

**R-08-37**

**Safety assessment for a  
KBS-3H spent nuclear fuel  
repository at Olkiluoto**

**Evolution report**

Paul Smith, Safety Assessment Management Ltd

Lawrence Johnson, Nagra

Margit Snellman, Barbara Pastina  
Saanio & Riekkola Oy

Peter Gribi, S+R Consult

January 2008

**Svensk Kärnbränslehantering AB**

Swedish Nuclear Fuel  
and Waste Management Co  
Box 250, SE-101 24 Stockholm  
Tel +46 8 459 84 00



ISSN 1402-3091

SKB Rapport R-08-37

# **Safety assessment for a KBS-3H spent nuclear fuel repository at Olkiluoto**

## **Evolution report**

Paul Smith, Safety Assessment Management Ltd

Lawrence Johnson, Nagra

Margit Snellman, Barbara Pastina  
Saanio & Riekkola Oy

Peter Gribi, S+R Consult

January 2008

*Keywords:* KBS-3H, Safety case, Safety assessment, Long-term safety, Evolution, Spent fuel, Nuclear waste, Disposal, Crystalline bedrock.

This report concerns a study which was conducted for SKB. The conclusions and viewpoints presented in the report are those of the authors and do not necessarily coincide with those of the client.

A pdf version of this document can be downloaded from [www.skb.se](http://www.skb.se).

# Abstract

The KBS-3 method, based on multiple barriers, is the proposed spent fuel disposal method both in Sweden and Finland. KBS-3H and KBS-3V are the two design alternatives of the KBS-3 method. Posiva and SKB have conducted a joint research, demonstration and development (RD&D) programme in 2002–2007 with the overall aim of establishing whether KBS-3H represents a feasible alternative to the reference alternative KBS-3V. The overall objectives of the present phase covering the period 2004–2007, have been to demonstrate that the horizontal deposition alternative is technically feasible and to demonstrate that it fulfils the same long-term safety requirements as KBS-3V. The safety studies conducted as part of this programme include a safety assessment of a preliminary design of a KBS-3H repository for spent nuclear fuel located about 400 m underground at the Olkiluoto site, which is the proposed site for a spent fuel repository in Finland. In the KBS-3H design alternative, each canister, with a surrounding layer of bentonite clay, is pre-packaged in a perforated steel cylinder prior to emplacement in the deposition drift; the entire assembly is called the supercontainer. Several supercontainers are positioned along parallel, 100–300 m long deposition drifts, which are sealed following waste emplacement using drift end plugs. Bentonite distance blocks separate the supercontainers, one from another, along the drift. Steel compartment plugs can be used to seal off drift sections with higher inflow, thus isolating the different compartments within the drift.

The present report describes the repository evolution in successive time frames, including key uncertainties. The description of evolution starts with the initial conditions at the time of emplacement of the first canisters. The repository evolves through an early, transient phase to a state where evolution is far slower. Particular attention is given to describing the transient phase, since this is where most of the important differences between KBS-3H and KBS-3V occur. The description of evolution in this phase addresses in turn the (i), thermal evolution, (ii), groundwater flow and evolution of groundwater composition, (iii), mechanical evolution, (iv), saturation and buffer swelling, (v) evolution of chemical and microbiological conditions and (vi), evolution of the canister surface and interior. A key issue is the local variability of the near-field rock around the KBS-3H repository drifts, which, together with the effects of gas from the corrosion of the supercontainer shells and other steel repository components, results in widely differing saturation times for different drift sections. Nevertheless, even in the tightest drift sections, the buffer is expected to retain its initial water content, and will eventually fully saturate, at which time it is expected to perform its full range of safety functions.

In the more distant future, the evolution of conditions at repository depth may be significantly affected by major climate change, and, in particular, by the formation of ice sheets at the ground surface. Key issues, which are common to KBS-3H and KBS-3V, are (i), the possibility that meltwater penetrating to repository depth may lead to some erosion of the buffer, and (ii), the impact of post-glacial earthquakes on canister integrity. The impact of anthropogenic emissions on the magnitude and timing of future major climate changes is a key uncertainty that is also common to the two alternatives. The description of repository evolution provides the basis for the identification of evolution scenarios, an assessment of canister longevity and the analysis of radionuclide release and transport in the event of canister failure.

Scenarios involving canister failure and radionuclide release are, however, also identified based on the discussion in this report and in the KBS-3H Process Report. These are initiated, in the first place, by:

- the presence of an initial, penetrating defect in one or more of the canisters;
- perturbations to the buffer and buffer/rock interface (some of which are specific to KBS-3H), giving rise to an increased rate of transport of sulphide from the geosphere to the canister surface and an increased canister corrosion rate;

- penetration of dilute glacial meltwater to repository depth, giving rise to chemical erosion of the buffer, an increased rate of transport of sulphide from the geosphere to the canister surface and an increased canister corrosion rate; and
- rock shear movements of sufficient magnitude to give rise to shear failure of the canisters.

No new canister failure modes have been identified compared with the KBS-3V design. The consequences of canister failure and radionuclide release are assessed in the KBS-3H Radionuclide Transport Report.

This report has been published also as a Posiva report, POSIVA 2007-08.

## Foreword

This study was coordinated by Margit Snellman from Saanio & Riekkola Oy on behalf of Posiva Oy. The progress of the study was supervised by a KBS-3H Review Group consisting of Aimo Hautojärvi (Posiva), Jukka-Pekka Salo (Posiva), Marjut Vähänen (Posiva), Barbara Pastina (Saanio & Riekkola Oy), Margit Snellman (Saanio & Riekkola Oy), Jorma Autio (Saanio & Riekkola Oy), Stig Pettersson (SKB), Erik Thurner (SKB), Börje Torstenfelt (Swedpower), Lennart Börgesson (Clay Technology) and Lawrence Johnson (Nagra). The Evolution Report was largely written by Paul Smith (Safety Assessment Management Ltd), with contributions from Daniel Suter (Science Solutions), Paul Wersin (Nagra), Paul Marschall (Nagra), Bill Lanyon (Fracture Systems) and the KBS-3H Review Group.

The interdisciplinary effort required the contributions of many individual scientists representing different areas of research. The flow of information was ensured by project meetings, reference reports and reviews by scientists in their respective fields of expertise. This report and its companion report, the KBS-3H Process Report /Gribi et al. 2007/, were cross-checked in several steps (outline, draft versions, final version) to ensure consistency.

Important contributions to scientific understanding of the evolution of the buffer have been made by Lennart Börgesson, Torbjörn Sanden and their co-workers at Clay Technology AB, Sweden, by way of laboratory tests, modelling and scenario analyses.

Modelling of cement/bentonite interaction was carried out by Jarmo Lehtikainen, Ari Luukkainen and Henrik Nordman (VTT), and estimates of grout take were made by Ursula Sievänen (Saanio & Riekkola Oy). The effects of cement on buffer evolution were summarised by Barbara Pastina (Saanio & Riekkola Oy).

The report was reviewed in draft form by members of the KBS-3H Review Group and by the following individuals: Jordi Bruno (Enviros Spain LS, Spain), Ivars Neretnieks KTH (Royal Institute of Technology, Sweden), Roland Pusch (Geodevelopment International AB, Sweden), Raymond Munier (SKB, Sweden), Johan Andersson (Streamflow AB, Sweden), Pirjo Hellä (Pöyry Environment, Finland), Nuria Marcos (Saanio & Riekkola Oy, Finland), and Christer Svemar (SKB, Sweden).

# Contents

<b>1</b>	<b>Introduction</b>	11
1.1	KBS-3H long-term safety studies	11
1.2	Reporting of KBS-3H long-term safety studies	13
1.3	Purpose and scope of this report	15
1.4	The regulatory context	16
1.5	Structure of this report	17
<b>2</b>	<b>Disposal site and KBS-3H repository description</b>	19
2.1	The spent fuel inventory	19
2.2	The Olkiluoto site	19
2.2.1	Reporting of site investigations	19
2.2.2	Surface conditions, overburden and bedrock geology	19
2.2.3	Rock fracturing and groundwater flow	21
2.2.4	Groundwater composition	22
2.2.5	Rock stress	23
2.2.6	Post-glacial adjustment	23
2.2.7	Repository layout and depth	24
2.2.8	Impact of repository excavation	26
2.3	Repository design	26
2.3.1	General description	26
2.3.2	Design options under consideration	27
2.3.3	Groundwater control and compartmentalisation of the drifts	28
2.3.4	Key components specific to KBS-3H in the current reference design	29
2.3.5	Use of cement and other construction materials	35
2.3.6	Use of steel	35
2.3.7	Operational procedure for implementing the current reference design	36
2.3.8	Possible deviations from planned operations and relevance to system evolution	36
2.4	Safety functions and how they are provided in the current design	37
2.4.1	Safety functions in KBS-3H	37
2.4.2	Design requirements to support the safety functions	38
2.5	Safety function indicators and criteria	41
2.5.1	Use of safety function indicators and criteria in safety assessment	41
2.5.2	Safety function indicators and criteria for the canisters	41
2.5.3	Safety function indicators and criteria for the buffer	42
2.5.4	Safety function indicators and criteria for the host rock	44
<b>3</b>	<b>Comparison of KBS-3V and KBS-3H</b>	45
<b>4</b>	<b>Initial conditions and operational phase</b>	51
4.1	Expected conditions	51
4.1.1	Impact of repository excavation on the near-field rock	51
4.1.2	The deposition drift	51
4.1.3	The spent fuel	54
4.1.4	The canister	55
4.1.5	Other engineered components	55
4.2	Possible deviations and remedial actions	56
4.2.1	Treatment of possible deviations in the description of repository evolution	56
4.2.2	Initial canister defects	56

4.2.3	Variations in buffer thickness and density	58
4.2.4	Accidents	58
4.2.5	Stray materials	59
4.2.6	Canister retrieval	59
<b>5</b>	<b>Early evolution</b>	<b>61</b>
5.1	Definition of the period and evolution of external conditions	61
5.2	Thermal evolution	62
5.2.1	Key aspects of thermal evolution in this period	62
5.2.2	Thermal evolution in the operational period	63
5.2.3	Thermal evolution in the longer term	64
5.2.4	Wider impact on system evolution and safety functions	66
5.3	Groundwater flow and evolution of groundwater composition	68
5.3.1	Key aspects of groundwater flow and evolution of groundwater composition in this period	68
5.3.2	Wider impact on system evolution and safety functions	69
5.4	Mechanical evolution	69
5.4.1	Key aspects of mechanical evolution in this period	69
5.4.2	Development of buffer swelling pressure and deformation of the supercontainer	70
5.4.3	Development of isostatic loads on canisters	71
5.4.4	Vertical displacement of the canisters	72
5.4.5	Mechanical evolution of the rock at its interface with the buffer	72
5.4.6	Rock shear movements	74
5.4.7	Hydromechanical heterogeneity along a KBS-3H drift	74
5.4.8	Mechanical evolution of the compartment and drift end plugs	74
5.4.9	Wider impact on system evolution and safety functions	75
5.5	Saturation and buffer swelling	76
5.5.1	Key aspects of saturation and buffer swelling	76
5.5.2	Expected evolution in less tight drift sections	77
5.5.3	Expected evolution in tighter drift sections	83
5.5.4	Expected evolution in tightest drift sections	86
5.5.5	Plugged sections	88
5.5.6	Possible deviations from expected evolution	89
5.5.7	Wider impact on system evolution and safety functions	92
5.6	Evolution of chemical and microbiological conditions	92
5.6.1	Key aspects of the evolution of chemical and microbiological conditions in this period	92
5.6.2	Chemical evolution of the buffer	93
5.6.3	Depletion of trapped oxygen and impact of microbial reactions	93
5.6.4	Corrosion of KBS-3H steel components	94
5.6.5	Interactions involving cement and stray materials	97
5.6.6	Wider impact on system evolution and safety functions	98
5.7	Evolution of the canister surface and interior	99
5.7.1	Canister temperature	99
5.7.2	Exposure of the canister surface to water	99
5.7.3	Mechanical load on the canister	99
5.7.4	Corrosion of the copper shell	99
5.7.5	Chemical evolution of the canister interior	101
5.7.6	Radioactive decay, radiolysis and the production of gas by decay	101
5.7.7	Redistribution of fissile material	101
5.7.8	Wider impact on system evolution and safety functions	101
<b>6</b>	<b>Subsequent evolution prior to the next major climate change</b>	<b>103</b>
6.1	Definition of the period and evolution of external conditions	103
6.2	Thermal evolution	103
6.3	Hydrogeological evolution	105

6.4	Mechanical evolution	105
6.4.1	General description	105
6.4.2	Potential for buffer extrusion and erosion in fractures	106
6.4.3	Potential for canister sinking	106
6.5	Chemical evolution	106
6.5.1	General description	106
6.5.2	Buffer intrusion into fractures and the stability of the gel water interface	107
6.5.3	Mineral transformation due to iron/bentonite interaction	107
6.5.4	Migration of oxygen introduced with surface water	108
6.6	Evolution of the canister surface and interior	109
6.6.1	Conditions at the canister surface	109
6.6.2	The canister interior	109
<b>7</b>	<b>Evolution affected by major climate change</b>	<b>111</b>
7.1	Climate evolution scenarios	111
7.2	Impact on the surface environment	111
7.3	Impact on the rock at repository depth	113
7.3.1	General description	113
7.3.2	Temperature evolution	113
7.3.3	Seismic activity and post-glacial earthquakes	114
7.3.4	Mechanical effects in the rock	114
7.3.5	Groundwater flow and composition	114
7.4	Impact on the engineered barrier system	116
7.4.1	General description	116
7.4.2	Freezing and thawing	117
7.4.3	Canister corrosion	117
7.4.4	Isostatic load on the canisters	117
7.4.5	Impact of earthquakes and rock shear on the canisters	118
7.4.6	Other potential impacts of rock shear	121
7.4.7	Changes in buffer swelling pressure and the possibility of buffer erosion	122
7.4.8	Buffer liquefaction	122
<b>8</b>	<b>Evolution of a canister with an initial penetrating defect</b>	<b>123</b>
8.1	Possibility of occurrence	123
8.2	Key phases in and aspects of evolution	123
8.3	Water ingress following penetration of the copper shell	123
8.4	Interaction of water with the cast iron insert	124
8.5	Impact of insert corrosion on the buffer	126
8.6	Contact of water with the cladding and fuel pellets and the effects of ionising radiation	126
8.7	Corrosion of the cladding and other metal components and impact on radionuclide release	127
8.8	Release of segregated radionuclides	127
8.9	Fuel dissolution and impact on radionuclide release	128
8.10	Fate of released radionuclides	129
8.10.1	Solubilities and speciation	129
8.10.2	Transport mechanisms	129
8.10.3	Conditions for gas-induced displacement of porewater	130
8.10.4	Formation of gas pathways in the buffer	131
8.11	Possibility of nuclear criticality	131
<b>9</b>	<b>The farthest future</b>	<b>133</b>
<b>10</b>	<b>Summary of system evolution of a KBS-3H repository at Olkiluoto</b>	<b>135</b>
10.1	Overall evolution	135
10.2	Early evolution	135



10.3	Subsequent evolution prior to major climate change	138
10.4	Effects of major climate change	139
10.5	Evolution of a canister with an initial penetrating defect	140
10.6	The farthest future	141
<b>11</b>	<b>Implications for radionuclide release and transport</b>	<b>143</b>
11.1	Scenarios and assessment cases	143
11.2	Finnish regulatory requirements regarding scenarios	144
11.3	Methodology for the identification of scenarios leading to canister failure and radionuclide release	145
11.4	Application to a KBS-3H repository at the Olkiluoto site	145
11.4.1	Carrying out the steps	145
11.4.2	Overview of scenarios	146
11.4.3	Scenarios involving an initial penetrating canister defect	150
11.4.4	Scenarios involving canister failure by corrosion	151
11.4.5	Scenarios involving canister rupture due to rock shear	152
11.5	Overview of assessment cases	153
<b>12</b>	<b>Issues requiring further work</b>	<b>157</b>
12.1	Issues related to the evolution of the repository and site	157
12.2	Design issues	161
	<b>References</b>	<b>163</b>
	<b>Appendix A</b> The DAWE design variant	<b>173</b>
	<b>Appendix B</b> Scoping calculations	<b>177</b>

# 1 Introduction

## 1.1 KBS-3H long-term safety studies

The KBS-3 method, based on multiple barriers, is the selected spent fuel disposal method in both Sweden and Finland. There are two design alternatives for the KBS-3 method: KBS-3V in which the canisters are emplaced in individual vertical deposition holes and KBS-3H in which several canisters are emplaced in horizontal deposition drifts (see Figure 1-1). The reference alternative for the implementing organisations, SKB in Sweden and Posiva in Finland, is KBS-3V. Posiva and SKB have conducted a joint research, demonstration and development (RD&D) programme in 2002–2007 with the overall aim of establishing whether KBS-3H represents a feasible alternative to KBS-3V. The overall objectives of the present phase, covering the period 2004–2007, have been to demonstrate that the horizontal deposition alternative is technically feasible and to demonstrate that it fulfils the same long-term safety requirements as the reference design KBS-3V. The safety studies conducted as part of this programme include an evolution report for a preliminary design of a KBS-3H repository, which is the present report.

Long-term safety studies specific to KBS-3H are complemented by detailed studies of:

- the function of the bentonite buffer;
- repository design and layout adaptation to the Olkiluoto site in Finland;
- deposition equipment;
- the retrievability of the canister in KBS-3H; and
- the comparative costs of the KBS-3H and KBS-3V alternatives.

These are intended to be sufficiently comprehensive that they can be used, along with other technical demonstration, environmental and cost studies, as a technical basis for a decision at the beginning of 2008 on whether or not to continue the development of KBS-3H. The main conclusions from these KBS-3H studies and answers to the high-level questions above will be presented in the Summary of the KBS-3H Project 2004–2007 /SKB/Posiva 2008/.

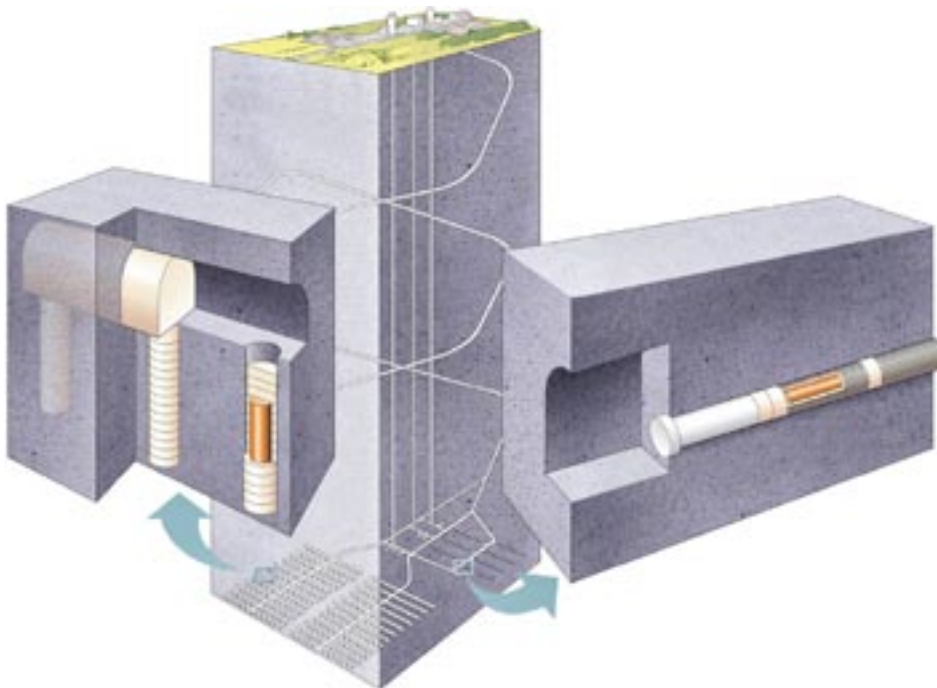


*Figure 1-1. The KBS-3V (left) and KBS-3H (right) alternatives of the KBS-3 spent fuel disposal method.*

There are currently a number of design variants under consideration for implementing KBS-3H, as well as differences between the fuel types, between the characteristics and inventories of the canisters, and between the designated repository site for a spent fuel repository in Finland and the sites still under consideration in Sweden. In order to focus the KBS-3H long-term safety studies, however, they are applied to the Olkiluoto site, in the municipality of Eurajoki, which is the proposed site for a spent fuel repository in Finland. The reference fuel is the Finnish BWR fuel from Olkiluoto 1 and 2 reactors and the reference design used in the KBS-3H safety assessment is the Basic Design as described in the Design Description 2006. This choice of reference design is preliminary and other design variants, also based on KBS-3H, are presented in the Design Description 2006. At the time of selection of the reference design for the long-term safety studies, no major differences between the Basic Design and the design alternative, termed DAWE (Drainage Artificial Watering and air Evacuation), had been identified that were relevant to long-term safety. The Basic Design is the outcome of several years of studies of different design options for the drift. DAWE was introduced at a later stage in the programme to address some uncertainties regarding the feasibility of implementing the Basic Design in less favourable locations along the drifts. At the time of selection, however, both designs were judged to be potentially feasible, and the Basic Design was chosen for the safety assessment. Since the present safety assessment addresses the long-term safety of a KBS-3H repository located at the Olkiluoto site in Finland, it is appropriate to base the assessment on Finnish regulatory requirements.

Specific high-level questions addressed by the KBS-3H long-term safety studies are:

- are there safety issues specific to KBS-3H with the potential to lead to unacceptable radiological consequences?
- is KBS-3H promising at a site with the broad characteristics of Olkiluoto from the long-term safety point of view?

Due to the limitations in the scope of the KBS-3H long-term safety studies, these do not currently address the questions:

- is KBS-3H more or less favourable than KBS-3V from a long-term safety point of view?
- does the specific realisation of the KBS-3H design considered in the safety studies satisfy all relevant regulatory guidelines?

KBS-3H and KBS-3V both have features that are favourable and less favourable to long-term safety and to its assessment. A comparative study of these favourable and less favourable features is beyond the scope of the long-term safety studies carried out so far. Regarding the second question, although the performance of a KBS-3H repository has been analysed in a number of cases representing alternative evolutions of the repository and its environment and the results compared with Finnish regulatory guidelines, the analyses have a number of limitations, as described in the KBS-3H Radionuclide Transport Report /Smith et al. 2007a/. These limitations would have to be addressed before it could be judged whether all relevant regulatory guidelines are satisfied.

In order to judge the feasibility of implementing KBS-3H from a long-term safety point of view, relevant safety issues must be understood as well for KBS-3H as they are for KBS-3V. There is a broad scientific and technical foundation that is common to both alternatives, and much of the work carried out by both Posiva and SKB in the context of KBS-3V is also directly applicable to KBS-3H. Thus, there is comparatively much more limited documentation that has been developed specifically relating to KBS-3H, and this documentation focuses primarily on the differences identified between the two alternatives in a systematic “difference analysis” reported in the KBS-3H Process Report<sup>1</sup> /Gribi et al. 2007/. Site properties and aspects of system evolution common to the two alternatives are described in more detail in the evolution report for a KBS-3V at Olkiluoto (/Pastina and Hellä 2006/ and references therein). Much of the information and analysis conducted by SKB in SR-Can /SKB 2006a–e/ for a KBS-3V repository

---

<sup>1</sup> Unless stated otherwise, the term Process Report refers to the KBS-3H Process Report /Gribi et al. 2007/.

in Sweden is also relevant, and drawn upon extensively in KBS-3H safety studies and their documentation.

Consistent with the “difference analysis” approach, at the start of the KBS-3H safety studies a decision was taken to follow the SR-Can approach for process selection and to accept the understanding and modelling basis presented in SR-Can in areas in which KBS-3H and KBS-3V are very similar, in particular in modelling canister and fuel processes. The reason for this is that major efforts would have to be made to advance the models beyond what was presented in SR-Can, and such advances were not part of the KBS-3H programme mandate. Such developments may, however, be considered in future project stages for both KBS-3H and 3V.

Safety studies refer to *long-term* or *post-emplacement* safety, i.e. safety from the time of emplacement of the first canisters in the repository. Construction and operation of the repository drifts will continue over several decades following emplacement of the first canisters, and long-term safety studies consider evolution and performance in this period, as well as in the period subsequent to repository closure. The safety of the workforce and the public during construction, operation and closure of the repository (operational safety) is, however, considered separately from the long-term safety studies.

Differences between the fuel, canisters and repository sites under consideration in Sweden and Finland will have to be considered in transferring the detailed findings of the current safety studies to a Swedish context. However, since the difference analysis shows that the key differences in the evolution and performance of the two alternatives relate mainly to the engineered barrier system, and, with the exception of overall inventory, these are broadly similar in the Swedish and Finnish contexts, many of the broad findings on the engineered barrier system are expected to be readily transferable.

## 1.2 Reporting of KBS-3H long-term safety studies

The several reports that document and support the safety studies of a KBS-3H repository at Olkiluoto are shown in Figure 1-2 (although some are common to KBS-3H and KBS-3V and will be developed in the context of Posiva’s KBS-3V programme). The reporting structure of the KBS-3H safety studies is based on Posiva’s 2005 safety case plan /Vieno and Ikonen 2005/.

The overall outcome of the KBS-3H safety studies is documented in the **summary report**, “Safety assessment for a KBS-3H repository for spent fuel at Olkiluoto” /Smith et al. 2007b/. The summary report is supported by a number of further high-level reports (those shown in Figure 1-2), one of which is this **Evolution Report**.

The geoscientific basis of the safety case is provided in **site reports** /Posiva 2003, 2005, Andersson et al. 2007/, including the present situation at, and past evolution of, the Olkiluoto site, and disturbances caused by ONKALO<sup>2</sup>, an underground characterisation facility that will also serve as an access route to the repository. Data from the most recent Olkiluoto Site Description 2006 /Andersson et al. 2007/ are referenced in the present report, although further work is required to incorporate this data fully in future safety assessments.

The engineering basis is provided by the reports on the **characteristics of spent fuel** /Anttila 2005a/, **canister design** /Raiko 2005/, and **repository design** /Autio 2007, Autio et al. 2007/. The preliminary “reference design” analysed in this report is presented in the “KBS-3H Design Description 2006” report /Autio et al. 2007/. The reference design for the KBS-3H safety studies (termed Basic Design) was frozen at the beginning of 2007. The KBS-3H repository design is still ongoing and subsequent design developments are presented in the Design Description 2007 report /Autio et al. 2008/.

---

<sup>2</sup> ONKALO is the Olkiluoto Underground Rock Characterisation facility for site-specific underground investigations. ONKALO has been under construction since mid-2004 and will serve as an access route to the repository and the first disposal tunnels are planned to be adjacent to ONKALO’s main characterization level.

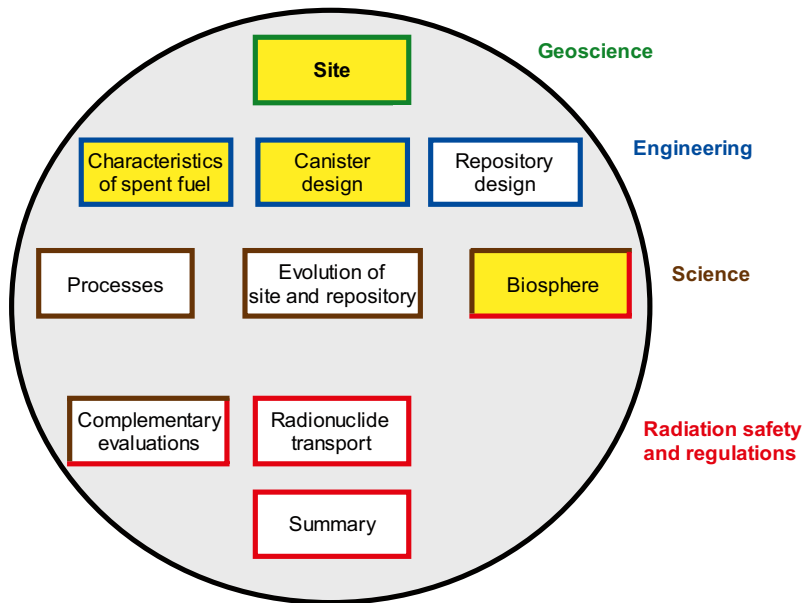


**Figure 1-2.** The reporting structure for KBS-3H long-term safety studies. The colours of the boxes indicate the areas covered by the reports (as listed on the right-hand side of the figure). Yellow filling indicates reports common to the KBS-3H and -3V safety studies. All the other boxes represent reports produced within the KBS-3H safety studies or design studies. The safety assessment for a KBS-3H spent nuclear fuel repository at Olkiluoto is presented in the Summary report. For details see the main text.

The scientific understanding supporting the long-term safety studies is described in a **Process Report** /Gribi et al. 2007/ and in the present **Evolution Report**. The Process Report, as its name indicates, describes the individual processes and discusses the relevance of selected processes (e.g. gas generation) through scoping calculations. The Evolution Report describes the most relevant processes identified in the Process report, but in broadly chronological order, highlighting the interactions between the processes and their coupling whenever possible, starting from repository construction and continuing up to one million years from the beginning of repository operations.<sup>3</sup>

The Process and Evolution Reports provide the basis for the selection of the assessment cases calculated in the **Radionuclide Transport Report** /Smith et al. 2007b/. A **Complementary Evaluations of Safety Report** /Neill et al. 2007/ provides additional arguments, mostly non quantitative, on the long-term safety aspects of a KBS-3H repository located at the Olkiluoto site. A **Biosphere Analysis Report** /Broed et al. 2007/ was produced in parallel to the above-mentioned reports using input from the KBS-3H radionuclide transport report and the main conclusions on the ensuing releases to the biosphere are summarised in the present safety assessment summary report.

These high-level reports are further supported by more detailed technical reports compiled in support of KBS-3H long-term safety studies, including reports on thermal analyses /Ikonen 2003, 2005/, thermo-mechanical analyses /Lönqvist and Hökmark 2007/, layout studies based on analyses of data from the Olkiluoto site /Hellä et al. 2006/, discrete fracture network modelling of the site /Lanyon and Marschall 2006/, analyses of hydro-mechanical, chemical, gaseous and microbiological (HMCCGB) processes related to the steel components /Johnson et al. 2005/, experimental and modelling studies on the interaction of iron and bentonite /Carlson et al. 2006, Wersin et al. 2007/, and solubility estimation in support of radionuclide release and transport calculations /Grivé et al. 2007/.

<sup>3</sup> A certain degree of overlap between the Process and the Evolution Reports is unavoidable and deemed beneficial if the reports are read separately. However, the authors recognise that it is preferable to read both the Evolution and Process Reports together to fully grasp the couplings and relative importance of processes in such a complex system.

### 1.3 Purpose and scope of this report

This report provides a description of the evolution of a preliminary design of a KBS-3H repository constructed deep underground at a depth of about 400–500 m at the Olkiluoto site in Finland, and identifies some of the current uncertainties affecting this evolution.

This report discusses in detail those aspects of the evolution of a KBS-3H repository that differ from those of KBS-3V, while mostly summarising other aspects. Many aspects are the same or very similar in both designs. Furthermore, the essential elements of the KBS-3H safety concept – i.e. the conceptualisation of how the proposed system provides safety – are shared with KBS-3V. This common KBS-3 safety concept is illustrated in Figure 1-3, which shows the primary roles and relationships between the different technical components of the disposal systems.

Early in the evolution of the repository, significant mass and energy fluxes occur as a result of the various gradients created by repository construction and emplacement of the spent fuel. In both KBS-3H and KBS-3V, the system evolves from the initial state through an early, transient phase towards a quasi-steady state, in which key safety-relevant physical and chemical characteristics (e.g. temperature, buffer density and swelling pressure) are subject to much slower changes than in the transient phase. It is in the transient phase that most of the significant differences in evolution between the two alternatives arise, although there are also some differences at later times (for example, in the impact of post-glacial faulting and in the gas-induced release of dissolved radionuclides in the case of a defective canister). Thus, the transient evolution of the repository and, in particular, the evolution of the KBS-3H buffer to a state of full saturation, receives particular attention in this report (Chapter 5).

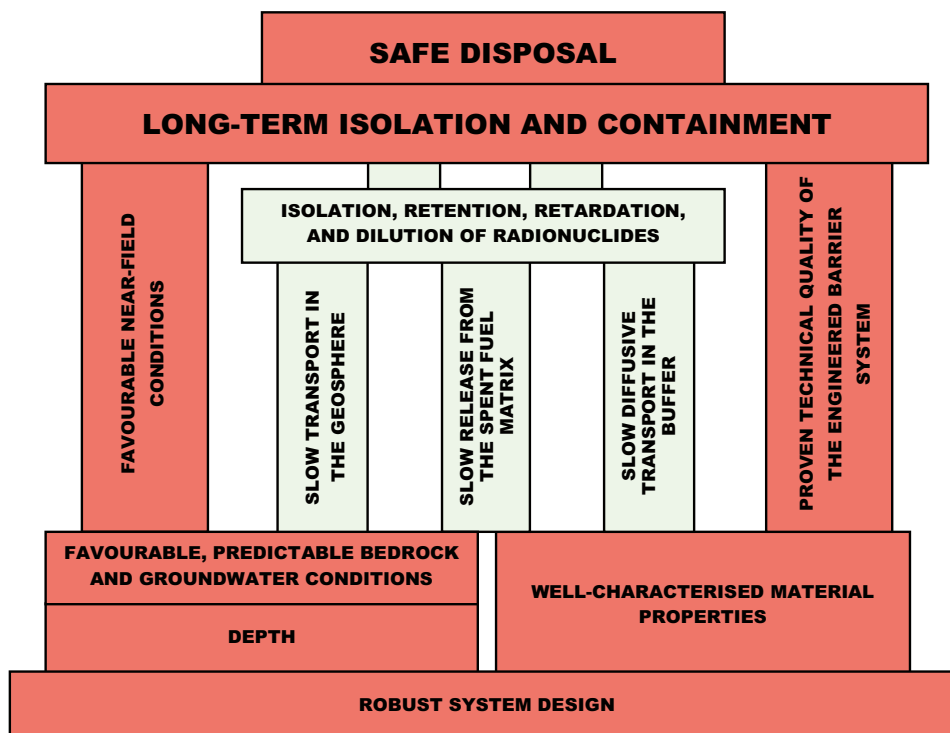


*Figure 1-3. Outline of the safety concept for a KBS-3 type repository for spent fuel in crystalline bedrock. Red pillars link characteristics of the disposal system to other characteristics on which they primarily depend. Green boxes and pillars indicate secondary characteristics and dependencies /after Posiva 2006/.*



## 1.4 The regulatory context

The present safety assessment addresses the long-term safety of a KBS-3H repository for Finnish spent fuel located at the Olkiluoto site in Finland. It is therefore appropriate to base the assessment on Finnish regulatory requirements<sup>4</sup>. The regulatory requirements for a spent fuel repository at Olkiluoto are set forth in the Government Decision on the safety of the disposal of spent nuclear fuel /STUK 1999/ and, in more detail, in Guide YVL 8.4 issued by the Finnish regulator /STUK 2001/. These requirements are, however, currently under revision. A detailed discussion of regulatory requirements related to the safety case, including dose and radionuclide release constraints in different time frames, is given in Posiva's TKS-2006 describing the programme for research, development and technical design /Posiva 2006/. Some key points relevant to the present report are summarised below.

Finnish regulations distinguish between the “environmentally predictable future” (lasting “several thousand years”), during which conservative estimates of dose must be made, and the “era of large-scale climate events” when periods of permafrost and glaciations are expected, and radiation protection criteria are based on constraints on nuclide-specific activity fluxes from the geosphere (“geo-bio flux” constraints). Posiva's interpretation of the duration of the “environmentally predictable future” is typically 10,000 years. The annual effective dose constraint for the most exposed members of the public applicable over this time frame is  $10^{-4}$  Sv per year, while the average annual effective doses to other members of the public should, according to the regulations, remain insignificantly low. It is also stated in YVL 8.4 that the radiation exposure of flora and fauna shall remain clearly below the levels that would cause decline in biodiversity or other significant detriment to any living population on the basis of the best available scientific knowledge. Moreover, rare animals and plants as well as domestic animals shall not be exposed detrimentally as individuals.

Regarding the characteristics and performance of the engineered barrier system, YVL 8.4 requires that:

*The barriers shall effectively hinder the release of disposed radioactive substances into the host rock for several thousands of years.*

The early (transient) evolution, which, as mentioned above, receives particular attention in this report, occurs within this time frame.

The importance to long-term safety of unlikely disruptive events shall, according to regulations, be assessed. According to STUK, these events are to include at least:

- boring a deep water well at the disposal site;
- core drilling hitting a spent fuel canister; and
- a substantial rock movement occurring in the environs of the repository.

The likelihood and consequence of the first two events is not considered to differ significantly between KBS-3V and KBS-3H repositories (although some differences in the probability of a vertical borehole intersecting vertically emplaced canister exist compared with horizontally emplaced canisters) and these are not discussed in the present report. The impact of substantial rock movement occurring in the environs of the repository is, however, discussed in Chapter 7 in the context of post-glacial earthquakes.

In the very long term, after at least several hundred thousand years, no rigorous quantitative safety assessment is required, but the judgement of safety can be based on more qualitative considerations.

---

<sup>4</sup> The differences between the Swedish and Finnish regulatory systems are discussed in Appendix C of the Complementary Evaluations of Safety Report /Neill et al. 2007/.

## 1.5 Structure of this report

The structure of this report is as follows:

Chapter 2 describes the Olkiluoto site, the KBS-3H design and the long-term safety requirements on the KBS-3H system components.

Chapter 3 provides a broad comparison of KBS-3V and KBS-3H, identifying where the important differences lie with respect to repository evolution.

Chapter 4 describes the initial conditions within and around a KBS-3H deposition drift, and gives a broad description of the KBS-3H engineered barrier system for the design variants currently under consideration.

Chapter 5 describes the evolution of a KBS-3H repository in the transient phase. The chapter deals separately and in turn with (i), thermal evolution, (ii), groundwater flow and evolution of groundwater composition, (iii), mechanical evolution, (iv), saturation and buffer swelling, (v) the evolution of chemical and microbiological conditions and (vi), the evolution of the canister surface and interior.

Chapter 6 deals with the evolution subsequent to the transient phase and prior to the next major climate change.

Chapter 7 deals with the effects of major climate change, focussing on aspects with a different significance to, or potential impact on, KBS-3H compared with KBS-3V.

Chapter 8 deals with evolution of a canister that is assumed to have an initial, penetrating defect.

Chapter 9 discusses evolution in the farthest future.

Chapter 10 provides a summary of the evolution of a KBS-3H repository, based on the descriptions in Chapters 5-9.

Chapter 11 discusses the implications of the evolution of a KBS-3H repository for radionuclide release and transport, providing a list of scenarios to be considered in the radionuclide release and transport calculations documented in the Radionuclide Transport Report /Smith et al. 2007a/.

Chapter 12 discusses various issues that will require further work.

The report has two appendices. The first describes the DAWE design variant, which is one of two broad realisations of KBS-3H currently under consideration. The description of system evolution in the main text concerns the Basic Design, which is the chosen reference design for the long-term safety studies<sup>5</sup> reports (including this report). The second appendix presents various scoping calculations that have been carried out to support some of the statements made in the main text. Much of the material in this second appendix is duplicated in, or slightly adapted from, sections of the KBS-3H Process Report /Gribi et al. 2007/.

---

<sup>5</sup> All further uses in this report of the term “safety studies” refer to long-term safety studies.



## 2 Disposal site and KBS-3H repository description

### 2.1 The spent fuel inventory

For the present safety studies, the working hypothesis is that a Finnish repository for spent fuel will need to accommodate approximately 5,500 tU of fuel, encapsulated in approximately 3,000 canisters /Pastina and Hellä 2006/. This comprises fuel from the following facilities:

- Loviisa 1–2: 700 canisters containing 1,020 tU of spent fuel
- Olkiluoto 1–2: 1,210 canisters containing 2,530 tU of spent fuel
- Olkiluoto 3: 930 canisters containing 1,980 tU of spent fuel
- **Total: 2,840 canisters and 5,530 tU from the spent fuel**

The reference fuel used in KBS-3H safety studies is the BWR fuel from the Olkiluoto 1 and 2 reactors. Finnish fuel has an average burn-up of 37–39 MWd/kgU and a maximum burnup of 45 MWd/kgU for Loviisa and 50 MWd/kgU for Olkiluoto. Spent fuel inventory estimates are based on maximum discharge burnup of 45 and 50 MWd/kgU. These estimates may change in the future along with the development of reactor load factors, fuel designs and burnup.

### 2.2 The Olkiluoto site

#### 2.2.1 Reporting of site investigations

The following sections give a brief description of the Olkiluoto site, the location of which is shown in Figure 2-1, which also indicates the Swedish sites at Forsmark and Laxemar that were the subject of SR-Can. The description, which focuses largely on those aspects most relevant to the present Evolution Report, is based on the comprehensive overview of investigations carried out at Olkiluoto up to the year 2005, most recently compiled into Site Report 2006 /Andersson et al. 2007/. This description is, in turn, an update of the descriptions provided in the Baseline Report /Posiva 2003/ and 2004 version of the site description /Posiva 2005/. An extensive summary of the site description is provided in Chapter 11 of /Andersson et al. 2007/.

#### 2.2.2 Surface conditions, overburden and bedrock geology

Olkiluoto is a relatively flat island with an average height of 5 m above sea level and with the highest point at 18 m above sea level. The island is covered by forest and shoreline vegetation. The sea around the island is shallow, with a depth mainly less than 12 m within 2 km of the current shoreline. The elevations relative to sea level are continuously changing, since the apparent rate of uplift is significant at 6 mm per year, mainly due to isostatic adjustment of the bedrock (Section 2.2.6).

The overburden, both onshore and offshore is mostly till. The other terrestrial sediment types are, in order of abundance, fine sand, sand and silt, with the thickness of the overburden mostly being between 2 and 4 m, although deposits up to 12 to 16 m in thickness have been observed in rock surface depressions /Lahdenperä et al. 2005, Posiva 2005/. The groundwater table follows the surface topography and is mainly 0 to 2 m below surface, with some exceptions. Olkiluoto Island forms its own hydrological unit; the surface waters flow directly into the sea /Lahdenperä et al. 2005, Posiva 2005/. Infiltration of surface water is currently being investigated. Current (and provisional) estimates are approximately 1–2% of the annual precipitation. The evolution of surface conditions and local ecosystem are described in more detail in the Terrain and Ecosystems Development Model Report /Ikonen et al. 2007/.



**Figure 2-1.** The location of the Olkiluoto site, which is the subject of the present study, and the Forsmark and Laxemar sites, which were the subject of SR-Can.

The bedrock at Olkiluoto belongs to the Svecofennian domain of Southern Finland and comprises a range of high-grade metamorphic and igneous rocks. The metamorphic rocks include various migmatitic gneisses and homogeneous, banded or only weakly migmatized gneisses, such as mica gneisses, quartz gneisses, mafic gneisses and tonalitic-granodioritic-granitic gneisses. The igneous rocks comprise abundant pegmatitic gneisses and sporadic narrow diabase dykes /Andersson et al. 2007/.

Three different alteration episodes can be identified at Olkiluoto, which have affected the chemical composition and mineralogical character of the altered rocks and, as a consequence, the physical properties of the bedrock:

- a *retrograde phase of metamorphism*, which affected the bedrock during the Svecofennian Orogeny about 1,900 to 1,800 million years ago;
- *hydrothermal alteration processes*, which are estimated to have taken place at temperatures from 50°C to slightly over 300°C and are thought to be related to the late stages of metamorphism, to the emplacement of rapakivi granites 1,580 to 1,570 million years ago and to the intrusion of olivine diabase dykes 1,270 to 1,250 million years ago; and
- *surface weathering*, which probably dates back some tens of millions of years and is currently still active.

The bedrock was deformed in a ductile manner during the Svecofennian Orogeny and was subsequently affected by several tectonic events that resulted in brittle deformation.

Large post-glacial earthquakes have been observed in Northern Finland and elsewhere in Northern Fennoscandia. In Southern Finland, however, although some small post-glacial faults with scarp heights up to 20 cm have been found, none have been identified so far at Olkiluoto /Lindberg 2007/. Seismic activity in the Olkiluoto region is currently low (see, e.g. /La Pointe and Hermanson 2002, Enescu et al. 2003, Saari 2006/). GPS and seismic measurements at Olkiluoto show rock movements of less than 0.1 mm per year /Posiva 2003/. Concerning past seismic movements, in particular those related to post-glacial earthquakes, no signs of rock displacements were found in a recent mapping campaign on outcrops in the islands surrounding Olkiluoto /Lindberg 2007/. On a larger spatial scale, a study of seismicity in the Olkiluoto area based on historical observations of earthquakes within 500 km of the site /Saari 1997/ showed that all significant earthquakes ( $M > 3.5$ ) are related to the Saaristomeri-Paldis-Pskov seismic zone, which is no closer than 35–40 km to Olkiluoto. Zones 20 km SW of Olkiluoto and 35 km NE of Olkiluoto have been identified that are possibly related small ( $2.7 < M < 3.1$ ) earthquakes /Saari 1997/. /Hutri 2007/ has studied traces of Holocene palaeoseismicity in the sea around Olkiluoto and identified possible relicts of post-glacial reactivation in soft sediment features in the straight just north of Olkiluoto (e.g. faults, slides, slumps and pockmarks). Dating results support the suggestion that major seismic activity was greatest during a short period after the last deglaciation. The lack of indications of recent significant seismic activity at Olkiluoto, together with indications of post-glacial reactivation in the past, suggest that major seismic activity in the future is also likely to occur with the greatest frequency following glaciations /Andersson et al. 2007/, although infrequent but significant seismic events during inter-glacial periods cannot be excluded.

Ongoing geological characterisation and modelling will give more insight into the characteristics of deformation zones at the site and their potential to host future large post-glacial earthquakes.

### **2.2.3 Rock fracturing and groundwater flow**

Polyphase deformation has resulted in a network of fractures and fracture zones with different scales within the Olkiluoto bedrock. The frequency, spatial distribution, size distribution, shape and orientation of these structures affect both the hydraulic and mechanical properties of the rock. The fracture zones often constitute dominant paths for groundwater flow and their size also determines the size of rock shear movements taking place in the zone. As noted above, hydrothermal alteration has occurred in certain domains in the rock mass, and this also affects its strength and transport properties.

Information has been gathered on the occurrence, frequency and orientation of transmissive fractures at Olkiluoto. Up till now, the focus of the hydrogeological modelling has been on identifying and characterising the major hydraulically active deformation zones, whereas the rock masses between these zones have been given average hydraulic properties. However, for assessing the evolution of the engineered barrier systems and for modelling the performance of the geosphere transport barrier, it is also necessary to describe the flow system at the scale of individual fractures. Detailed data on the fractures exist, but so far the analyses of these data have focused on those fractures reflecting likely conditions in the deposition drifts /Hellä et al. 2006/.

According to these analyses, transmissive fractures at relevant depths, especially those with transmissivities higher than  $10^{-8} \text{ m}^2 \text{ s}^{-1}$ , are concentrated mainly in local zones of abundant fracturing. Fractures with lower transmissivities occur outside these zones, but also tend to form clusters /Hellä et al. 2006/. The rock matrix between fractures has an average porosity of 0.14% /Autio et al. 2003/ and a low hydraulic conductivity so that water fluxes through it are negligible compared to that through fractures. The estimates of /Hellä et al. 2006/ may be revised as a result of the ongoing detailed site characterisation work at ONKALO and associated modelling.

Calcite and a range of clay minerals (illite, smectite, kaolinite, vermiculite and chlorite) make up most of the fracture filling. Pyrite is also abundant, mainly as coatings on calcite grains. Pyrite has been observed in all boreholes studied so far at the site. These fracture fillings play an important role in the hydrogeochemical conditions at Olkiluoto and their evolution.

## 2.2.4 Groundwater composition

Groundwater composition at Olkiluoto has been extensively investigated, and baseline conditions are described in /Posiva 2003/ and /Pitkänen et al. 2004/. Generally, chemical conditions in the groundwater are stable at depth at Olkiluoto and reactions and transport processes proceed slowly, but may be perturbed by the presence of the repository and by external events occurring in the far future, such as major climate change. Thus, a description of the present-day flow distribution and groundwater composition at the site, and also their history and prognoses for future evolution, have also been developed based on hydrogeological and hydrogeochemical studies and modelling.

The groundwater composition over the depth range 0 to 1,000 m at Olkiluoto is characterised by a significant range in salinity (see, e.g. Figure 11-8 in /Andersson et al. 2007/). Fresh groundwater with low total dissolved solids (TDS less than about 1 g/l) is found only at shallow depths, in the uppermost tens of metres. Brackish groundwater, with TDS up to 10 g/l dominates at depths between 30 m and about 400 m. Saline groundwaters (TDS > 10 g/l) dominate at still greater depths. The current salinity of groundwater at repository depth (400 to 500 m below ground) ranges from 10 to 20 g per litre TDS /Andersson et al. 2007/. Chloride is normally the dominant anion in all bedrock groundwaters. Near-surface groundwater is also rich in dissolved carbonate and groundwater at depths between about 100 and 300 m is characterised by high sulphate concentrations. The sulphate content in the sulphate-rich brackish groundwater is at maximum about 500 mg/l. Both carbonate and sulphate concentrations decrease significantly at greater depths. Sodium and calcium dominate as main cations in all groundwaters, and magnesium is also notably enriched in sulphate-rich waters.

The ions dominating in different groundwater types reflect the origins of their salinity. In crystalline rocks, high dissolved carbonate content is typical of meteoric groundwaters that have infiltrated through organic soil layers. High sulphate content indicates a marine origin in crystalline rocks without sulphate mineral phases. More generally, the wide groundwater salinity variations at Olkiluoto can be interpreted in terms of varying degrees of mixing of certain reference water types, together with a range of water/rock interactions that buffer pH and redox conditions and stabilise groundwater composition. The reference water types are present-day *Baltic seawater* and four different groundwater types, termed, in order of decreasing age, *brine reference*, *glacial reference*, *Littorina (Sea) reference* and *meteoric water*. The groundwater flow and composition near to the surface is characterised by a dynamic hydraulic regime and a significant imprint of young meteoric waters. Below about 300 m depth, studies of methane and of isotopic composition indicate that the deep stable groundwater system has not been disturbed by glacial and post-glacial transients and that neither oxidising glacial meltwater<sup>6</sup> nor marine water have mixed in this deeper system.

Redox conditions deep underground are reducing, and are buffered by a range of redox processes, with microbes playing an important role. The anaerobic reduction of sulphate to sulphide at the interface where sulphate-rich marine derived brackish groundwater comes into contact with deeper, methane-rich saline groundwater results in an abundance of sulphide in the groundwater at repository depth, the highest measured sulphide concentration being 12 mg per litre. In a repository, sulphide may diffuse through the buffer and react with the copper canister, as described in various sections of this report. Sulphide ions thus play an important role in considerations of canister lifetime.

---

<sup>6</sup> Glacial meltwater is a very dilute ice-melting water. Saline groundwater represents a water with a salinity, expressed as Total Dissolved Solids of about 20 g/l. For detailed composition of the waters used in the assessment, see Appendix D of Radionuclide Transport report.

The variation of dissolved gas composition with depth at Olkiluoto, the origin of gases and their coupling to chemical reactions with other dissolved species is discussed in detail in /Pitkänen and Partamies 2007/. Dissolved nitrogen and methane content is high in Olkiluoto groundwater, nitrogen being the dominant dissolved gas in the upper 300 m with methane being dominant at greater depths. Methane is potentially relevant to canister corrosion in that it may participate in the reduction of sulphate in the groundwater to sulphide in the presence of sulphate reducing bacteria. Methane in the groundwater is thought to have two primary sources. Thermal abiogenic hydrocarbons (a crustal inorganic carbon source without biogenic processes) dominate in the deepest sampled groundwaters, where the highest methane concentrations are found, and are near to saturation values. It may be speculated that methane percolates from great depths or even from the Earth's mantle and that the source term is practically infinite. At shallow depths, the methane content of the water decreases and the fraction of biogenic methane increases steadily. At repository depth, biogenic methane dominates. The concentration is lower here than at greater depths and is far from saturation, but, as noted in Chapter 12, the role of methane in the reduction of sulphate to sulphide, its evolution over time and its impact on canister lifetime are issues requiring further investigation. In sulphate-rich groundwater above about 300 m depth, only traces of hydrocarbons are observed, consistent with the possibility that dissolved methane reacts with sulphate in a system where sulphate reducing bacteria are present.

The pH conditions in the deep aquifer system at Olkiluoto are well buffered by the presence of abundant carbonate and clay minerals found in fracture fillings. The pH values at relevant depths are generally in the range 7.5–8.2 /Pitkänen et al. 2004/.

### **2.2.5 Rock stress**

The stress state at the Olkiluoto site has been determined for different depths /Johansson et al. 2002a, Posiva 2005, Andersson et al. 2007/. The repository drifts will be aligned as much as possible with the direction of the maximal horizontal stress for reasons of mechanical stability (see Section 2.2.7). Regional data indicate that the mean orientation of the maximum horizontal stress is roughly E-W, but the data display a large scatter, so that it is currently uncertain whether the stress orientation at the site differs from the mean regional orientation. At 500 m, the maximal horizontal stress is estimated to be between 15 and 31 MPa and the minimum horizontal stress is estimated to be in the range 10 to 18 MPa. The vertical stress is estimated to be between 7 and 15 MPa at 500 m. The major principal stress is subhorizontally orientated, and is thus slightly larger in magnitude than the maximum horizontal stress. The other two principal stress components vary significantly in magnitude and orientation between the different measurement locations, indicating the need to relate the stress field to geological structure and to conduct associated numerical analyses. The minimal principal rock stress is relevant to the early evolution of the repository in that it may affect, for example, the maximum gas pressures that can develop around the repository as a result of gas generation by the corrosion of steel components. In Section 5.5, a minimal principal rock stress of 9 MPa is tentatively assumed.

### **2.2.6 Post-glacial adjustment**

During the last glacial maximum, 17–22 thousand years ago, the Fennoscandian ice sheet reached as far south as northern Germany. The thickness of the ice sheet at that time is thought to have been about 2 km over Finland /Lambeck et al. 1998/. The weight of the ice mass against the viscous mantle caused the Earth's crust to sink some hundreds of metres. As the ice sheet started to melt about 13,500–10,300 years ago, the crust started to rise. The crust is currently still in the process of returning to its position of isostatic equilibrium.

The most obvious consequences of postglacial adjustment in Fennoscandia are the land uplift along both sides of the northern part of the Baltic Sea and the concomitant retreat of the shoreline. Olkiluoto Island began to emerge from the Baltic Sea about 3,000–2,500 years ago. Currently, the rate of isostatic post-glacial uplift at the site is estimated to be 6.8 mm per year /Johansson et al. 2002b, Kahma et al. 2001, Eronen et al. 1995/. The apparent uplift rate, which



is the rate of isostatic uplift minus the eustatic component due to sea-level change associated with the changing shapes of the sea basins, is 6 mm per year (this does not include the impact of global sea level change). The land uplift rate is expected to vary little over the next few centuries, but will decrease significantly within the next few thousand years /Mäkiäho 2005, Pässe 1996, 1997, 1998/. Such post-glacial land uplift is not to be confused with tectonic uplift, which in Finland is very slow, as discussed in the Complementary Evaluations of Safety Report /Neall et al. 2007/.

### 2.2.7 Repository layout and depth

The layout of a repository at Olkiluoto will be adapted according to the locations of major deformation zones, which will be avoided when constructing deposition drifts. Two broad arrangements of deposition drifts are currently under consideration: 1) a one-storey facility with deposition drifts at a depth of approximately 400 metres (reference design) or 2) a two-storey facility with deposition drifts at depths of approximately 400 and 500 metres (alternative design). This report addresses the evolution of a one-storey repository only, although any differences compared with the alternative design are expected to be minor.

The number, length and orientations of the drifts themselves will be constrained by a range of factors, including safety-related requirements regarding:

- the hydraulic properties of fractures intersecting the deposition drifts at canister and buffer emplacement locations;
- the maximum allowable temperature within the deposition drifts; and
- the extent and hydraulic conductivities of the excavation-damaged zones (EDZs) around the drifts, including the risk of rock spalling.

Efforts will be made to avoid fractures at canister emplacement locations that could undergo shear movements that could damage the canisters in the event of a large post-glacial earthquake (Section 7.4.5). The extent to which it will be possible to identify and avoid fractures capable of undergoing potentially damaging displacements is currently under investigation for both KBS-3V and KBS-3H. The amount of shear movement that will occur as a result of future post-glacial earthquakes is uncertain, but is related to fracture size. The size of fractures will, to some (uncertain) extent, be correlated to their transmissivity, and the more transmissive fractures (and fractures with the highest initial inflow) will be avoided for reasons outlined below and in Appendix B.2.

According to the simulations by /Hellä et al. 2006/ (see Section 4.1.2), repository drifts are likely to pass through long relatively tight, sparsely fractured sections of rock between localised clusters of transmissive fractures. In the current reference design, ~ 10 m long drift sections<sup>7</sup> with initial inflows higher than 0.1 litres per minute will be excluded as canister and buffer emplacement locations in order to limit the possibility of piping and erosion during the operational period and subsequent period of buffer saturation (Section 5.5.6 and Appendix L of /Autio et al. 2007/). This implies that transmissive fractures that could give rise to relatively high flows around the repository drift in the longer term, once the drift is saturated, will also be avoided.

The relationship between initial inflow and longer-term flow is, however, complicated by a number of factors. On the one hand, grouting may reduce the observed inflow of some larger aperture fractures. On the other hand, a larger leakage elsewhere may reduce the hydrostatic pressure at the observation point and thus give a wrong interpretation of the observed inflow. Furthermore, initial inflows may also be reduced by drawdown of the water table, which will give a reduction in the hydrostatic pressure at repository depth; the impact of other open repository tunnels and drifts; and potentially by mineral precipitation and degassing in the fracture.

---

<sup>7</sup> 10 m is the approximate combined length of a supercontainer and distance block, as defined in Section 2.3.

These are generally transient effects which do not affect flow in the longer term, once the drifts are saturated. Finally, inflow is determined not only by the hydraulic properties of fractures intersecting the drift, but also by those of other connected fractures in the wider fracture network.

The grout is likely to become degraded and ineffective in reducing flow in the longer term. In view of current uncertainties in the performance of any grout, an inflow of less than 0.1 litres per minute prior to grouting is used as a criterion for a drift section to be suitable for the emplacement of canisters and buffer in deriving a preliminary repository layout.

In many of the scoping calculations and radionuclide release and transport calculations carried out for the KBS-3H safety studies, it is tentatively assumed that the highest transmissivity of any fracture intersecting a drift at locations where canisters and buffer are emplaced is  $3 \times 10^{-9} \text{ m}^2 \text{ s}^{-1}$ . This assumption, which is discussed further in Appendix B.2, is based on an application of Darcy's law in a radial configuration (Thiem's equation; Eq. B.2-1) to a single fracture giving an inflow of 0.1 litres per minute, assuming a 4 MPa pressure difference between the drift and the undisturbed rock during saturation and a distance of 50 m between the drift wall and the nearest major fracture zone. In view of the factors mentioned above, higher transmissivities cannot currently be excluded (radionuclide release and transport calculations include the possibility that a higher transmissivity fracture intersects the drift at the location of a failed canister in a variant case – see /Smith et al. 2007a/), but a transmissivity of  $3 \times 10^{-9} \text{ m}^2 \text{ s}^{-1}$  at a canister and buffer emplacement location is nevertheless considered to be towards the high end of the expected distribution.

The maximum allowable temperature in the buffer is currently set at 100°C. This limit should favour the thermal and mineralogical stability of bentonite. According to /Pusch and Karnland 1990/, irreversible chemical changes such as illite formation<sup>8</sup> and cementation that would reduce swelling capacity are expected to be insignificant below 100°C (Section 2.5.9 of /SKB 2006b/), although, as noted in Chapter 12, the possibility of cementation due to silica precipitation is an issue requiring further investigation. The 100°C limit is met through an adequate spacing of the canisters along the drift using distance blocks of sufficient length (Section 2.3), and through an adequate spacing between the drifts /Ikonen 2003/.

Finally, the orientations of the drifts in relation to the stress field in the rock are selected, in part, to minimise the extent and hydraulic conductivities of the excavation-damaged zones (EDZs) around the drifts and in part to minimise the risk of rock spalling (although additional design measures may be needed to avoid thermally-induced rock spalling in tight drift sections – Section 5.4.5).

A preliminary layout for a one-storey facility based on the current bedrock model and the hydraulic, thermal and mechanical considerations described above is given in /Johansson et al. 2007/. In this preliminary layout, which is illustrated in Figure 2-2, the repository is constructed in a single layer at a depth in the range 400 to 420 m below ground (note that the drifts are slightly inclined to the horizontal to facilitate drainage during construction and operation – see Figure 2-4). The layout is based on a drift separation of 25 m, and a canister pitch ranging from 9.1 to 11 m, depending on the specific Finnish fuel type under consideration (see Table 4-1). The layout features 170 deposition drifts with an average length of 272 m. It is estimated by /Johansson et al. 2007/ that about 25% of the total drift length is unusable for canister and buffer emplacement (see the discussion of groundwater control and compartmentalisation of the drifts in Section 2.3.3). Thus, the total “usable” drift length is about 34,700 m, which is sufficient for the approximately 3,000 canisters to be emplaced in the current KBS-3H reference design, as described in Section 2.3. The drifts are orientated at 120°, with their axes close to the direction of maximum horizontal stress (Section 2.2.5).

---

<sup>8</sup> Illitisation also requires a supply of potassium from the groundwater, which may limit the rate at which this process can occur at higher temperatures.

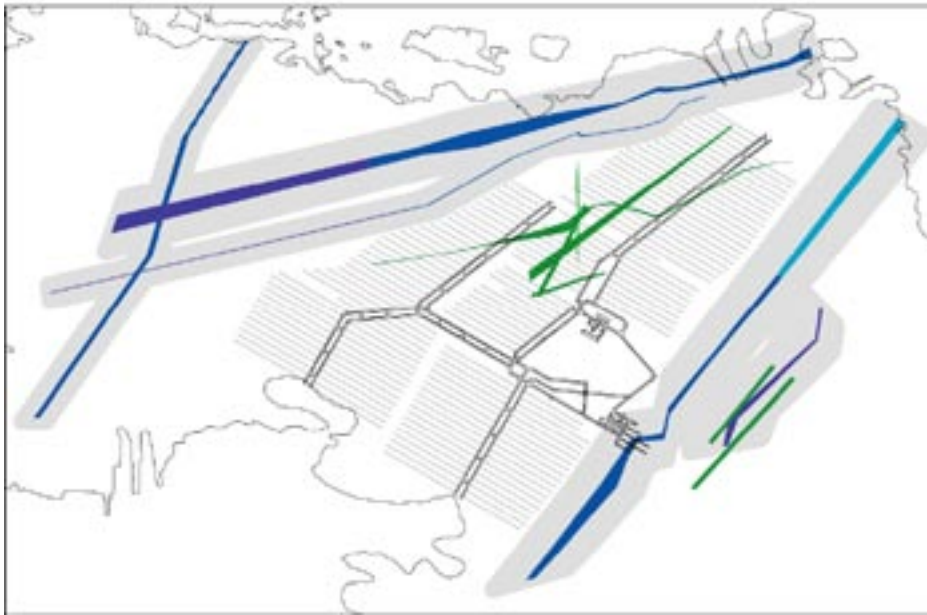


**Figure 2-2.** Example layout adaptation of a KBS-3H repository at Olkiluoto at a depth of about 420 m below ground /after Johansson et al. 2007/. Grey areas indicate the area that the layout is not allowed to intersect due to the proximity of hydraulically conductive zones (termed “hydrogeological zones” in the Site Description 2006 /Andersson et al. 2007/). These zones are shown in blue. Features shown in green are not considered to be layout determining, and may thus intersect the deposition drifts. The layout is based on the bedrock model presented in the Site Description 2006, in which the hydraulically conductive zones and their extensions are taken into account.

This preliminary layout uses about 95% of the currently well-characterised and available bedrock resource<sup>9</sup> at Olkiluoto, which takes into account the major fracture zones shown in Figure 2-2, respect distances to investigation boreholes, the access tunnel to the ONKALO, the shoreline of Olkiluoto Island, and the boundaries of the current investigation area. Although the margin for uncertainties is therefore small in this layout, it would, if necessary, be possible to increase this margin by extending the current investigation area (there is, for example, land to the east that is potentially available) or constructing the repository in multiple layers.

## 2.2.8 Impact of repository excavation

Construction of the repository will significantly perturb mechanical, hydrogeological and geochemical conditions deep underground. The resulting state of the bedrock at repository depth at the time of emplacement of the first canister, including rock stress, ambient rock temperature, fractures and fracture zones and groundwater composition and flow are described in Section 4.1.1. Transient perturbations are also described in Chapter 5.

## 2.3 Repository design

### 2.3.1 General description

In KBS-3H, the spent fuel is encapsulated in copper canisters with cast iron inserts. Each canister, with a surrounding partly saturated layer of bentonite clay, is placed in a perforated steel cylinder prior to emplacement and the entire assembly is called the supercontainer.

<sup>9</sup> For comparison, the current reference KBS-3V layout at Olkiluoto uses about 80% of the available bedrock resource /Johansson et al. 2007/.



The supercontainers are deposited coaxially in the drifts, supported on steel feet to leave an annular gap to the drift wall (about 4 cm in the current reference design). Bentonite distance blocks separate the supercontainers, one from another, along the drift. A section of drift with two supercontainers and two distance blocks is shown in Figure 2-3. Void spaces around the supercontainers and distance blocks will become filled with bentonite as the drift saturates and the bentonite swells, although the rate at which this occurs may vary considerably along the drift due to the heterogeneity of the rock and the variability of water inflow, as discussed at length in Chapter 5. The bentonite inside the supercontainers and the bentonite distance blocks are jointly termed the buffer.

### 2.3.2 Design options under consideration

Localised water inflow along the drift may potentially give rise to large hydraulic pressure differences along the drift between the void spaces around neighbouring supercontainers. A key consideration in the development of the present reference and alternative designs is to minimise the possibility that these pressure differences develop rapidly, before the bentonite of the distance blocks swells and contacts the drift walls and a high swelling pressure and bentonite density develop at this interface. The concern is that, if high pressure differences develop too rapidly, this could result in movement of the distance blocks and supercontainers, or in transient water flows (“piping”) along the interface, which could in turn lead to erosion and loss of bentonite density in some supercontainer sections, and possibly an increase in density in others.

Two broad design options are currently being developed in parallel. The Basic Design is the current reference design chosen for safety studies and is described below (some alternative realisations of the Basic Design are described in Appendix K of /Autio et al. 2007/). The Drainage, Artificial Watering and air Evacuation (DAWE) design variant is described briefly in Appendix A.

Each design option has a number of open design issues (e.g. physical dimensions of some components) that are still under consideration, thus both design options are considered to be preliminary. After the main design features have been fixed, development will concentrate on dimensioning of components and confirmation that they will perform their intended design functions. The current reference design, Basic Design, as described in the following sections, is the basis for description of repository evolution in this report.

In all design options, the copper canisters are fully retrievable, as will be described in the coming Design Description 2007 /Autio et al. 2008/. An SKB report evaluating canister retrievability techniques for both KBS-3H and KBS-3V /Kalbantner and Sjöblom 2000/ concluded that canister retrieval feasibility is equivalent for both horizontal and vertical disposal alternatives.

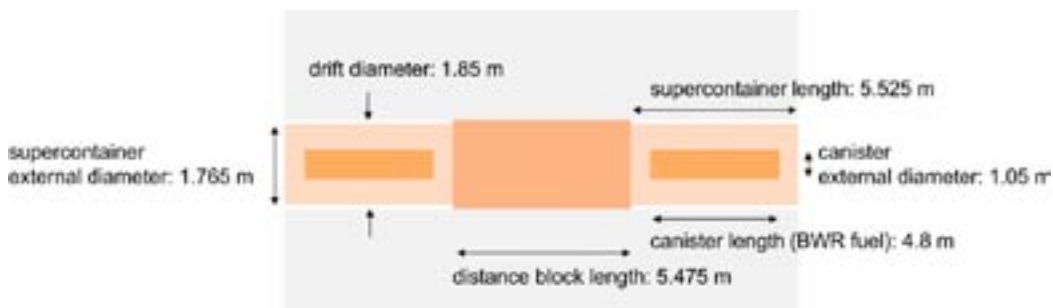


**Figure 2-3.** Illustration of a section of a KBS-3H deposition drift with two supercontainers separated by a distance block. The 5.475 m distance block length is for the reference fuel for the present safety studies (BWR spent fuel from the Olkiluoto 1 and 2 reactors).

### 2.3.3 Groundwater control and compartmentalisation of the drifts

Groundwater control measures in the form of pre- or post-grouting to reduce inflow to the drifts will be implemented for reasons of engineering practicality and operational safety, and to limit the possibility of piping and erosion of the buffer during the operational period. Currently, the possibility of using a large-scale post-grouting device (called Mega-Packer, see /Autio et al. 2007/) to inject Silica Sol, or other types of grout (low-pH cement) into transmissive fractures is being investigated

The performance of grout in reducing inflows is currently uncertain, and grout cannot be relied upon in the long term to reduce groundwater flow around the drifts. Thus, irrespective of any grouting that is undertaken, transmissive fractures intersecting the drift may render particular sections unsuitable for the emplacement of supercontainers and distance blocks. In the current reference design, additional “filling blocks” are emplaced in those ~ 10 m long drift sections where the total inflow to the section exceeds about 0.1 litres per minute, but excluding those higher inflow drift sections where inflow exceeds about 1 litre per minute even after grouting<sup>10</sup>.

The maximum allowable inflow of 1 litre per minute is thus higher in the case of filling blocks compared with the 0.1 litres per minute allowed for distance blocks. This is because of the different functions of these two components. The distance blocks should prevent significant water flow by piping between adjacent supercontainer drift sections during saturation of the drift, which could otherwise lead to buffer erosion. The limit of 0.1 litres per minute is related to this requirement. The filling blocks, on the other hand, are not used to separate adjacent supercontainers and so the prevention of piping is not a primary consideration in deciding where they can be emplaced. There is, however, a requirement to avoid erosion of these blocks by water flowing around the drift through intersecting transmissive fractures and erosion, as discussed in Section 5.5.6 and in Sections 4.5.2 and 4.6.1 of the Process Report /Gribi et al. 2007/. The relevant inflow criterion is expected to be higher, although the present choice of 1 litre per minute is preliminary and somewhat arbitrary value that may be updated in view of future studies and possible design changes. Steel compartment plugs are used to seal off drift sections where inflows are higher than 1 litre per minute after grouting, thus dividing the drift into compartments. Main features of a KBS-3H drift are shown in Figure 2-4.

According to the discrete fracture network modelling carried out by /Lanyon and Marschall 2006/, based on hydrogeological considerations, a 300-metre long KBS-3H drift at Olkiluoto contains, on average, two compartments, one drift section (30 m long) isolated by compartment plugs, 3–4 filling blocks (10 m each) and 22 to 23 supercontainers on average considering all fuel/canister types (or 17 to 18 considering only Olkiluoto BWR fuel, which is the reference fuel considered in this report). On average, 17% of the drift is unusable due to high water inflow.

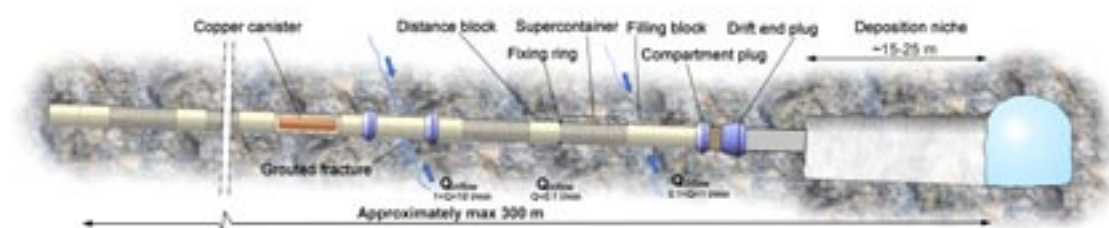


**Figure 2-4.** Illustration of a generic KBS-3H drift showing one canister in copper colour for better visualisation. At one end of the drift, a wider area (deposition niche) hosts the deposition equipment while the other end of the drift is closed off. The different components are described in Section 2.3.4.

<sup>10</sup> Note that fractures giving inflows of less than 0.1 litres per minute may not be amenable to further flow reduction by grouting on account of their small apertures.

A higher figure of 25% is tentatively and conservatively assumed in the layout adaptation (Section 2.2.7). This takes into account the possibility that some relatively tight fractures that have the potential to undergo shear movements sufficiently large to damage the canisters in the event of a large earthquake are identified and avoided. The impact of earthquakes and rock shear on canister integrity is discussed in Section 7.4.5 in the context of future glaciation and post-glacial earthquakes.

### 2.3.4 Key components specific to KBS-3H in the current reference design

The KBS-3H deposition drifts, and key engineered system components emplaced within a drift that are specific to KBS-3H, as realised in the current reference design, are described individually in the following sections.

#### **The drifts**

In the preliminary layout described in Section 2.2.7, the drifts have an average length of 272 m, and have a shallow dip of 1.5 to 2 degrees towards the tunnels from which they are bored to provide drainage during the operational period. In the current reference design, the drift diameter is 1.85 m. At the beginning of each deposition drift, before the drift end plug, is a 15-metre long, wider section of the drift, termed the deposition niche, with a 50 m<sup>2</sup> cross section, which is used to host the deposition equipment for supercontainers and distance blocks (Figure 2-5). The maximum length of the drifts is 300 m, the estimated minimum length is 100 m and the average length is about 272 m, based on site-specific features /Autio et al. 2007/. In the current design, the drifts are dead-ended, i.e. there is no access tunnel on the other end.

#### **The supercontainers**

The supercontainers are 1.765 m in diameter. Their lengths will vary according to fuel type that they contain. They are, for example, 5.525 m long for BWR fuel from the Olkiluoto 1–2 reactors. The buffer inside each supercontainer is comprised of a set of MX-80 bentonite ring blocks surrounding the canister and two end blocks (Figure 2-6).

The cylindrical steel shell that contains the buffer and canister is 8 mm thick and perforated with 100 mm diameter holes covering 62% of the cylindrical surface (Figure 2-7). The buffer inside the supercontainers will swell through these perforations as it saturates. The surfaces of the end plates are unperforated, to minimise the gap in order to favour a good contact between the supercontainers and the adjacent distance blocks. The mass of the steel components (cylindrical shell, end plates and feet) is 1,071 kg.



**Figure 2-5.** The main tunnel and deposition drifts including the deposition niche (after Figure 4-2 of /Autio et al. 2007/).

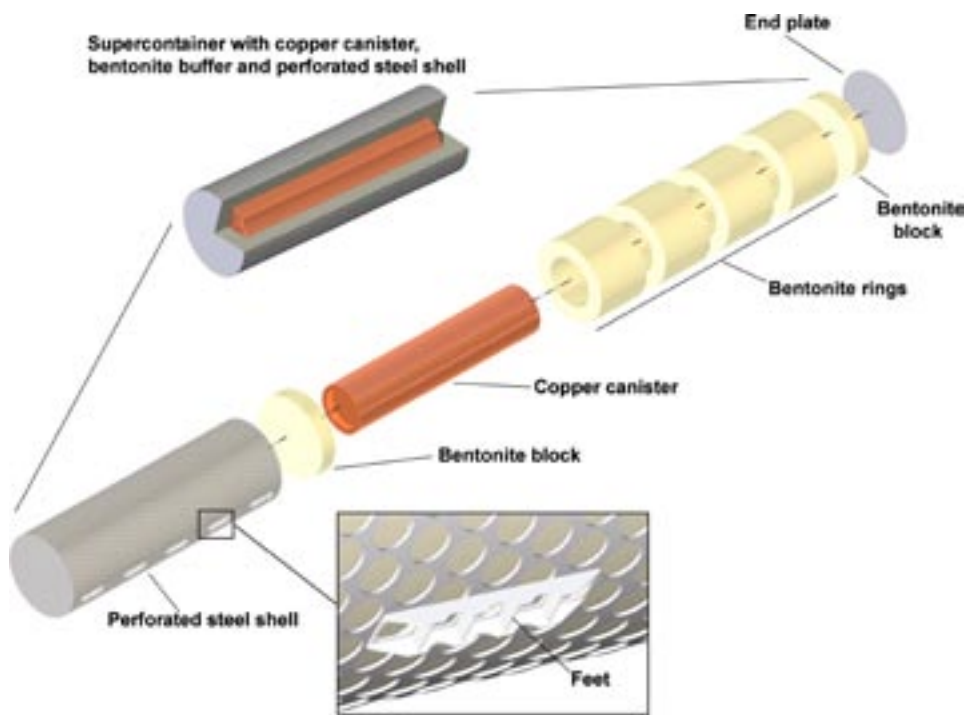


Figure 2-6. The supercontainer with buffer and copper canister.

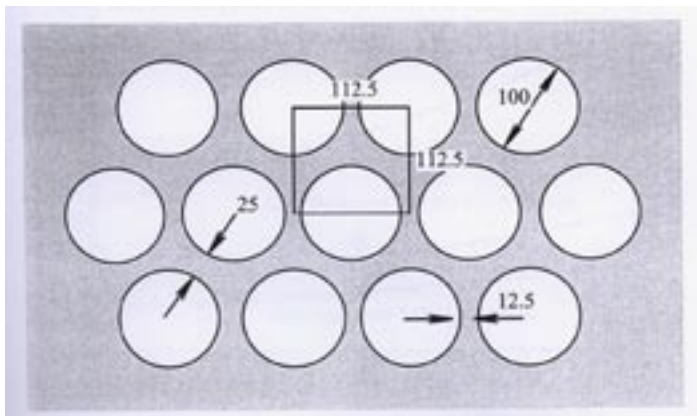


Figure 2-7. Section of supercontainer cylindrical shell surface, showing dimensions [mm] of the perforations.

The ring blocks have a 10% initial water content and a dry density of  $1,885 \text{ kg m}^{-3}$ . The end blocks also have a 10% initial water content, but have a lower dry density ( $1,753 \text{ kg m}^{-3}$ ). The design density and porosity of these buffer components following saturation and swelling into the gap around the supercontainer are  $2,000 \text{ kg m}^{-3}$  and 0.44, respectively. Differences in buffer density are, however, likely to occur, especially between the saturated buffer inside and outside the supercontainer. These differences will reduce over time, but some residual differences may persist indefinitely because friction limits buffer homogenisation (Section 5.5).

### The distance blocks

The distance blocks, which hydraulically separate the supercontainers one from another, are also composed of MX-80 bentonite. In the current reference design, the distance block consists of two different bentonite components in series; a “tight” block and a “loose” block as shown in Figure 2-8. The gap between the distance block and the drift wall is made small (a few mm in the case of the “tight” blocks and up to a maximum of 15 mm in the case of the “loose blocks”) to favour rapid closing and sealing /Autio et al. 2007/.



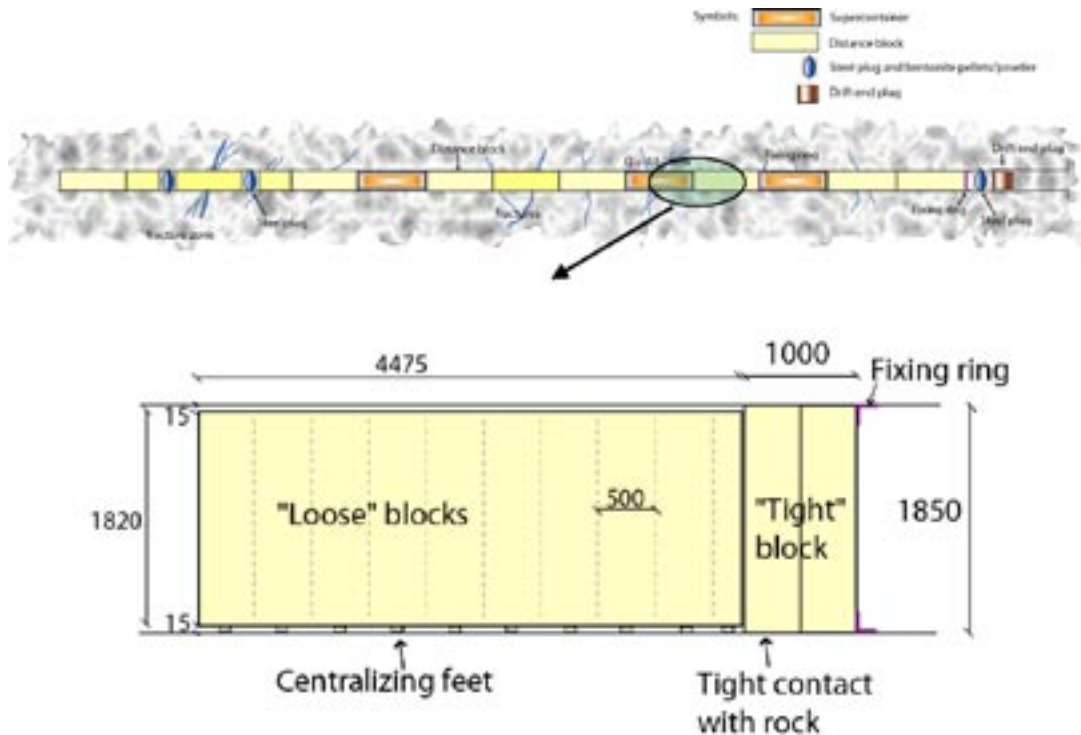


**Figure 2-8.** “Tight” and “loose” components of the distance block (after Figure 5-2 of /Autio et al. 2007/).

Large hydraulic pressure differences may develop along the drift during and after operation due to localised water inflow. A distance block separating a tighter drift section from a drift section in which the gaps become rapidly water filled may full hydrostatic pressure around the periphery of one vertical face, while the pressure on the opposite vertical face remains low. The vertical gaps between distance blocks and supercontainer are minimised to prevent the possibility of exposing the entire vertical face of a distance block to full hydrostatic pressure, which could otherwise lead to the possibility of pressure-induced movement of distance blocks and supercontainers. If the gap is made small (a few millimetres), the full hydrostatic pressure is initially expected to be exerted only around the periphery of the face, reducing the overall force on the face. There is, however, uncertainty concerning the possible deformation of the distance block, which could result in greater forces being exerted on the face, and this is being addressed in current design studies. In current safety studies, it is assumed that friction, together with the presence of fixing rings (below), will prevent and significant movement prior to the installation of compartment and drift end plugs. These issues are discussed further in Section 5.5.

The length of the distance blocks is determined by the thermal management requirements on the spent fuel (see Section 5.2 for a description of thermal evolution in the early phase). The distance blocks for BWR fuel from the Olkiluoto 1–2 reactors are 5.475 m long (Figure 2-3 and Figure 2-8).

The “loose and “tight” blocks both have a 24% initial water content, The “loose” blocks have an initial dry density of  $1,610 \text{ kg m}^{-3}$ , and the “tight” blocks an initial dry density of  $1,559 \text{ kg m}^{-3}$ . As in the case of the buffer originally inside the supercontainers, the design saturated density and porosity are  $2,000 \text{ kg m}^{-3}$  and 0.44, respectively, for both the “loose” blocks and the “tight” blocks.

### **Filling blocks**

The MX-80 bentonite filling blocks are similar in design to the distance block units. Their use is illustrated in Figure 2-9.

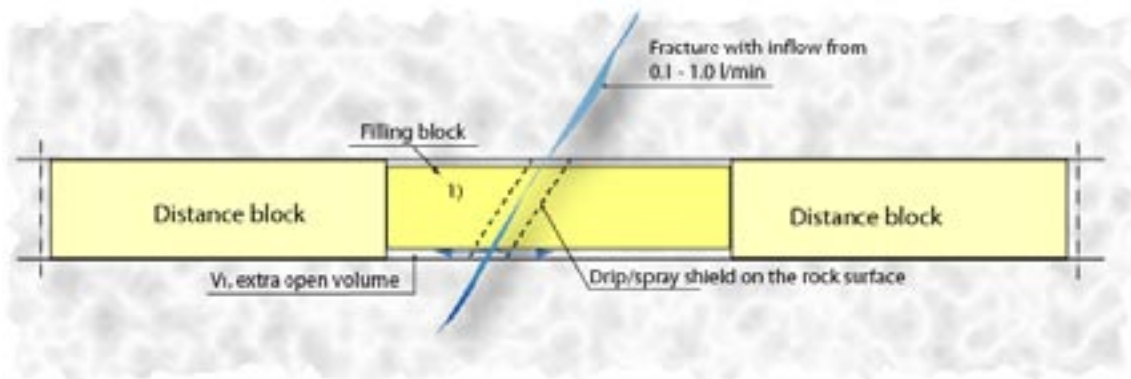


Figure 2-9. Filling block between two distance blocks (after Figure 5-15 in /Autio et al. 2007/).

### Fixing rings

Steel fixing rings are installed, where necessary, to avoid displacement of the distance blocks prior to the installation of compartment and drift end plugs. Such displacements could otherwise arise as a result of large hydraulic pressure differences along the drift due to localised water inflow. Displacement in case of limited pressure exerted over the end face of a distance block can be prevented during compartment operation by the fixing rings that are installed along the drift and, following operations, by the compartment plug, which is designed to withstand full hydrostatic pressure at repository depth.

The principle of using fixing rings to prevent displacement during drift operation is described in Section 5.2.3 of /Autio et al. 2007/ and illustrated in Figure 2-10.

The fixing ring consists of a 10 mm-thick steel plate, supported by a steel collar grouted and bolted into the rock, as described in Section 5.2.3 of /Autio et al. 2007/. In the current reference design, fixing rings are installed in every position where the inflow to a “supercontainer unit” (comprising one supercontainer and distance block) exceeds 0.01 litres per minute. This tentative criterion will, however, need to be confirmed by further studies.

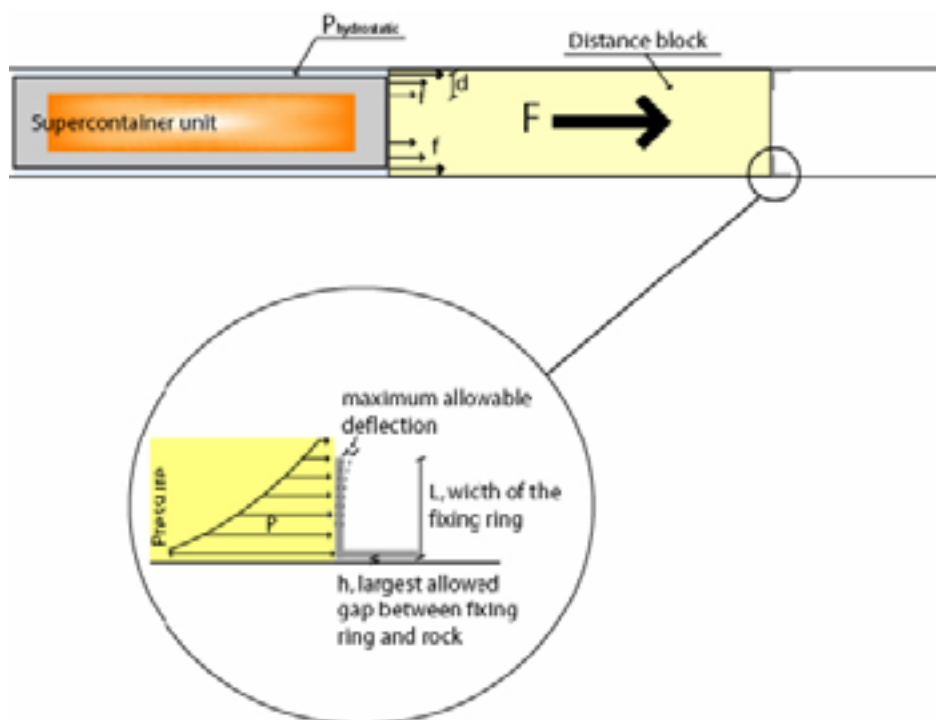


Figure 2-10. The principle of using fixing rings to prevent displacement of a distance block during drift operation.  $P_{hydrostatic}$  is the rock matrix pore pressure (after Figure 5-8 of /Autio et al. 2007/).

### Compartment plugs

Steel compartment plugs will be used to seal off drift sections where inflows are higher than 1 litre per minute (after grouting). The design of the compartment plugs is still under development and demonstration tests are planned to be performed at the Äspö Hard Rock Laboratory. In the current provisional design, the compartment plugs are steel structures, and these are described in detail in Section 4.3 of /Autio et al. 2007/. At each location where a plug is required, a steel collar structure will be attached to the drift surface before drift operation starts and sealed using concrete. The centre part of the plug, which takes the form of one or two dome-shaped caps attached to a flange (see Figure 4-12 in /Autio et al. 2007/), will then be installed rapidly during drift operation following emplacement of the supercontainers and distance blocks in a compartment. The plugs are designed to withstand full hydrostatic pressure exerted on the convex side of the cap. If the hydrostatic pressure is exerted on both sides, the double-capped version of the plug is used.

### Filling adjacent to, within and between compartment plugs

Void spaces within and around the compartment plugs will be filled to avoid the presence of large void spaces within the drift that could eventually lead to a loss in buffer density. Spaces to be filled are:

- the space between the compartment plugs and the adjacent distance blocks;
- the space between the concave surfaces of the compartment plugs; and
- the drift section unsuitable for distance blocks and supercontainer emplacement that is sealed off by compartment plugs.

The design of filling components has not yet been finalised. In the current reference design, cylindrical transition blocks are placed between the compartment plugs and the adjacent distance blocks. The transition blocks are similar to the “loose” component of the distance blocks. The remaining void space next to the convex surfaces of the plugs will be filled with MX-80 bentonite pellets or sand (Figure 2-11). The space between the concave surfaces of the compartment plugs will also be filled with sand, according to preliminary considerations.

As described in Section 2.3.7, after the filling of a compartment and the installation of compartment plugs, operations may be interrupted to monitor the development of hydraulic pressure in the sealed compartment. The high-inflow drift section (leakage > 1 litre per minute) enclosed by compartment plugs will be backfilled and drained during this period. No detailed design has as yet been developed for the backfill between the plugs in the enclosed high-inflow section. One tentative possibility is illustrated in Figure 2-12.

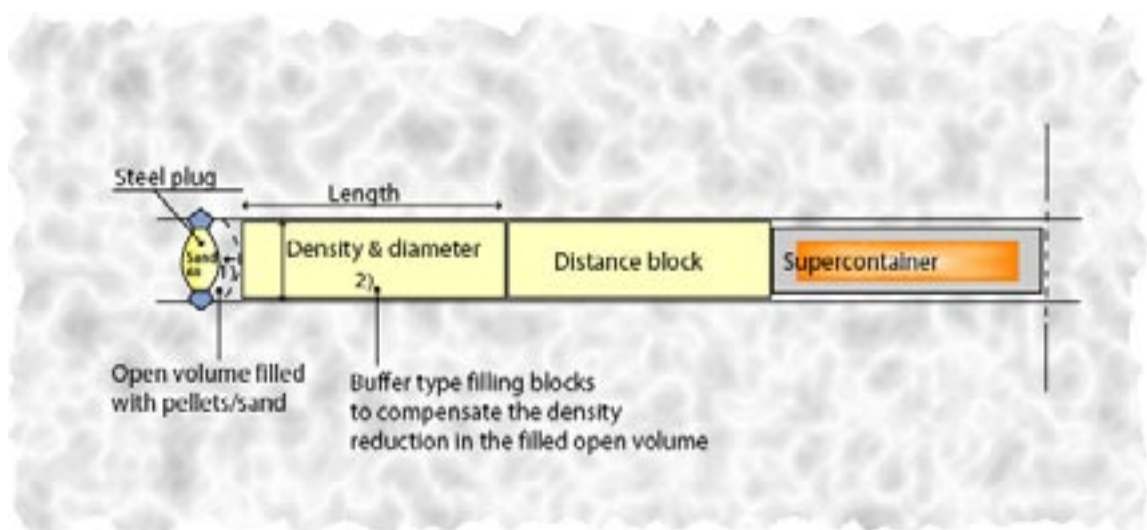


**Figure 2-11.** Filling adjacent to and within compartment plugs (after Figure 5-12 of /Autio et al. 2007/).

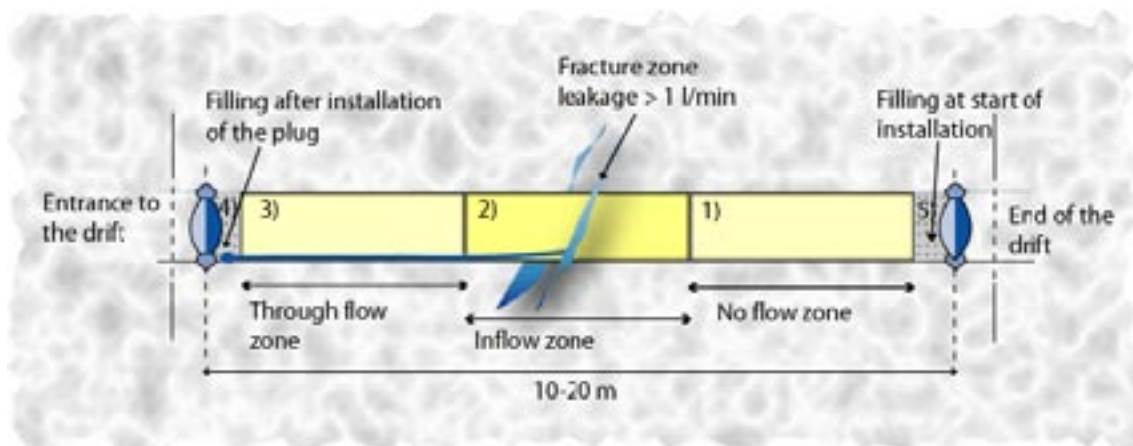


**Figure 2-12.** Filling between steel compartment plugs (after Figure 5-14 of /Autio et al. 2007/). The design of filling components between the steel plugs will be presented in the coming Design Description 2007 /Autio et al. 2008/.

In this possible design, the inflow zone is filled with a permeable material, such as crushed rock, which is graded to prevent the bentonite used to fill the “no-flow zone” and the “through-flow zone” from swelling into interstitial spaces. It should be noted that, in the term “through flow zone”, “through-flow” refers to flow along the floor of the drift prior to installation of the plug nearest to the entrance to the drift. Once the plug is installed and the bentonite saturates, the only long-term flow will be into and out of the fracture zone.

### **Spray and drip shields**

The possibility of erosion of bentonite due to the spraying, dripping and squirting of water from the drift walls onto the distance blocks and supercontainers will be prevented by placing thin steel spray and drip shields over inflow points (Section 4.2.2 of /Autio et al. 2007/). It is anticipated that four to five drip and spray shields will be used in each drift. These shields will be left in place after plugging the drift.

### **Drift end plugs**

Drift end plugs are placed at the ends of the drifts at their intersection with the deposition niche (Figure 2-4). The reference design for the drift end plugs is a steel-reinforced low-pH concrete bulkhead positioned in a notch (Figure 4-6 of /Autio et al. 2007/). A steel plug similar to the single-cap compartment plug is installed first, where necessary, to provide rapid sealing while the concrete structure is emplaced and hardens. It is also likely that one or more filling blocks is/are installed in the drift adjacent to the drift end plugs, to isolate the canisters and their surrounding buffer from any leachates from the concrete bulkhead (see Section 5.6.5). The detailed composition of the concrete is yet to be developed, but one example of a possible composition is given in Table 4-3 of /Autio et al. 2007/.

### **The backfill and seals of other repository cavities**

The backfilling and sealing of other repository cavities (e.g. deposition niche, central tunnel, shafts, characterisation boreholes) with impermeable material is required to prevent the formation of water-conductive flow paths. It is also required to keep the drift end plug in place once the backfill has reached the desired swelling pressure. Backfilling and sealing materials and methods are likely to be similar to those envisioned for the KBS-3V design, as outlined below.

The current candidate backfill materials are Friedland clay and/or a mixture of bentonite (MX-80) and crushed rock (30% bentonite and 70% crushed rock or 15% bentonite 85% crushed rock, depending on the backfill location). Friedland clay and bentonite/crushed rock



mixtures both carry impurities into the repository, such as organic carbon, pyrite and gypsum, which may have long-term safety implications (Section 4.2.5).

The design of plugs for sealing boreholes, shafts and other access routes to the surface is ongoing for the KBS-3V design. The current plan is to employ a combination of bentonite and cementitious material for the different types of plugs to be emplaced at different places (e.g. characterisation boreholes, shafts). The same type of plugs are expected to be used in KBS-3H.

### **2.3.5 Use of cement and other construction materials**

Cement and other construction materials are being used in the construction of ONKALO and will be used in the construction and operation of a repository, whether based on KBS-3V or on KBS-3H. The purposes of such materials include limitation of groundwater inflow (grouting), stabilisation of the rock (shotcrete, castings of rock bolts), construction of various plugs and seals, and use in temporary structures required for construction and for operational safety purposes (floors, supporting walls etc).

Detailed descriptions and inventories of cement and other construction materials are presented in /Hagros 2007ab/. Grouting materials considered for both the KBS-3H and KBS-3V designs in various parts of the repository include:

- ordinary cement;
- low-pH cement; and
- Silica Sol (colloidal silica).

High alkalinity materials, such as Ordinary Portland Cement, are not envisaged in the deposition drift. The composition of the low-pH cement and Silica Sol considered for grouting in the current reference design are given in Appendix A of /Gribi et al. 2007/.

Shotcreting is not envisaged in the deposition drifts, although other parts of the repository, including the deposition niches, which have a larger diameter and height than the rest of the deposition drifts (Figure 2-5), may require support by shotcreting /Hagros 2007b/. As in the KBS-3V case, ordinary and low-pH cement are both considered as shotcreting materials. The detailed composition of shotcrete in both designs is described in /Hagros 2007a/.

Shotcrete and other temporary structures made from cementitious materials will be removed as far as possible before the final closure of the repository but, according to the estimates of residual materials in the KBS-3H repository, between 1,200,000 and 1,800,000 kg<sup>11</sup> of cement will be left in the repository (including ONKALO). Of these, an average of 2,600 to 3,900 kg of cement will be located in each drift /Hagros 2007a/.

Cement has the potential to interact with the host rock and with the bentonite buffer. Furthermore, additives, such as accelerators (i.e. inorganic salts) and superplasticisers (i.e. organic substances), also have the potential to perturb the safety functions of the repository. The impact of cement and stray materials on the repository safety functions is discussed in Section 5.6.5. A joint (Nagra, NUMO, Posiva and SKB) study on the potential effect of organic cement additives on the sorption of radionuclides on rock is ongoing.

### **2.3.6 Use of steel**

A key difference between KBS-3V and KBS-3H is the use, in KBS-3H, of additional steel components external to the canisters that will corrode and generate gases. As part of the safety case, the overall effect of these steel components thus needs to be evaluated with respect to corrosion, gas formation, the potential for the creation of gas overpressures, and the chemical interaction with, and consequences for, the bentonite buffer.

---

<sup>11</sup> Estimates depend on the alternatives for design, rock support, grouting, backfill and drift end plug.

The uncertainties discussed in Chapter 5 associated with gas production and pressure development arising from the corrosion of steel, and with the interaction of steel corrosion products with the buffer, give some incentive to minimise the volume of steel used in the repository. Amounts of steel in a repository constructed according to the current reference design are shown in Table 2-1.

### 2.3.7 Operational procedure for implementing the current reference design

The operational procedure for implementing the current reference design is given in Box 2-1. Assuming that a drift is divided into two compartments of similar length, the period required to emplace supercontainers, distance blocks and a compartment plug in the first compartment is in the order of 10–14 days, depending on the length and capacity of the compartment and, to some extent, on the requirement for fixing rings, as described in /Autio et al. 2007/. After the filling of this compartment, it may be necessary to interrupt operations and monitor the development of groundwater pressure for, say, a further week before proceeding with the installation of filling material and a second compartment plug to isolate the drift section considered unsuitable for supercontainer and distance block (or filling block) emplacement. This is likely to require in the order of another week. Finally another 10–14 days will be required to emplace supercontainers, distance blocks and a drift end plug in the second compartment, giving an overall operational period for a drift in the order of about 6 weeks (the drift end plug will require time to harden, but, as noted in Section 2.3.4, there is a steel plug next to the end plug to enable rapid sealing if needed).

The operational procedure for the DAWE alternative design is described in Appendix D of the Process Report /Gribi et al. 2007/. Operational risks, such as fires, rock falling, sudden water inflow during the operational period are being addressed in the coming report Design Description 2007 /Autio et al. 2008/.

### 2.3.8 Possible deviations from planned operations and relevance to system evolution

The feasibility of implementing the Basic Design without significant safety-relevant deviations is assumed, although several design issues remain to be addressed, as discussed in Section 12.2. The feasibility of implementing the chosen design must be justified as part of any future safety case. Feasibility issues are discussed in the Design Description 2007 report /Autio et al. 2008/.

Sections 4.7.1 and 5.5.1 of /Autio et al. 2007/ list a number of possible deviations from planned operations (for both the current reference design and for the DAWE design alternative). All of these can be addressed by remedial measures of some kind, including the disassembly and replacement of defective components or the reversal and repetition of supercontainer and distance block emplacement steps. The operational period would become longer, but provided it remained in the order of a couple of months, the effects on longer-term repository evolution are expected to be minor. If deviations from planned operations result in longer delays, recent buffer tests /Sandén et al. 2007/ indicate that the humidity-induced cracking of the distance blocks could occur (experimental studies have shown humidity-induced cracking after about 3 months for bentonite with an initial water content of 10% – see Appendix L of /Autio et al. 2007/).

**Table 2-1. Steel components and masses in a KBS-3H repository at Olkiluoto (data from /Hagros 2007a/).**

Steel component	Mass (whole repository) [kg]
Supercontainer shells (incl. feet)	3,041,640 (1,071 kg per supercontainer)
Compartment plugs	872,100 (5,100 kg per set of 2 plugs)
Steel plug (adjacent to drift end plug)	360,810 (2,110 kg per plug)
Fixing rings (4.5 per drift assumed)	461,700 (600 kg per ring)
Spray and drip shields (4.5 per drift assumed)	462 (0.6 kg per shield)

**Box 2-1** *The operational procedure for implementing the current reference design in a single compartment*

- Planning of drift specific implementation and definition of positions for design components (e.g. supercontainers, distance blocks, fixing rings, filling blocks, compartment plugs). The positions of compartment borders and of each component are determined before operation starts.
- Preparatory rock works (e.g. installation of drip shields, excavation of grooves and notches). Preparation of positions for steel plugs and fixing rings.
- Installation of attachments to steel structures (mainly plugs and fixing rings).
- Emplacement of distance blocks, supercontainers and other design components to one compartment. The estimated longest time for this step without attachment of fixing rings is around 10 days. Installation of two fixing rings would increase the operation time to approximately 14 days.
- The compartment plug is installed. The estimated longest time for this is one day.
- The free space behind the plug is filled (see Figure 2-11).
- An option currently kept open is to fill the free gap and adjacent open volume with water to speed up the saturation in proximity to the plug.
- When the drift is plugged and sealed the deposition operation of the compartment is completed.

The impact that this would have on continued operations and on long-term safety is again likely to be minor, but requires further investigation. Some bentonite fragments could fall through the holes in the supercontainer walls. This is unimportant in the case of the current reference design, but could be more problematic in the case of DAWE (Appendix A). It is also conceivable that a) cracking of distance block next to fixing rings may cause reduction in strength followed by movement of the distance block, or that b) plastic deformation of distance block could occur, so that it could start to be extruded through the centre hole in fixing ring. It is expected that these potential problems can be solved by design if found to be critical. The possibility to precision handle thousands of large bentonite blocks will be discussed in the Design Description 2007 report /Autio et al. 2008/.

## **2.4 Safety functions and how they are provided in the current design**

### **2.4.1 Safety functions in KBS-3H**

The canister, the buffer (i.e. the bentonite material originally inside the supercontainers, together with the distance blocks) and the host rock are the main KBS-3H system components that together ensure isolation of the spent fuel and containment of radionuclides according to the safety concept shown in Figure 1-3. Other system components, including the filling blocks, the compartment and drift end plugs, the steel supercontainer shells, fixing rings and other structural materials, have not been assigned safety functions. They are, however, designed to be compatible with, and support the safety functions of, the canister, the buffer and the host rock.

The safety function on the canister is common to the KBS-3V. The main safety function of the canisters is to ensure a prolonged period of complete containment of the spent fuel as in the case of KBS-3V (see Figure 1-3). As long as its copper shell is not breached, a canister will provide complete containment of radionuclides, and the spent fuel will interact with the environment only by means of heat generation and low level gamma and neutron radiation penetrating through the canister walls.

Safety functions of the buffer are (a), protection of the canisters, and (b), limitation and retardation of radionuclide releases in the event of canister failure. These safety functions are also common for KBS-3V and KBS-3H. The current KBS-3H design includes the use of steel components external to the canisters that will corrode over time and give rise to potentially porous or fractured corrosion products (Section 5.6.4). These may interact chemically with adjacent bentonite and the slow formation of an altered zone with perturbed mass-transport properties at the bentonite/rock interface at supercontainer locations cannot be excluded (Section 6.5.3). A final safety function of the KBS-3H buffer (or, more specifically, the distance blocks) is, therefore, (c), to separate the supercontainers hydraulically one from another, thus preventing the possibility of preferential pathways for flow and advective transport within the drifts through the corrosion products or altered buffer.

The safety functions of the host rock are again the same as for the KBS-3V. They are (a), to isolate the spent fuel from the biosphere, (b), to provide favourable and predictable mechanical, geochemical and hydrogeological conditions for the engineered barriers, protecting them from potentially detrimental processes taking place above and near the ground surface, and (c), to limit and retard both the inflow of harmful substances<sup>12</sup> to the engineered barrier system and radionuclide releases to the biosphere.

## 2.4.2 Design requirements to support the safety functions

### *Design requirements related to mutual compatibility of the system components*

A requirement common to all engineered system components, including not only the canister and the buffer, but also the filling blocks, the compartment and drift end plugs, the steel supercontainers shells and other structural materials, is that they should be mutually compatible. Although all components will inevitably undergo physical and chemical changes over time (e.g. due to chemical alteration or corrosion, saturation, swelling), none should evolve in such a way as to significantly undermine either the long-term safety functions or the design functions of the others. Thus:

- no component should contain any chemical constituents that lead to significant negative effects on the performance of the others;
- no component should generate gases at rates that could lead to a build-up of potentially damaging gas pressure (taking into account the gas permeability of the other components);
- no component should give rise to mechanical stresses that could lead to significant damage to the canisters or host rock; and
- no component should undergo volume changes (due, e.g. to swelling, compaction, corrosion or alteration) that could lead to significant changes in density of the adjacent buffer.

The degree to which the current reference design meets these requirements is discussed in various places throughout this report. In particular:

- the significance of interactions of iron and cement with the buffer and (in the case of cement) the host rock is discussed in Sections 5.6.4 and 6.5.3 (iron) and 5.6.5 (cement);
- the issue of gas generation and pressurisation is discussed in Section 5.5;
- the potential for buffer swelling pressure and gas pressure to damage the rock is discussed in Section 5.4.5; and
- the stability of the canister under isostatic loading is discussed in Section 5.4.3.

Scoping calculations of potential buffer density changes during the early phase of evolution are discussed in Section 5.5 (and described in detail in Appendix B.4). The range of densities compatible with the buffer fulfilling its safety functions taking into account the evolution of groundwater and buffer porewater salinity (1,890 to 2,050 kg m<sup>-3</sup>) is discussed in Section 5.3.2.

---

<sup>12</sup> Including the chemically toxic components of spent fuel, as discussed in the Complementary Evaluations of Safety Report /Neill et al. 2007/.

The following sections describe design requirements over and above the general requirement of mutual compatibility, which are intended to support the safety functions, and indicate how they are met in the current design.

### ***Design requirements to support the safety function of the canister***

The requirements on the canister are common to KBS-3V and KBS-3H. The canisters have a design lifetime of at least 100,000 years. This means that the canisters are designed to maintain their integrity taking into account the processes and events that are considered likely to take place in the repository over a design basis period of 100,000 years. It does not exclude the possibility that canister integrity will be retained significantly beyond the design basis period, nor that (less likely) extreme conditions will give rise to earlier canister failures, and these possibilities must be considered in the safety assessment. The terminology is similar to that used in the reactor safety area: a design basis is defined to reflect the most likely conditions for the system but the safety assessment must address less likely situations as well.

In order to achieve its minimum design lifetime, canisters are required to have:

1. a low probability of occurrence of initial penetrating defects;
2. corrosion resistance; and
3. mechanical strength.

The probability of occurrence of initial penetrating defects is still under investigation. In the current design, corrosion resistance is provided by the copper canister shell, and mechanical strength primarily by the cast iron insert.

The minimum design lifetime also implies a number of design requirements on repository layout (avoidance of fractures that may undergo shear movements that could damage the canisters – Section 2.2.7) and the buffer.

If the copper shell is breached, then a canister is considered to have failed, even though it may continue to offer some resistance to the ingress of water and the release of radionuclides for a significant period thereafter (Chapter 8).

### ***Design requirements to support the safety functions of the buffer***

The first safety function of the buffer (a, above in Section 2.4.1) is to protect the canisters from external processes that could compromise their safety function of the complete containment of the spent fuel. Corresponding design requirements on the buffer are that it should be:

- sufficiently plastic (or ductile) to protect the canister from small rock movements, including shear displacements smaller than 10 cm at canister locations (the issue of potential larger shear movements caused by large earthquakes is discussed in Section 7.4.5);
- sufficiently stiff to support the weight of the canisters and maintain their central vertical positions in the drift in the long term;
- sufficiently dense that microbes are metabolically barely active in the buffer and thus do not give rise to unfavourable chemical conditions at the canister surface; and
- sufficiently impermeable, once saturated, that the movement of water is insignificant and diffusion is the dominant transport mechanism for corrosive agents present in the ground-water that may reduce the lifetime of the canisters.

A further safety function of the buffer (b, above in Section 2.4.1) is to limit and retard the release of any radionuclides from the canisters, should any be damaged. This implies design requirements that the buffer be:

- again sufficiently impermeable, once saturated, that the movement of water is insignificant and diffusion is the dominant radionuclide transport mechanism;



and have:

- a sufficiently fine pore structure such that microbes and colloids are immobile (filtered) and microbe- or colloid-facilitated radionuclide transport will not occur.

It also implies a self-healing capability of the buffer, which means that any potential advective pathways for flow and transport that may arise, for example, as a result of piping and erosion, sudden rock movements or the release of gas formed in a damaged canister are rapidly closed.

These safety functions are common to KBS-3V and KBS-3H. In addition, for the KBS-3H design the final safety function of the buffer (c, Section 2.4.1) is to separate the supercontainers hydraulically one from another. This implies a design requirement that the buffer should provide:

- tight interfaces with the host rock within a reasonable time.

Competing requirements on buffer density are balanced in the design process. For example, excessive density would lead to a correspondingly high swelling pressure and to a risk of damage to the rock. It would also offer less protection of the canisters from rock movements. On the other hand, insufficient density would lead to the possibility of colloid-facilitated radionuclide transport. The choice of MX-80 bentonite as a buffer material with a design target for saturated density of  $2,000 \text{ kg m}^{-3}$  (Section 2.3.4) is made with a view to balancing these various requirements.

The filling blocks are not considered part of the buffer and are not assigned any long-term safety functions – i.e. they are not required to contribute directly to the isolation of the spent fuel and containment of radionuclides. On the other hand, in the current design, they have the same properties as the buffer as they are likely, in practice, to contribute to the limitation and retardation of the release of any radionuclides from the canisters, should any canisters be damaged.

During the saturation of the repository, high hydraulic pressure gradients and gradients in buffer swelling pressure may develop along the drifts, which could potentially lead to phenomena such as piping and erosion of the buffer and displacement of the distance blocks and supercontainers (Section 5.5.6). The distance blocks and filling blocks, together with the compartment and drift end plugs, have the important design function of keeping the adjoining buffer in place, and not allowing any significant loss or redistribution of buffer mass by piping and erosion during the operational period and subsequent period of buffer saturation. The fixing rings also have the short-term safety-related design function of preventing displacement of a distance block while the adjoining components are installed. The distance blocks and filling blocks have a low hydraulic conductivity at saturation and will develop swelling pressure against the drift wall, such that friction will resist buffer displacement. Furthermore, each compartment plug is designed to stay in place under the applied loads (i.e. no significant displacement are allowed) until the next compartment is filled and a further compartment plug or drift end plug installed. Likewise, the drift end plug is designed to stay in place under the applied loads (no significant displacement allowed) until the adjoining transport tunnels are backfilled.

The temperature of the buffer is kept below  $100^\circ\text{C}$  to avoid significant chemical alteration of the buffer that could undermine its ability to satisfy the above requirements. This in turn imposes requirements on buffer layout and dimensioning (Section 2.2.7).

### ***Design requirements to support the safety functions of the host rock***

Unlike the engineered components of the repository, the implementer has no control over the undisturbed properties of the host rock, except in as far as by grouting of intersecting transmissive fractures during construction to avoid drawdown of surface waters and upconing of saline groundwaters, and by adaption of the depth and layout of the repository, for example, to avoid unacceptable features (Section 2.2.7). It should be noted, however, that grouting also affects the rock mass properties (Section 2.3.3). Furthermore it should be noted, however, that backfilling

and sealing of the repository cavities support the safety functions of the host rock, being carried out with the main purpose of preventing the formation of water conductive flow paths, and making the inadvertent human intrusion to the repository more difficult. Requirements on the host rock related to site selection are similar to those for the KBS-3V design and will not be further discussed here.

### ***Design requirements related to the issue of repository-generated gas***

The repository must be designed so as to avoid the build-up of potentially damaging pressures due to repository-generated hydrogen gas formed due to corrosion of supercontainer steel shell and structural components in the drift, and after canister failure also corrosion gases formed due to corrosion of the cast iron insert. This does not imply that the drifts and access tunnels need to be gas permeable, provided gas can escape to from the drift by other routes, e.g. via transmissive fractures in the rock. The issue of gas pressurisation in the repository near field is discussed in Section 5.5.

## **2.5 Safety function indicators and criteria**

### **2.5.1 Use of safety function indicators and criteria in safety assessment**

To assess the performance and safety of a KBS-3H or KBS-3V repository, it is necessary to determine the conditions under which the identified safety functions will operate as intended, and the conditions under which they will fail, or operate with reduced effectiveness. Following the methodology adopted in the Swedish SR-Can safety assessment /SKB 2006a/, KBS-3H safety studies make use of the concept of safety function indicators and associated criteria. One or more safety function indicators are assigned to each safety function. A safety function indicator is a measurable or calculable property of the system that is critical to a safety function being fulfilled. If the safety function indicators fulfil certain criteria, then the safety functions can be assumed to be provided. If, however, plausible situations can be identified where the criteria for one or more safety function indicators are not fulfilled, then the consequences of loss or degraded performance of the corresponding safety function should be evaluated in the safety assessment.

It is important to distinguish design requirements, as discussed in Section 2.4.2, from the criteria for safety function indicators. In general, design requirements refer to attributes that the repository is ensured to have by design at the time of emplacement of the first canister, or during the early evolution of the repository in the period leading up to saturation, although some design requirements also affect the long-term evolution of the system. Repository design also aims to ensure that the criteria for the safety function indicators are fulfilled over the required time frames, but this is seen as a target, rather than as a design requirement.

Adherence to design requirements is primarily the concern of design studies, whereas safety studies focus more on the fulfilment of safety function indicator criteria, taking into account the associated uncertainties. It is emphasised that, if there are plausible situations where one or more criteria for safety function indicators are not satisfied, this does not imply that the system as a whole is unsafe. Such situations must, however, be carefully analysed, for example by means of radionuclide release and transport calculations, as described in the Radionuclide Transport Report /Smith et al. 2007a/.

### **2.5.2 Safety function indicators and criteria for the canisters**

Four fundamental modes have been identified by which, in principle, one or more canisters could fail to provide their safety function of complete containment of the spent fuel and associated radionuclides /SKB 2006a/: i) initial, penetrating defects, ii) failure due to corrosion of

copper shell, iii) rupture due to rock shear and the transfer of shear stresses from the rock via the buffer to the canister (in particular, in the event of a large earthquake), and iv) collapse due to isostatic loading. The probability of initial penetrating defects for the Finnish and Swedish canister designs is discussed in Section 4.2.2. The slow corrosion of the copper shell in the various phases of system evolution is described in Sections 5.7.4, 6.5.1 and 7.4.3. The mechanical strength of the canisters, which must be such as to allow them to withstand that isostatic pressures and shear stresses to which they will be exposed over time, is discussed in /Raiko 2005/.

Safety function indicators for the canister are (i), minimum copper thickness – failure occurs if this is zero at any point on the canister surface, due to the presence of an initial defect that penetrates the entire thickness of the shell or due to localised and general corrosion processes leading to the gradual thinning of the shell, (ii), the isostatic pressure on the canister – failure occurs if this exceeds the isostatic pressure for collapse, and (iii), the shear stress on the canister – failure occurs if this exceeds the rupture limit. The canister safety function indicators and associated criteria, as presented in SR-Can /SKB 2006a/, are summarised in Table 2-2.

### **2.5.3 Safety function indicators and criteria for the buffer**

Three broad modes can be envisaged by which the bentonite buffer could conceivably cease to perform its safety functions fully: loss or redistribution of buffer mass, mineral alteration of the buffer, freezing of the buffer.

#### **1. Loss or redistribution of buffer mass**

The loss or redistribution of buffer mass due, for example, to piping and erosion by flowing water could in principle lead to:

- a loss of swelling pressure at the drift wall, which could, if sufficiently large, lead to a loss of tightness of the contact between the buffer and the rock, and, in turn, enhance the transfer of mass (dissolved corrosive agents – especially sulphide – and radionuclides) between the rock and the buffer and thus compromise or reduce the ability of the buffer to perform any of its three safety functions;
- a loss of swelling pressure at the drift wall, which could also lead to enhanced thermal spalling due to reduction in confining pressure associated with time-dependent degradation of rock strength;
- a more general loss of swelling pressure, which could, if sufficiently large, lead to increased microbial activity within the buffer, potentially increasing the rate of canister corrosion by reducing dissolved sulphate to sulphide, and, for still larger losses in swelling pressure, the possibility of canister sinking;
- an increase in buffer hydraulic conductivity, which, if sufficiently high, could lead to advective transport of dissolved corrosive agents and radionuclides in the buffer and hence compromise the ability of the buffer to perform any of its three safety functions (note that isolated regions of higher hydraulic conductivity around the canisters would have a less significant affect);
- a reduction in buffer density, which, if sufficiently large, could lead to the possibility of colloid-facilitated radionuclide transport in the buffer and reduce the ability of the buffer to limit and retard radionuclide releases (note again that isolated regions affected in this way would have a less significant affect); and
- an increase in buffer density at some locations along the drift, which, if sufficiently large, could lead to mechanical damage of the rock, and compromise the ability of the buffer to protect the canisters from rock shear movements of less than 10 cm.



## 2. Mineral alteration of the buffer

Mineral alteration of the buffer due, for example, to high temperatures around the canisters or to chemical interactions between the buffer and the steel or cementitious components could in principle lead to:

- a change to a less plastic material, which, if it affects a significant proportion of the buffer between the canisters and the drift wall, could compromise the ability of the buffer to protect the canister from rock movements, including shear displacements at canister locations;
- a loss of swelling pressure, with potential consequences as described above in the context of loss or redistribution of buffer mass; and
- a loss of self-healing capacity, which could lead to fracturing of the buffer and an increase in hydraulic conductivity, again with potential consequences as described above in the context of loss or redistribution of buffer mass.

## 3. Freezing of the buffer

Freezing of the buffer as a result, for example, of the deep penetration of permafrost following a major climate change would, if it were to occur, detrimental changes in buffer properties that could compromise its capacity to protect the canister and to limit and retard radionuclide releases from a failed canister. As noted in Section 12.4.1 of /SKB 2006a/, it is uncertain what transport properties the buffer would have after thawing. According to present knowledge based on past glaciations, the permafrost layer is not expected to reach more than 180 metres below ground at Olkiluoto /Hartikainen 2006/ and is thus not considered as a potential cause of major loss of buffer safety functions in the present study. The possibility that conditions at Olkiluoto could in the future differ significantly compared with those during the past glaciations and lead to buffer freezing may, however, require further consideration in future studies.

Consideration of these three possible modes for loss or degradation of the buffer safety functions leads to the safety function indicators and associated criteria that are summarised in Table 2-3. Most are taken directly from SR-Can. However, the criterion that there is a negligible impact on the rheological and hydraulic properties of the buffer due to mineral alteration replaces the SR-Can criterion for a Swedish KBS-3V repository that buffer temperature remains below 100°C. The potential chemical processes that may occur at elevated temperature are, for example, silica dissolution close to the canister followed by transport outwards by diffusion to colder parts and precipitation, as well as buffer cementation due to the dissolution, transport and precipitation of silica or aluminosilicate minerals. But neither experimental nor natural analogue studies have shown that these processes will actually occur. The effect of buffer cementation due to silica precipitation is, however, an issue for further work. The present criterion also takes account of the concern that the buffer of a KBS-3H repository may be more affected by certain chemical interactions, and particularly those between the corrosion products of steel components external to the canisters and bentonite (see Sections 5.6.4 and 6.5.3) and those between cementitious materials and bentonite (see Section 5.6.5), than is the case for a KBS-3V repository.

**Table 2-2. Safety function indicators and criteria for the canister (after Figure 7-2 of /SKB 2006a/).**

Safety function indicator	Criterion	Rationale
Minimum copper thickness	> 0 mm	Zero copper thickness anywhere on the copper surface would allow relatively rapid water ingress to the canister interior and radionuclide release
Isostatic pressure on canister	< pressure for isostatic collapse (varies between canisters, but probability of collapse at 44 MPa is vanishingly small)	An isostatic pressure on the canister greater than 44 MPa would imply a more significant possibility of failure due to isostatic collapse (see Section 7.4.4)
Shear stress on canister	< rupture limit	A shear stress on the canister greater than the rupture limit would imply failure due to rupture

**Table 2-3. Safety function indicators and criteria for the buffer (adapted for KBS-3H from Figure 7-2 of /SKB 2006a/).**

Safety function indicator	Criterion	Rationale
Bulk hydraulic conductivity	$< 10^{-12} \text{ m s}^{-1}$	Avoid advective transport in buffer
Swelling pressure at drift wall	$> 1 \text{ MPa}$	Ensure tightness, self sealing
Swelling pressure in bulk of buffer	$> 2 \text{ MPa}$	Prevent significant microbial activity
	$> 0.2 \text{ MPa}^1$	Prevent canister sinking
Saturated density	$> 1,650 \text{ kg m}^{-3}$	Prevent colloid-facilitated radionuclide transport
	$< 2,050 \text{ kg m}^{-3}$	Ensure protection of canister against rock shear
Mineralogical composition	No changes resulting in significant perturbations to the rheological and hydraulic properties of the buffer (e.g. from iron or cement interaction or related to temperature)	See main text
Minimum buffer temperature	$> -5^\circ\text{C}$	Avoid freezing

<sup>1</sup> Although developed for KBS-3V, this criterion is also expected to be applicable to KBS-3H, and is likely to be more conservative for this alternative since, in KBS-3H, the weight of the canister is distributed over a larger horizontal area compared with KBS-3V.

#### 2.5.4 Safety function indicators and criteria for the host rock

Loss or degradation of the isolation function of the host rock would occur if the Precambrian Shield were to erode away sufficiently to expose the repository at the surface (this situation, which concerns the farthest future, is discussed in Chapter 9). Loss or degradation of the protective function of the host rock could occur if chemical conditions in the groundwater become unfavourable to buffer and canister longevity, or if a fracture intersecting the deposition drifts near a canister location were to slip sufficiently to cause rupturing of the canister. Finally, there are several rock properties that can favour its performance as a radionuclide transport barrier (for example, absence or low frequency of highly transmissive fractures, low hydraulic gradient, mineralogical and geochemical characteristics giving high retention by sorption). Some of these may vary over time (especially geochemical characteristics), potentially leading to some degradation of the host rock as a transport barrier.

The host rock safety function indicators and associated criteria, as presented in SR-Can, are summarised in Table 2-4.

**Table 2-4. Safety function indicators and criteria for the host rock (adapted for KBS-3H from Figure 7-2 of /SKB 2006a/).**

Safety function indicator	Criterion	Rationale
Redox conditions	No dissolved oxygen	The presence of measurable $\text{O}_2$ would imply oxidising conditions
Minimum ionic strength	Total divalent cation concentration $> 10^{-3} \text{ M}$	Avoid buffer erosion
Maximum chloride concentration or minimum pH	$\text{pH}^{\text{GW}} > 4$ or $[\text{Cl}^-]^{\text{GW}} < 3 \text{ M}$	Avoid chloride corrosion of canister
Limited alkalinity	$\text{pH}^{\text{GW}} < 11$	Avoid dissolution of buffer smectite
Limited salinity (expressed in terms of total dissolved solids, TDS)	$[\text{NaCl}] < 100 \text{ g/l}$ (or other compositions of equivalent ionic strength)	Avoid detrimental effects, in particular on swelling pressure of buffer and distance block
Limited concentration of detrimental agents for buffer, distance block and canister	Applies to $\text{HS}^-$ , $\text{K}^+$ and $\text{Fe(II)/Fe(III)}$ . The lower the better (no quantitative criterion)	Avoid canister corrosion by sulphide, avoid illitisation ( $\text{K}^+$ ) and chloritisation ( $\text{Fe}$ ) of buffer and distance block
Limited rock shear at canister/distance block locations in deposition drift	$< 10 \text{ cm}$	Avoid canister failure due to rock shear in deposition drift

### 3 Comparison of KBS-3V and KBS-3H

A comparison of the features, events and processes (FEPs) relevant to KBS-3H and KBS-3V is reported in /Johnson et al. 2005/. The Swedish Nuclear Power Inspectorate (SKI) also carried out a comparison of the alternatives /Bennett and Hicks 2005/.

In /Johnson et al. 2005/, FEPs that have different significance to, or potential impact on, KBS-3H compared with KBS-3V were identified as those related to gas issues, to the evolution of steel components external to the canisters, and to the distance blocks.

SKI noted that key technical issues for KBS-3H are associated with:

1. the accuracy of deposition drift construction;
2. water inflow to the deposition drifts from fractures in the host rock and the ability to seal such fractures;
3. the ability of the buffer to seal the deposition drifts;
4. piping and erosion of the buffer;
5. steel corrosion and interactions of corrosion products with bentonite;
6. evolution of processes and materials within failed canisters; and
7. gas generation and flow.

Of these, the most important were identified by SKI as probably the interrelated issues of water inflow from fractures and buffer performance (Issues 2, 3 and 4), and the evolution of processes and materials within failed canisters (Issue 6). It was noted that, although issues 1 to 7 represent potentially important uncertainties for the KBS-3H repository design, the most important issues (Issues 2, 3, 4, 6) also apply to some extent to the KBS-3V design. It was further noted that there are also issues and uncertainties specific to the KBS-3V design, such as the ability of the backfill to achieve its performance requirements in that system.

A systematic difference analysis of KBS-3V and KBS-3H is described in the Process Report /Gribi et al. 2007/. The principal objective of this analysis is to identify issues relevant to KBS-3H that may have been missing or differently treated in previous studies of KBS-3V and need to be specifically addressed in the analysis of KBS-3H. The analysis is based on the Olkiluoto site, although the main outcomes may also be applicable to other repository sites for spent fuel in crystalline rock.

For many aspects of the two alternatives, the processes to be considered and their expected impacts on the systems are similar or identical. In a few instances, however, major differences are identified. These are shown in Table 3-1, which also indicates where in the present report the impact of these major differences in terms of system evolution are discussed.

**Table 3-1. Major differences identified in the difference analysis of safety-relevant features and processes in KBS-3V and KBS-3H.**

System components/ (groups of) processes	KBS-3V	KBS-3H	Discussion of impact on system evolution in present report
<b>1 Fuel/cavity in canister</b>			
No major differences identified			
<b>2 Cast iron insert/copper canister</b>			
No major differences identified			
<b>3 Buffer/distance block</b>			
Materials, geometry, properties	Major differences related to compartment plugs, distance blocks, etc.		Throughout report.
Piping/erosion by water and gas, chemical erosion	Within deposition hole at buffer/rock interface in the case of high initial inflow rates (however, the holes can be selected individually and those with larger inflows will be rejected). Also, in the longer term, chemical erosion is possible in the event of an influx of glacial meltwater. Loss of buffer around one canister due to piping/erosion or chemical erosion by glacial meltwater will not affect the buffer around neighbouring canisters.	Piping/erosion may affect buffer density at bentonite/rock interface in canister sections with high initial inflow rates and in canister sections adjacent to these; mitigating the effects of piping/erosion is considered to be a major challenge in the design of KBS-3H and has led to the consideration of two candidate designs and various design alternatives. Deposition drift sections with inflows larger than a specified limit are not used for deposition – but sealed tightly. This will affect the utilisation degree of deposition drifts. Design is still under development /Autio et al. 2007/. Chemical erosion is possible in the event of an influx of glacial meltwater. Loss of buffer around one canister due to piping/erosion or chemical erosion by glacial meltwater may affect the buffer around neighbouring canisters, since the buffer density along the drift will tend to homogenise over time.	Discussion of early, transient phase – <b>Section 5.5</b> , and evolution affected by climatic change – <b>Section 7.4.7</b> .
Displacement of buffer/distance block (leading to a reduction in bentonite density)	Swelling of buffer from deposition hole into drift above the hole may lead to lowering of bentonite density; rock stress distribution leads to risk of rock slabs at mouth of deposition hole.	Axial displacement of distance block by hydraulic pressure build-up may lead to lowering of bentonite density and must be counteracted by a rapid emplacement rate and by the use of steel plugs and steel rings bolted to rock, as described in the current reference design /Autio et al. 2007, Börgesson et al. 2005/. Axial displacement due to heterogeneous swelling is limited by friction and by drift end plug.	Discussion of early, transient phase – <b>Section 5.5</b> .

System components/ (groups of) processes	KBS-3V	KBS-3H	Discussion of impact on system evolution in present report
Iron/bentonite interaction	Relevant only for failed canisters.	In addition to the processes relevant to KBS-3V, significant geochemical interactions between supercontainer and buffer will take place (iron/smectite interaction, iron-silicate formation, cation exchange, etc); these processes may affect the buffer density, swelling pressure, hydraulic conductivity and other properties; these effects are locally limited at early times, but may develop with time and affect larger parts of the buffer /Johnson et al. 2005, Carlson et al. 2006, Wersin et al. 2007/.	Discussion of early, transient phase – <b>Section 5.6.</b> Discussion of subsequent evolution prior to next major climate change – <b>Section 6.5.</b> Discussion of canister with initial, penetrating defect – <b>Section 8.5.</b>
Gas transport and possibly gas-induced porewater displacement	Relevant only for failed canisters.	In addition to the processes relevant to KBS-3V, significant gas effects are expected /Johnson et al. 2005/ due to anaerobic corrosion of supercontainer and other steel components (retarded resaturation, air trapping, gas dissolution/diffusion/advection, gas pressure build-up, gas leakage, gas pathways along drifts, etc); during this early phase, no radionuclide transport is expected.	Discussion of early, transient phase – <b>Section 5.5.</b> Discussion of canister with initial, penetrating defect – <b>Sections 8.3–8.6.</b>
Effects of engineering and stray materials	Effects of concrete bottom plate, stray materials, bentonite pellets.	Effects of steel rings, rock bolts, steel feet, water/gas evacuation pipes, grouting, spray and drip shields, cement.	Depending on the types and quantities of these materials, all safety function indicators of buffer may be affected to some extent; under reasonable assumptions (e.g. functioning sealing of pipes), however, all buffer safety function indicator criteria are expected to be met both in KBS-3V and KBS-3H ( <b>Sections 5.6.4 and 5.6.5</b> ).
<b>4 Supercontainer and other structural components within the deposition drifts</b>			
Materials, geometry, properties	N/A		Throughout report.
Steel corrosion and formation of corrosion products	N/A	For the expected steel corrosion rate, complete conversion to oxidised species occurs within a few thousand years.	Discussion of early, transient phase – <b>Section 5.6.</b>
Gas generation by anaerobic corrosion of steel	N/A	Gas generation rates are significant although the overall amount of gas produced is moderate; for the effects of gas, see buffer.	Discussion of early, transient phase – <b>Section 5.5.</b>



System components/ (groups of) processes	KBS-3V	KBS-3H	Discussion of impact on system evolution in present report
Effects of volume expansion (magnetite formation)	N/A	Volume expansion of corrosion products may increase buffer density and swelling pressure.	Discussion of early, transient phase – <b>Section 5.4.</b>
Ion release to bentonite porewater	N/A	Leads to iron/bentonite interaction.	See buffer, above
Effect of supercontainer on water flow paths along the periphery of the drift	N/A	The physical properties of the corroded supercontainer have not been evaluated. Although the porosity and hydraulic conductivity of the corrosion products may be low, the possibility that fracturing could lead to the formation of pathways for water flow and advective transport cannot currently be excluded. Selected radionuclide transport calculation cases cover the case of a disturbed buffer/rock interface due to the presence of iron corrosion products in contact with bentonite.	Consequences for radionuclide transport – <b>Chapter 11.</b>
Displacement of supercontainer/ buffer by swelling of distance blocks	N/A	See buffer.	Discussion of early, transient phase – <b>Section 5.5.</b>
Breaching of supercontainer shells by bentonite swelling	N/A	The supercontainer shell may be breached by the different forces due to bentonite swelling acting inside and outside the supercontainer shell (secondary effect, because the supercontainer has no safety function).	Discussion of early, transient phase – <b>Section 5.4.</b>

##### 5 Deposition drift, central tunnel, access tunnel, shafts, boreholes

A major difference is in the geometry and backfilling of the KBS-3H deposition drifts compared with the KBS-3V deposition tunnels. In KBS-3H, supercontainers are emplaced along relatively narrow deposition drifts, separated by compacted bentonite distance blocks. In KBS-3V, deposition holes are bored from relatively large diameter deposition tunnels, backfilled with swelling clay or clay/crushed rock mixture.

For other underground openings (transport and main drifts, ramp shaft, boreholes) no major differences have been identified.

System components/ (groups of) processes	KBS-3V	KBS-3H	Discussion of impact on system evolution in present report
<b>6 Geosphere</b>			
Gas transport, gas-induced porewater displacement	Relevant only for failed canisters.	<p>Limited storage volume and transport capacity within deposition drift, combined with increased gas generation (rates and total amount).</p> <p>Gas dissolution/diffusion/advection in groundwater, gas pressure build-up, gas-induced porewater displacement, capillary leakage.</p> <p>For tight canister sections: gas transport along drift (EDZ) to the next transmissive fracture, possibly involving reactivation of fractures in near-field rock, when minimal principal stress is exceeded.</p>	<p>Discussion of early, transient phase – <b>Section 5.5.</b></p> <p>Consequences for radionuclide transport – <b>Chapter 11.</b></p>
Transmissive fractures and flow conditions	The selection of deposition hole locations is more flexible than in KBS-3H because rock sections with larger inflows can be rejected.	Local variations in groundwater flow conditions along the drift may lead to variable saturation time for the buffer along the drift (see Figure 10-2).	Consequences for radionuclide transport – <b>Chapter 11.</b>
Mechanical stability of the drift/ tunnel	High stresses at the mouth of deposition holes and at the top of backfill tunnel.	Lower rock stresses than in KBS-3V because the deposition drifts can be better adapted to the stress field.	Potential for rock spalling, hence consequences for radionuclide transport – <b>Chapter 11.</b>
Orientation of fractures	KBS-3V is more sensitive to sub-horizontal than to sub-vertical fractures with respect to potential damage to the engineered barrier system by rock shear.	KBS-3H is more sensitive to sub-vertical fractures with respect to potential damage to the engineered barrier system by rock shear.	Discussion of impact of earthquakes and rock shear on canisters – <b>Section 7.4.5.</b>
<b>7 Biosphere</b>			
No major differences identified			
<b>8 Human activities</b>			
No major differences identified			

## 4 Initial conditions and operational phase

### 4.1 Expected conditions

#### 4.1.1 Impact of repository excavation on the near-field rock

Undisturbed hydrogeological and geochemical conditions at Olkiluoto are summarised in Section 2.2. Excavation of ONKALO and of the repository tunnel and drift system will, however, significantly perturb these conditions, causing a transient drawdown of the water table and an associated reduction in the hydrostatic pressure at repository depth /Pastina and Hellä 2006/. Grouting of fractures in the rock is, however, likely to be used (Section 2.3.3), and this will significantly reduce hydraulic disturbance caused by excavation.

Excavation is also likely to cause a transient increase in the mixing of water types. In particular, there will be mixing of fresh water and brackish, sulphate-rich marine-derived waters from closer to the surface as well as of saline water from greater depths. The mixing of the waters from closer to the surface may induce some changes in pH and Eh of the groundwaters, although buffering by the host rock should prevent significant Eh and pH changes. Preliminary calculations have been carried out based on the estimation of the lifetime of fracture mineral buffers, such as calcite and pyrite in the fractures, against acid pH and oxygen containing infiltrating waters from the surface /Andersson et al. 2007/. Further field studies and more advanced modelling are planned. At the time of emplacement of the first canister, the water is expected to be diluted as compared with the undisturbed conditions prior to excavations. During the operational phase (100 years) the salinity (TDS, total dissolved solids) may rise from a maximum of 12 g per litre at the time of emplacement of the first canister to a maximum of 25 g per litre in the vicinity of the excavations at repository level, about 400 m below ground (and from a maximum of 30 g per litre to a maximum of 47 g per litre at 550 m depth) according to groundwater flow simulations, depending on the extent of fracture grouting used /Vieno 2000, Vieno et al. 2003, Löfman 2005, Pastina and Hellä 2006/. This is due to upconing of deeper, saline waters while the repository is open. Figure 4-1 shows the evolution of the salinity at repository depth (about 400 m below ground) and at 550 m below ground from the beginning of repository operations (2020) until 100,000 years later /Pastina and Hellä 2006/.

Groundwater monitoring will be performed during the construction of ONKALO to better understand these effects (see summary of ongoing and planned activities in /Ahokas et al. 2006/ and /Posiva 2006/). The monitoring results will also be analysed with the site descriptive model and used to verify or, where necessary, update the hydrogeological model, see e.g. Section 9.4 of the Olkiluoto Site Description 2006 /Andersson et al. 2007/.

In addition to these transient hydrogeological and geochemical perturbations, excavation of underground openings will also give rise to irreversible mechanical disturbances and, in particular, to the formation of excavation-damaged zones (EDZs) around the openings. The EDZs around the deposition drifts are potentially of significance to long-term safety because, if sufficiently conductive, they could create additional pathways for groundwater flow along the drifts. EDZ properties are described in Section 4.1.2, below.

#### 4.1.2 The deposition drift

##### **Excavation disturbance**

A description of the expected characteristics of the EDZs adjacent to the deposition drifts of a KBS-3H repository at Olkiluoto, together with associated uncertainties, is given in Appendix D of /Johnson et al. 2005/. A drift excavation technique is being designed that should ensure that the degree of excavation disturbance is small. EDZ properties are, however, subject to considerable uncertainties, being dependent on a variety of rock-specific and site-specific factors as well as on the repository layout (see the discussion in Section 2.4 of /Johnson et al. 2005/).

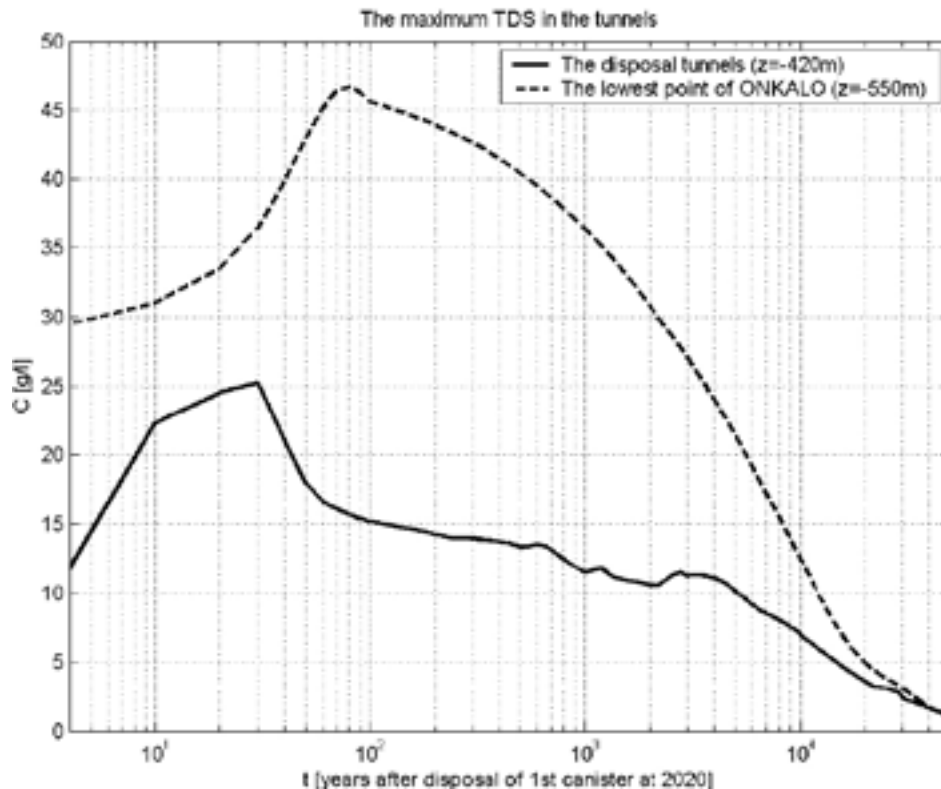


**Figure 4-1.** Evolution of maximum salinity at the repository level (about 400 m below ground, solid line) expected from the beginning of repository operations (2020) onward. The starting salinity takes into account the effect of construction on salinity. The maximum salinity at the lowest point in the ONKALO-repository tunnel system (550 m below ground, dotted line) is also shown for comparison. Salinity is expressed in g per litre of Total Dissolved Solids (TDS). The figure (after Figure 6-19 of /Pastina and Hellä 2006/) was developed for KBS-3V disposal tunnels, but is also expected to be applicable to KBS-3H deposition drifts.

Furthermore, the measurements made so far have been on a limited number of samples taken from the Research Tunnel located in the intermediate and low-level waste repository (the VLJ repository) at Olkiluoto. These may not correspond fully to the properties at repository depth. In particular, measurements of intrinsic gas permeability were based on unfractured samples. Samples containing fractures or microfractures were rejected. Thus, the EDZ is likely, on average, to have a higher intrinsic permeability than suggested by the measured values. Nevertheless, current understanding is that the hydraulic significance of the EDZ is low, as assumed in the radionuclide release calculations described in the Radionuclide Transport Report /Smith et al. 2007a/. The significance of the EDZ with respect to gas pressurisation is discussed in Section 5.5.

### **Drift temperature**

The air temperature in open deposition drift sections will be controlled during operations. Following the sealing of a drift compartment, however, the heat generated by the fuel, the heat-transfer properties of the system components and the ambient rock temperature will determine subsequent temperature evolution. The ambient rock temperature at depths of 400 m and 500 m are 10.5°C and 12°C, respectively /Anttila et al. 1999/. The evolution of temperature in the drift during the operational period and at later times is discussed in Section 5.2.

### **Air humidity**

Water vapour in the air in the deposition drifts will originate from the rock and, during the operational period, from the water cushion system that is proposed for the deposition vehicle /Autio et al. 2007/. The humidity in the deposition drifts is expected to be close to 100% at the start of operations. Although evaporation from wet surfaces within the drift will tend to maintain high levels of humidity, this could be affected during the operational period by design features, such as the use of spray and drip shields, which would cover such surfaces, and will remain in place following sealing of a drift compartment. Humidity could also be reduced as bentonite is emplaced in the drifts and starts to take up moisture from the air. The rate of uptake of moisture by bentonite in an open drift is, however, affected by significant uncertainties (Section 5.5).

### **Water inflow**

As described in Section 2.2, groundwater flow at Olkiluoto is concentrated in transmissive fractures. These are likely to intersect the deposition drifts at irregularly spaced locations, and will lead to water inflow and saturation of the initially air filled voids during the early, transient phase. Some water inflow to the drifts will occur at discrete locations due to intersections with transmissive fractures (or channels within those fractures), while some may be more dispersed by the EDZs surrounding the drifts.

/Hellä et al. 2006/ have generated different realisations of the flow conditions in a deposition drift, based on the available field data. It has been inferred from the simulations and from borehole data that:

- the total leakage into a drift may be up to 10 litres per minute<sup>13</sup>;
- the average frequency with which fractures with transmissivities greater than  $10^{-9} \text{ m}^2 \text{ s}^{-1}$  intersect a drift is 4 per 100 m ( $10^{-9} \text{ m}^2 \text{ s}^{-1}$  is the detection limit – fractures of this transmissivity would be expected each to give rise to an initial inflow of about 0.04 litres per minute into the drift – see, however, the discussion of the relationship between initial inflow and transmissivity in Section 2.2.7);
- the initial inflow into 5 m drift intervals (corresponding to the length of a KBS-3H super-container) is less than 0.1 litres per minute over more than 90% percent of the drift length;
- the initial inflow into 10 m drift intervals (corresponding to the length of a KBS-3H “super-container unit” comprising one supercontainer and one distance block) is less than 0.1 litres per minute (with fracture transmissivities less than  $10^{-8.5} \text{ m}^2 \text{ s}^{-1}$ ) over about 85% percent of the drift length; and
- there are long sections (100 m or more) of the drift that are intersected by no fractures with transmissivities greater than  $10^{-8} \text{ m}^2 \text{ s}^{-1}$ .

The drifts will have a shallow dip of 1.5 to 2 degrees towards the tunnels from which they are bored to provide drainage during the operational period, as illustrated in Figure 2-4. As noted above, spray and drip shields will be used to avoid the possibility of dripping water, which could otherwise damage the engineered barrier system by causing erosion of bentonite /Autio et al. 2007/.

As described in Section 2.3.3, the possibility of controlling water inflow, for example by injecting Silica Sol into transmissive fractures using a Mega-Packer-type grouting device is currently under investigation.

---

<sup>13</sup> From Figures 16 and 17 in /Hellä et al. 2006/. It has, however, been observed at Äspö and in the interim storage facilities for low-level waste at Loviisa and Olkiluoto (VLJ repositories) that inflows have a tendency to decrease over time, possibly due to precipitation in fractures (see, e.g. /Hagros and Öhberg 2007/). See also Section 7.5 in the Process Report /Gribi et al. 2007/.



### 4.1.3 The spent fuel

Spent fuel consists of cylindrical pellets of uranium dioxide, stacked in closed tubes (fuel rods) of zirconium alloy cladding (Zircaloy). Collections of fuel rods are integrated to form fuel assemblies, held together with spacers and plates.

The material compositions of typical Olkiluoto and Loviisa fuel assemblies are presented in Table 4-1 (data from /Anttila 2005a/). Figures and dimensions of the Olkiluoto and Loviisa fuel assemblies are presented in TVO-92 /Vieno et al. 1992/, in TILA-96 /Vieno and Nordman 1996/ and in /Pastina and Hellä 2006/.

Activity inventories, heat production and other radioactive properties of three spent fuel types have been evaluated as functions of cooling time for different burnups, void history, and enrichment /Anttila 2005a/. The three fuel types are VVER-440 PWR fuel from the Loviisa 1 and 2 reactors, BWR fuel from the Olkiluoto 1 and 2 reactors and EPR fuel from Olkiluoto 3. The reference fuel type for the KBS-3H safety case reports is the BWR fuel from Olkiluoto 1–2.

The cladding tubes are expected to limit the migration of water to fuel surfaces and the migration of radionuclides away from these surfaces in the event of canister failure. The majority of the cladding tubes should provide a complete barrier to migration for at least 100,000 years, based on a maximal corrosion rate of 8 nm per year /SKB 2006a/. Damage may, however, occur during handling. Furthermore, if tubes experience high temperatures during dry storage, this will lead to increased gas pressure inside the tubes that can cause immediate failure or, in the longer term, failure by creep (the timescale is uncertain).

Irradiation of the fuel assemblies produces a large number of radionuclides. These radionuclides include those produced by the fission of uranium and plutonium in the fuel pellets (fission products), as well as activation products arising from neutron absorption. The majority of fission products and higher actinides in the fuel exist as a solid solution in the uranium dioxide matrix. However, some of the activation products, such as <sup>14</sup>C and <sup>36</sup>Cl, are present in both the fuel pellets and structural materials. Certain radionuclides are also enriched at grain boundaries in the fuel, at pellet cracks and in the fuel/sheath gap as a result of thermally driven segregation during irradiation of the fuel in the reactor, as illustrated in Figure 4-2.

For the purpose of radionuclide transport calculations, as reported in /Smith et al. 2007a/, the radionuclide inventory is assigned to three characteristic locations in a fuel rod:

- the fuel matrix;
- the grain boundaries and gaps (instant release fraction); and
- structural materials (cladding).

**Table 4-1. Material compositions of the fuel assemblies for each of the spent fuel types at Olkiluoto and Loviisa /after Anttila 2005a/. The reference fuel type for KBS-3H safety studies is the BWR fuel from Olkiluoto 1–2.**

	BWR (Olkiluoto 1–2)	VVER-440 (PWR) (Loviisa 1–2)	EPR (Olkiluoto 3)
	Mass (kg per tonne UO <sub>2</sub> )	Mass (kg per tonne UO <sub>2</sub> )	Mass (kg per tonne UO <sub>2</sub> )
Cladding (Zry-2 in BWR, ZrNb1 in VVER, M5 in EPR)	265	342.62	282.55
Flow channel (Zry-4 in BWR, ZrNb2.5 in VVER)	190	112.31	–
Inconel parts	2.9	–	4.8
Stainless steel parts	53	194.30	50.90

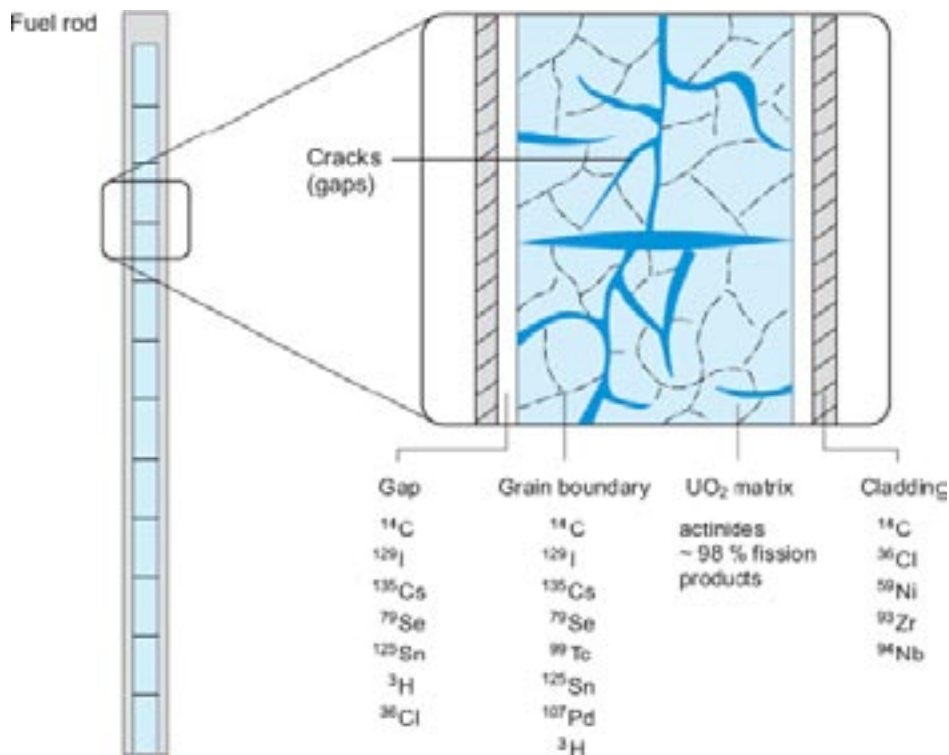


**Figure 4-2.** Schematic illustration of the distribution of radionuclides within a fuel rod (from /Nagra 2002/, based on /Johnson and Tait 1997/).

#### 4.1.4 The canister

The spent fuel assemblies are sealed in copper canisters. The canisters are designed for long-term integrity, i.e. gas and water-tightness, and have a design lifetime of at least 100,000 years (the concept of design lifetime is described in Section 2.4.2).

There are three versions of the canister, one for each reactor type in Finland, the main dimensions and masses of which are given in Table 4-2. The total number of canisters is estimated to be approximately 3,000. For comparison purpose, the total number of canisters for the Swedish spent fuel inventory is about 6,000. The design and dimensioning of the canisters, as well as the manufacturing and encapsulation procedures and quality control, are described in detail by /Raiko 2005/.

The canisters have iron inserts with channels for the fuel assemblies. The canister cavity may initially be filled with air containing a small amount of water vapour (600 g). Alternatively, the air in the canister cavity may be replaced by an inert gas (argon or helium) if this is considered necessary to prevent radiolytic formation of nitric acid from nitrogen and moisture remaining in the canister. Nitric acid could potentially promote stress corrosion cracking /SKB 2004, Raiko 2005/.

Induced fission inside intact canisters is not expected for the entire range of Finnish burnups, due to the lack of any moderator. In particular, no significant amount of liquid water will be present inside the canisters prior to failure. The issue of nuclear criticality in the case of an initial penetrating defect is discussed in Section 8.11 (the discussion also applies to canisters that fail at later times).

#### 4.1.5 Other engineered components

Other components in the current reference design have been described in Section 2.3 of this report. These include the supercontainer, the compartment plugs, the drift end plugs, fixing rings and grout to control water flows.

**Table 4-2. Main dimensions and masses of canisters for different types of spent fuel /after Raiko 2005/.**

	Loviisa 1–2 (VVER-440)	Olkiluoto 1–2 (BWR)	Olkiluoto 3 (EPR)
Outer diameter (m)	1.05	1.05	1.05
Height (m)	3.60	4.80	5.25
Thickness of copper cylinder (mm)	48	48	48
Thickness of copper lid and bottom (mm)	50	50	50
Total volume (m <sup>3</sup> )	3.0	4.1	4.5
Fuel assemblies	12	12	4
Amount of spent fuel (tU)	1.4	2.2	2.1
Void space (m <sup>3</sup> )	0.61	0.95	0.67
Mass of fuel assemblies (tonnes)	2.6	3.6	3.1
Mass of iron and steel (tonnes)	10.4	13.4	18.0
Mass of copper (tonnes)	5.7	7.4	8.0
Total mass (tonnes)	18.6	24.3	29.1

## 4.2 Possible deviations and remedial actions

### 4.2.1 Treatment of possible deviations in the description of repository evolution

The following sections discuss briefly some possible deviations during the manufacture of canisters and during the construction, operation and closure of the repository that could affect its future evolution, as well remedial actions (canister retrieval). In general, the description of repository evolution given in the present report is based on the assumption that the canisters are manufactured and the repository constructed, operated and closed according to design specifications. As discussed below, however, the possibility of initial canister defects, variations in buffer density, and the presence of some stray materials in the repository following closure cannot be excluded, and these possibilities are included in the description of evolution (see e.g. Section 5.6.5 on interactions involving cement and stray materials and Chapter 8 on the evolution of a canister with an initial penetrating defect). No attempt has so far been made to assess the likelihood of such deviations. Other possible deviations include accidents during construction and operation and poor canister emplacement within a drift. These possibilities are discussed briefly in the following sections, but, at the current programme stage, they are regarded as design and operational issues and are dealt with in the coming report Design Description 2007 /Autio et al. 2008/.

### 4.2.2 Initial canister defects

Given the long (100,000 year at least) design lifetime of the canisters, which relies on the corrosion resistance of the copper shell, the possibility of initial defects that penetrate the copper shell is of crucial importance in the safety assessment. In principle, such defects could occur anywhere in the copper shell, but they are most likely to occur along welds and, in particular, at the seal of the canister top lid, which is less amenable to inspection than other welds.

SKB has made a first evaluation of the reliability of the friction stir welding process for canister sealing, which is the reference method assumed in SR-Can, and concluded that “the welding process produces reproducible results which satisfy stipulated requirements on minimum

copper thickness with very good margins” /Ronneteg et al. 2006/. According to SR-Can, there are expected to be no canisters with initial penetrating defects in their copper shells /SKB 2006b/. Furthermore, out of the entire canister inventory considered in the SR-Can assessment (4,500 canisters), it has been estimated that 99% have no defect deeper than 10 mm and 1% have no defect deeper than 15 mm. SKB also studied the reliability of non-destructive testing (NDT) of the copper seal welds and concluded that the proposed NDT methods are well suited to checking the weld quality /Müller et al. 2006/.

SKB has conducted tests on 20 canister lids welded by friction stir welding under production-like conditions (/SKB 2006e/ and references therein). SKB’s conclusion on the reliability of the friction stir welding method is that the welding process produces reproducible results which satisfy stipulated requirements on minimum copper thickness with very good margins /Ronneteg et al. 2006/. After the lids were welded, each weld was examined using the Non Destructive Testing (NDT) methods available at the SKB Canister Laboratory. SKB conclusion on the proposed NDT methods is that they are suitable to indicate the weld quality /Müller et al. 2006/. After NDT, the welds were further analysed using destructive methods to determine the exact size and, for some welds, the material composition in the defects. The maximum defect sizes obtained for this demonstration series were then used to predict the expected maximum defect size for the total production series using extreme value statistics, i.e. by fitting the measured defect sizes to a generalised extreme value distribution /SKB 2006b/.

Based on the results of these tests, for the purpose of the SR-Can safety assessment, the defect distribution was assumed to be as follows (see Table 4-1 in /SKB 2006b/):

- 99% of all canisters have a maximum defect size smaller than 10 mm
- 1% of all canisters have a maximum defect size smaller than 15 mm

In other words, one percent of canisters have a maximum defect size between 10 and 15 mm and none have larger defects. No initial penetrating defects are expected.

Posiva plans to seal the lid of the copper overpack with electron beam welding, but currently retains friction stir welding as an alternative option. Although there are differences in Posiva’s and SKB’s canister designs, including the chosen reference welding techniques, the probability of initial penetrating defects in Finnish canisters is also expected to be low. On the other hand, in Finland, the quality assurance program for NDT techniques is still in an early phase of development. A non-destructive examination method for canister component manufacture and sealing will only be selected by the end of 2008. A qualification programme for the applicable examination procedures will be made by the end of 2009 and executed by the end of 2012, before the application of the encapsulation plant construction license is submitted. Thus, Posiva is not yet taking any position on the likelihood of occurrence of canisters with initial penetrating defects.

In both methods, the seal location is on, or within a few centimetres of, the end-face of the canister, so that no differences can be identified between electron beam welding and friction stir welding from the long-term safety point of view if an initial penetrating defect is assumed to be present.

The evolution of a canister with a postulated initial penetrating defect is described in Chapter 8. In the Radionuclide Transport Report /Smith et al. 2007a/, a scenario in which a canister has an initially penetrated canister is used to illustrate the impact of a range of uncertainties affecting release and transport processes in the event of canister failure, whatever the cause or the timing the failure event. In SR-Can, although no initial penetrating defects are expected, evolution in case of a growing pinhole failure was described and its consequences evaluated (Section 10.5 of /SKB 2006a/).

### 4.2.3 Variations in buffer thickness and density

The design saturated buffer density is  $2,000 \text{ kg m}^{-3}$ . The density will, however, have a statistical spread due to small variations in the drift diameter and variations in the density of the emplaced bentonite. As discussed in Section 5.5, there is also expected to be a difference in the density of the buffer inside the supercontainers and the buffer extruded into the surrounding gaps through perforations in the supercontainer walls. These differences will reduce over time, but some residual differences may persist indefinitely because friction limits buffer homogenisation.

The initial spread of buffer densities following saturation has been calculated in the case of a KBS-3V repository using data from the Prototype Repository experiment at the Äspö Hard Rock Laboratory /Birgersson and Johannesson 2006/. The mean density 95% confidence interval for a complete deposition hole was calculated to be 2024–2038 (the mean density was higher than the KBS-3V and -3H design saturated buffer density, due to limited information when planning the experiment). No similar experiment or calculation has as yet been performed for KBS-3H.

Poor emplacement of canisters in the drift, such as off-centred or tilted deposition, could also have potentially detrimental effects on the safety functions of the buffer with respect to protection of the canisters and the limitation and retardation of radionuclide release from a failed canister. The thickness of the diffusion barrier provided by the buffer could be reduced. The swelling pressure could also be reduced, although a swelling pressure reduction leading to a significant increase of the hydraulic conductivity of the buffer is less likely; it is noted in SR-Can that substantial loss of buffer density would be required for advection in the buffer to be an important process (Section 9.4.8 of /SKB 2006a/). Either situation, if it were to occur, would result in an increase in the rate of transport of sulphide from the groundwater to the canister surface, thereby increasing the copper corrosion rate, and, in the event of canister failure, an increase of the radionuclide release rates at the interface between buffer and rock. During the early, transient phase, no impact on the integrity of either intact or initially defective canisters is, however, expected.

### 4.2.4 Accidents

Handling and transport of canisters from the encapsulation plant to a KBS-3H deposition drift is expected to be performed according to prescribed QA procedures and the emplacement of canisters is expected to take place as designed. Nevertheless, accidents or mishaps during the operational period can never be completely excluded, and must either be demonstrated not to have any significant impact on the long-term behaviour of the canisters, or, if such a demonstration is not possible, affected canisters will have to be removed from the drift and returned to the encapsulation plant, where appropriate measures would be taken to fully restore their functionality. Extreme cases, such as major mishaps or accidents during construction or operation of the repository, rock fall, failure of grouting causing sudden inflow to a compartment, sabotage, as well as a repository left open or unsealed after the operation period, have not so far been considered in KBS-3H safety studies.

/Knuutila 2001/ has studied the impact of possible accidents involving falling or dropping of canisters during encapsulation or transport to the underground facilities in the context of a KBS-3V repository. The findings are also largely applicable to KBS-3H. The strength and rigidity of the canister insert and the ductility of the copper shell ensure that the canisters remain gas tight even in the event of accidents that cause significant deformations of the insert. The fire resistance of the canister, when transferred in a rubber wheeled transfer lorry in the ramp or central tunnel of the repository, has been analysed in /Lautkaski et al. 2003/. According to simulation results, the spent fuel in its transportation cask would endure a fire with a flame temperature of  $1,000 \pm 100^\circ\text{C}$  for 3–4 hours, and in a radiation shield for 2.5–3 hours, without any resulting damage.

Off-normal conditions, including accidents, will be addressed in the coming report Design Description 2007 /Autio et al. 2008/.



#### **4.2.5 Stray materials**

Stray materials, if present in sufficient amounts, could damage the canister surfaces or otherwise adversely affect the repository safety functions. Stray materials of interest include those containing nitrogen compounds, such as ammonium nitrates and NO<sub>x</sub> species injected into bedrock during blasting, which could have detrimental effects e.g. on the stress corrosion of copper. These are, however, generally expected to be decomposed or reacted relatively soon after blasting and it is likely that there will be very limited amounts of these present after the operational period. Organic substances or their degradation products could, however, form complexes with radionuclides that would lower radionuclide sorption and thus increase radionuclide release and transport rates in the event of canister failure. These organic substances and their association with some metals could be particularly relevant when assessing the chemical risks associated with the repository system. The impact of these substances on the radiological consequences of the repository remains an issue for future safety assessments.

Where practicable, the introduction of potentially detrimental stray materials into the repository will be avoided, or such materials will be removed or cleaned during repository operations. Some stray materials will, however, inevitably remain in the repository and the surrounding rock after the closure. Potential amounts have been estimated, based on the reference layout described in Section 2.2.7 /Hagros 2007a/. The impact of stray materials on the repository safety functions is discussed briefly in Section 5.6.5.

#### **4.2.6 Canister retrieval**

If considered beneficial or necessary due to accidents, mishaps or poor emplacement, some or all canisters could be retrieved from a single drift or from the entire repository. It is currently assumed that any measures to facilitate retrieval will be realised in such a way that they will not harm the performance and long-term safety of the repository.

## 5 Early evolution

### 5.1 Definition of the period and evolution of external conditions

Early evolution covers evolution in the transient phase following the emplacement of the first canister in the repository. Significant mass and energy fluxes occur during this phase as a result of the various gradients created by the construction of the repository and emplacement of the spent fuel. The end-point of early evolution is not well defined; many of the transient processes that occur during this period do not suddenly cease, but rather gradually diminish over time. Nevertheless, two key transient processes – heat dissipation from the spent fuel and saturation of the repository external to the canisters – may take up to several thousands of years (or even longer in the case of saturation of the tightest sections) and this may be taken as the rough duration of the period discussed in this chapter.

External conditions, and especially the climate, are expected to vary significantly over this period. /Ruosteenoja 2003/ has described possible paths of climatic evolution at Olkiluoto in the near future (2010–2350), which corresponds roughly to the transient period described in this chapter (see also Section 5.2 of /Pastina and Hellä 2006/). An increase in temperature is predicted during the current century, due largely to the burning of fossil fuels (the “greenhouse effect”). High latitude temperature increase is expected to be larger than the global average (e.g. a high latitude increase of 8°C requires a global rise of only 2.5 to 6.7°C). By 2070–2099 winter temperatures at Olkiluoto are estimated to have risen by 3.8–10.4°C and summer temperatures by 1.6–5.6°C. Relative humidity will tend to decrease in all seasons except winter.

According to the Intergovernmental Panel on Climate Change /IPCC 2001/<sup>14</sup>, global average sea level will rise 0.11–0.77 m in the next century. Factors taken into account in this estimate are: thermal expansion, which accounts for a sea level rise of 0.09–0.37 m, melting of glaciers and ice caps, melting of the Greenland and Antarctic ice sheets, the thawing of permafrost, and the effects of sedimentation. This rise is counterbalanced at Olkiluoto by post-glacial land uplift, which is expected to remain roughly constant at 6 to 6.8 mm per year for the next few centuries (but to slow significantly over a time frame of a few thousand years – Section 2.2.6).

Before the end of the operational phase, it is possible that every winter will be practically snow/ice free. Thereafter, there are significant uncertainties in the magnitude of greenhouse effect (see the discussion of the Weichselian-R and Emission-M scenarios in Section 7.1). Within the next thousand years, according to the most radical scenario, the Greenland ice sheet will totally melt and raise the global average sea level by 6 m /IPCC 2001/. The maximum sea level rise caused by thermal expansion is 4 m. Thus, sea level could rise by a total of 10 m during this thousand-year period. Nevertheless, due to continuing post-glacial rebound, the shoreline will be displaced away from the Olkiluoto site, even in this most radical scenario. Within a few thousand years, the sea will have no impact on groundwater flow and composition around the repository, and thus the impact of anthropogenic changes in global average sea level on repository evolution will be negligible.

It could be speculated that the burning of fossil fuels, because of its impact on overall temperatures and on the CO<sub>2</sub> content of rainwater, could affect the reactivity of water infiltrating into the bedrock. This could, in principle, eventually lead to changes in groundwater flow patterns as a result of precipitation and/or dissolution on fracture surfaces, although there is currently no

---

<sup>14</sup> A new IPCC report is being compiled at the time of writing (2006–2007). Draft sections that are publicly available confirm the information presented in the earlier study /IPCC 2001/, which has been used in the present report.

evidence for any significant effects. The effect of increased  $p\text{CO}_2$ , as estimated in the base case scenario of /IPPC 2001/, on groundwater composition and the extent and depth of this perturbation could be an issue for further work in both the KBS-3H and KBS-3V programmes.

In the longer term, beyond the period of early evolution, the burning of fossil fuels could also affect the occurrence and timing of future glacial episodes. For safety studies, two scenarios for future climatic evolution have been selected on which to base the description of the evolution of a repository (either KBS-3H or KBS-3V) at Olkiluoto: the Weichselian-R scenario (Scenario B in /Cedercreutz 2004/) and the Emissions-M scenario (Scenario D in /Cedercreutz 2004/). The Weichselian-R scenario assumes a repetition (R) in the future of the last glacial cycle from the Eemian interglacial to the end of the Weichselian glaciation, which lasted about 125,000 years. The Emissions-M scenario takes into account the warming effects of moderate (M) levels of anthropogenic emissions (especially  $\text{CO}_2$ ) from human activities. The Weichselian-R and the Emissions-M scenarios provide alternative timelines for climate evolution consistent with current understanding. No attempt has been made to assess their respective likelihoods of occurrence. Both the Weichselian-R and Emissions-M scenarios are described further in Chapter 7 and are covered in detail in /Pastina and Hellä 2006/.

## 5.2 Thermal evolution

### 5.2.1 Key aspects of thermal evolution in this period

Heat will be generated by the decay of radionuclides in the repository at a time-dependent rate. This heat will be transferred continuously to the surrounding media by:

- conduction through metal components, bentonite, rock and any gas- or water-filled gaps between these media;
- radiation from surfaces; and
- convection of gas or water in gaps and voids.

Upon emplacement of the first supercontainer, the thermal evolution of the interior of the supercontainer (which begins prior to emplacement) will continue. In addition, heat will be transferred to air within the open part of the deposition drift and to the host rock. When the first distance block is emplaced, its temperature will start to rise as a result of heat transfer from the first supercontainer, from the next supercontainer as soon as it is emplaced, and so on until emplacement operations are complete. The thermal evolution within and around any individual supercontainer and distance block is thus, to some extent, dependent on the emplacement schedule and the duration of the operational period for a deposition drift. It is also dependent on the position of a given supercontainer with respect to other supercontainers in a drift.

In the longer term, the temperature within and around the repository will peak and then start to decline due to the diminishing heat output from the spent fuel. Repository temperature will tend towards the ambient rock temperature over a few thousand years. The thermal analysis results for KBS-3H, which are summarised in the following sections, are very similar to those for KBS-3V repository, particularly in the longer term.

Well-established physical laws describe the heat-transfer processes controlling thermal evolution. Nevertheless, there are some significant uncertainties in the parameter values that are appropriate when applying these laws to a KBS-3H repository at Olkiluoto. The emissivity of copper, for example, a parameter relevant to radiative heat transfer from the canister surface, depends on the quality of the surface, which will be a function of the manufacturing process and will also vary with time as the surface oxidises (see Section 2.3 of /Ikonen 2005/). The thermal conductivity of bentonite and the presence of gaps around the peripheries of the bentonite blocks depend on the saturation state. Heat transfer rates are thus affected by the various uncertainties that also affect the saturation process (Section 5.5). There is further uncertainty, as well as spatial variability and anisotropy, in the thermal conductivity of the host rock at Olkiluoto.

Uncertainty arises, in particular, from the use of spatially averaged thermal properties obtained from small sample data applied to the entire rock mass for thermal analyses. Thermal conductivity values for the host rock, which are relatively low compared with many crystalline rocks, are reported in Chapter 5 of the Site Description 2006 /Andersson et al. 2007/.

In /Ikonen 2003/ and /Ikonen 2005/, where the calculations are described in detail, such uncertainties are either argued to be of negligible consequence, or are handled by conservative parameter value selection (i.e. values are used that lead to an over-estimate of temperatures<sup>15</sup>). For example, in view of the uncertainty and variability in measured values, rather low values for thermal conductivity data were used in thermal analyses to avoid overestimating the heat transfer through the rock. Model simplifications are also made to facilitate the analyses, such as the neglect of convective heat transfer and of thermal anisotropy in the host rock. These are again argued either to be of negligible consequence or conservative. For example, the consequences of the thermal anisotropy of the host rock been evaluated and are minor with respect to thermal behaviour.

Because of the conservative parameter values used and model simplifications made, the temperature maxima reached in reality during the operational period and in the longer-term are expected to be lower than those calculated.

## 5.2.2 Thermal evolution in the operational period

/Ikonen 2005/ carried out an analysis of thermal evolution for BWR spent fuel in two limiting cases. In the first of these, the hypothetical assumption was made that an infinite row of supercontainers and distance blocks is emplaced in a drift instantaneously at time zero – i.e. the operational period is, in effect, instantaneous and all supercontainers evolve identically. This assumption is expected to lead to an over-estimate of temperatures at times when the thermal influences of different canisters begin to interact.

Figure 5-1 shows the calculated temperature evolution over a 30-day period in a vertical plane normal to the drift axis and passing through the centre of a supercontainer (i.e. where temperatures are highest) at three radial distances from the drift axis, corresponding to:

- the canister surface;
- the outer surface of the bentonite buffer; and
- the rock surface.

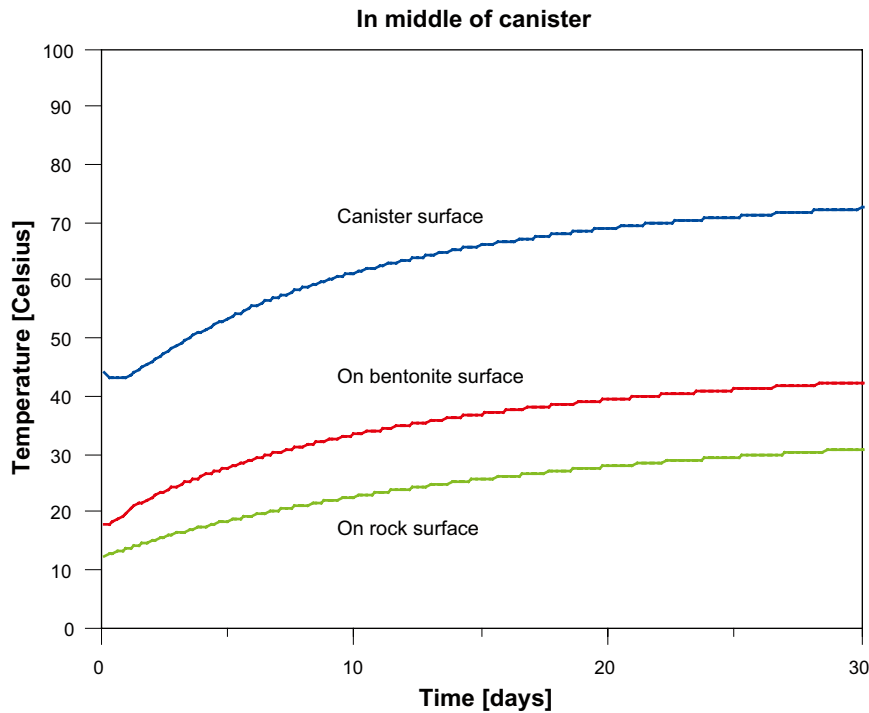
Gaps were assumed to exist between the canister surface and the buffer, between the buffer and the supercontainer and between the supercontainer and the drift surface<sup>16</sup>. These gaps were assumed to be air filled for the duration of the calculated period, with heat transfer across the gaps by thermal conduction and radiation.

Figure 5-2 shows the temperature profile parallel to the drift axis at each of these radial positions. According to this analysis, the air temperature in the gap between the supercontainer and the rock midway along the canister rises to between about 30 and 40°C over 30 days. The temperature on the canister surface rises to a little over 70°C.

---

<sup>15</sup> Such values are viewed as conservative, since the object of the modelling studies was to determine values for canister pitch and tunnel separation that ensure that *maximum* temperature criteria are satisfied.

<sup>16</sup> In reality, canisters are not likely to be located fully coaxially in the drifts. The buffer and canister will, for example, be in contact immediately below the canister, whereas an initial gap will exist above the canister. To simplify modelling, however, full axial symmetry was assumed. To ensure that the bentonite temperature assessment was conservative, the bentonite temperature at all points on its inner boundary was set equal to copper canister surface temperature.



Note: The 46°C initial temperature at the canister surface is the estimated steady surface temperature of the canister in ventilated storage at the encapsulation plant. A decay heat of 1,700 W per canister dissipated through a canister surface area (cylinder and top lid) of 16.7 m<sup>2</sup> with a heat transfer coefficient at the canister surface of 4 W m<sup>-2</sup> °C<sup>-1</sup> gives rise to a 26°C higher temperature at the canister surface compared with ambient air temperature, which is assumed to be 20°C.

*Figure 5-1. The temperature evolution over a 30-day period in a vertical plane normal to the drift axis and passing through the centre of a supercontainer at three radial distances from the drift axis – the canister surface, the (outer) bentonite surface and the rock surface /after Ikonen 2005/.*

Ikonen carried out a further analysis based on an alternative limiting case in which the operational period is, in effect, infinite – only a single supercontainer and single distance block are present from time zero and throughout the entire calculational period. This assumption leads to an under-estimate of temperatures at times when the thermal influences of different canisters begin to interact. The actual evolution of temperature will follow a path somewhere between these two limiting cases. However, the maximum temperatures calculated by Ikonen – i.e. the temperatures in a vertical plane passing through the centre of a supercontainer – are similar in both cases, indicating that neither the duration of the operational period, nor the position of one supercontainer with respect to other supercontainers in a drift, are important factors influencing the evolution of temperature in this plane.

### 5.2.3 Thermal evolution in the longer term

As the thermal influence of the fuel extends to increasingly large distances, the evolution of the temperature around a canister will be affected not only by heat output from canisters in the same drift, but also by the heat output from canisters in neighbouring drifts. /Ikonen 2003/ carried out analyses of the thermal evolution of a repository panel with different BWR canister pitches in a drift, and with either 25 m or 40 m drift separation. As noted above, the process of saturation of the buffer will affect its thermal properties, and will close air-filled gaps. In the calculations, however, fixed thermal properties were assumed for the bentonite and the gaps were (conservatively) assumed to remain open.

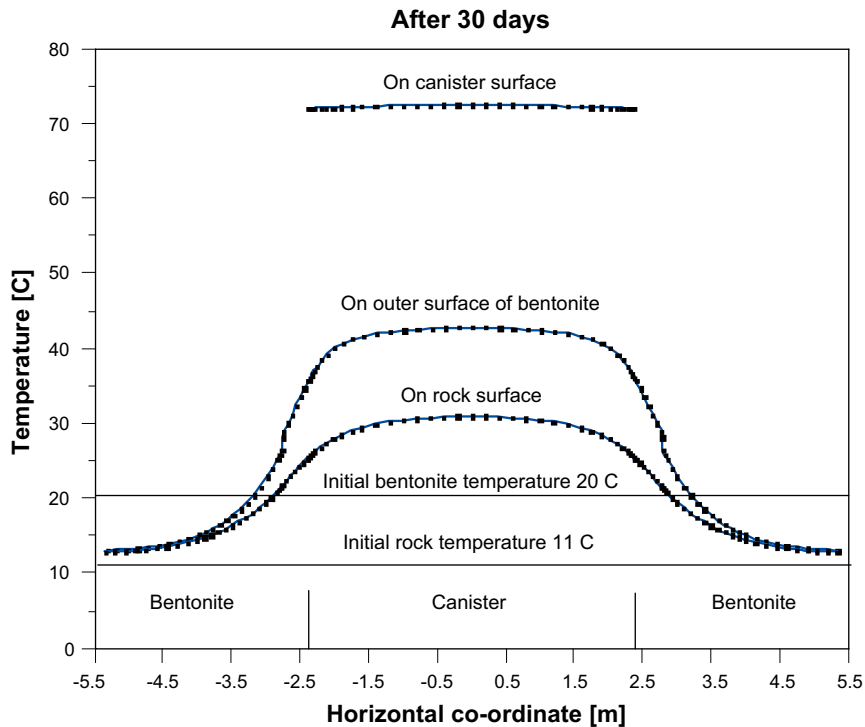


**Figure 5-2.** The temperature profile parallel to the drift axis at each of the radial positions shown in Figure 5-1 /after Ikonen 2005/.

The results showed that, for a canister pitch of 11 m and a drift separation of 25 m, the temperature at the canister/bentonite interface at the centre of the highest-temperature canister peaks at 90°C after 50 years of repository operation – or about 20 years after deposition of the canister<sup>17</sup>. For a 40 m drift spacing, the temperature maximum is slightly lower (84°C) and reached somewhat earlier (after 40 years from the start of repository operation – or about 10 years after deposition of the canister).

For the longer term, no temperature calculations specific to a KBS-3H repository at Olkiluoto have been carried out. The temperatures within the rock surrounding a KBS-3H repository are, however, expected to be similar to those around a KBS-3V repository, given the similarity of the emplacement density in the two alternatives. The results of calculations of coupled heat and solute (salinity) transport and flow carried out in connection with a KBS-3V repository at Olkiluoto and reported in /Pastina and Hellä 2006/ are therefore also expected to be broadly representative of a KBS-3H repository. The results indicate that the decay heat of spent nuclear fuel raises the temperature of the repository and the surrounding bedrock by several tens of degrees for many centuries and by a few degrees for several thousand years. Five thousand years after disposal, the temperature of the canister was calculated to be between 11 and 6°C higher than the undisturbed ambient temperature at repository depth (see Figure 5-3).

Climatic evolution and its associated uncertainties will have only a small impact on rock temperatures at repository depth up until the occurrence of the next period of permafrost (expected around 12,500 years at the earliest; see Chapter 7, Figure 7-2). By this time, the heat output from spent fuel will be negligible.

<sup>17</sup> Canisters are modelled as being deposited at a rate of 45 canisters per year. The canister experiencing the highest temperature in this case is in the 12th canister row of the 28th tunnel, with 50 canisters per tunnel (Table 5 of /Ikonen 2003/), and so it is deposited about 30 years after the start of operations. All canisters are assumed to have the same thermal output upon deposition.



## 5.2.4 Wider impact on system evolution and safety functions

### General

Thermal effects will significantly influence several of the processes involved in the evolution of a KBS-3H repository. Early thermal evolution has an important impact on design, in that avoiding thermally-induced detrimental changes is a major consideration determining deposition drift spacing and the spacing of canisters within a drift (i.e. the axial dimension of the distance blocks). In particular, considerations of thermal evolution reported in /Ikonen 2003/ are the basis of the 11-m canister pitch in the current KBS-3H layout for Finnish BWR spent fuel (Figure 2-3).

Specific thermal effects on the evolution and properties of the KBS-3H system are described below.

### Impact on pore pressures, saturation and flow

Heat generated by the spent fuel will cause water initially contained in the buffer near to the canister surface to evaporate and migrate outwards by vapour diffusion, followed by condensation in the outer part of the buffer or at the rock surface. Heat generation will not, however, significantly affect the rate of buffer saturation, since the increased hydraulic conductivity of the buffer at elevated temperatures largely compensates for the thermally driven transport of vapour outwards from the buffer (Section 5.5).

Increased temperatures will also lead to thermal expansion of water and decreased water viscosity. In the buffer, the thermal expansion of pore water will lead to significant increases in pore pressure only once full saturation is achieved in hydraulically isolated parts of the drift, due to the high compressibility of any trapped or repository-generated gas /Rasilainen 2004/.

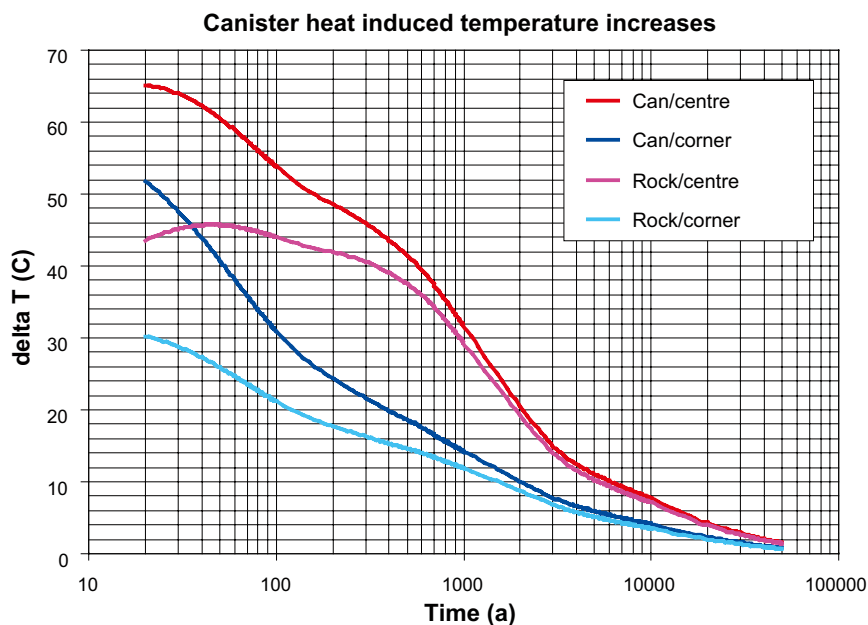


**Figure 5-3.** Increase in canister and buffer temperature above the undisturbed ambient value in a KBS-3V repository. To obtain temperatures in °C, the ambient rock temperature (10.5°C at the depth of 400 m in Olkiluoto) can be added to delta T. Further details are given in /Pastina and Hellä 2006/. As the spent fuel emplacement densities are similar for KBS-3V and KBS-3H, this figure also gives an indication of the magnitude and duration of the elevated temperatures occurring within and around a KBS-3H repository.

In the near-field rock, increased pore pressures and decreased groundwater viscosity will tend to increase water inflows towards the drift. Furthermore, thermal expansion of the rock may alter fractures apertures, increasing or decreasing flow<sup>18</sup>. Nevertheless, because of the declining heat output from the fuel, insignificant effects on the hydraulic, chemical and mechanical evolution of the repository and its surroundings are expected after a few hundred years.

### ***Impact on gas generation and transport***

Heat output from the fuel is expected to have no significant impact on gas generation or transport. Long-term steel corrosion (which gives rise to most repository generated gas) shows low sensitivity to the temperature within the range of 30–85°C /Smart et al. 2001/. Furthermore, although gas pressure and temperature are strongly related, and the solubility of gas is somewhat decreased at higher temperatures, the timeframe for the buildup of significant gas pressures is expected to be in the order of hundreds of years or more (see Section 5.5), by which time the thermal transient will be largely complete.

### ***Impact on the properties of the canisters and buffer***

The layout of the repository is chosen such that temperature within the buffer will remain below 100°C, in which case thermal effects will have no major impact on long-term safety functions of the canisters or the buffer (see Section 2.2.7). During the period of elevated temperature, some limited chemical changes may occur in the buffer, as described in Section 5.6. These are not, however, expected to perturb the properties of the buffer significantly in terms of the criteria for the buffer safety function indicators (Table 2-3). Cooling of the canister will cause tensile strain of the copper shells of the canisters over the iron inserts, but this will be negligible relative to the maximum allowable creep strain (Section 5.7.3).

### ***Mechanical impact on the rock***

Thermal loading will increase the principal stresses in the rock mass, and is expected to lead to some thermally-induced rock spalling (see Section 5.4.5). Subsequently, as the thermal load declines, the rock mass will readjust to the decreasing temperature, but some irreversible changes are likely to remain. The impact of thermally-induced rock spalling, along with other processes that may perturb mass transfer across the buffer/rock interface, is considered in Appendix B.7 in the context of canister corrosion, and in the Radionuclide Transport Report /Smith et al. 2007a/ in the context of the release and transport of radionuclides.

### ***Impact on chemical reactions in the near-field rock***

Elevated temperatures within and around the repository will affect chemical thermodynamic equilibria. They will also affect (and generally accelerate) the kinetics of aqueous and mineral reactions and will tend to increase the activity of microbes naturally present in the rock, as well as those introduced during repository construction and operation. Elevated temperatures will therefore influence the chemical evolution of the engineered barriers and the host rock, including the impact of cement, organics, nitrogen compounds and the various stray materials that may be introduced underground. The impact of elevated temperatures (together with an increase in pCO<sub>2</sub>) on the rock is expected to be largely reversible and may include precipitation of calcite in fractures and accelerated dissolution of silicates – as the rock mass subsequently cools, calcite will redissolve and silica will precipitate.

---

<sup>18</sup> In SR-Can, it was found that there could be some significant but very local effects on fractures close to deposition holes (see Figure 9-20 of /SKB 2006a/).

## 5.3 Groundwater flow and evolution of groundwater composition

### 5.3.1 Key aspects of groundwater flow and evolution of groundwater composition in this period

At the start of the early, transient phase, excavation of the repository will have caused drawdown of the groundwater table and a reduction in the hydrostatic pressure at repository depth. It will also have caused drawdown of sulphate-rich waters from closer to the surface and upconing of more saline, deep groundwaters (Section 4.1.1). After the underground openings are backfilled and sealed, groundwater flow analyses conducted in connection with the construction and operation of the ONKALO underground rock characterisation facility indicate that the groundwater table will recover within a couple of years of backfilling and sealing the facility /Vieno et al. 2003/. Perturbed geochemical and hydrogeological conditions will, however, persist in the immediate vicinity of the repository due to the residual thermal output from the spent fuel, which is expected to create a “groundwater convective cell”, drawing cooler and more saline waters from underneath the repository and discharging warmer waters above the repository. Calculations performed for a KBS-3V repository at Olkiluoto /Löfman 2005/ indicate that there will be increased upward groundwater flow and increased salinity compared with unperturbed conditions for a period of up to several hundreds of years (see Figure 4-1).

A further process potentially relevant to groundwater flow and geochemical composition in the transient phase (though not included in the calculations of /Löfman 2005/) is the gas rising through the fracture network – see Section 6.3.3 of /Pastina and Hellä 2006/. There are indications that deep saline groundwaters below repository depth contain gases, and in particular methane, at near-saturation concentrations (Section 2.2.4). The convective cell created by the thermal gradients around the repository will draw up dissolved gases from depth, and elevated temperatures will promote degassing and bubble formation. Repository-generated gas, principally hydrogen from the corrosion of steel components may also form bubbles. Furthermore, as gas rises through the fracture network within the host rock, it may carry water with it, and perturb groundwater flow to a degree not currently fully understood. However, the formation of bubbles from either natural dissolved gas or from repository-generated hydrogen gas formation is only likely to occur during the first few thousand years of repository evolution (during the period of elevated temperatures in the case of natural dissolved gas and during the period of steel corrosion in the case of repository-generated gas), and any perturbation to groundwater flow will have largely ceased by the time any radionuclides are released from failed canisters. For example, in the case of a canister with an initial penetrating defect through the copper shell, it may take around a thousand years for a transport pathway to be established between the canister interior and exterior and releases are initially expected to be relatively small due to the large transport resistance of the defect – it is likely to take several thousands of years more for the transport resistance of the defect to be lost – see the Radionuclide Transport Report, /Smith et al. 2007a/.

Methane and hydrogen gases migrating upwards may also participate in diverse redox processes in the groundwater, such as reduction of sulphate to sulphide in the presence of sulphate reducing bacteria. This is discussed in detail in /Pitkänen and Partamies 2007/, but is also noted in Chapter 12 as an issue for further investigation.

Although sealed, boreholes may play a significant role in hydrogeological evolution in the transient phase and beyond. This is because no currently available sealing techniques can be relied upon to prevent flow over timescales beyond a few centuries, and boreholes may thus become preferential flow and transport paths. As also noted in the context of a KBS-3V repository at Olkiluoto (Section 6.2.3 of /Pastina and Hellä 2006/), the long-term role of the boreholes will be clarified as more specific information about the technical method to seal them becomes available.

### 5.3.2 Wider impact on system evolution and safety functions

The evolution of the hydrostatic pressure and groundwater composition will to some extent affect buffer saturation and swelling, which are described in detail in Section 5.5. The hydrostatic pressure, which will be perturbed over a timescale of a few years by drawdown of the groundwater table, will affect the rate of inflow of water to the drift during saturation (Section 5.5). The salinity of the groundwater, which will be increased with respect to ambient conditions over a few hundred years, will affect both the rate of uptake of water by the bentonite buffer and the buffer swelling pressure (and thus, indirectly, the buffer hydraulic conductivity). As discussed below, however, provided the saturated buffer density remains in the range of about 1,890 to 2,050 kg m<sup>-3</sup> (the design density of 2,000 kg m<sup>-3</sup>), changes in swelling pressure and hydraulic conductivity caused by salinity variations are expected to be minor, and the criteria for the buffer safety function indicators will continue to be met. Processes that may lead to changes and non-uniformity in buffer density in the early evolution phase and beyond are discussed in various sections throughout this report.

The upper bound for saturated buffer density so that the buffer can be assumed to perform its safety functions (2,050 kg m<sup>-3</sup>) is taken directly from Table 2-3 and is based on the requirement on the buffer to protect the canisters in the event of rock shear movements. The lower bound of 1,890 kg m<sup>-3</sup> is derived firstly from the requirement on the buffer to prevent significant microbial activity. The corresponding safety function indicator criterion given in Table 2-3 is a swelling pressure of 2 MPa. Studies indicate that bacterial activity will be suppressed, and both culturability and viability will decrease, at swelling pressures exceeding 2 MPa /Stroes-Gascoyne et al. 2006, Masurat 2006/. It is likely that microbes are barely active under these conditions (although this is an issue that is still under investigation). Below about 2 MPa, however, significant microbial activity cannot be excluded. This lower bound for swelling pressure is met for 0.3 M NaCl solution (corresponding roughly to the present-day 10–20 g per litre total dissolved solids – TDS – at Olkiluoto) if the dry density is above about 1,300 kg m<sup>-3</sup> (1,830 kg m<sup>-3</sup> saturated) (see Figure 4-7 of /SKB 2006a/). A conservative estimate of the maximum salinity that could occur at a depth of about 550 m at Olkiluoto at future times is 30–45 g per litre. There is currently about 12 g per litre of TDS at repository depth (420 m below ground), which may rise transiently to around 25 g per litre as a result of the upcoming associated with excavations, before decreasing again as a result of continuing post-glacial uplift (Figure 4-1). For a 1 M NaCl solution (which corresponds to about 60 g per litre TDS) a 2 MPa swelling pressure is achieved at a dry density of about 1,400 kg m<sup>-3</sup> (1,890 kg m<sup>-3</sup> saturated).

In addition to preventing significant microbial activity, a saturated density of 1,890 kg m<sup>-3</sup> will prevent colloid-facilitated radionuclide transport (Table 2-3 of the present report – see also Section 2.5.4 of /SKB 2006c/ for further discussion). Furthermore, since the swelling pressure will never be less than 2 MPa, irrespective of salinity variations in the expected range, it will also prevent the possibility of canister sinking and ensure tightness at the drift wall and self sealing capability (Table 2-3). Finally, it will ensure diffusion-dominated transport in the buffer, given that hydraulic conductivities of less than 10<sup>-12</sup> m<sup>2</sup> s<sup>-1</sup> are measured in MX-80 bentonite in saline conditions at dry densities above about 1,200 kg m<sup>-3</sup> (1,760 kg m<sup>-3</sup> saturated) (see Figure 4-8 of /SKB 2006a/). Diffusion dominates over advection as a transport process at these low conductivities.

## 5.4 Mechanical evolution

### 5.4.1 Key aspects of mechanical evolution in this period

During early evolution, thermal gradients, gas generation, buffer saturation and swelling and the volume expansion of steel components as they corrode will result in mechanical forces being exerted on the canisters, on the surfaces of the supercontainer shells and on the drift walls.

The development of buffer swelling pressure (including the resulting deformation of the supercontainer shells) is described in Section 5.4.2. Section 5.4.3 describes the development of isostatic loads on the canisters. The potential for vertical displacement of canisters within the drift is described in Section 5.4.4. The mechanical evolution of the rock at its interface with the buffer and, in particular, the issue of rock spalling is discussed in Section 5.4.5. The impact of rock shear movements is described in Section 5.4.6. The impact of heterogeneous water inflow and saturation along the drift is discussed in Section 5.4.7. The mechanical evolution of the compartment and drift end plugs is described in Section 5.4.8. A discussion of the wider impact of the mechanical phenomena on system evolution and safety functions is given in Section 5.4.9.

#### **5.4.2 Development of buffer swelling pressure and deformation of the supercontainer**

A single KBS-3H drift is likely to pass through sections of relatively tight rock and rock intersected by transmissive fractures, so that saturation, swelling and the development of swelling pressure occur at different rates along the drift (an important difference between KBS-3H and 3V is the length of the KBS-3H deposition drift compared with the KBS-3V deposition holes). The saturation and swelling of the KBS-3H buffer is described in detail in Section 5.5, and is summarised below.

The buffer will start to absorb water from the high-humidity air immediately upon emplacement of the supercontainers and distance blocks. Water infiltrating through the drift walls will enter the bentonite pore spaces causing further swelling. Swelling bentonite will fill the gap between the distance blocks and the drift wall, hydraulically isolating the supercontainers from each other. Bentonite will also be extruded through the perforations in the cylindrical shell of the supercontainer. The extruded bentonite outside the supercontainers will initially be of low density, and exert a small swelling pressure on the supercontainer shells and drift walls, while the buffer inside the supercontainers will exert a relatively large swelling pressure on the inner surfaces of the shells. The difference in pressure exerted on the inner and outer surfaces of the supercontainer shells will lead to elasto-plastic deformation and possibly to rupturing of the shells after a period of a few months. This has been observed experimentally in 1:10 scale tests (Figure 4-13 in /Börgesson et al. 2005/). The exact form that any rupturing will take is uncertain, although it is most likely to take place initially at the intersection between the lid and the supercontainer cylinder.

As further water is absorbed, confinement of the buffer will cause the swelling pressure exerted on the drift walls, on the canisters and on the compartment and drift end plugs to increase. The weight of the supercontainers will be transferred from the supporting feet to the buffer, which will be sufficiently dense to prevent any significant sinking as the supporting feet corrode (although the supporting feet, when corroded, may themselves form a high density, low porosity corrosion product, which will have some mechanical strength).

The corrosion of steel components external to the canisters is described in detail in Section 5.6.4. Corrosion will affect buffer saturation by producing gas, leading to the development of gas overpressures, and possibly delaying saturation in tight drift sections (Section 5.5). There is also the possibility of gas flow at the buffer/rock interface. Gas overpressures and flow could be maintained over a prolonged period of up to several thousands of years. The buffer swelling pressure is, however, expected to reseal gas pathways once the gas pressures fall. As corrosion products form on the surfaces of the steel components, the volume occupied by the buffer will be reduced. This is due to the higher volume occupied by the corrosion products compared with the original metal. It will lead to an increase in buffer density and swelling pressure in the vicinity of the corroded components (see the scoping calculations in Appendix B.4). This may homogenise to some extent over time, but internal friction within the clay means that some inhomogeneity in buffer porosity near to the corroded components may persist indefinitely. Complete conversion of the supercontainer shells, the most significant



of the steel components, to magnetite<sup>19</sup> over a few thousand years would lead to a porosity decrease in the bentonite of about 2%, and a corresponding small increase in swelling pressure of about 1 MPa. Higher volume expansion would occur if other possible corrosion products such as iron sulphide and siderite were to form. Too high a buffer density could compromise the protection afforded to the canisters against rock movements, and could also result in swelling pressures that could damage the rock. The scoping calculations given in Appendix B.4 indicate that the increase in buffer density following conversion of the steel of the supercontainers to magnetite will be less than 2,050 kg m<sup>-3</sup>, and thus the buffer is expected to retain its protective function, irrespective of variations in groundwater salinity (Section 5.3.2). Buffer densities above 2,050 kg m<sup>-3</sup> this might occur if the supercontainer were to be completely converted to siderite, rather than magnetite. There is, however, clear evidence that the transformation of iron to siderite is limited by the availability of carbonate (Appendix B.4).

The buffer that swells into void spaces around the distance blocks and supercontainers will be of lower density than the rest of the buffer. Together with the heterogeneity of water inflow and the impact of the volume expansion of steel corrosion products, this will lead to an inhomogeneous stress distribution in the buffer, which may in turn result in some creep of the buffer over time. Eventually, however, a quasi-stationary state of stress equilibrium is likely to be reached when all forces acting within the bentonite (including the swelling pressure itself, the force caused by volume expansion of steel corrosion products and by gas pressure build-up, the hydrostatic pressure and rock stress, internal friction within the buffer and between the buffer and other components) are balanced, resulting in a partial homogenisation of bentonite swelling pressure throughout the buffer.

The saturated bentonite density and porosity following full homogenisation would be 2,000 kg m<sup>-3</sup> and 44%, respectively (although some differences in density within the buffer, and especially between the buffer inside and outside the supercontainer, may, however, persist indefinitely due to friction). The corresponding maximum swelling pressure within the buffer is in the order of 7–8 MPa (affected slightly by uncertainty in the volume expansion of the steel corrosion products, as explained above). Lower values are possible, due to the interaction of bentonite with saline water from upconing at Olkiluoto, although, as discussed in Section 5.3.2, the safety functions of the buffer are not expected to be compromised provided the saturated buffer density remains in the range of about 1,890 to 2,050 kg m<sup>-3</sup>.

### 5.4.3 Development of isostatic loads on canisters

As the buffer saturates and swells, it will exert an increasing mechanical load on the canisters. This load is expected to develop unevenly during the saturation process, due to the variability in water inflow along the drift. The canisters will also experience transient thermomechanical loads induced by the progressive cooling of the spent fuel. As the temperature of the canister increases, the copper shell will expand more than the iron insert because of its higher thermal expansion coefficient. This will result in a small widening of the gap between the insert and the shell. When the temperature decreases, a tensile strain in the copper shell will be induced due to the greater shrinkage of the copper compared with iron. The plastic strain of copper due to this thermo-mechanical loading is estimated at 0.054%, which is negligible compared with the allowable creep strain in copper (5%) (Section 6.1.2 in /Pastina and Hellä 2006/).

Uneven loading at the canister surface may cause localised mechanical stresses on the canister, which could in principle result in movement, tilt or deformation. These effects have, however, been demonstrated to be negligible in studies of KBS-3V /SKB 1999/. This conclusion is also expected to hold for KBS-3H. As noted above, differences in density and swelling pressure around individual canisters and also along the drift are expected to diminish over time due to homogenisation of the bentonite and, although some inhomogeneity may remain, the load on

---

<sup>19</sup> As discussed in Section 5.6.4, magnetite is the expected initial corrosion product of steel in the presence of bentonite, although, depending on solution conditions, some iron sulphide and siderite may also form. Subsequent film dissolution can produce iron silicates.



the canisters is expected to become approximately isostatic (i.e. equally large over the entire canister surface area) and similar for all canisters.

The isostatic load on the canisters will be about 11–12 MPa, which is the sum of the swelling pressure of the bentonite (7–8 MPa, see Section 5.4.2) and the groundwater pressure at repository depth (about 4 MPa following recovery of the groundwater table from drawdown during construction and operation). This is well below the expected pressure for total collapse of the canister, estimated to be 80–114 MPa (Section 4.3.1 of /Pastina and Hellä 2006/), depending on the insert type. It is also significantly less than the pressure required for a significant probability of local collapse (Section 7.4.4).

#### **5.4.4 Vertical displacement of the canisters**

The weight of the canisters, which have a much higher density than the buffer, will result in a gradual vertical sinking through the plastic buffer material as a result of consolidation and creep (both volumetric and deviatoric).

Provided the buffer swelling pressure exceeds about 0.2 MPa, no significant canister sinking is expected to occur (Table 2-3). Although there are some significant uncertainties, the scoping calculations described in Appendix B.4 indicate that none of the identified processes that could give rise to loss of buffer mass or redistribution of buffer mass along the drift have the potential to cause a buffer density and swelling pressure decrease that could lead to significant sinking. Furthermore, for KBS-3V, the calculations of /Börgesson and Hernelind 2006a/ indicate that even a reduced swelling pressure of 80 kPa (compared with a reference value of 7–8 MPa) only results in only a limited amount of sinking (23 mm over  $10^5$  years). Thus the amount of sinking will be negligible during the transient phase (and also in the longer term – Section 6.4.3).

Buffer material extruded through the perforations in the supercontainer shells will be of lower density than the bulk of the buffer, and may initially and locally take the form of a gel. Although relatively soft compared with the bulk of the buffer, internal friction and friction with the supercontainer shell and drift wall is expected to prevent any significant flow of the gel within the gap between the supercontainer shell and the drift wall.

There may, however, be some transient upward vertical displacement of the canister during the saturation process. This could occur if the lower part of the buffer inside a supercontainer is saturated more rapidly than the upper part. In this case, the wetted bentonite in the lower part of the buffer will have a higher thermal conductivity than the drier buffer above, further accentuating the asymmetry of the saturation process. The swelling pressure of the buffer material extruded through the perforations on the lower side of the supercontainer could lift the supercontainer, together with the canister, until the supercontainer contacts the top of the drift. The resulting difference in buffer density above and below the canister is considered in a scoping calculation in Appendix B.4. As the remaining buffer saturates, the initially higher density in the upper part of the drift will tend to homogenise and the canister will return to a more central position in the drift, although some small eccentricity may remain.

#### **5.4.5 Mechanical evolution of the rock at its interface with the buffer**

Buffer swelling will exert forces on the drift wall that could, in principle, open existing fractures or generate new fractures in the adjacent rock. A modelling study by /Lönngqvist and Hökmark 2007/ found that, for a KBS-3H repository at Olkiluoto, a pressure on the drift wall of at least 10 MPa is required to open a pre-existing horizontal fracture intersecting the drift at mid-height, although the effects are expected to be small, in terms of increase in fracture aperture and distance from the drift wall to which such effects extend, even at pressures of 20 to 25 MPa. Gas generation from the corrosion of steel components external to the canisters will also lead to a pressure build up on the drift wall, especially in tight drift sections where there are no transmissive fractures to act as pathways for gas migration. The outward migration of gas in tight drift sections, including the possibility of the reactivation of tight fractures, is discussed in Section 5.5.4.

A further mechanical process that may take place during the transient phase, but which could also affect repository performance at later times, is that of rock spalling around the deposition drifts walls. Spalling is the brittle fracturing of the rock surface into splinters, chips or fragments. It could potentially occur as a result of the relief of high initial rock stresses upon rock excavation, especially at the interface between the niche and the main part of a drift with smaller diameter (Figure 2-5). Thermally-induced spalling could also occur as a result of the decay heat from the spent fuel.

Thermo-mechanical analyses of a KBS-3H repository at Olkiluoto by /Lönnqvist and Hökmark 2007/ indicate that, in the reference layout in which the deposition drifts are aligned with the direction of the principal stress in the rock, little or no spalling will occur prior to the emplacement of spent fuel. Boundary element modelling results of two KBS-3H drifts, niches and a transport tunnel presented in the Process Report show that stress values in the drifts are moderate and below the spalling strength of 65 MPa (Section 7.6.3, /Gribi et al. 2007/). Significant thermally-induced spalling could occur on a timescale of a few years, although it is most likely around supercontainers in relatively tight drift sections, since in less tight drift sections and around the relatively tightly fitted distance blocks, where the gaps around supercontainers require only a few weeks or less to fill with water, and a further few months to fill with bentonite (Section 5.5), buffer swelling pressure is likely to stabilise the drift wall before spalling occurs.

For example, the maximum allowable inflow rate to a ~ 10 m supercontainer/distance block drift section is set at 0.1 litres per minute (Section 2.2.7). In such a drift section, it will thus require about 10 days to fill the 1.5 m<sup>3</sup> void space around a supercontainer, and thermally induced rock spalling is not expected. In the case of tighter drift sections with much smaller inflows, water will probably not spread and fill the entire void space, but will rather be absorbed directly by the partly saturated buffer. In such drift sections, the possibility of thermally-induced rock spalling cannot be excluded. The proportion of drift sections that will be affected cannot currently be estimated with confidence, since the precise inflow conditions to prevent spalling have not been investigated. The proportion is, however, likely to be high – note that 60% of supercontainer drift sections are estimated to be intersected only by fractures with transmissivities of 10<sup>-10</sup> m<sup>2</sup> s<sup>-1</sup> or less, and would be expected to give inflows more than an order of magnitude lower than the 0.1 litre per minute criterion (Appendix B, p.126 of /Lanyon and Marschall 2006/).

Similar conclusions have been reached in the case a KBS-3V repository at the sites currently considered in the Swedish programme. The properties of the potential host rocks are such that no rock spalling is expected in the deposition holes prior to canister deposition /Hökmark et al. 2006/. Furthermore, SR-Can notes that, even if it were to occur, detached rock fragments could be removed and filled with bentonite. On the other hand, following spent fuel emplacement, there will almost certainly be some thermally-induced spalling on a timescale of years to centuries at any of the Swedish sites. Spalling is most likely in dry deposition holes where the development of some bentonite swelling pressure at the interface with the rock is slow.

Pressures much smaller than the full buffer swelling pressure – possibly in the order of 150 to 200 kPa – are likely to be sufficient to suppress spalling (/Chou et al. 2002/, and the APSE experiment at the Äspö hard rock laboratory, reported in /Andersson and Eng 2005/). Filling the buffer/rock gap around the KBS-3H supercontainers with bentonite pellets at the time of deposition would, for example, either prevent spalling, or at least stabilise the walls and limit the growth of fractures (see also the discussion of the DAWE design variant in Appendix A). The use of pellets to prevent spalling is being studied in the context of KBS-3V, and such measures may also be considered in future KBS-3H design studies.

While the hydraulic conductivity of the host rock near the drift wall around supercontainers in tighter drift sections may be substantially increased by thermally-induced spalling, it is likely that the pressure on the drift wall exerted by the distance blocks will suppress spalling and will prevent the formation of continuous flow and transport pathways along the drift. Although this

is an issue that requires further investigation<sup>20</sup>, the possibility of continuous pathways along the drift is therefore currently excluded in defining radionuclide release and transport calculations addressing the issue of spalling, which consider only the possibility of local perturbation to the buffer/rock interface (see the Radionuclide Transport Report, /Smith et al. 2007a/).

#### **5.4.6 Rock shear movements**

During the early evolution of the repository, shear movement on fractures intersecting the deposition drifts may take place as a result of rock excavation and heat load, leading to mechanical forces on the canisters (/SKB 2006a/, Section 9.3.1). Shear movements as a result of these processes that are significant in the sense that they could damage the engineered barrier system are, however, considered highly unlikely (the plasticity of the buffer is expected to protect the canisters from any small shear movements that do occur).

Movement on one of the major lineaments bounding Olkiluoto Island, or on the major brittle deformations adjacent to or within the repository rock mass volume, could significantly affect rock stress around the deposition drifts. The repository will, however, be designed taking into account local fluctuations of the principal stress magnitudes and orientations, and such changes should not have any safety implications.

The possibility that a large earthquake will give rise to secondary shear movements on fractures intersecting the drifts that are sufficiently large to damage the canisters cannot be completely excluded in the early, transient phase, but such earthquakes are most likely to occur in association with future glaciation; the issue of engineered barrier damage due to post-glacial earthquakes is discussed in Section 7.4.4.

#### **5.4.7 Hydromechanical heterogeneity along a KBS-3H drift**

Heterogeneous water inflow will lead to the development hydraulic pressure differences along the drift as the drift saturates. As illustrated in Figure 5-4, which is taken from the discrete fracture network study by /Lanyon and Marschall 2006/, the variability in the rate of saturation and water pressurisation along the drift will result, within the first year from the start of emplacement in a drift, in a system of neighbouring supercontainers and distance blocks in which there can be full hydrostatic pressure on one side of a distance block, and a pressure close to the initial atmospheric pressure on the other side.

In the longer term, as the buffer saturates at variable rates, axial swelling pressure gradients will also develop along the drift.

These pressure differences and swelling pressure gradients are of concern because of their potential to cause any erosion the buffer by flowing water (“piping”) and deformation, displacement and compaction of the supercontainers and distance blocks during saturation. As discussed in Section 5.5.6, these effects are not, however, expected to be significant in terms of their impact on the capacity of the buffer to satisfy the criteria for safety function indicators (Table 2-3), although some unresolved issues remain.

#### **5.4.8 Mechanical evolution of the compartment and drift end plugs**

The mechanical strength of the compartment plugs, as emplaced, is insufficient to withstand full buffer swelling pressure. The filling material between the plugs may therefore undergo some compaction as the swelling pressure of the buffer increases (only a tentative design has so far been developed for the backfill between the plugs in a sealed off section – Section 2.3.4). The compressibility of this material is, however, likely to be limited, and certainly insufficient for the adjoining buffer to expand into the sealed off section, and become exposed to high water flows.

---

<sup>20</sup> SKB is embarking on a modelling study and a field experiment programme at the Äspö Hard Rock Laboratory to address this issue.

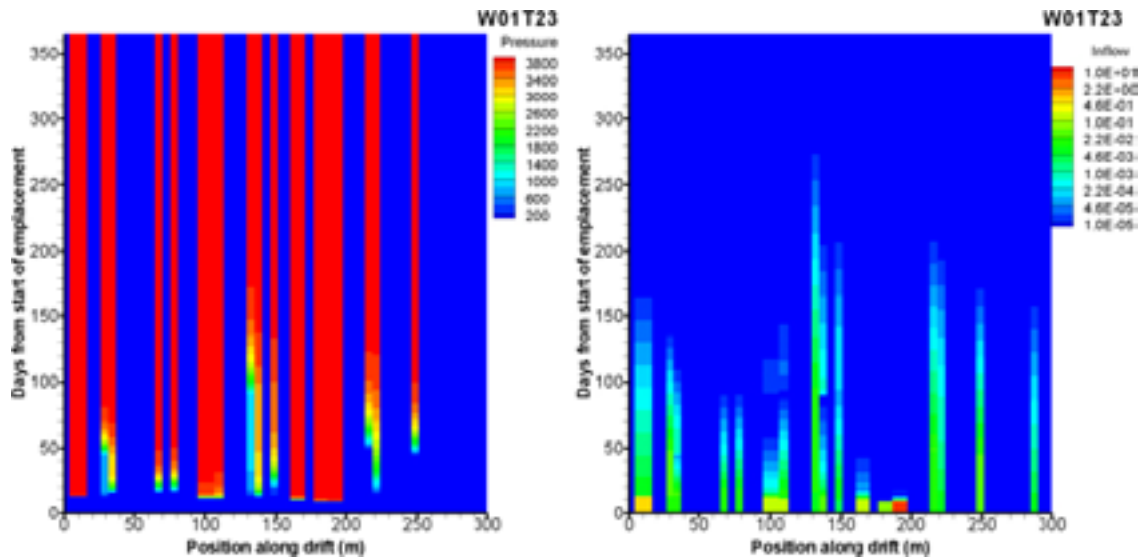


*Figure 5-4. Example of pressure (on left) and inflow (on right) as a function of time and position along a drift (after Figure 6-2 of /Lanyon and Marschall 2006/).*

The mechanical strength of the drift end plugs, as emplaced, will prevent the buffer from expanding into the main tunnels. The loss of mechanical strength due to the chemical degradation of the cement parts of the drift end plugs (Section 5.6.5) may, however, eventually lead to some limited displacement of the plugs towards the main tunnel.

#### 5.4.9 Wider impact on system evolution and safety functions

The development of buffer swelling pressure and isostatic load on the canisters is part of the expected evolution of a KBS-3H repository in the transient phase. Relevant safety function indicator criteria for the canister and buffer (Tables 2-2 and 2-3) are expected to be met. In particular, the isostatic pressure on the canister will not lead to collapse and shear stresses on the canister are likely to be significantly less than the rupture limit. The swelling pressure that develops will be sufficient to ensure a tight seal at the interface with the host rock, and to prevent or minimise:

- water flow and advective transport through the buffer;
- canister sinking;
- microbial activity; and
- colloid transport.

At the same time, the buffer density will not be so high as to compromise the protection of the canister against rock shear, and the swelling pressure will not be sufficient to damage the canisters or the rock.

Only limited vertical displacement of the canisters during the buffer saturation process is expected.

The likelihood of rock spalling due to stress relief is considered to be low. After emplacement of the supercontainers, however, thermally-induced rock spalling is likely to occur, especially in tighter drift sections. Its impact on long-term safety relates to the potential increase in both the rate of groundwater flow at the buffer/rock interface and also the residence time of solutes in contact with the interface, which affects mass transfer between the buffer and the rock. This is relevant to:

- canister corrosion due to the migration of sulphide from the rock through the buffer to the canister surface (Sections 5.7.4 and 6.6.1); and

- radionuclide migration from the buffer to the rock in the event of canister failure (Radionuclide Transport Report – /Smith et al. 2007a/).

Hydromechanical heterogeneity along the drift may cause some small displacement of the supercontainers and distance blocks during saturation. No significant impact on the safety functions of buffer and canister are expected. However, an issue for further study and design development is the possible deformation of the distance blocks as a result of hydraulic pressure differences between less tight and tighter drift sections, which could, if not avoided by design, lead to more significant displacement. These issues are discussed further in the context of saturation and buffer swelling in Section 5.5.6.

## 5.5 Saturation and buffer swelling

### 5.5.1 Key aspects of saturation and buffer swelling

Groundwater will flow into the KBS-3H drifts as soon as they are excavated. This water will enter the drift through transmissive fractures that intersect the drift walls and will flow around the drift walls to the drift floor, and along the drift floor down the incline towards the transport tunnel.

As supercontainers and distance blocks are emplaced, the bentonite they contain will absorb moisture from the air. They will also absorb liquid water as this fills the gaps between the distance blocks and the drift walls, and between the supercontainers and the drift walls.

In the current reference design, free drainage of water along the floor during the operation of a drift compartment will be interrupted during the operation of the compartment by the fixing rings that will be fitted at intervals along the drift, and later by the swelling of the distance blocks. Water flowing into the drift will therefore accumulate in the gaps around supercontainers and migrate into the buffer.

The details and duration of the evolution of the buffer to a final state in which full saturation and the required buffer density and swelling pressure are attained will vary significantly along the drift. This is because the intersecting fractures will have variable transmissivities and be unevenly spaced, resulting in significant variability in the rate of water inflow at different locations along a drift (Figure 5-4). The impact of gas generated by the corrosion of steel in the supercontainers and other steel components on the saturation and swelling processes will also vary along the drift, as this also depends strongly on the properties of intersecting transmissive fractures. Furthermore, as noted in Section 4.1.1, excavation will cause a mixing of groundwater types. It may well be that one part of a drift takes in less saline water from above and another more saline water from below, also contributing to transient swelling pressure differences.

In describing the evolution of saturation and buffer swelling, it is convenient to categorise drift sections as follows.

1. Less tight drift sections, the expected evolution of which is discussed in Section 5.5.2.

These are defined as drift sections in which the average hydraulic conductivity of the adjoining wallrock is about  $10^{-12} \text{ m s}^{-1}$  or more. This corresponds, for example, to a fracture spacing of ten metres and a fracture transmissivity of  $10^{-11} \text{ m}^2 \text{ s}^{-1}$  or more, or  $10^{-12} \text{ m}^2 \text{ s}^{-1}$  or more for a one-metre fracture spacing. It also corresponds roughly to an initial inflow to a 10 m drift section of about 0.4 ml per minute or more, based on Darcy's law in a radial configuration (Thiem's equation; see Appendix B.2, Eq. B.2-1), and using the same geometrical parameters and assumed maximum hydraulic pressure difference as in Appendix B.2 (see, however, the discussion of the relationship between initial inflow and transmissivity in Section 2.2.7). Assuming that inflow is fairly evenly distributed along the drift, the rate of buffer saturation in these sections will not be limited by the hydraulic conductivity of the rock, but rather by the rate at which water can migrate into the buffer. Repository-generated gas can readily escape via the



intersecting fractures, and thus plays no significant role in the saturation process. Such sections are expected to be the most common: all but one of the supercontainer sections in an example drift considered in discrete fracture network modelling for KBS-3H fall into this category /Lanyon and Marschall 2006/.

## 2. Tighter drift sections, discussed in Section 5.5.3.

These are defined as drift sections in which the average hydraulic conductivity of the rock is in the range  $10^{-13}$  to  $10^{-12}$  m s<sup>-1</sup>. In these sections, the rate of buffer saturation is largely controlled by the hydrogeological properties of the host rock, which will give rise to little or no detectable initial inflow, and later, potentially, by the rate of hydrogen gas generation.

## 3. Tightest drift sections, discussed in Section 5.5.4.

These are defined as drift sections in which the average hydraulic conductivity of the rock is in less than  $10^{-13}$  m s<sup>-1</sup>. It may not, in practice, be possible to differentiate such sections from the tighter drift sections defined above, since neither may give rise to detectable initial water inflow<sup>21</sup>. Nevertheless, the existence of these tightest drift sections cannot currently be excluded, and the saturation of the buffer may proceed somewhat differently compared with other drift sections due to their tightness with respect to both groundwater flow and the flow of repository generated gas. In these sections, repository-generated gas may hinder or prevent altogether the saturation of the buffer until gas generation by steel corrosion ceases and gas pressure falls (which is expected to take several thousands of years).

In each case, the drift section described may contain just a single supercontainer (as depicted, for example, in Figure 5-5), or a sequence of several adjacent supercontainers and distance blocks.

### 5.5.2 Expected evolution in less tight drift sections

Saturation and buffer swelling of a less tight drift section (as defined above) can be described in terms of the following broad stages.

#### ***Water inflow to the gaps around the supercontainers and distance blocks***

As illustrated schematically in Figure 5-5, water will enter less tight drift sections through transmissive fractures and accumulate in the lower part of the drift, flow along the drift floor being prevented by the fixing rings and/or fallen fragments of bentonite from the distance blocks. Because of the narrowness of the gap between the distance blocks and the drift walls, this gap will fill with bentonite and seal rapidly as the water level rises, isolating each supercontainer from its neighbours hydraulically. Any cracks in the bentonite and the gaps between the distance blocks and adjoining supercontainers will also fill and seal with the rising water level.

The rate at which the gaps around the supercontainers fill with water will be determined by the local rate of supply of water from the host rock on the one hand, and the rate at which the bentonite inside the supercontainers and in the adjacent distance blocks takes up water on the other. As the gaps around the supercontainers fill with water, the buffer inside the supercontainers will absorb water through the perforations in the supercontainer walls due to capillary forces. In drift sections with higher initial inflow rates (flow rates of up to around 0.1 litres per minute, which is the maximum allowable rate of water inflow in a drift section suitable for canister and buffer emplacement in the current reference design; see Section 2.2.7), it is unlikely that uptake by the buffer will balance the rate of inflow from the rock, and the gaps around the supercontainers will initially fill with water. In such drift sections, and neglecting uptake by the bentonite, the 1.5 m<sup>3</sup> open volume around a supercontainer will fill with water within about 10 days (see also

<sup>21</sup> An inflow as low as about one millilitre per minute can be observed, e.g. by ventilation tests or, if the inflow is localised is a small number of leakage points, as damp locations on the drift wall.



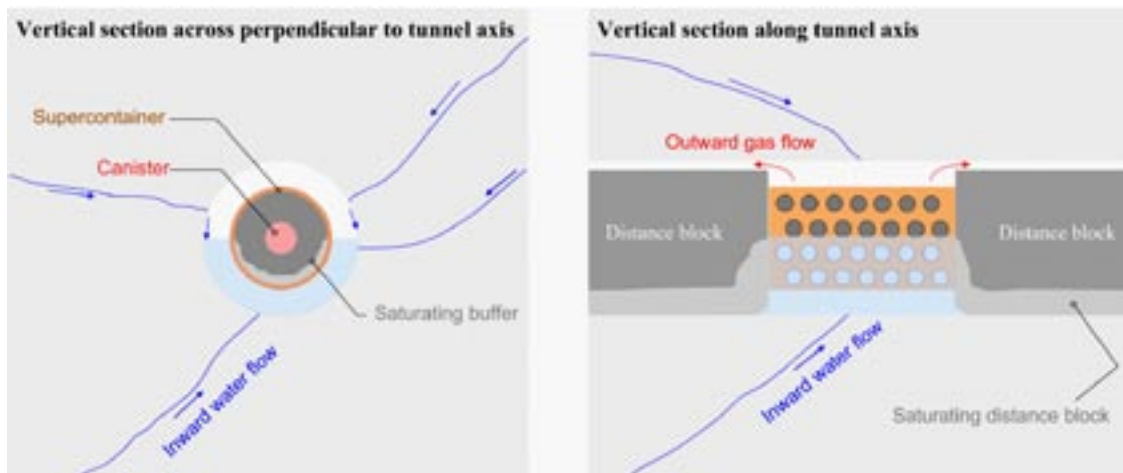


**Figure 5-5.** Water inflow to the gaps around the supercontainers and distance blocks (gap size exaggerated).

/Lanyon and Marschall 2006/). As water enters, air will be forced towards the top of the drift and axially along gaps above the distance blocks towards tighter (drier) drift sections (see the right-hand side of Figure 5-5). However, once the water level approaches the top of the drift, the gaps between the distance blocks and the drift wall will seal completely, resisting any further flow of trapped air along these routes. The rising water will then compress any remaining air.

Once filled with water (possibly with a small amount of trapped air at the top of the gap), the fluid pressure inside the gap will increase to a value close to the hydrostatic pressure (which, in the short term, may be less than the equilibrium hydrostatic pressure of 4 MPa due to drawdown during construction and operation) and water inflow will be substantially reduced. The fluid pressure increase rate has been considered in a discrete fracture network modelling study by /Lanyon and Marschall 2006/. There are significant uncertainties, particularly with respect to the storativity assigned to the system, which is related, in part, to the assumptions made about the presence of trapped air. Increasing pressure could also give rise to some internal piping in the adjacent distance blocks (i.e. piping that does not penetrate to the gaps around neighbouring supercontainers), which would moderate the rate of pressure increase (internal piping has been observed in laboratory tests – see Appendix L of /Autio et al. 2007/). It is currently estimated that the pressure increase rate could be as high as a few MPa per hour (see also the discussion in Section 3.3 of /Autio et al. 2007/).

Even after the pressure in the gap has risen to near the hydrostatic pressure, some small net inflow from the rock will continue, since the buffer will still be only partially saturated at this time (full saturation requiring a minimum of about 10 years; see Figure 5-7), and capillary forces will continue to draw water into unsaturated bentonite pores. Before the gaps become filled with bentonite, transmissive fractures intersecting the drift will also carry a small water flow into and out of the drift, driven by the natural hydraulic gradient. There may, however, be much higher gradients during the transient period, arising from the lower fluid pressures in other parts of the same drift compartment that are more slowly saturated, in neighbouring unplugged compartments in the same drift, and in adjacent drifts if these are also yet to be plugged. These gradients may drive water flows through the intersecting transmissive fractures or, to lesser extent, create axial flow through the EDZ and buffer. These flows may contribute to the eventual saturation of some tighter drift sections, but are expected to be too small to have any detrimental impact on the buffer in terms of erosion (Appendix B.3 and Section 5.5.6).

The differences in fluid pressure acting on the vertical faces of the distance blocks in sections intersected by transmissive fractures and tighter drift sections have the potential to cause some mechanical displacement of the supercontainers and distance blocks along the drift.

It is currently assumed that friction between the distance blocks and the drift wall, together with the installation of fixing rings, all prevent significant displacement at early times, and especially during the operation of each drift compartment before the compartment plug or drift end plug is installed (although ensuring that this is the case is the subject of continuing design studies). The potential for displacement is also reduced over time as the buffer swelling exerted on the drift wall increases. These issues are discussed further in Section 5.5.6.

### **Filling of gaps with bentonite and continuing buffer saturation**

Uptake of water by the buffer will result in a swelling pressure that will cause bentonite to be extruded as a gel through the perforations in the supercontainers and into the gaps between the supercontainers and the rock. The bentonite gel will continue to expand into the gaps around the supercontainers until prevented from doing so by the drift walls, whereupon its swelling pressure will start to increase.

Buffer swelling pressure differences between the inside and outside of the supercontainer shell will cause the supercontainer shells to deform and possibly rupture (Figure 5-6). This is also discussed in Section 5.4.2. The various strain mechanisms that are involved in the early evolution of the supercontainer shells could have a detrimental effect on the outer part of the buffer depending on how the shells deform and they may generate heterogeneities in the buffer. This is an issue for further study. In relatively dry conditions (inflows at the lower end of the range for less tight drift sections) the possibility that the shell could subsequently peel open (probably along its weld) and partially contact the rock cannot currently be excluded. In wetter conditions, the supercontainer will also rupture, but extruded bentonite already present outside the supercontainer before the swelling pressure becomes large enough to cause rupturing is likely to prevent contact with the drift wall. The impact of supercontainer rupture on the homogeneity of the buffer clay is uncertain. Design solutions are being considered to optimise the size of the holes in the steel supercontainer shell to ensure that it does not breach during the buffer maturation period. Alternative materials are also being considered and will be addressed in the summary report of the KBS-3H project 2004–2007 /SKB/Posiva 2008/.

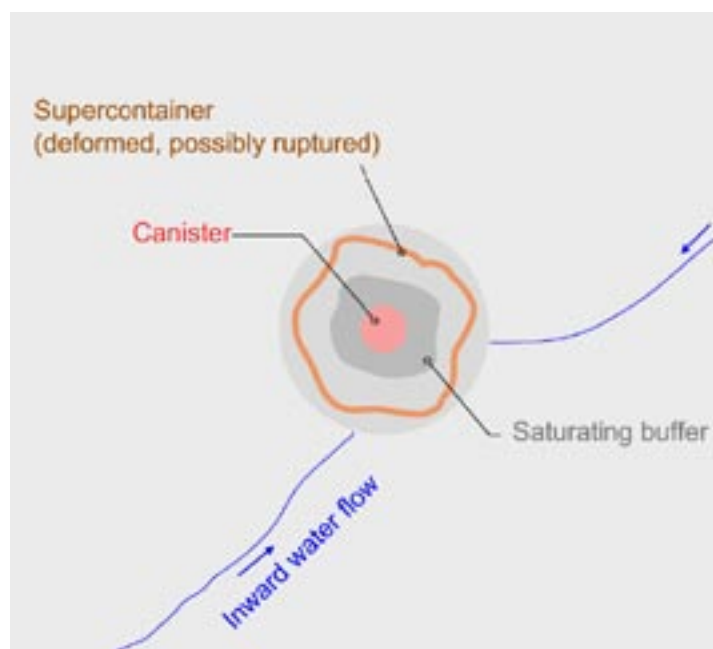


**Figure 5-6.** Filling of the gaps with bentonite and continuing buffer saturation.

Eventually, the buffer will become fully saturated and full swelling pressure will be reached. Figure 5-7 shows the results of finite element modelling of buffer saturation as a function of host rock hydraulic conductivity, in which the rock is treated as a homogeneous porous medium. The model, which takes coupled thermohydraulic processes<sup>22</sup> and water vapour transport into account, indicates that the saturation rate becomes insensitive to the hydraulic conductivity of the rock, with a minimum saturation time of about a decade, in less tight drift sections with hydraulic conductivities above about  $10^{-11} \text{ m s}^{-1}$ , where saturation is controlled by the ability of the bentonite to take up water (principally by capillary flow). This is in accordance with the minimum saturation times calculated for KBS-3V /SKB 2006c/. The rate of uptake of water by the buffer is, however, uncertain, and is affected by the salinity of the water. /Börgesson et al. 2005/ have shown that the rate of water uptake by bentonite and the consequent rate of increase of swelling pressure where the bentonite is confined are higher for saline water than for dilute water, although the final swelling pressure is lower for saline water than for more dilute water.

### Gas generation and migration

Gas, principally in the form of hydrogen, will be generated as a result of the anaerobic corrosion of steel components (principally the supercontainers shells, but also other steel components such as fixing rings – see Section 5.6.4). There is the possibility that some of this hydrogen will be consumed by microbially mediated reduction of sulphate to sulphide, or of carbonate to acetic acid or methane. The total volume of gas generated is, however, expected to be large /Gribi et al. 2007/. The gas generation rate will be determined by the corrosion rate, the surface area of the corroding components (which will vary only slowly with time) and by the availability of water (in the form of liquid or water vapour).

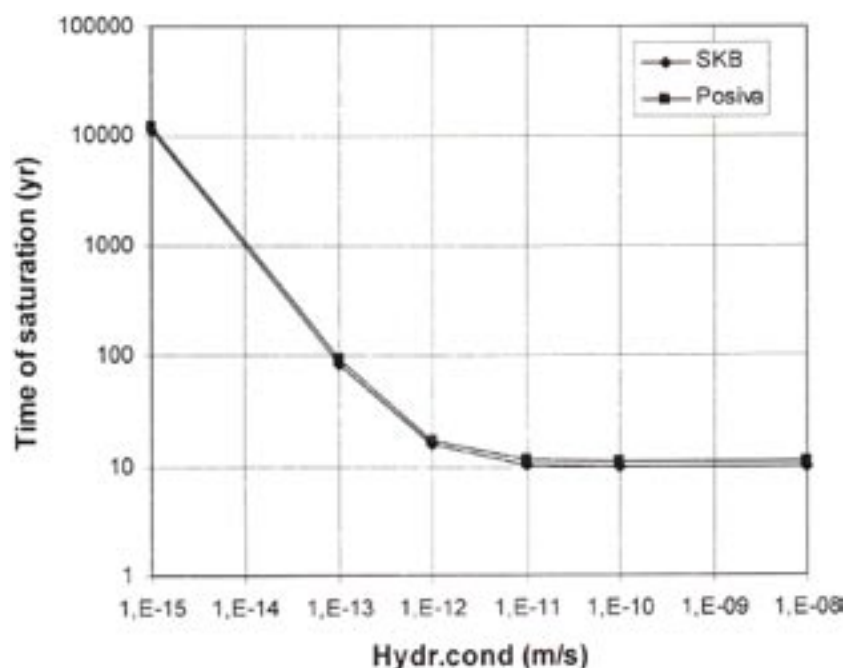


**Figure 5-7.** Time to saturation for different hydraulic conductivities. The curves are plotted according to SKB's and Posiva's different model geometry for the canister (e.g. length of the canister) and the near field. (from Figure 8-14 of /Börgesson et al. 2005/).

<sup>22</sup> As noted in Section 5.2.4, heat generated by the spent fuel will not significantly slow the rate of saturation, since the increased hydraulic conductivity of the buffer at elevated temperatures largely compensates for the thermally driven transport of vapour outwards from the buffer.

Gas will dissolve in the liquid water contacting the corroding surfaces and will migrate away from the surfaces by diffusion. However, assuming a corrosion rate of 1–2  $\mu\text{m}$  per year (see Section 5.6.4 for a discussion of corrosion rates), the rate of hydrogen generation exceeds the rate at which it can be removed by dissolution<sup>23</sup> and diffusion (Appendix C or /Gribi et al. 2007/) and a gas phase will therefore form.

Depending on if and how they rupture, the supercontainers may become surrounded by bentonite or bentonite gel, or be pushed against the drift wall. Those surfaces in contact with bentonite will be subjected to an increasing swelling pressure, which will provide resistance to the migration of the gas that accumulates there. As gas pressure increases, so will the amount of gas dissolved in the porewater at the porewater/gas interface, increasing the concentration gradient for diffusion. Nevertheless, calculations reported in Appendix C of /Gribi et al. 2007/ indicate that dissolution and diffusion remain insufficient to balance the rate of gas generation, and pressure will continue to increase until it is sufficient to create pathways for migration through the buffer to the drift wall (Figure 5-8).

The detailed processes involved in gas migration through bentonite are still under debate /Nagra 2002, Rodwell 2005/. Fracturing or micro-fracturing are the most likely mechanisms /Harrington and Horseman 2003/. Laboratory studies by /Pusch et al. 1985, Horseman et al. 1999/ and /Tanai et al. 1997/ show that gas breakthrough within bentonite occurs at a pressure approximately equal to the sum of the bentonite swelling pressure (7–8 MPa at full saturation)

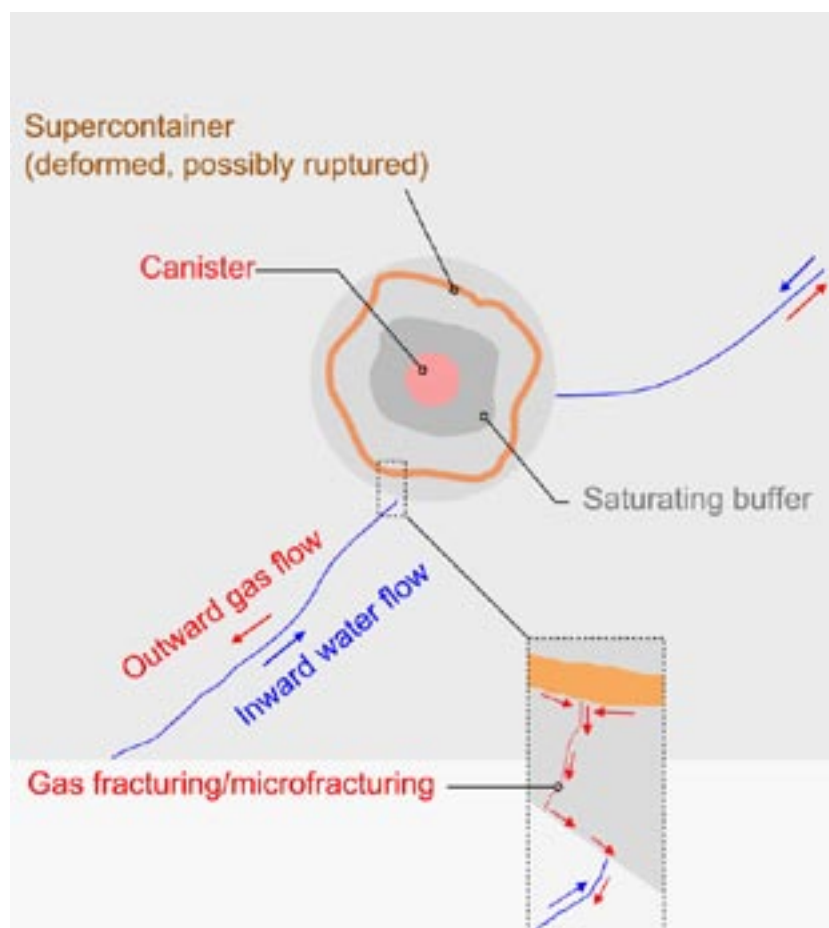


**Figure 5-8.** Gas generation and migration.

<sup>23</sup> The background hydrogen concentration at Olkiluoto is far from the solubility limit and may be neglected in the context of the evaluation of gas dissolution /Rasilainen 2004/.

and the hydrostatic pressure (4 MPa at a depth of 400 m), i.e. at approximately 11–12 MPa at full saturation. Some recent experiments have shown that the breakthrough pressure of gas through bentonite can be substantially higher than this (above 20 MPa for bentonite with a swelling pressure of ~ 6 MPa), although, after gas breakthrough has occurred, the gas pressure drops to the sum of bentonite swelling pressure and porewater pressure (Section 2.3.3 in /SKB 2006c, Harrington and Horseman 2003/). The gas breakthrough pressure is probably significantly less for the thin layer of low density bentonite or bentonite gel between the supercontainer shell and the drift wall compared with the bulk of the buffer, although gas pressure increase could compress the lower density material to some extent and thereby increase the gas pressure required for breakthrough. The formation of gas pockets and resulting compression of the clay could in principle also cause delay and non-uniformity in the saturation of the buffer, some opening of fractures intersecting the drift, and some transient increase in the load on the canister. Although these effects have not been evaluated quantitatively, they are transient in nature and are not expected to have any significant impact on the final saturated state of the buffer and rock, or to compromise canister integrity (the expected minimum pressure giving rise to total collapse of an intact canister is 80–114 MPa – see, e.g. Section 4.3.1 of /Pastina and Hellä 2006/).

Another source of uncertainty is the impact of chemical interaction with corroding iron on the gas migration properties of the buffer. The interaction of iron corrosion products with the buffer is discussed in Section 5.6.4 and 6.5.3. Although there is only limited understanding of gas migration in chemically altered smectite, it is known that the microstructural constitution of iron-saturated MX-80 is characterised by channels, allowing gas migration at rather low pressures, which may cause erosion and widening of the channels with little chance of self-sealing. This is an issue for further investigation that is also relevant to KBS-3V because of the iron in the canister insert.

Having reached the drift wall, gas will migrate along the drift, until it enters the host rock, probably via intersecting transmissive fractures. Whether this gas flows predominantly along the interface between the buffer and the drift wall or along the EDZ is uncertain. To create pathways along the interface, gas must overcome the swelling pressure exerted by the buffer on the drift wall (7–8 MPa at full saturation). On the other hand, to migrate along the EDZ, gas must displace groundwater in EDZ fractures. In order to do so, its pressure must exceed the sum of the hydrostatic pressure (4 MPa) and the capillary forces in these fractures (which are rather small compared with the hydrostatic pressure – about 0.15 MPa<sup>24</sup>). Thus, some gas migration along the EDZ is likely. In less tight drift sections intersected by transmissive fractures, the intrinsic permeability of the EDZ will largely determine the rate of gas migration for a given pressure gradient. Its value is, however, uncertain (Section 4.1.2), and may also change over time. There is a range of processes that could lead to partial or complete closing of fractures or microfractures within the EDZ, such as the development of buffer swelling pressure on the drift wall, bentonite intrusion and mineral precipitation. There is currently no quantitative evaluation of these effects. Finally, the EDZ will not be fully gas saturated and the effective permeability will be less than the intrinsic permeability. The saturation state of the EDZ and its evolution with time has not been quantitatively evaluated.

Whatever the predominant migration route, once gas migration pathways are created, a situation of equilibrium is likely to be established between gas generation and loss to the host rock by two-phase flow in fractures, as well as, to a lesser extent, dissolution and diffusion. Considering gas migration along the EDZ, and assuming a permeability of the EDZ which is 10% of the measured intrinsic permeability, calculations reported in Appendix C of /Gribi et al. 2007/ indicate that, in drift sections intersected by transmissive, larger-aperture fractures (with hydraulic

---

<sup>24</sup> The gas entry pressure into EDZ fractures depends on fracture aperture, the expected range for which has been evaluated based on microfractographic characterisation of samples from the Research Tunnel at Olkiluoto. Although there are significant uncertainties in the characterisation of apertures over a wide range, the fact that the calculated gas entry pressure is only about 5% of the hydrostatic pressure means that these uncertainties are not important in the evaluation of gas overpressures /Autio et al. 2005/.



transmissivities calculated by the cubic law exceeding about  $10^{-10} \text{ m}^2 \text{ s}^{-1}$ ), the maximum gas pressures reached at the drift wall in this equilibrium situation will be only slightly above the hydrostatic pressure of 4 MPa; gas will be readily dissipated via these fractures and there will be no significant volume of compressed gas at the drift wall.

Having migrated to the buffer/rock interface and into the rock, it is possible that hydrogen will cause some transient perturbation to the groundwater flow, and that it will participate in the reduction of sulphate to sulphide by sulphate reducing bacteria, giving rise to a transient increase the rate of canister corrosion. These issues are discussed in Sections 5.3.1 and Appendix B.7, respectively.

### ***Cessation of gas production and dissipation of gas pressure***

The rate of gas generation will eventually fall as smaller steel components (components with the highest surface area to volume ratio) are consumed, and will cease altogether upon the complete corrosion of all steel components, which is expected to take a few thousand years. Gas pressure will then fall until it is no longer sufficient to drive two-phase flow in transmissive fractures intersecting the drift section, in the rock matrix or in the EDZ, or is insufficient to maintain gas pathways along the bentonite/rock interface. Thereafter, gas pressure within the buffer will continue to fall more slowly as gas dissolves and is dissipated by diffusion. Complete dissolution of the gas and dissipation by diffusion may take a further several thousand years.

### **5.5.3 Expected evolution in tighter drift sections**

Saturation and buffer swelling in tighter drift section can again be described in terms of a series of broad stages.

#### ***Inflow and the filling of the gaps around the supercontainers with bentonite***

In tighter drift sections, water will again enter through transmissive fractures and accumulate in the lower part of the drift, but will do so more slowly than in the case of less tight drift sections. The gap between the distance blocks will fill with swelling bentonite, either as a result of the uptake of inflowing water, or, where the rate of inflow is sufficiently small, uptake moisture from the air in the drift (Section 4.1.2). At least during the operational period, the physical integrity of the buffer around the canisters will be largely maintained, and the buffer contained, by the presence of the supercontainers, but the distance blocks will begin to swell and may crack even where there is little free, liquid water present.

Experimental and modelling studies indicate that the time required for the gap between the distance blocks and the drift wall to be filled by humidity-induced swelling of the buffer is in the order of three months (Section 10.3.2 of /Börgesson et al. 2005/; Appendix L of /Autio et al. 2007/). The rate is determined by the vapour transport rate in air between the drift wall and the buffer. This in turn is determined by the relative humidity (RH) at the rock surface (which was assumed to be 100% in the scoping calculations, but may be less if the water flux in the rock is sufficiently small), the RH at the distance block surface (which depends on the water ratio in the bentonite at the distance block surface) and the transport mechanism in air (which was assumed in the scoping calculations to be purely diffusive).

The buffer inside the supercontainers will also absorb water either due to contact with free water accumulated at the bottom of the gap or, more likely, by the uptake of humidity from the air. In either case, this will increase the swelling pressure exerted on the inner surfaces of the supercontainer shells. If free water is present, bentonite will be extruded as a gel through the perforations in the lower part of the supercontainer. The bentonite outside the supercontainers will initially be of low density, and exert a smaller swelling pressure than the bentonite inside, leading to elasto-plastic deformation and possibly to rupturing of the supercontainer (Figure 5-9). If no free water is present, there will be no extrusion of bentonite through the



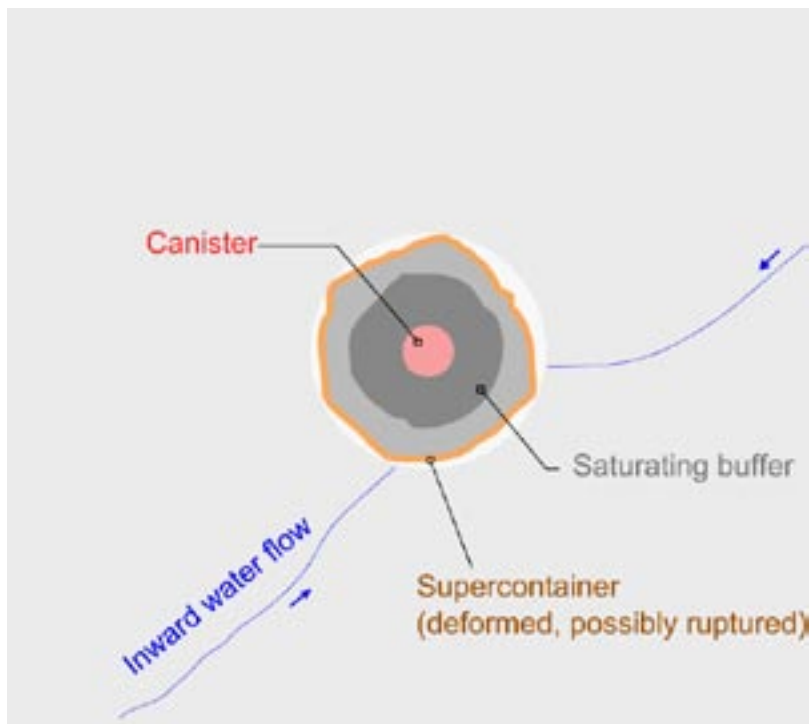


**Figure 5-9.** Water inflow and filling of the gaps around the supercontainers with bentonite (no free water present in drift).

supercontainer perforations. Some cracking of the buffer is likely after a few months, and some small fragments may fall to the drift floor though the perforations in the supercontainer shells (experimental studies have shown humidity-induced cracking after about 3 months for bentonite with an initial water content of 10% – see Appendix L of /Autio et al. 2007/). The increase in swelling pressure inside the supercontainers due to the absorption of water vapour will eventually be sufficient to cause supercontainer deformation or rupture. Timing of rupture is uncertain, but is estimated to require a few months. In these tighter drift sections there is a possibility that ruptured supercontainers will contact the drift wall. The buffer will then swell into the remaining void spaces as a relatively stiff mass, rather than as a gel.

### **Continuing buffer saturation**

The rate of continuing buffer saturation in these tighter drift sections will be controlled principally by the (more limited) rate of inflow from the rock. The transition between buffer saturation times controlled by the rate of inflow from the rock in tighter drift sections and those controlled by the rate of uptake by the buffer in less tight drift sections is shown by the change in gradient in Figure 5-7 at average rock hydraulic conductivities of around  $10^{-12}$  to  $10^{-11}$  m s<sup>-1</sup>. Calculations in Appendix B.3 indicate that saturation of a drift section by inflow from rock with an average hydraulic conductivity of  $10^{-12}$  m s<sup>-1</sup> will require about 23 years, with 230 years being the saturation time in the case of an average rock hydraulic conductivity of  $10^{-13}$  m s<sup>-1</sup> (roughly consistent with the results of more detailed modelling shown in Figure 5-7).

As well as direct inflow from fractures in the rock, there are potential pathways that run parallel to the drift axis and via which water may, in principle, enter a tighter drift section from a less tight drift section. These are illustrated in Figure 5-10, and comprise:

- (i) the distance block matrix;
- (ii) the EDZ around the drift, and
- (iii) the buffer/rock interface – i.e. piping.

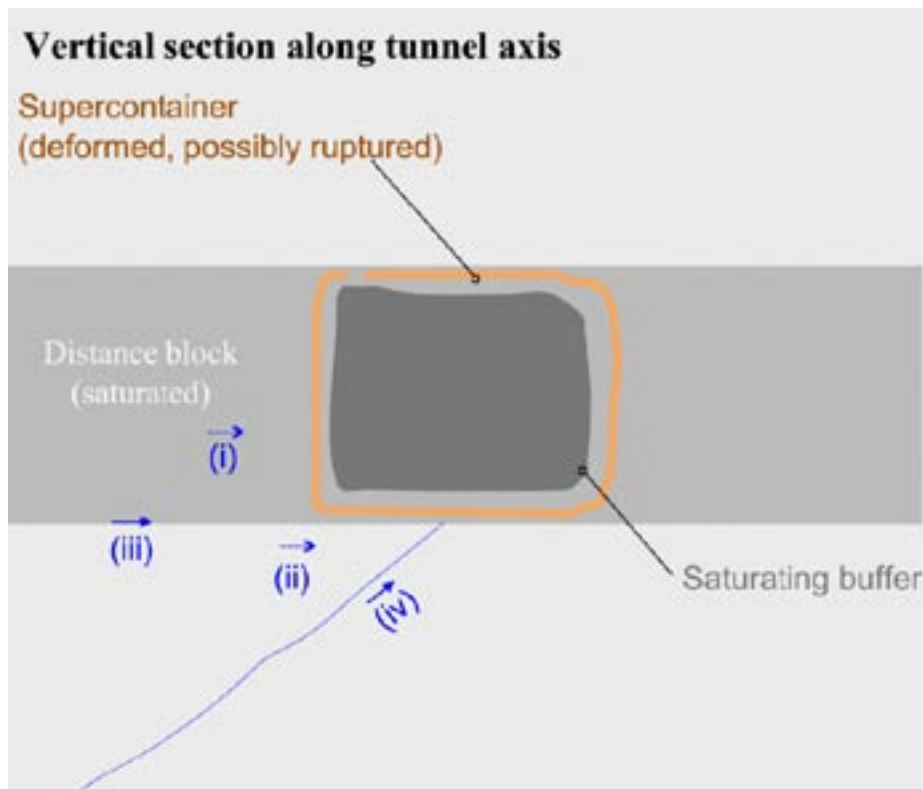


**Figure 5-10.** Continuing buffer saturation – potential inflow pathways through (i), the distance block matrix, (ii), the EDZ around the drift, (iii), the buffer/rock interface (i.e. piping) and (iv), a fracture intersecting the supercontainer volume.

Water migration along these pathways will be driven by hydraulic pressure differences across the distance blocks separating the less tight and tighter sections. These pressure differences will develop as the hydraulic pressure in the water around the supercontainers in the less tight sections increases towards equilibrium pressure, while water/trapped air pressures in the tighter sections remain relatively low.

Scoping calculations of the impact of migration along a drift via these axial paths on saturation times are described in Appendix B.3. The hydraulic conductivities of the distance blocks and the drift EDZ are low. Although there are significant uncertainties, the scoping calculations suggest that saturation of the buffer by pathways (i) and (ii) alone would require at least about a thousand years to complete, and possibly up to some tens of thousands of years. Referring to Figure 5-7, these pathways are unlikely to dominate over inflow from the host rock (pathway (iv) in Figure 5-10) unless the hydraulic conductivity of the rock is about  $10^{-14} \text{ m s}^{-1}$  or less (Section 5.5.4, below).

Situations that could lead to piping (i.e. pathway (iii) in Figure 5-10) are avoided by design and, even if it were to occur, its impact on saturation times would be limited (Section 5.5.6).

### **Gas migration through the bentonite-filled gaps**

As in the case of less tight drift sections, gas will be generated continuously by the corrosion of steel components as the buffer saturates and swells. Again, an equilibrium situation will be established between gas generation and the outward gas migration through the host rock, probably via intersecting fractures. Gas will, however, be less readily dissipated via these fractures compared with the case of less tight sections, and there will be a more significant volume of compressed gas near the drift wall, probably in the EDZ or at the interfaces between the supercontainer and the buffer and between the buffer and the drift wall. This gas will also be

present at higher pressures. Calculations reported in Appendix C or /Gribi et al. 2007/ indicate that pressures of up to about 7 MPa are developed in a drift section intersected by a fracture with a hydraulic transmissivity of  $10^{-12} \text{ m}^2 \text{ s}^{-1}$ . On the other hand, the calculations also indicate that development of gas over-pressures will require in the order of 100 years, by which time the buffer is expected to be largely saturated. Thus, although a gas phase will remain in or around the drift for as long as gas generation continues (a few thousand years), the presence of this gas is not expected to affect the saturation of the buffer significantly.

### ***Cessation of gas production and dissipation of gas pressure***

Once gas generation ceases after a few thousand years, gas pressure will fall until it is no longer sufficient to drive two-phase flow in the transmissive fractures intersecting the drift section, in the rock matrix or in the EDZ, or is insufficient to maintain gas pathways along the bentonite/rock interface. Thereafter, gas pressure will continue to fall more slowly as gas dissolves and is dissipated by diffusion.

## **5.5.4 Expected evolution in tightest drift sections**

In the tightest drift sections, saturation and buffer swelling can be described in terms of the following broad stages.

### ***Humidity-induced changes in the first few months***

Following buffer emplacement, the bentonite will take up moisture from the air in the drift, mainly in the form of water vapour originating from the rock. The water cushion system used by the deposition vehicle may also provide a source of water vapour during the operational period (see Section 4.1.2). Significant inflow and accumulation of liquid water in the gaps around the supercontainers and distance blocks in these tightest drift sections is unlikely. The rate at which moisture uptake from the rock occurs will be reduced if the rock has undergone any desaturation during the time that the drift stays open (which will be less than a month, according to /Autio et al. 2007/). From an examination of the moisture retention curves of buffer and rock, desaturation of the rock is not, however, expected to lead to any loss of water from the buffer surface. For example, based on the curve<sup>25</sup> reported by /Börgesson and Hernelind 1999/, the suction of the buffer exceeds that of the rock by a factor of 8 for an equivalent degree of saturation of 0.5.

Humidity-induced swelling of the distance blocks will cause the gaps between the distance blocks and the drifts wall to fill with bentonite in about three months. The buffer inside the supercontainers will also absorb water vapour from the air and will exert a swelling pressure on the supercontainer walls. Some cracking of the buffer is likely after a few months, and some small fragments may fall to the drift floor through the perforations in the supercontainer shells. Swelling pressure may eventually increase sufficiently to deform or rupture the supercontainers, but this could take up to several years. Thereafter, the buffer will swell into the gaps around the supercontainers as a relatively stiff mass. Some gas-filled void spaces may remain.

### ***Increasing gas pressure***

Humidity will also lead to gas generation by corrosion of the supercontainers (and other steel components) and the gas pressure in remaining void spaces will rise. The rate of generation of hydrogen has been estimated at about  $0.2 \text{ m}^3 \text{ STP a}^{-1}$  for each supercontainer, assuming a steel corrosion rate of  $1 \text{ } \mu\text{m}$  per year (see Section 5.6.4 for a discussion of corrosion rates).

---

<sup>25</sup> The applicability of the curve is, however, subject to some uncertainty, since it is based on measurements at the Grimsel test Site in Switzerland, rather than at the Olkiluoto site.

Considering the gaps around the supercontainers and disregarding the possible rupturing of the supercontainer and filling of these gaps with bentonite, the time taken for repository-generated gas to pressurise the 1.5 m<sup>3</sup> open volume to the hydrostatic pressure (about 4 MPa once the drawdown due to repository construction and operation has subsided) will be approximately<sup>26</sup>:

$$\frac{1.5 \text{ m}^3}{0.2 \text{ m}^3 \text{ STP a}^{-1}} \times \frac{4 \text{ MPa}}{0.1 \text{ MPa}} = 300 \text{ years} \quad (\text{Eq. 5-1})$$

As the gas pressure around the supercontainers approaches the equilibrium pressure, the rate of any small water inflow to remaining void spaces via paths (i)–(iv) in Figure 5-10 will be further reduced, and will largely cease once the equilibrium pressure is reached, although some water may continue to enter the buffer, drawn in from the rock by capillary forces.

The reduction or prevention of water inflow as a result of gas pressurisation was not taken into account in the calculations used to derive Figure 5-7, which is therefore expected to provide an underestimate of saturation times in the tightest drift sections.

Both steel corrosion and suction/condensation in the buffer will take up moisture in the form of vapour and tend thus to maintain a vapour pressure gradient from the rock towards the interior of the drift (see Appendix B.6, Figure B.6-1). It is, however, important to note that the conversion of water to corrosion products is an irreversible process and is thus a true sink, whereas the uptake/condensation of moisture in buffer may be reversed by evaporation/removal (drying of bentonite – note that drying of bentonite is common in the fabrication of bentonite blocks or pellets). After a transient period, a steady-state vapour flux is likely to be established, where the consumption of water at the steel surface (the sink) is balanced by transport of vapour towards this sink from the rock and, if the supply of moisture from the rock is small, from the interior of the buffer. Thus, provided a sufficiently high relative humidity can be maintained at the corroding surfaces<sup>27</sup>, corrosion is expected to continue, maintained by the supply of water from the buffer, even if there is no significant supply of water in the form of vapour from the rock.

### **Outward migration of gas**

As corrosion of the supercontainers proceeds, the gas pressure in the drift section will continue to increase above the hydrostatic pressure until it is sufficient to create and maintain pathways for further migration. In the absence of transmissive fractures, possible routes for the outward migration of gas include:

- migration along the deposition drift via the distance block/rock interface or through the EDZ, eventually reaching either a drift section in fractured rock or the transport tunnel system; and
- reactivation of existing but hydraulically tight fractures.

Whatever the pathways for outward migration from tight drift sections, an equilibrium situation will again develop between gas generation and outward gas migration. The equilibrium gas overpressure in the drift will continue to prevent water inflow.

If the EDZ is too tight to allow significant gas flow, the equilibrium gas overpressure will correspond to the pressure required either to reactivate existing but hydraulically tight fractures in the EDZ or the surrounding rock, or to create gas pathways along the distance block/rock interface. Reactivation of fractures in the host rock could occur if the gas pressure exceeds the minimum principal rock stress component, which is assumed to be about 9 MPa at a repository

<sup>26</sup> The calculation disregards the loss of gas due to dissolution and diffusion, which will lead to slightly longer gas pressurisation times. It also disregards any open volume that may remain around the distance blocks in tight drift sections, although humidity-induced swelling will reduce this.

<sup>27</sup> As also noted in Appendix B.7, corrosion is strongly reduced for relative humidities below 0.6. In the presence of hygroscopic salts on the steel surface, the threshold value for the relative humidity allowing corrosion may be even lower (in the order of 0.4).

depth of 400 m (Section 2.2.5). If, on the other hand, the EDZ is sufficiently gas permeable that it forms the principle pathway for gas flow, it will be the effective gas permeability of the EDZ that determines the equilibrium overpressure that is established. The gas permeability of the EDZ will in turn depend on the intrinsic permeability of the EDZ (permeability at full gas saturation – see Section 5.5.2) and the EDZ saturation state.

Calculations reported in Appendix C of /Gribi et al. 2007/, which assume a permeability of the EDZ which is 10% of the measured intrinsic permeability, indicate that gas pressures will be a few MPa higher than the hydrostatic pressure in these drift sections, but still below the sum of the bentonite swelling pressure and the hydrostatic pressure (11–12 MPa), and also below the minimal principal stress at Olkiluoto (about 9 MPa). Thus, the EDZ is a potential migration route for gas away from tight drift sections; neither the reactivation of hydraulically tight fractures nor the formation of pathways along the bentonite/host rock interface is expected in such sections.

### ***Cessation of gas production and dissipation of gas pressure***

Once gas generation ceases after a few thousand years, gas pressure will fall until it is no longer sufficient to drive two-phase flow in transmissive fractures intersecting the drift section (pre-existing or reactivated), in the rock matrix or in the EDZ, or is insufficient to maintain gas pathways along the bentonite/rock interface. Thereafter, gas pressure will continue to fall more slowly as gas dissolves and is dissipated by diffusion. Once the gas pressure falls below the hydrostatic pressure, water will slowly migrate into the drift section via host rock fractures, the distance block matrix and/or the EDZ. Gradual saturation of the buffer will then continue until a state of full buffer saturation is reached.

### **5.5.5 Plugged sections**

As described in Section 2.3.3, highly transmissive fractures intersecting the drift may render particular sections unsuitable for the emplacement of supercontainers and distance blocks. Pairs of steel compartment plugs will be used to seal off drift sections where inflows are higher than 1 litre per minute (after grouting), thus dividing the drift into compartments. The space in between the plugs will be filled with a permeable, erosion-resistant material, although only a tentative design has so far been developed.

These drift sections are expected to become rapidly saturated following installation of the second compartment plug. Water inside the pore spaces of the filling material will then exert a pressure on the compartment plugs equal to the hydrostatic pressure (about 4 MPa once transient drawdown effects have ceased). The plugs are, however, designed to withstand a load of 5 MPa from either side and should, therefore, remain functional and not be significantly deformed or displaced by the hydraulic pressure differences across them.

As the buffer adjacent to the compartment plugs swells and saturates, any flow past the compartment plugs will largely cease due to the low hydraulic conductivity of the saturated buffer and the high swelling pressure exerted on the drift wall. There may be some transient, early water flow past the plug from the sealed off section to the adjacent compartments before full saturation occurs. It is a design criterion on the compartment plugs that this water flow should not be large enough to lead to piping at the buffer/rock interface and erosion of the buffer (Section 2.4.2).

The steel compartment plugs will corrode over time (Section 5.6.4), releasing hydrogen gas. On the side of the plugs adjacent to the buffer, the migration of gas through the bentonite will take place as described in the previous sections. No significant build up of gas pressure is expected to take place within a sealed off section, due to the high gas permeability of the intersecting fracture zone.



## 5.5.6 Possible deviations from expected evolution

### ***Potential for transient water flows to cause erosion***

Transient water flows from less tight drift sections with rapidly water-filled gaps to tighter, drier drift sections could, in principle, lead to erosion that could perturb the safety functions of the buffer. Gas piping could also occur as a result of gas pressure differences between less tight drift sections, with intersecting transmissive fractures along which gas from the corrosion of steel components can readily escape, and tighter drift sections, where high gas pressures can develop. Gas piping is not expected to have any impact on the capacity of the buffer to fulfil its safety functions and is not discussed further in this report, although no quantitative evaluations have been made.

Potential paths for the migration of water from a drift section with a water-saturated gap are sketched in Figure 5-11. Path (i), which is through the distance block matrix, is not relevant in this context, since any suspended buffer material would be filtered by the fine matrix pore structure. Paths (ii) and (iii), i.e. through the EDZ around the drift and along the buffer/rock interface, could, however, in principle convey suspended buffer material from one part of the drift to another. Water and suspended buffer material could also, in principle, migrate via path (iv) through transmissive fractures (if they exist and are not avoided in selecting supercontainer emplacement positions) to other parts of the same drift compartment that are more slowly saturated, to neighbouring open compartments in the same drift, or to adjacent open drifts or transport tunnels.

Scoping calculations presented in Appendix B.4 indicate that the redistribution of bentonite by erosion into a transmissive fracture – path (iv) – is unlikely to have a detrimental effect on the capacity of the eroded buffer to perform its safety functions (i.e. buffer density remains within the range 1,890 to 2,050 kg m<sup>-3</sup> discussed in Section 5.3.2), even if flow to other underground openings persists for a year or more.

The hydraulic properties of the EDZ are currently not well characterised (Section 4.1.2), and processes may occur that could lead to the closing of fractures within the EDZ (e.g. the swelling of the bentonite, bentonite intrusion, mineral precipitation) have not been evaluated quantitatively. In spite of these uncertainties, the hydraulic conductivity of the EDZ is expected to be low and, although the pressure differences along it may be large, flow via path (ii) is expected to be small.

Flow along the distance block/host rock interface from the water-filled gap around one supercontainer to the unfilled void space around another (path (iii) in Figure 5-11) has been experimentally observed under certain conditions. Flow occurs in discrete channels and is termed “piping”. The creation and maintenance of such channels along the bentonite/host rock interface is, on the one hand, favoured by the hydraulic pressure differences that drive the flow, which will develop over time as drift sections fill with water at different rates. On the other hand, the increasing density of the bentonite adjacent to the drift wall and the increasing swelling pressure exerted on the interface inhibits the creation of new pathways, and will tend to close those that may already exist (although, if piping occurs, some residual loss of buffer density and swelling pressure along the paths is likely to remain – see the modelling study by /Börgesson and Hernelind 2006b/). Thus, both the rate at which hydraulic pressure differences develop and the magnitude of these differences are critical factors in determining whether, and for how long, piping will occur; both are subject to uncertainties.

The issues of piping and erosion of the buffer by piping have been investigated in a series of experimental and modelling studies (Appendix L of /Autio et al. 2007/). These studies have been used to guide repository design and, in particular, the dimensioning of the distance blocks, to avoid the possibility that significant piping and erosion will occur. As described in Section 2.3.4, the reference distance block design uses two different bentonite components in series; a “tight” block and a “loose” block. It is the “tight” block that seals most rapidly, giving protection against piping and erosion. The current reference design for the “tight” block has been shown experimentally not to undergo piping in both a reference scenario and a more



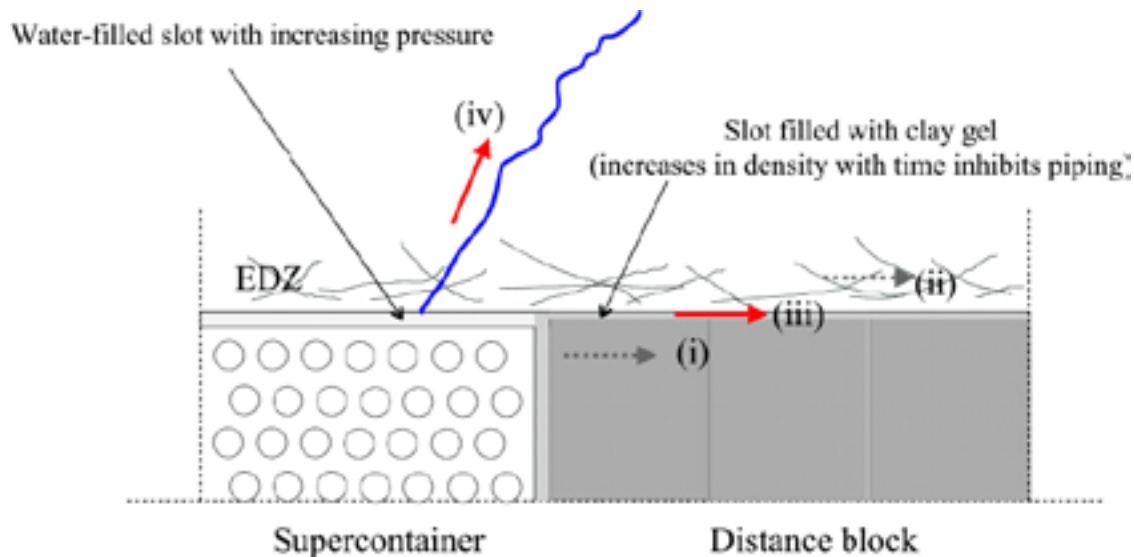


**Figure 5-11.** Potential paths for the transport of water and suspended buffer material (ii), (iii) and (iv). In the case of path (i), suspended buffer material would be filtered and unable to migrate.

pessimistic scenario, assuming there is no significant mechanical displacement of the distance blocks (see Potential for mechanical displacement and compaction of supercontainers and distance blocks, below). The reference scenario involves a 0.1 litre per minute inflow to the gaps around a supercontainer adjoining the block, a 100 kPa per hour rate of hydraulic pressure increase following filling of the gaps with water and a maximum hydraulic pressure difference across the block of 2 MPa. In the more pessimistic scenario, the conditions are 1 litre per minute inflow, a 1 MPa per hour rate of hydraulic pressure increase and a 5 MPa maximum hydraulic pressure difference. On the basis of these studies, it is concluded that piping and erosion are unlikely to occur in the reference design given the current criterion on the maximum inflow rate to a supercontainer drift section of 0.1 litres per minute (again assuming there is no significant mechanical displacement of the distance blocks). However, it is unclear whether all possibilities regarding piping and erosion can be addressed in such calculations, because of uncertainties associated with some of the assumptions. Therefore, these results are not sufficient to give guidance on the design requirements regarding the avoidance of piping and erosion. As described in Section 2.3.3, where drift sections do not fulfil this criterion, either filling blocks are installed, or, if significant subsequent erosion of these blocks cannot be excluded, the drift sections will be isolated using compartment plugs.

Even if piping or significant flow along the EDZ were to occur, the effects on the saturation time of the tighter drift section at the downstream end of these flows would be limited (see the scoping calculations in Appendix B.3). Water flows via paths (ii) and (iii) in Figure 5-11 could only be maintained while a “sink” at the downstream end of the paths exists. If, at the downstream end, further water flow is prevented (i.e. by a compartment plug or a distance block that has swollen sufficiently to seal the gap to the drift wall) then flow along the path will essentially cease once the gaps in the downstream drift section become water filled. The flows could lead to the relatively rapid saturation of the downstream gap, following which the pressure gradient driving flow would diminish and (in the case of path (iii)) the pipes reseal. The buffer inside the supercontainer would remain only partly saturated once piping had ceased. The limited duration of flow also means that the potential of piping (should it occur) to cause redistribution of buffer mass is limited once a compartment has been plugged. Assuming rapid homogenisation of any local density reductions, the scoping calculations presented in Appendix B.4 indicate that any redistribution of buffer mass would not significantly perturb the safety functions of the buffer (i.e. buffer density remains within the range 1,890 to 2,050 kg m<sup>-3</sup> discussed in Section 5.3.2) provided:

- the total suspended solids ratio of the bentonite suspension carried by the paths is not too large (in the order of a few weight %); and
- the volume available to be filled with bentonite suspension carried by the pipes is not too large (a few supercontainer units).

There are, however, significant uncertainties in the degree to which the buffer would homogenise following significant localised erosion. Homogenisation will be resisted by internal friction within the buffer and friction between the buffer and fixed surfaces. /Börgesson and Hernelind 2006b/ carried out a modelling study of the homogenisation of a KBS-3V buffer, including the resealing of pipes and buffer swelling following a local loss of buffer mass, e.g. due to piping. The calculations showed that, due to friction, locally decreased densities and swelling pressures and increased hydraulic conductivities will persist indefinitely. A loss of swelling pressure in some supercontainer sections due to piping and erosion could lead to enhanced thermal spalling due to reduction in confining pressure associated with time-dependent degradation of rock strength (see Section 5.4.5). Thus, avoidance of piping remains a critical issue in repository design.

### ***Potential for mechanical displacement and compaction of supercontainers and distance blocks***

The hydraulic pressure differences between water-filled gaps in less tight drift sections and other, tighter parts of the drift could potentially give rise to deformation, mechanical displacement or compaction of distance blocks and supercontainer units. In the current reference design, displacement is prevented during compartment operation by the fixing rings that are installed along the drift and, following operations, by the compartment plug, which is designed to withstand full hydrostatic pressure at repository depth (Section 2.3.4). A critical issue, however, is the possibility that even a small deformation or movement of a distance block relative to an adjoining supercontainer could create an open gap along the vertical face of the block. Hydraulic pressure would then be exerted on the full surface area of the face, rather than the narrow annulus shown in Figure 2-10. In this situation, the fixing rings would not be adequate to prevent a more serious movement of the distance block, which would then increase the likelihood of piping along the bentonite/host rock interface. As noted in Section 2.3.2, further design developments are being considered to improve the robustness of the engineered barrier system with respect to possible distance block deformation and displacement by hydraulic pressure differences.

In the longer term, as the buffer swells and swelling pressure develops, some displacement and compaction of distance blocks and supercontainer units by differential buffer swelling pressure along the drift cannot be excluded. The scoping calculations given in Appendix B.4 indicate that any displacement and compaction that occurs will not be sufficient to cause significant change in the safety-relevant properties of the bentonite provided:

- the total linear compaction per supercontainer unit is not too large (a few centimetres, say); and
- the number of supercontainer units affected is also not too large.

Displacement and compaction will be resisted by friction between buffer (including the filling blocks) and the drift walls, which will increase with time as swelling pressure develops. The fixing rings and compartment plugs are not designed to withstand full buffer swelling pressure, and may undergo some small displacement. The installation of drift end plug and the backfilling of the repository access tunnels will, however, greatly limit the maximum extent of any displacement and compaction along the drift.

## 5.5.7 Wider impact on system evolution and safety functions

Saturation and swelling of the buffer are necessary for the buffer to fulfil its safety functions, as specified in Section 2.4.1, which are:

- protection of the canisters;
- limitation of radionuclide releases;

and, in the case of the distance blocks,

- separation of the supercontainers hydraulically one from another, thus preventing the possibility of preferential pathways for flow and advective transport within the drifts through the corrosion products or altered buffer.

Even in the tightest drift sections, the buffer is expected to retain its initial water content, and will eventually fully saturate, at which time it is expected to perform its full range of safety functions. Heterogeneity of the near-field rock will, however, result in widely differing saturation rates for different drift sections, with the tightest drift sections potentially remaining only partly saturated for up to thousands of years. Changes may occur during this time, including, for example, mechanical failure of the supercontainer shell, steel corrosion and the slow interaction of the corrosion products with the buffer (Section 5.6.4). The rates or timing of these changes may, to some extent, be affected by the saturation state of the buffer, but the processes themselves are expected to be the same in all drift sections. On the other hand, on a timescale of a few years, thermally-induced rock spalling may occur, but is most likely in drift sections in which the buffer does not sufficiently rapidly exert swelling pressure on the drift wall (Section 5.4.5).

In the course of the saturation process, the heterogeneity of the near-field rock results in gradients in hydraulic and swelling pressures that could, in principle, result in water flows (including piping), buffer erosion and the mechanical displacement of the supercontainers and distance blocks. These effects are not expected to perturb the final properties of the buffer to an extent that affects its safety functions, although some design issues related to the deformation and displacement of the distance blocks due to early hydraulic pressure differences along the drift remain.

Although significant perturbations to the buffer safety functions due to deviations from expected early evolution can probably be excluded, there remains the possibility that some limited redistribution of buffer mass may lead to somewhat modified diffusion coefficients. A radionuclide release and transport assessment case is defined in the Radionuclide Transport Report to evaluate the potential impact of an increase in diffusion coefficients in the case of a canister with an initial penetrating defect /Smith et al. 2007a/.

## 5.6 Evolution of chemical and microbiological conditions

### 5.6.1 Key aspects of the evolution of chemical and microbiological conditions in this period

A range of chemical and microbiological processes will take place during the transient phase, starting as soon as the first canister is emplaced in the repository:

- water infiltrating into the drift and entering the buffer will interact chemically with minerals in the bentonite;
- oxygen, which will be trapped within the drift by the compartment and drift end plugs, will be depleted due to microbially induced reactions or as it interacts with various system components;
- the steel components will corrode; and
- cement and various stray materials will interact with the host rock and with the buffer.

The impacts of these processes on the evolution of conditions within and around the repository are discussed in turn in the following sections.

### 5.6.2 Chemical evolution of the buffer

During the transient period, a range of chemical interactions between groundwater and bentonite will occur. Ion exchange in the buffer porewater will gradually reduce the swelling pressure and increase the permeability of the buffer, and impurities in the buffer will dissolve and be transported, while new minerals may precipitate.

Silica in the buffer close to the canister is expected to dissolve during the period of elevated temperature and be transported outwards by diffusion to colder parts where precipitation may take place. Buffer cementation could in principle take place due to the dissolution, transport and precipitation of silica or aluminosilicate minerals, but neither experimental nor natural analogue studies have shown that this process will actually occur. The effect of buffer cementation due to silica precipitation is, however, an issue for further work (see Chapter 12).

Cementation by precipitation of sulphates due to elevated temperatures around the canisters may lead to the formation of a zone in the buffer adjacent to the canisters with increased strength but reduced plasticity /SKB 2006c/. As temperatures and temperature gradients decrease however, it is likely that the precipitated solids will redissolve, and disperse within the buffer by diffusion.

Strongly reducing conditions will be maintained in the buffer following the depletion of trapped oxygen (Section 5.6.3). Under such conditions, structural iron in smectites, which occur in the buffer mainly as Fe(III), may be reduced to Fe(II). This could, in principle, have consequences for the stability and to some extent the hydraulic properties of the buffer /e.g. Foster 1953, Stucki et al. 1984, Karnland and Birgersson 2006/, although the mechanism of this redox process is still controversial and available experimental data are not representative of repository conditions.

At sufficiently high temperature, there is the possibility of a permanent collapse of the smectite stacks in a partly saturated buffer, which would modify its properties /Karnland and Birgersson 2006/. However, at the lower buffer temperatures that will arise in the repository (Section 5.2), collapse of the smectite stacks is not expected<sup>28</sup>.

### 5.6.3 Depletion of trapped oxygen and impact of microbial reactions

There are several chemical processes that may contribute to the depletion of trapped oxygen within the repository drifts, including microbially induced reactions near the bentonite/host rock interface and inorganic reactions with:

- minerals (especially pyrite) in the bentonite;
- the copper canister; and
- the KBS-3H steel supercontainer and other steel components (see also Section 5.6.4).

In the case of KBS-3V, numerical simulations of oxygen depletion have been carried out that account for oxidation of copper, microbially-induced oxygen consumption and oxidation of Fe(II)-bearing mineral impurities in the bentonite (Section 6.2.4 of /Pastina and Hellä 2006/). Furthermore, large-scale tests to evaluate oxygen consumption in bentonite have been carried out in the framework of the LOT project /Muurinen 2006/. Although there are significant uncertainties and variability between different locations within the repository, the numerical simulations and large-scale tests indicate that the timescale for oxygen depletion from individual KBS-3V deposition holes is no more than a few hundred years at most, and could be as little as a few years /Muurinen 2006/.

---

<sup>28</sup> The consequences of hypothetical cementation and cracking of the buffer in terms of solute transport through a damaged buffer have been investigated by /Neretnieks 2006/.

In KBS-3H, oxygen in the gap between the supercontainer and the rock will be consumed rapidly (on a timescale of months to a few years) by microbially-induced reactions and by steel corrosion. The oxygen trapped deeper inside the buffer will be depleted more slowly. In the outer part of the buffer, if this is near saturation, the rate of depletion will be controlled the slow rate at which oxygen will migrate by aqueous diffusion to the outer surface, where again it will be consumed by relatively rapid microbially-induced reactions and by steel corrosion. In the inner part of the buffer, if this is unsaturated, oxygen will be transported relatively rapidly to the copper canister surface, but reaction with the copper will be slow. Much of this oxygen may again, therefore, ultimately be consumed by microbially-induced reactions and by steel corrosion at the outer boundary of the buffer.

Since the presence of the steel supercontainer shell and other steel components in KBS-3H provides an additional sink for oxygen depletion, in addition to those present in and around a KBS-3V deposition hole, the timescale for oxygen depletion will certainly be no higher in KBS-3H than in KBS-3V (a few years to, pessimistically, a few hundred years), and could be somewhat less. Because the depletion timescale is likely to be controlled by the transport rate of oxygen within the buffer, rather than by reaction rates, any differences are likely to be quite limited, but they have not so far been possible to quantify.

After conditions have returned to anoxic, the presence of sulphate and corrosion-derived hydrogen gas or natural methane gas in the rock may nurture a population of sulphate-reducing bacteria at the buffer/rock interface, which may have some impact on the corrosion rate of the copper canisters by producing sulphide (Section 5.7.4). In the bulk of the buffer, however, both the culturability and the viability of microbes are expected to decrease with time. Provided the swelling pressure remains above about 2 MPa, microbes will be metabolically barely active after buffer saturation (see the buffer safety function indicator criteria, Table 2-3), due to the low water activity in combination with the high density and a swelling pressure that is less than the turgor pressure of the bacteria, which is reported to be around 2 MPa /Masurat 2006/. Low microbial activity is supported by the experimental findings of:

- /Pusch 1999/, who showed that SRB are immobile in bentonite exceeding  $1.9 \text{ Mg m}^{-3}$  saturated density;
- Pedersen and co-workers /e.g. Pedersen 2000/, who showed that the activity of SRB in bentonite ceases at densities higher than  $1.5 \text{ Mg m}^{-3}$ ;
- /Motamedi et al. 1996/, who showed that SRB did not survive the experimental period of 60 days at bentonite densities above  $1.8 \text{ Mg m}^{-3}$ ; and
- /Stroes-Gascoyne et al. 2006/, who noted that microbial activity is negligible above a swelling pressure of 2 MPa.

Thus, although the issue of microbial activity in the buffer is still under investigation, it is unlikely that significant microbially induced on the canister surface will occur.

#### **5.6.4 Corrosion of KBS-3H steel components**

A key difference between KBS-3H, as realised in the current reference design, and KBS-3V is the presence in KBS-3H of additional steel components (supercontainer and structural materials such as rings, supporting feet and compartment plugs) in the deposition drifts. These will start to corrode immediately upon emplacement, with corrosion continuing over a period possibly extending over a few thousand years after spent fuel emplacement. Eventually, corrosion products will replace the original steel components. The final corrosion products are stable and poorly soluble, but Fe(II) will nevertheless be slowly released to, migrate in and react with the buffer, potentially affecting its safety-relevant properties, as described below.



### **Initial period of aerobic corrosion**

During the operation of a drift compartment and for a short time thereafter (a few years to a few decades – see /Johnson et al. 2005/), some relatively rapid aerobic corrosion of the steel components will occur, but its overall contribution to the corrosion of the steel components is not expected to be significant.

### **Long-term corrosion rate and corrosion products**

Once oxygen is depleted, anoxic corrosion will take place. The expected initial corrosion product is magnetite, although, depending on solution conditions, some iron sulphide and siderite may also form (see e.g. Section 4.3.3 in /Johnson et al. 2005, Smart et al. 2001, 2004/). Subsequent film dissolution can produce iron silicates, as discussed below.

The conversion to magnetite proceeds according to the reaction:



and thus results in the production of hydrogen gas.

Magnetite can be made to form a thin but protective layer against corrosion with little or no connected porosity when produced under high pressure and temperature. In the repository, steel components external to the canister will be converted to magnetite under a high buffer swelling pressure, although the temperature will not be high. The porosity and hydraulic conductivity of the magnetite formed under these conditions are uncertain, and may be very low, although it may also be fractured and the possibility of it forming a hydraulically conductive layer at the buffer/rock interface cannot currently be excluded.

On the basis of corrosion studies in water and bentonite under anaerobic conditions lasting for a couple of years (see e.g. /Andra 2005/), the rate of corrosion is expected to decrease from an initially relatively high rate to a rate of a few microns per year, due to the formation of a protective layer of corrosion products. Long-term corrosion rates of about one micrometre per year, (see Section 5.7.1 in the Process report, /Gribi et al. 2007/), which are also corroborated by investigations on archaeological analogues /David 2001/, are insensitive to temperature over the temperature range expected (Section 5.2). They imply complete conversion of the 8 mm thick steel plate of the supercontainer, for example, in about 4,000 years.

In tight drift sections, the limited availability of water prior to buffer saturation may reduce the corrosion rate still further, as examined in scoping calculations in Appendix B.6. These calculations indicate that, if there is no inflow of liquid water (e.g. because of a lack of transmissive fractures or because of a build up of gas pressure, as discussed in Section 5.5.4), then transport of water vapour from the buffer is sufficient to maintain a corrosion rate of only about 0.1 µm per year.

The presence of bacteria on the steel surfaces could result in increased pitting and/or in the precipitation of iron sulphide phases. As noted in Section 5.6.3, provided, as expected, the buffer swelling pressure remains above about 2 MPa, no significant microbial activity is expected to occur in the buffer, and there will thus be no significant microbial activity on steel components embedded within the buffer. Studies performed by /JNC 2000/ confirmed that sulphate-reducing bacteria (SRB) introduced into bentonite surrounding steel samples had no effect on corrosion rates and were not cultivatable after the test. Bacteria may, however, be present on steel surfaces:

- where steel components contact the drift walls (e.g. the fixing rings, or possibly the supercontainer if this is ruptured and pressed against the drift wall by the swelling buffer);
- in tight drift sections, before there is significant extrusion of bentonite into the open space between the supercontainers and the drift walls; and
- where the bentonite contacting steel components is chemically altered by interaction with corrosion products, and locally loses some of its density and swelling pressure (as discussed below).



Natural analogue observations of low steel corrosion rates /e.g. David 2001/ in soils and sediments in which microbial populations are relatively large suggest, however, that the effect of bacteria on overall corrosion rates is not large.

The reduction of sulphate by SRB external to the buffer may result in some increase in steel corrosion rates. On the other hand, corrosion-derived Fe may form Fe(II) silicate phases which could, in principle, compete with the formation of oxide or carbonate corrosion products. The thermodynamics and kinetics of this Fe-clay interaction process are still not well known, as noted below.

### ***Interaction of iron with the buffer***

The magnetite, iron sulphide or siderite formed as iron corrosion products have a low solubility under expected repository conditions, but will nevertheless slowly dissolve, releasing Fe(II) to the buffer porewater. Some Fe(II) will also be present in the buffer as a result of the slow dissolution of any iron sulphide and siderite present as mineral impurities (see Table 4-14 of /Gribi et al. 2007/ for the iron fractions of different components in the KBS-3H near field). In addition, Fe(II) diffusion from the surrounding groundwater will occur. The interaction of Fe(II) with bentonite is discussed in /Marcos 2003, Johnson et al. 2005/ and /Wersin et al. 2007/, and was recently the subject of a workshop held in Basel, Switzerland /Wersin and Mettler 2006/. There is currently significant uncertainty in the extent of this interaction and its consequences for buffer properties. Current understanding is, however, summarised below.

Dissolved Fe(II) will undergo molecular diffusion and will also interact strongly with clay minerals by:

- Sorbing onto clay surfaces by cation exchange in the interlayers and by surface complexation to edge sites.

Sorption to edge sites has been shown to dominate under non-acidic conditions and to involve complex redox/precipitation reactions at pH values of above 7.

- Mineral transformation.

Although process understanding is not currently well developed, experimental work performed mainly in France /e.g. Cathelineau et al. 2006, Lanson 2006/ suggests two possible mineral transformations that the buffer may undergo in the presence of iron:

- Fe-poor smectite + Fe → berthierine, chlorite; and (Eq. 5-3)
- Fe-poor smectite + Fe → Fe-rich smectite. (Eq. 5-4)

The first transformation has the greatest potential to impair the performance of the buffer, since berthierine and chlorite, unlike Fe-rich smectite, are not swelling clays.

The experimentally observed reaction products are generally in agreement with thermodynamic predictions, as indicated in the recent study by /Wilson et al. 2006/.

Mineral transformation of the buffer is expected to proceed slowly, due to the slow diffusive migration rate of Fe(II), which is retarded by sorption, and the slow kinetics of the transformation processes. The supercontainer shell is the largest source of reactive iron in the system. During the transient phase, mineral transformation due to the presence of the supercontainer shell is only expected to affect a thin layer adjacent to or near the buffer/rock interface (as indicated by the results of 1-D reactive transport modelling – /Wersin et al. 2007/). This transformation could, however, significantly affect mass transport at the interface of the buffer and the rock, if the transformation products have a high hydraulic conductivity. In principle, both smectite transformation and cementation may result in reduced buffer performance. A preliminary study /Carlson et al. 2006/ suggests that swelling properties may be much less affected than hydraulic conductivity by these processes. The reason for the observed hydraulic conductivity increase in that study remains however, unclear (see also discussion in Section 4.7.1 of the Process report, /Gribi et al. 2007/).

Beyond the period of early, transient evolution, the extent of the zone of mineral transformation may extend further into the buffer, as described in Section 6.5, affecting the possibility of canister failure by corrosion in the very long term (after 100,000 years, see below), and the transfer of radionuclides across the buffer/rock interface in the event of canister failure.

### ***Interactions involving hydrogen from steel corrosion***

Methane and hydrogen are present naturally in the groundwater and hydrogen will also be generated by the corrosion of the steel repository components, principally the supercontainer shell. These gases could participate in the reduction of groundwater sulphate to sulphide in the presence of sulphate-reducing bacteria, which could then corrode the copper canister. This issue is discussed further in Section 5.7.4.

It is generally assumed that there is no significant interaction between hydrogen from the corrosion of steel and minerals in the buffer. This assumption, however, still awaits experimental verification, and is noted as an issue requiring further investigation in Chapter 12. Furthermore, the presence of high hydrogen partial pressures due to the corrosion of the supercontainer shells and the other steel components may have an effect on the bentonite porewater chemistry. Various factors need to be considered, including acid-base equilibria and the pH buffering capacity of bentonite, as well as the limited timeframe of hydrogen production of several thousand years. This is also noted as an issue requiring further investigation in Chapter 12.

### **5.6.5 Interactions involving cement and stray materials**

Cementitious materials in the repository (Section 2.3.5) will slowly degrade. Degradation will lead to the formation of calcium-silicate-hydrates (CSH) phases, and to the leaching of alkaline porewater, which may react with the surroundings (see, e.g. Section 6.2.4 of /Pastina and Hellä 2006/).

Current knowledge of cement chemistry and microstructure is sufficient to predict the broad evolution of Ordinary Portland Cement (OPC) in controlled systems, such as laboratory experiments /Pastina and Hellä 2006/. On this basis, the structural integrity of OPC when exposed to various water types ranging from saline to fresh is expected to be maintained during the operational period (approximately 100 years). Furthermore, the lifetime of cementitious components is, at a minimum, expected to be of the same order as the duration of the early evolution period (a few thousand years after closure) during which the buffer saturates /Pastina and Hellä 2006/. In the deposition drifts, however, it is currently foreseen that low-pH cement and/or Silica Sol (colloidal silica) grouts<sup>29</sup> will be used (Section 2.3.5). These may have reduced detrimental effects on other system components (notably the buffer) compared with OPC because of the reduced alkalinity of their porewater leachates, although the long-term durability and evolution of such materials is not as well understood as in the case of OPC. In either case, there are significant uncertainties concerning the duration and the spatial extent of the alkaline plume leaching from cement.

Cementitious porewater leachate will first react with the host rock. Reacting minerals will dissolve and new minerals will be precipitated, creating a zone of altered mineralogy around the cementitious components. Quantitative understanding of these processes is, however, limited, with poor knowledge of the possible reaction products and of mineral dissolution and growth kinetics.

---

<sup>29</sup> Silica Sol is being considered as a grouting material for narrow fractures /Autio et al. 2007/. Silica Sol is a stable dispersion of discrete nonporous particles of amorphous silicon dioxide (SiO<sub>2</sub>). The long-term durability and evolution of colloidal silica grouts has not been as well characterised as that of cementitious grouts /Ahokas et al. 2006/. For example, the potential for forming colloids with radionuclides is under investigation.

When the leachate reaches the buffer, the most significant potential impact will be the dissolution of montmorillonite. Secondary minerals could also dissolve or precipitate in the buffer. Alteration products are expected to be a succession of calcium-silicate hydrates, illites and zeolites as the distance from the cementitious source is increased. The reaction products are likely to be amorphous with no expandability, but their porosity is low with very low hydraulic conductivity. The long-term safety concern is the possibility of a loss of buffer swelling pressure, increased hydraulic conductivity, and possibly fracturing of bentonite at cement/bentonite interfaces due to cementation.

Mass balance calculation results (Appendix F in /Gribi et al. 2007/) indicate that the maximum mass of bentonite altered by cement in a KBS-3H drift is small – in the order of 1 %, assuming that all the cementitious material used for grouting of the rock in ONKALO and in the repository below a depth of 150 m is distributed evenly among the repository drifts. There could, however, be more significant local effects on the buffer.

The period during which the buffer is exposed to high alkalinity, and hence the extent of alteration, depends on the amount of cement used in the drift and for grouting as well as the flow conditions. The spatial extent of any altered zone is expected to be in the order of a few tens of centimetres if bentonite is in direct contact with a cement source. Direct contact between cement and bentonite occurs at the drift end plug/filling block interface. This situation is, however, not greatly safety relevant as the filling block is planned to be more than 10 m long and even a significant alteration zone would have no impact on buffer function. In general, however, any cement-bearing components in a drift will be separated from the supercontainers by at least one 5-m long compacted bentonite block (about 20 tons of bentonite).

Potentially, the most significant scenario of cement/bentonite interaction occurs through indirect contact of alkaline cementitious porewater transported from a grouted fracture by groundwater to the supercontainer area through the fracture network. However, the leachate from a grouted fracture along the drift is likely to affect only a small percentage of the buffer in 100,000 years (Appendix F in /Gribi et al. 2007/). Mass balance and mass transport calculation results indicate that the thickness of the altered buffer zone can be up to 4 cm at most. These calculations are conservative, neglecting several mitigating factors, such as dilution of the leachate in the host rock dilution, the presence of pH-buffering minerals, the effect of the secondary minerals in the buffer, and the limited release rate of OH<sup>-</sup> from low pH cement.

The above discussion indicates that exposure of the canisters to high-pH leachates is not expected, although there remain significant uncertainties. However, even if exposure were to occur, it is likely to have a favourable impact on corrosion of the canister surfaces, through the production of a passivating film /King 2002/.

Organic materials (including stray materials such as plastics, cellulose, hydraulic oil and surfactants, and also cement additives released as cement degrades) will be decomposed in microbially mediated reactions, and therefore add reducing capacity to the repository near field. As noted in Section 4.2.5, these materials may, however, also enhance the rate of radionuclide transport in groundwater in the event of canister failure.

## **5.6.6 Wider impact on system evolution and safety functions**

The chemical and microbiological evolution of the repository in the transient phase will affect the saturation and the development of buffer swelling pressure, mainly through the generation of gas, but also to a lesser extent through volume expansion as the steel components corrode. Although repository-generated gas can significantly delay saturation, it is expected to have no effect on the final saturated state of the buffer (Section 5.5). Furthermore, as noted in Section 5.4.2, the impact of volume expansion on the final density and swelling pressure of the buffer is not expected to be significant in terms of the criteria for buffer safety function indicators.

The corrosion of the steel components will produce potentially porous or fractured materials, some of which will be embedded within the buffer, while others may be in direct contact with the drift walls. The former are not expected to have any significant impact on the safety functions of the repository. The latter may give rise to locally enhanced flow at the buffer/rock interface. Mineral transformation due to the interaction of corrosion-derived Fe with the buffer could also lead to the formation of a highly conductive layer at the buffer/rock interface. As in the case of rock spalling (Section 5.4.9), this is relevant to:

- canister corrosion due to the migration of sulphide from the rock through the buffer to the canister surface (Sections 5.7.4, 6.6.1 and Appendix B.7); and
- radionuclide migration from the buffer to the rock in the event of canister failure (Radionuclide Transport Report – /Smith et al. 2007a/).

Interactions involving cement and stray materials are subject to significant uncertainties. They are not expected to have significant adverse effects on the safety functions of the canister, buffer or host rock, but are likely to be the subject of further studies.

## **5.7 Evolution of the canister surface and interior**

### **5.7.1 Canister temperature**

The temperatures inside and outside the canister will increase rapidly after supercontainer emplacement, due to the ongoing generation of radiogenic heat and due to the thermal resistance of the unsaturated engineered barrier system (in particular, air-filled void space around the canister and at the interface between rock and buffer inside the deposition hole). The peak temperature in the fuel will be reached shortly after deposition, and will decline over the following several thousand years, as described in Section 5.2.

### **5.7.2 Exposure of the canister surface to water**

Water initially contained in the buffer near to the canister surface will evaporate and migrate outwards by vapour diffusion, followed by condensation in the outer part of the buffer or at the rock surface (Section 5.2.4). The canister surface will thus remain essentially dry until the buffer is slowly saturated from the outside.

### **5.7.3 Mechanical load on the canister**

The development of an isostatic load on the canister and the potential impact of rock shear movements are discussed in Sections 5.4.3 and 5.4.6, respectively. It should also be noted that, in studies of a KBS-3V repository at Olkiluoto, canister stability in a range of unfavourable load conditions, including, for example, higher than expected pore water pressure, has been considered (Section 6.1.2 of /Pastina and Hellä 2006/). In all conceivable situations, the stability of the canister is ensured with a large safety margin. This conclusion is also expected to apply in the case of KBS-3H.

### **5.7.4 Corrosion of the copper shell**

The corrosion of copper in the first several thousand years after emplacement is discussed in detail in Sections 6.1.4 and 7.1.4 of /Pastina and Hellä 2006/ in the case of a KBS-3V repository, and is likely to be similar in the case of KBS-3H.

The presence of initially entrapped oxygen will cause some limited corrosion of copper until the available oxygen is depleted and the environment changes from oxic to anoxic (Section 5.6.3). Microbially influenced corrosion (MIC) may have some impact on the chemical evolution of the

canister surface before the buffer reaches full saturation, since microbes are present both in the groundwater and in the bentonite. The development of a fine, homogeneous pore structure and the high swelling pressure of the saturated buffer mean, however, that microbes are not expected to stay active and viable near the canister surface in the longer term (Section 5.6.3).

In /Pastina and Hellä 2006/, it is argued that localised corrosion of the copper shell, including stress corrosion cracking (SCC), is unlikely, even in the period of hot and oxic conditions at the canister surface. Based on the work of /King 2004/, it is further argued that, although welding gives regions of non-uniformity of the surface, weld discontinuities will not lead to significant localised corrosion behaviour of the copper canister and that grain boundary corrosion of copper weld material is very unlikely to adversely affect the copper canisters under the expected conditions in the repository.

Changes in the chemical composition of the bentonite porewater may occur in the transient phase (Section 5.6.2), but are not expected to jeopardise the integrity of the copper shell. For example, the presence of high hydrogen partial pressures due to the corrosion of the supercontainer shells and the other steel components of a KBS-3H repository, may have an effect on the bentonite porewater chemistry. The impact of hydrogen gas on the bentonite porewater chemistry has not yet been fully evaluated. Various factors need to be considered, including acid-base equilibria and the pH buffering capacity of bentonite, as well as the limited timeframe of hydrogen production of several thousand years. The overall impacts, in particular any effects on the buffer, should be taken into account in future studies.

Once the entire repository is fully saturated and has reached anoxic conditions, the only significant corrosion agent will be sulphide that diffuses through the buffer to the canister surface. Sulphide is abundant in the groundwater at repository depth, the present highest measured sulphide concentration at repository depth at Olkiluoto being 12 mg per litre (Section 2.2.4). The sulphate content in the sulphate-rich brackish groundwater is at maximum about 500 mg/l, decreasing to a negligible concentration in the methane-rich saline groundwater /Pitkänen et al. 2004/. Furthermore, the hydrogen generated by the corrosion of the steel repository components external to the canister (Section 5.6.4) could, along with methane and hydrogen naturally present in the groundwater, participate in the reduction of groundwater sulphate to sulphide in the presence of sulphate-reducing bacteria, increasing the sulphide concentration. The concentration of sulphide in the groundwater will however, be limited by the concentration of iron in the groundwater, which contributes to formations of iron sulphides with low solubility.

Some of the sulphide entering the buffer will react with the supercontainer and other steel components, and with amorphous iron present in the bentonite. The resulting iron sulphides have a low solubility and will precipitate, reducing the flux of sulphide to the canister surface. Reaction with sulphide, by increasing the corrosion rate of the steel components, could reduce the period of hydrogen generation, and the period during which sulphate is potentially reduced to sulphide in the presence of repository-generated hydrogen and sulphate-reducing bacteria. It is argued in Appendix B.7 that the impact of repository-generated hydrogen on canister lifetime is in any case small, although the impact of methane in the groundwater remains an issue for further study.

In a few thousand years, once the steel has corroded, the sulphide scavenging effect of the iron from steel components will be lost. Nevertheless, amorphous iron present in the bentonite is still likely to scavenge at least some of the migrating sulphide (see e.g. discussions in Chapter 11 of /Pastina and Hellä 2006/). Furthermore, the low rate of migration of any sulphide reaching the canister surface will keep the rate of copper corrosion very low (see Appendix B.7, which also includes a discussion of the uncertainty in sulphide transport rate and canister lifetime due to the impact of potential perturbations to the mass transfer properties of the buffer/rock interface due, for example, to rock spalling – Section 5.4.5 – and iron/bentonite interaction – Section 5.6.4).



### **5.7.5 Chemical evolution of the canister interior**

Following encapsulation of the fuel, any residual water inside the canister (maximally 600g, Section 4.3.2, /Pastina and Hellä 2006/) will evaporate. Some nitric acid could be formed by radiolysis, possibly resulting in some stress corrosion cracking of the insert /Raiko 2005/. As noted in Section 4.14, this possibility can, if required, be avoided by filling the canister voids with inert gases (Ar or He), in the presence of which no significant radiation-induced effects are expected.

### **5.7.6 Radioactive decay, radiolysis and the production of gas by decay**

The radionuclide inventory inside the canisters will evolve by decay and ingrowth. These processes will produce small amounts of decay gases that may accumulate within the fuel rods or escape to the canister voids. Gamma radiolysis of air and water inside the canister, associated mainly with the decay of Cs-137, will also occur over a period of a few decades, until this radionuclide has substantially decayed.

Most of the gas produced by decay will be trapped within the fuel matrix. Over time, this has the potential to detrimentally affect mechanical stability of the fuel. In SR-Can, however, it is concluded that there will be no detrimental effects on the fuel for the burn-up range that is relevant for Swedish conditions, and this conclusion is also expected to hold for a KBS-3H repository for Finnish fuel at Olkiluoto.

Stress on the fuel cladding may also increase with time as gas accumulates in the gap between the fuel pellets and the inner walls of the cladding tubes. This will increase the risk of cladding tube failure by delayed hydrogen cracking (DHC) (Section 4.1.3). Studies performed in association with the Spent Fuel Stability Project have been unable to clarify the effects of pressure build-up on cladding integrity (see, e.g., Section 6.4.3 of /SKB 2006a/). However, even if the pressure increase does lead to damage of the cladding tubes, this is not expected to lead to gas pressures inside the canisters that could compromise canister integrity, even after prolonged periods of time /SKB 2006a/.

### **5.7.7 Redistribution of fissile material**

Redistribution of fissile material inside the canister cannot be ruled out over long periods of time through mechanical degradation of fuel rods and pieces detaching and accumulating along the lower sides of the horizontally oriented fuel channels. This is discussed in the context of the potential for criticality in the case of a canister with an initial penetrating defect in Section 8.11.

### **5.7.8 Wider impact on system evolution and safety functions**

During the early phase of evolution, as the buffer saturates, the canisters are expected to experience elevated temperatures, increasing water pressure, differential pressures from the swelling bentonite, and corrosion, mainly due to sulphide and initially entrapped oxygen during the transient phase. Nevertheless, the copper canisters are expected to remain intact, and with a large safety margin (assuming appropriate quality control procedures during canister encapsulation and emplacement). As a consequence, spent fuel and radionuclides are expected to be totally isolated within the canisters throughout the early evolution period.



## 6 Subsequent evolution prior to the next major climate change

### 6.1 Definition of the period and evolution of external conditions

Following the early, transient phase, the repository and its geological environment will evolve to a quasi-steady state, in which key safety-relevant physical and chemical characteristics (e.g. temperature, buffer density and swelling pressure) are subject to much slower changes.

The period covered in this chapter is that prior to any major future climate change that could impact the evolution and performance of a KBS-3H repository at Olkiluoto. Future climatic events that could potentially have a significant impact on evolution and performance include the formation of permafrost and of ice sheets, and their subsequent melting.

The future evolution of the climate and the occurrence of future glaciations are subject to considerable uncertainty, particularly in regard to the long-term impact of anthropogenic emissions, especially greenhouse gasses. Two scenarios for future climatic evolution, the Weichselian-R scenario and the Emissions-M scenario, have been introduced in Section 5.1. The Weichselian-R scenario assumes a repetition (R) in the future of the last glacial cycle. The Emissions-M scenario takes into account the warming effects of moderate (M) levels of anthropogenic emissions (especially CO<sub>2</sub>) from human activities.

An important climate-related process affecting groundwater flow and composition is post-glacial land uplift. Post-glacial land uplift will progressively displace the shoreline away from the repository site, and will do so more rapidly in the Weichselian-R scenario compared with the Emissions-M scenario, due to the significant rise in global average sea level in the latter scenario. In the next 4,000 years, for example, the shoreline is expected to move several kilometres to the west in the Weichselian-R scenario, but only a few hundred metres to the west in the warmer, Emissions-M scenario. This is illustrated in Figure 6-1, which shows the evolution of the shoreline in the two scenarios, and also the main bedrock lineaments, which may indicate dominant hydraulic features from beyond which the sea level has relatively little effect on groundwater head.

In the longer term, however, on a timescale of 10,000 years or more, the shoreline will be displaced several kilometres to the west in both scenarios. The rate of land uplift will gradually slow over time. /Löfman 1999/ predicted land surface uplift as a function of time for the next 10,000 years, based on the mathematical theory of /Påsse 1996/ and a regional land uplift dating study by /Eronen et al. 1995/. In the KBS-3V Evolution Report, an extrapolation of that prediction further into the future indicates a land uplift of about 70 m at 50,000 years, with uplift remaining below 90 m during the next 100,000 years, assuming that no glaciation occurs within this timeframe, which is the case in the Emission-M scenario (Figure 7-9 in /Pastina and Hella 2006/). This extrapolation is subject to uncertainty, but is considered to be a plausible estimate of the magnitude of future uplift; the depression of the bedrock due to the previous ice sheets was about 90 m /Lambeck et al. 1998/

### 6.2 Thermal evolution

By definition, the heat output of the spent fuel will have declined to a level that has no significant effect on the evolution of the repository and its environment by the start of this phase (the end of the transient phase). Climatic evolution and its associated uncertainties will have only a small impact on rock temperatures at repository depth up until the occurrence of the next period of permafrost (expected around 12,500 years at the earliest; see Chapter 7, Figure 7-2).

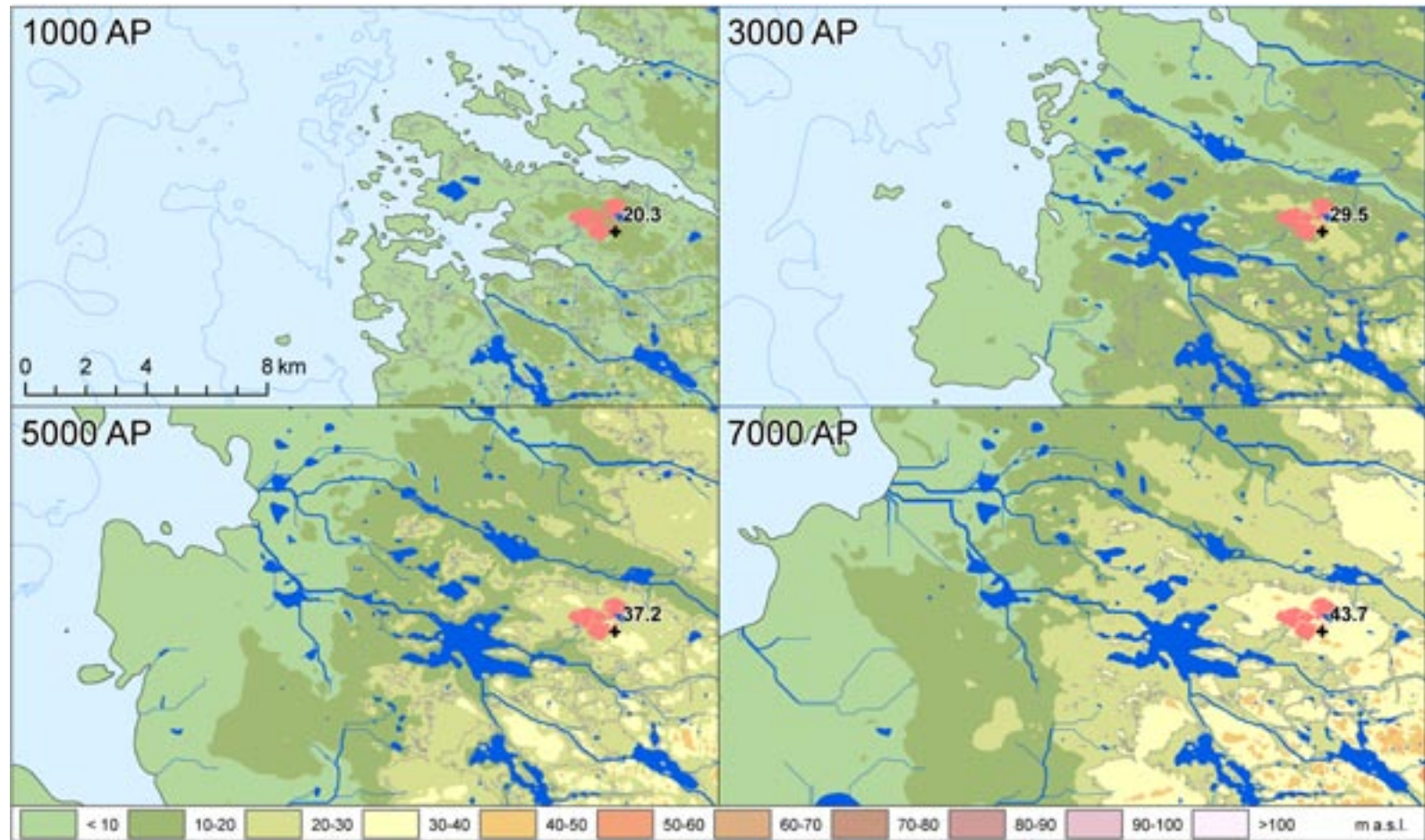


**Figure 6-1.** Terrain and surface water body forecasts for selected times, assuming a repetition of the last glacial cycle. Colours show elevation in intervals of 10 metres. The present coastline is shown with a grey line, 10-m depth contours of the sea in blue, and illustrative repository layout in red /from Ikonen et al. 2007/. Top elevation of the hill above the ramp entrance is indicated in for each time point (m a.s.l.).

## 6.3 Hydrogeological evolution

As a result of continuing post-glacial uplift, the saline water currently at repository depth will start to be replaced by brackish, sulphate-rich and fresher groundwater currently present at shallower depths. Furthermore, the receding shoreline will uncover topographic features that will affect the shape of the water table and hence the driving forces for groundwater flow. Changes in the salinity of the Baltic Sea are also expected, but shoreline displacement means that the effect of seawater salinity on groundwater flow around the repository will be reduced such that it is negligible.

The sea level will have a progressively diminishing effect on hydrogeological conditions as the shoreline is displaced away from the repository site due to land uplift. The shoreline is expected to recede in both the Weichselian-R and the Emissions-M scenarios, though less rapidly in the Emissions-M scenario because of global average sea-level rise. Within a few thousand years after repository closure (after about 2,000 in the Weichselian-R scenario and after about 4,000 years in the Emission-M scenario; see Figure 6-1), the groundwater flow in the vicinity of the repository will no longer be affected by sea level because, in both scenarios, the shoreline will have receded by several kilometres and beyond the borders of the expected hydraulic block of the Olkiluoto site. Therefore, after a few thousand years and prior to the next permafrost episode, a similar hydrogeological evolution is expected in both scenarios. According to the Weichselian-R scenario, the first 40,000 years are characterised by alternating permafrost and temperate climate phases, with the present temperate phase continuing for 12,000 years. According to the Emissions-M scenario, a permafrost stage will be reached 170,000 years from now (although no ice sheet will be formed before 350,000 years).

It is conceivable that, in the Emissions-M Scenario, because of the higher overall temperatures and CO<sub>2</sub> content in rainwater and the change in the vegetation and microbial activity in soil, there will be a difference in reactivity of infiltrating water. This difference in reactivity could, in principle, eventually lead to differences in groundwater flow pattern (as a result, say, of precipitation and/or dissolution of fracture surface minerals and infills). Currently, however, there is no evidence for significantly different deep groundwater flow patterns arising from possible differences in the chemical properties of infiltrated water.

Groundwater flow was modelled for the Emissions-M scenario in the KBS-3V Evolution Report during the first 50,000 years of the post-closure temperate phase (Figure 7-9 in /Pastina and Hellä 2006/). Modelling results indicate that increasingly fresh water will penetrate to greater depths over time and that the repository level will be flushed by brackish water in about 20,000 years time. Modelling results based on the assumption of continuing but decreasing uplift over the next 50,000 years, with more than 70 m of uplift at the end of the simulation period, indicate that the repository level will eventually be flushed by meteoric water from the surface, although, as noted above, the rate at which uplift slows, and hence the timing of this event, is highly uncertain. It should also be noted that surface water slowly infiltrating to repository depth will also interact with soil layers and rock minerals, and mix with groundwater present in the rock which will increase its ionic strength (Section 6.5.2).

## 6.4 Mechanical evolution

### 6.4.1 General description

The mechanical evolution of the repository and its geological environment will be similar to that of a KBS-3V repository in this period. The reduction in thermal output from the fuel will result in rock stress levels returning to values similar to those prior to spent fuel emplacement and in a reduction in the thermo-mechanical loads on the canisters. The swelling pressure exerted by the saturated buffer on the rock may, however, result in some increase in the apertures and transmissivities of fractures around the drift walls. The probability of significant tectonic earthquakes will remain low, and rock fracturing and creep deformation of drifts will be limited.

The changes in the salinity of the groundwater over time noted in Section 6.3 will affect the swelling pressure of the buffer (with lower salinities giving higher swelling pressures), and its susceptibility to erosion by water flowing through fractures intersecting the drift walls (Section 6.5).

#### **6.4.2 Potential for buffer extrusion and erosion in fractures**

The swelling pressure that develops in the buffer (and also the filling blocks) is likely to cause bentonite to intrude into some of the open fractures intersecting the drift. If sufficiently large, the flow of groundwater through these fractures could potentially lead to some mechanical erosion of the gel at the bentonite/groundwater interface and the release of bentonite colloids. However, once the deposition drifts and transport tunnels have been filled and sealed and have saturated, and transient hydraulic pressure gradients within and around the repository have dissipated, flowrates are expected to be low, with hydraulic gradients comparable to the undisturbed situation at Olkiluoto. Erosion of bentonite extruded into fracture openings by flowing water (mechanical erosion – see the scoping calculations in Appendix B.2) is then not expected because of the particle bond strength between the clay particles forming the gel, as long as this bond strength is not adversely affected by changes in groundwater ionic strength (Section 6.5.2).

#### **6.4.3 Potential for canister sinking**

As discussed in Section 5.4.4, the canister, having a higher density than the surrounding buffer, may sink slightly under its own weight. No specific analyses have been carried out for KBS-3H. The situation is, however, somewhat simpler than in the case of KBS-3V, where sinking is offset by an upward displacement due to compaction of the backfill – see Section 2.4.1 of /SKB 2006c/. /Börgesson and Hernelind 2006a/ have modelled the net vertical sinking of a KBS-3V canister both with and without consideration of compaction of the backfill. Where compaction of the backfill is neglected, the total settlement of the canisters in  $10^5$  years is calculated as being only 0.35 mm (a net upward displacement is calculated if backfill compaction is included). For a given buffer density, if canister sinking (neglecting backfill compaction) is of little concern for KBS-3V, then it is even less a concern for KBS-3H. This is because the pressure exerted by the KBS-3H canister on the bentonite that supports it is less than in the case of KBS-3V, due to the weight of the KBS-3H canister being distributed over a larger horizontal area.

### **6.5 Chemical evolution**

#### **6.5.1 General description**

Further gradual chemical evolution of the rock and the buffer will continue throughout this period. Geochemical conditions will be affected in particular if there are climatic variations that have an impact on the relative infiltration of water in the form of precipitation and seawater. The buffer will also continue to evolve chemically, important processes being ion exchange and the dissolution/precipitation of calcite (Section 2.5 of /SKB 2006a/). Other specific issues of concern are the chemical stability of the bentonite gel at its interface with the groundwater where the buffer has intruded into fractures and the continuing interaction of the buffer with corroding steel components and the possibility of oxygen penetration to repository depth. These issues are discussed in Sections 6.5.2, 6.5.3 and 6.5.4, respectively.



### 6.5.2 Buffer intrusion into fractures and the stability of the gel water interface

Bentonite gel that has intruded into fractures intersecting the drift could potentially break up and disperse in the form of colloids if the concentration of cations in solution at the gel/water interface falls below the Critical Coagulation Concentration (CCC), as discussed in detail in Section 2.5.10 of /SKB 2006c/. The cation concentration at the interface is determined by the cation concentration in the groundwater, and also by the supply of cations to the interface through the dissolution of Ca and Mg minerals in the buffer and subsequent diffusion of these ions to the interface. The CCC is uncertain but, according to Section 2.5.10 of /SKB 2006c/, is around 1 mmol per litre in the case of divalent ions.

Currently, very dilute groundwaters occur in Olkiluoto practically only in the overburden, and the ionic strength of Olkiluoto groundwater at repository depth exceeds the CCC by a significant margin (the sum of  $\text{Ca}^{2+}$  and  $\text{Mg}^{2+}$  concentrations at repository depth at Olkiluoto is in the range 50–80 mmol per litre). The ionic strength is expected to increase temporarily during the transient period due to the upconing of deeper, more saline waters (Section 4.1.1).

In the longer term, continuing isostatic uplift will result in the gradual replacement of the saline water at repository depth with more brackish water of lower ionic strength. In the Emissions-M scenario, prolonged temperate conditions without glaciation will result in more prolonged uplift and a longer period of seepage of surface water towards repository level compared with the Weichselian-R scenario. In the main report of SR-Can, SKB concludes that the groundwater conditions during the post-closure temperate phase under the greenhouse variant of SKB's reference evolution scenario will be similar to those of the reference evolution, with the difference that a longer period of exposure to groundwaters of meteoric origin is expected at repository depth /SKB 2006a/. Nevertheless, compared with glacial meltwater penetration (Section 7.3.5), surface water infiltration is a slow process because it is driven only by the hydraulic gradient created by the residual land uplift, expected to be some tens of metres in the next few tens of thousands of years (Section 6.1). Slowly infiltrating surface water will interact with rock minerals and mix with deeper, more saline groundwater layers. This, together with organic activity in the soil layers, will increase its ionic strength.

The CCC is, therefore, expected to continue to be exceeded in both the Weichselian-R and Emissions-M scenarios. Although uncertainty remains and the issue is noted in Chapter 12 as requiring further investigation, the stability of the gel/water interface is expected to be maintained, and no significant erosion of the buffer is expected to occur prior to any future change to glacial conditions and the penetration of glacial meltwater to repository depth. The issue of erosion as a result of the infiltration of glacial meltwater to repository depth, discussed in Section 7.4.7, is still under study.

### 6.5.3 Mineral transformation due to iron/bentonite interaction

Mineral transformation of the buffer due to the presence of corroding steel components, as described in Section 5.6.4, is likely to extend further into the buffer during this period. A simple mass balance calculation described in /Wersin et al. 2007/, assuming complete dissolution of the corrosion products, indicates that 10–30% of the swelling clay in the buffer could eventually be converted to a non-swelling iron silicate, depending on the reaction product assumed (berthierine or chamosite, which is an iron-rich chlorite). The migration of Fe(II) through the buffer, which gives rise to mineral transformation, is, however, likely to be slow. The final steel corrosion products that provide the source of Fe(II) have low solubilities. Furthermore, the clay has a strong affinity for Fe(II), so that diffusion of Fe(II) through the buffer will be retarded significantly. To estimate the timescales required for transformation of a significant proportion of the buffer, a 1-D reactive transport model was set up (also described in /Wersin et al. 2007/) using site-specific information from Olkiluoto, such as groundwater and mineralogical data. Results indicate that the extent of the zone potentially undergoing mineral transformation is likely to remain spatially limited (a few centimetres) for very long times (hundreds of thousands of years or more).



The impact of mineral transformation on the hydraulic and rheological properties of the transformed clay is uncertain. In the zones where transformation occurs, there is the possibility of a substantial loss of swelling capacity and cementation by mineral precipitation leading to an increase in brittleness and a significant increase in hydraulic conductivity. Available data are by no means conclusive on the effect of iron on bentonite. Examples from natural systems reported refer to cementation effects induced by iron oxide precipitation under oxic, but not anoxic conditions. There is no natural analogue known to us which would indicate significant cementation effects in swelling clays under anoxic conditions. The cementation effect is still not well understood and is an issue for further investigation (Section 12.1, Iron corrosion, gas generation and the interaction of the buffer with iron corrosion products and hydrogen). These altered zones are, however, likely to remain hydraulically isolated from each other by the distance blocks, which will be largely unaffected by mineral transformation because they are spatially well separated from the steel components.

Mineral transformation is not expected to affect the sorption properties of the buffer adversely, because the surfaces of the mineral phases formed by transformation to, for example, berthierine or chamosite also have high sorption affinities for radionuclides. The presence of corrosion products and of iron silicates formed by iron/bentonite interaction will considerably enhance the reducing capacity of the buffer adjacent to the supercontainer. This area will then act as a sink for redox-sensitive radionuclides, such as isotopes of U, Se and Tc that may have escaped from a failed canister in oxidised form. The pH conditions will not be significantly altered because of the large acid-base buffering capacity of bentonite. Although these changes in the capacity of the buffer to retain and retard radionuclides are broadly favourable to safety, it is also possible that changes in geochemical conditions and/or ageing and transformation of the surfaces of the corrosion and alteration products could result in the release of some radionuclides accumulated in the buffer. This situation is discussed in the Radionuclide Transport Report /Smith et al. 2007a/.

The potential formation of a highly conductive layer of mineralogically altered bentonite at the buffer/rock interface is relevant to:

- canister corrosion due to the migration of sulphide from the rock through the buffer to the canister surface (Sections 5.7.4, 6.6.1 and Appendix B.7); and
- radionuclide migration from the buffer to the rock in the event of canister failure (Radionuclide Transport Report – /Smith et al. 2007a/).

Fracturing of the transformed buffer may allow microbial activity, which may in turn have some impact on the rate of corrosion of any remaining uncorroded steel – this is discussed in Section 5.6.4. Furthermore, an increase in the stiffness of the transformed buffer, if this affects a significant proportion of the buffer thickness around the canisters, could in principle compromise the capacity of the buffer to protect the canisters from rock shear movements, and make the canisters more vulnerable to post-glacial earthquakes, although this is not expected due to the slowness of the transformation process (Section 7.4.5).

#### **6.5.4 Migration of oxygen introduced with surface water**

Microbial activity and organic respiration in general are high near the ground surface. Oxygen in the surface water will therefore be largely consumed by aerobic microbial bacterial oxidation of organic matter to carbon dioxide in the soil cover, before this water penetrates deeper into the rock. Any residual oxygen will react readily with Fe(II) minerals in the rock. Anaerobic microbial processes at repository level are discussed in Section 6.6.1. Thus, in neither the Weichselian-R scenario nor the Emission-M scenario any oxygen introduced with surface water is expected to reach the repository depth.

## **6.6 Evolution of the canister surface and interior**

### **6.6.1 Conditions at the canister surface**

During this period, the canister surface will approach ambient rock temperature. Isostatic pressure conditions will be established and maintained at a value equal to sum of the groundwater pressure and the buffer swelling pressure. Given the expected anoxic conditions at the canister surface, the only corrosion agent will be sulphide that diffuses through the buffer from the rock.

Because the rate of transport of sulphide to the canister surface by diffusion is small, the rate of copper corrosion is expected to be very low, although there is some uncertainty related to transport properties, particularly at the buffer/rock interface.

Features and processes with the potential to perturb the buffer/rock interface, and a limited layer of buffer or rock adjacent to the interface, include:

- thermally-induced rock spalling (Section 5.4.5);
- the presence of potentially porous or fractured corrosion products in contact with the drift wall tighter drift sections (see Section 5.5.2);
- chemical interaction of the buffer with these corrosion products (Sections 5.6.4 and 6.5.3); and
- chemical interaction of the buffer with high-pH leachates from cementitious components (Section 5.6.5).

Scoping calculations to illustrate the potential impact of these features and processes on the mass transfer of sulphide from groundwater to the buffer, and hence on canister corrosion and lifetime, are described in Appendix B.7. It is concluded that a combination of pessimistic assumptions must be made before the canister lifetime drops to one million years or less.

For the reasons outlined in Section 6.5.4, it is not expected that amounts of oxygen that could have a significant impact on canister corrosion will penetrate to repository depth. The saline water currently at repository depth will be gradually replaced by brackish, sulphate-rich and fresher groundwater (Section 6.3). If adequate nutrients are available, the presence of sulphate-reducing bacteria could lead to increased sulphide concentrations around the repository and increased canister corrosion rates in both the Weichselian-R and Emissions-M scenarios. However, increasingly dilute groundwater will provide reduced amounts of nutrients, such as sulphate for microbially-mediated redox processes, and microbial activity and sulphide production may decrease. Thus, the impact of isostatic uplift on the canisters could be either to increase or to decrease corrosion rates, but in either case the effect is not expected to be large. This is, however, an issue that requires further investigation.

Overall, it is concluded that no canister failure by corrosion of the copper shell is expected prior to the next glaciation. In this respect, the Emissions-M scenario is believed to be as favourable to the safety functions of the engineered barrier system as the Weichselian-R for the time period considered.

### **6.6.2 The canister interior**

The radionuclide inventory inside the canisters will continue to evolve by decay and ingrowth. There will also be further production of decay gases, but this will not be sufficient to compromise canister integrity (see also Section 5.7.6).

The redistribution of fissile material inside the canister described in Section 5.7.7 may continue due to the further mechanical degradation of the fuel rods, with additional fissile accumulating along the lower sides of the horizontally oriented fuel channels. This is discussed in the context of the potential for criticality in the case of a canister with an initial penetrating defect in Section 8.11.

## 7 Evolution affected by major climate change

### 7.1 Climate evolution scenarios

The evolution of conditions at repository depth could be significantly affected by major climate change, and, in particular, by the formation of permafrost and ice sheets at the ground surface in response to any future change to much colder climatic conditions.

/Cedercreutz 2004/ has identified possible scenarios for climatic evolution at Olkiluoto on a timescale of 125,000 to 450,000 years. Two scenarios, already introduced in the previous chapters, are judged to be representative of the range of plausible possibilities for future climate development: (i), the Weichselian-R scenario, which assumes a repetition of conditions that are believed to have occurred during the last glacial cycle, and (ii), the Emissions-M scenario, which assumes a moderate climatic warming due to anthropogenic emissions, especially greenhouse gases that delays the formation of permafrost and ice sheets at Olkiluoto. Climatic evolution following the development of an ice sheet is similar in both scenarios.

### 7.2 Impact on the surface environment

In general terms, the changes expected in the surface environment during a glacial cycle are as follows:

- the glacial cycle will be initiated by a cooling of the climate;
- as the climate grows progressively cooler, periglacial conditions will become established; at first, the land surface temperature will fluctuate around freezing point, and then will fall further, such that the ground remains frozen year round (permafrost);
- at some point, an advancing ice sheet will reach the repository location, thicken gradually and then retreat relatively rapidly by melting;
- after the ice has gone, periglacial conditions will resume, characterised by permafrost and near-freezing average annual air temperatures;
- a warming trend will restore average annual temperatures to near-present-day values.

During future glaciations, the load of up to 2 km-thick ice sheets is expected to depress the Earth's crust, leaving the Olkiluoto area submerged below sea level. The site will experience a gradual uplift following ice-sheet melting and return to the temperate condition, as in past glacial cycles.

Figure 7-1 illustrates modelling results for the evolution of air and ground-surface temperature, ice sheet thickness and vegetation cover in the Weichselian-R scenario. Temperature reconstructions are based on the Greenland Ice Core Project and from temperature data from the northern European climate archives (/Pastina and Hellä 2006/ and references therein).

The main differences between the Weichselian-R and Emissions-M scenarios are in the timing of climatic changes (permafrost, ice sheet, glacial melting) and the effects of prolonged infiltration of surface water in the Emissions-M scenario (Section 6.3).

In this scenario, the next 40,000 years are characterised by alternating permafrost and temperate climate phases. After about 50,000 years, the area will be covered with ice and snow, and this cover will remain for the following 25,000 years. Olkiluoto will be submerged as the glacier retreats and will remain submerged until the next glaciation, at about 87,000 to 112,000 years from now. The maximum permafrost depth during this period will be 180 metres, as illustrated in Figure 7-2. The next interglacial is expected in about 112,000 to 115,000 years. Climatic

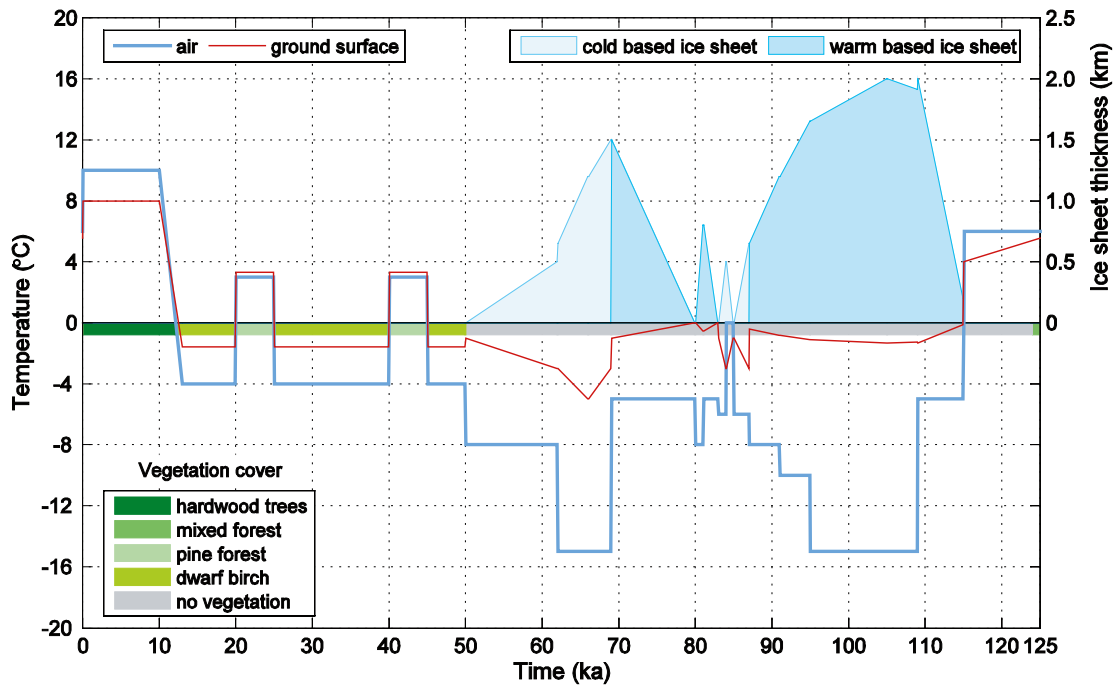


Figure 7-1. Evolution of air and ground-surface temperature, ice sheet thickness and vegetation cover in the Weichselian-R scenario (after Figure 2-7 of /Hartikainen 2006/).

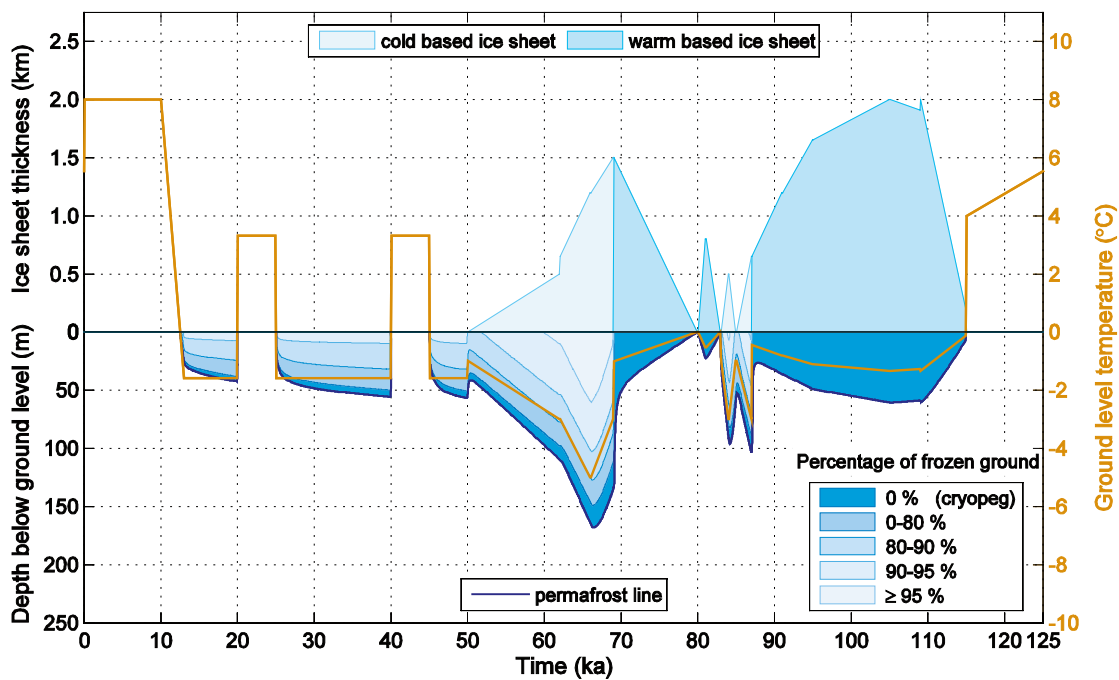


Figure 7-2. Evolution permafrost and frozen ground in the Weichselian-R scenario – vegetation cover taken into account (after Figure 4-1 of /Hartikainen 2006/).

conditions similar to the current ones will return in about 125,000 years, when a new glacial cycle will begin. For most of this glacial cycle (from 50,000 to 125,000 years from now), Olkiluoto will be covered either by ice or by water.

Thus, the next glacial retreat, and hence the next possibility for penetration of glacial meltwater to repository depth, is in 70,000 years time, based on a repetition of previous glacial cycles.

In the Emissions-M scenario, as shown in Figure 7-3, surface temperatures will continue to rise, effectively leading to snowless and frostless winters, before starting to fall again in about 20,000 years from now. A permafrost stage will be reached at 170,000 years, but no ice sheet will be formed before 350,000 years. During the sole periglacial period (between about 170,000 to 180,000 years in the future), the maximum permafrost depth will be between 10 m and less than 80 m, depending on the types of vegetation present at the surface.

## 7.3 Impact on the rock at repository depth

### 7.3.1 General description

Underground, the most significant effects associated with major climate change are related to:

- temperature;
- seismic activity and post-glacial faulting;
- changes in rock stress; and
- changes in the groundwater flow regime, pore pressure and chemical composition.

These effects are described in the following sections, with reference, where relevant, to the Weichselian-R and Emissions-M scenarios. The impact of glaciation and deglaciation is, however, generally limited and similar in the two scenarios, with many of the features of the system and slow processes occurring prior to glaciation continuing relatively unchanged.

### 7.3.2 Temperature evolution

Rock temperatures diverge significantly in the two scenarios with the occurrence of the first permafrost period in Weichselian R-scenario (around 12,500 years; see Figure 7-2). Because the thermal output from the spent fuel will be negligible, the temperature of the repository at this time will be approximately equal to the ambient rock temperature at repository depth, which will be somewhat higher in the Emissions-M scenario compared with the Weichselian-R scenario.

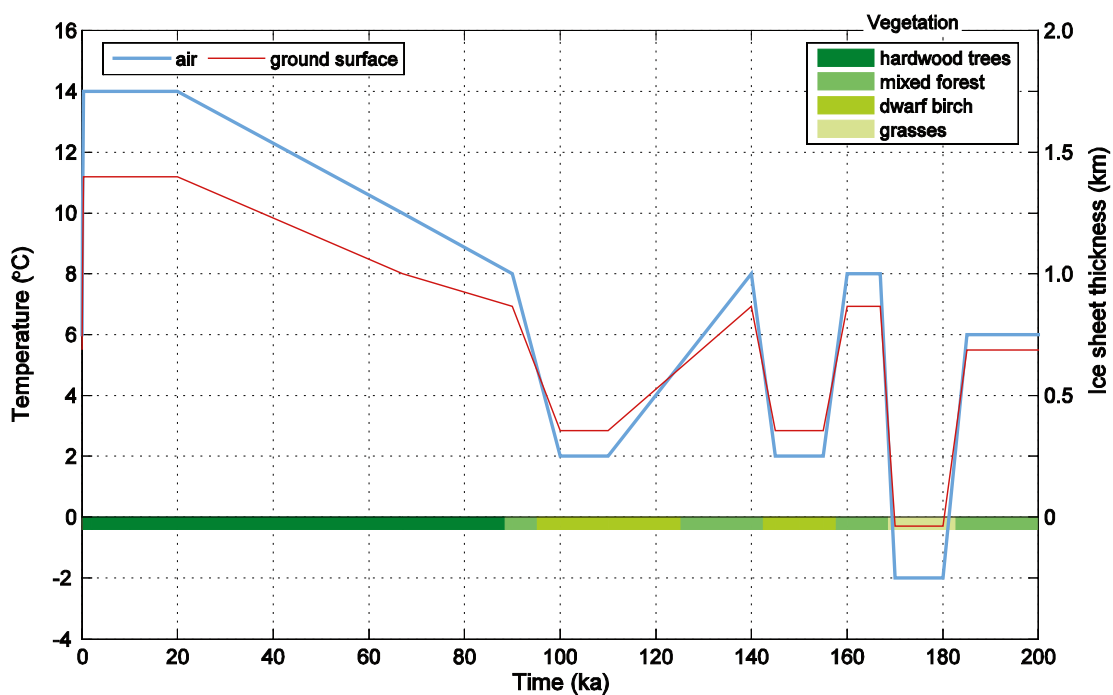


Figure 7-3. Evolution of air and ground-surface temperature, ice sheet thickness and vegetation cover in the Emissions-M scenario (after Figure 2-8 of /Hartikainen 2006/).



Even then, however, the development of permafrost and frozen ground and the advance and retreat of ice sheets is expected to have only limited effects on ambient rock temperature. According to the numerical simulations of /Hartikainen 2006/, the lowest temperature reached at repository depth will be about 4°C lower than the present-day ambient temperature, and this temperature minimum will occur at about 68,000 years in the future in the Weichselian-R scenario. In the Emissions-M, the lowest temperature reached at repository depth will be about 1°C lower than the present-day ambient temperature at about 181,000 years in the future. Calculated pore water pressures indicate that the development of permafrost will have only a minor influence on hydro-mechanical pressure conditions at repository depth, whereas the creation of ice sheets will result in large water pressures and hydraulic gradients in the subsurface, as discussed further in Section 7.3.5.

### **7.3.3 Seismic activity and post-glacial earthquakes**

Seismic activity, which is in any case low in the Olkiluoto region (Section 2.2.2), will be further suppressed by the weight of the ice while an ice sheet is present at the repository location. Post-glacial earthquakes may, however, occur following the retreat of the ice sheet, triggered by rapid crustal uplift and the release of vertical stresses. Post-glacial earthquakes are expected to occur on existing major deformation zones. Major deformation zones capable of accommodating significant slip should be readily identified and KBS-3H drifts will not be constructed within, or in the immediate vicinity of such zones. As noted in Section 2.2.2, ongoing geological characterisation and modelling will give more insight into the characteristics of deformation zones at the site and their potential to host such earthquakes in the future.

Even if it occurs at some distance from the repository, a large earthquake occurring on a major deformation zone may give rise to stress changes in the rock that trigger shear movements on smaller-scale fractures that are not detected or cannot be avoided when constructing the drifts. /Hutri 2007/ has carried out computer simulations of the bedrock behaviour during future glaciations applying different glacial scenarios, suggesting that the maximum shear displacements will be no more than a few centimetres at repository depth. The potential impact of such displacements on the repository engineered barrier system is discussed in Section 7.4.5.

### **7.3.4 Mechanical effects in the rock**

Bedrock freezing may cause frost wedging, leading to the propagation of cracks and joints in the rock (Section 6.3.2 of /Pastina and Hellä 2006/). This may affect the evolution of the geosphere transport barrier. As noted above, however, frozen conditions are not expected to penetrate to repository depth, and conditions around the repository will be unaffected.

Glacial loading will give rise to additional rock stresses and increased pore pressures. According to SR-Can /SKB 2006d/, processes related to glaciation could lead to the creation the reactivation or hydraulic jacking of existing fractures, potentially increasing fracture transmissivity (these effects are not specific to KBS-3H and are not discussed further in this report). They could also potentially result in creep movement and possible convergence of the drifts (see also Section 7.4.4), and to seismicity and faulting, that could imply shear movements on fractures intersecting deposition drifts and also increase the transmissivity of the sheared fractures (Section 7.4.5).

### **7.3.5 Groundwater flow and composition**

The impact of major climate change on groundwater flow and composition is described in detail in Section 8.3.3 of /Pastina and Hellä 2006/. The following is a brief summary of the effects of permafrost and of ice sheets that are of particular relevance to the evolution and performance of the repository engineered barrier system.

### Effects of permafrost

The development of permafrost is likely to lead to a more stagnant flow pattern at repository depth. If a continuous layer of permafrost is present, surface water cannot penetrate the frozen ground, topographically-driven flow will diminish, and only a minute groundwater flow driven by salinity gradients and weak residual heat generation from the spent fuel will remain. The possibility of open taliks (i.e. unfrozen windows in the permafrost region under lakes or rivers) cannot, however, be disregarded. These will tend to provide a hydraulic gradient similar to the regional topographic gradients, and thus give rise to more significant groundwater flow in (Section 8.3.3 of /Pastina and Hellä 2006/).

Although it has been suggested that the gradual formation of permafrost could lead to increasing salinity of the underlying water, and also that salt-water inclusions within the frozen ground or saline pockets could be formed /Pastina and Hellä 2006/, these effects have not so far been observed in real systems in crystalline rock areas. A period of permafrost is not therefore expected to have any significant effect on composition of groundwater surrounding a repository at Olkiluoto.

Current understanding is that methane is continuously produced in the bedrock (Section 2.2.4), and so the build-up of methane during periods of permafrost may lead to transient hydraulic effects when thawing takes place, although the magnitude of such effects is uncertain.

The issue of possible freezing and thawing on the engineered barrier system is discussed in Section 7.4.2.

### Effects of ice sheets

In the first stages of a glacial cycle, deep extensive permafrost and the presence of a cold-based ice sheet will lead to a reduction in groundwater recharge. For most of the time that an ice sheet is present, however, the ice sheet will be warm based. The high pressure exerted by the overlying ice on the liquid water between the ice and the rock could conceivably force large volumes of low-salinity and possibly oxidising meltwater into deeper parts of the bedrock. Conversely, hydraulic upconing effects could also increase salinity in front of the ice margin (Figure 7-4), as indicated, for example, in modelling studies by /Jaquet and Siegel 2003/.

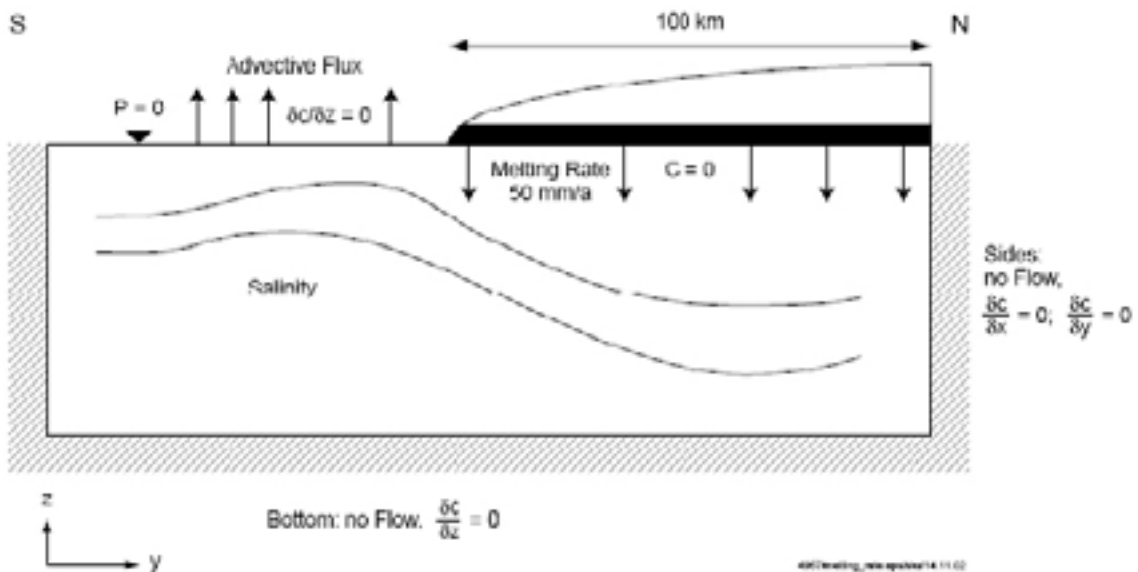


**Figure 7-4.** Schematic illustration of the distribution of salinity below an ice margin and the boundary conditions used by Jaquet and Siegel to model this situation (from Figure 6 of /Jaquet and Siegel 2003/).

Coupled and transient modelling of groundwater flow and solute transport has been used to investigate flow conditions for Olkiluoto under the load of a melting ice sheet for a period of up to 1,000 years. Although there are significant uncertainties, the results indicate that penetration of meltwater to below repository depth could occur if a melting ice sheet remains at the site for hundreds of years. This is consistent with analyses of groundwater composition at Olkiluoto, which indicate that some glacial meltwater has penetrated to such depths in the past and mixed with deeper groundwaters /Pastina and Hellä 2006/.

Although glacial meltwater may penetrate to repository depth, the recent interpretation of hydrogeochemical site data, and especially gas data, from Olkiluoto by /Pitkänen and Partamies 2007/ and /Andersson et al. 2007/ gives no evidence for intrusion of oxygen to repository depth in the past although more information to support this tentative finding will be required in future studies. This can be attributed to consumption of oxygen by microbially mediated processes and the interaction of oxygen with minerals in the rock (Section 6.5.4).

Oxygen intrusion to the repository depth would imply extensive flushing of the groundwater system at this depth with glacial meltwater. Current understanding of the history of the Olkiluoto site does not, however, support this scenario, but rather suggests only moderate dilution of groundwater as a result of meltwater intrusion. Currently at repository depth, the glacial meltwater component is less than 20% /Andersson et al. 2007/, which can include not only the most recent glaciation, but also earlier ones. Detailed fracture mineralogy studies have not been carried out for all drill cores taken from the site, but recently precipitated iron hydroxides, which would be indicative of the migration of dissolved oxygen, have not so far been observed. In addition, calcite with very low methane-based C-13 values, which would be indicative of dissolved oxygen mixing with the methanic groundwater system below about 300 m depth, has not been found. The isotopic composition of methane also suggests that no oxidation of methane, anaerobic or aerobic, has occurred in the deeper groundwater system below sulphate-rich groundwater (i.e. –300 m and deeper). This indicates that neither oxidising glacial meltwater nor marine water, which can cause either aerobic or anaerobic oxidation of methane, respectively, have affected the composition of this deeper system, although this could have taken place on several occasions due to the periodic glacial cycles during the Quaternary. It should also be noted that, even if oxygen-rich glacial meltwater were to reach the repository, an additional scavenger for oxygen in a KBS-3H repository of the current reference design would be the iron in divalent form originating from the corrosion of the steel supercontainer shell.

Based on these arguments, the future intrusion of oxygen-rich glacial meltwater into the deep groundwater system at Olkiluoto is unlikely. A transient reduction in salinity in association with glacial retreat is, however, possible and has implications for the evolution of the canister and buffer (Sections 7.4.3 and 7.4.7, respectively). Ongoing site characterisation work is exploring whether or not such events have happened in the past.

## **7.4 Impact on the engineered barrier system**

### **7.4.1 General description**

Potential effects of major climate change on the engineered barrier system concern:

- freezing and thawing;
- canister corrosion;
- isostatic load on the canisters;
- rock shear associated with post-glacial earthquakes, including its effects on the canister, the buffer and on the fractures undergoing shear movement;
- changes in buffer swelling pressure and the possibility of buffer erosion; and
- buffer liquefaction.

These potential effects are discussed in the following sections without specific reference to the timing of glaciation and deglaciation (the Weichselian-R and Emissions-M scenarios). According to the KBS-3V Evolution Report /Pastina and Hellä 2006/ and SR-Can Main Report /SKB 2006a/, the Emissions-M scenario is no less favourable than the Weichselian-R scenario in terms of its impact on the engineered barrier system because the same processes are expected to occur during future glacial phases, whenever these phases take place. Moreover, in the Emissions-M scenario, these processes are expected to occur at a much later time, when the radioactivity of the fuel has decayed to lower levels.

#### **7.4.2 Freezing and thawing**

Based on studies of past climatic evolution, future permafrost at Olkiluoto is not expected to reach more than 180 metres below ground at (Figure 7-2). Thus, excavations in the upper parts of the repository, e.g., entrance to shafts and transport tunnels, are likely to be subject to freeze-thaw cycling, which may change the properties of bentonite- and cement-based backfill and seals (the impact on bentonite and bentonite mixtures is discussed in /Saarelainen and Kivikoski 2002/). However, the canisters and buffer are not expected to be affected by freeze-thaw cycling. This conclusion applies in both the Weichselian-R and the Emissions-M scenarios. However, the possibility that conditions at Olkiluoto in the future could differ significantly compared with those during the past glaciations and lead to buffer freezing may require further consideration in future studies.

#### **7.4.3 Canister corrosion**

During the next glacial cycle and in the far future, slow corrosion of the copper surfaces of the canisters will continue to take place by reaction with sulphide from the groundwater, which will diffuse to the canister surface through the buffer.

As noted in Section 7.3.5, the migration of oxygen to repository depth in association with future glacial cycles is unlikely. Furthermore, even if this were to occur, scoping calculations by /Ahonen and Vieno 1994/ indicate that canister failure by corrosion would hypothetically require exposure to oxygenated water to be maintained for at least 100,000 years. The possibility of dilute glacial meltwater penetrating to repository depth cannot, however, be ruled out as yet, and may lead to some chemical erosion of the buffer (Section 7.4.7).

If, during repeated glacial cycles, the density of the buffer were to be reduced by erosion to such an extent that advective transport could take place within the buffer, this could increase the rate at which sulphide migrates to the copper surface, and hence increase the copper corrosion rate, reduce canister lifetime and increase radionuclide migration rates in the event of canister failure (the implications for radionuclide release and transport are assessed in the Radionuclide Transport Report, /Smith et al. 2007a/). It should be noted, however, that the next glacial retreat, and hence the next possibility for penetration of glacial meltwater to repository depth, is in 70,000 years time according to the Weichselian-R scenario. Even following partial erosion of the buffer, the rate of corrosion is expected to remain low due to the limited supply of sulphide from the groundwater. Thus, although canister lifetime may be reduced, it is expected to remain at least in the order of a hundred thousand years.

#### **7.4.4 Isostatic load on the canisters**

Glacial loading will affect pore pressures in the rock and in the saturated buffer and the isostatic load exerted on the canisters. The isostatic load will be equal to the sum of the groundwater pressure at repository depth and the swelling pressure of the bentonite. At Olkiluoto, the maximum expected isostatic load on the canister in the absence of an ice sheet is about 11–12 MPa, which is the sum of the swelling pressure of the bentonite and the hydrostatic pressure at repository depth (Section 5.4.3). The maximum ice thickness over Olkiluoto is estimated to have been about 2 km during the last glacial maximum /Lambeck et al. 1998/. A 2 km-thick ice sheet will

increase the load on the canisters by about 18 MPa and a 3 km thick ice sheet by about 27 MPa (/SKB 1999, Rasilainen 2004/; assuming an average ice density of 900 kg m<sup>-3</sup>).

The expected minimum pressure giving rise to total collapse of an intact canister is significantly higher than this (80–114 MPa – see, e.g. Section 4.3.1 of /Pastina and Hellä 2006/), and so no failure of canisters is expected by this mechanism without prior weakening of the insert by corrosion (which could occur, for example, in the case of a canister with an initial penetrating defect – Chapter 8). A more localised failure may be possible at lower pressures. /Dillström 2005/ has carried out a probabilistic analysis in which two failure modes are considered:

- local plastic collapse of the insert; and
- crack growth from an assumed initial defect in the insert.

The results of the analysis showed that, in all cases where crack growth occurred to a significant extent, local plastic collapse occurred at a smaller load. For a base case pressure of 44 MPa, the probability of failure by either mode is insignificant ( $\sim 2 \times 10^{-9}$ ), although the probability of local plastic collapse was found to be strongly dependent on the outer corner radius of the fuel channels and the eccentricity of the steel section cassette. In the base case, it was assumed that the cassette was centred and the outer corner radius was 20 mm.

Additional rock stresses due to glacial loading could potentially result in creep movement and possible convergence of repository drifts, which would in turn affect the density and the swelling pressure of the buffer, and indirectly give rise to some further loading on the canisters. In /Rasilainen 2004/, however, it is stated that time-dependent deformations (creep) are not considered to be a significant factor for intact crystalline rock in the case of a KBS-3V repository. This conclusion is also expected to hold for KBS-3H.

#### **7.4.5 Impact of earthquakes and rock shear on the canisters**

Although seismic activity is currently low at the Olkiluoto site, the possibility that large earthquakes may occur in the future cannot be excluded, and their impact on the repository has to be evaluated.

Any future earthquakes occurring at the Olkiluoto site are not expected to be uniformly distributed in time. Palaeoseismicity studies support the suggestion that major seismic activity was, in the past, limited to a short period after deglaciation, and it is inferred that this will also be the case in the future (Section 2.2.2).

Ongoing geological characterisation and modelling is expected to give insight into the characteristics of deformation zones at the site and their potential to host future large earthquakes, such that major zones capable of undergoing such earthquakes will be avoided when constructing the deposition drifts (Sections 2.2.2 and 2.2.7). A large earthquake occurring on a major deformation zone may, however, trigger shear movements on smaller-scale fractures. These could lead to a deformation of the bentonite buffer and to additional stresses being exerted on the canisters. A movement of 0.1 m or more on a fracture intersecting a deposition drift at a canister position is cautiously defined as “potentially damaging” to the canister, assuming the properties of the buffer are as expected /Börgesson et al. 2004, Börgesson and Hernelind 2006c/. The following sections discuss:

- the probability of canister damage due to shear movements on fractures with the potential to undergo shear movements of 0.1 m or more assuming that they are not detected and avoided (and assuming that the buffer protects the canister against smaller rock movements); and
- the possibility that changes will occur in the properties of the buffer that reduce its capacity to protect the canisters in the event of smaller rock shear movements.

The potential of a fracture to undergo shear movements is related to its size, as well as its distance from the earthquake, and orientation effects /Munier and Hökmark 2004, Fäth and Hökmark 2006/. The probability that fractures with the potential to undergo shear movements of 0.1 m or greater will, in practice, be detected and avoided has not yet been evaluated. As far



as practically possible, the likelihood of canister damage will be reduced by applying suitable canister deposition criteria. These may be related to distance from deformation zones (see, e.g. Section 8.3.2 of /Pastina and Hellä 2006/, where it is noted that criteria in the form of respect distances developed by /Munier and Hökmark 2004/ for a repository in Sweden are also applicable at Olkiluoto) and possibly the size of fractures intersecting the drift. In SR-Can, the calculated probability of canister failure is significantly reduced by assuming that the Expanded Full Perimeter Criterion (EFPC) is applied, whereby large fractures intersecting both the full perimeter of a KBS-3V deposition tunnel and the deposition hole are assumed to be readily observable and avoided /Munier 2006/. It is uncertain, however, whether or not a similar line of reasoning can be applied to a KBS-3H repository, without rendering a large proportion of the drift unusable. Thus, no criterion similar to the EFPC is applied in the calculation of the likelihood of canister damage described below, although this remains an issue for further study.

### ***Likelihood of canister damage***

A method for calculating the probability of a KBS-3V canister location being intersected by a fracture capable of slipping by more than a prescribed amount, assuming that such fractures are not detected and avoided when the canisters are deposited, is given in /Hedin 2005/. The method is applied in SR-Can to the sites under consideration in Sweden. The method is based on the notion that, if the distributions of fracture sizes and orientations in a host rock are known, and if a canister is emplaced randomly in that host rock, then it is possible to calculate the probability that the canister is intersected by fractures of specified properties, and in particular by fractures that exceed a certain size. It is further assumed that the maximum slip that a fracture can undergo is proportional to its size, and so the fractures of interest are those large enough to slip by more than 0.1 m. The fracture population is described as several fracture sets, each with specified distributions of sizes and orientations. The distributions of sizes and orientations within a set are assumed to be uncorrelated. Furthermore, all fractures are treated as infinitesimally thin, circular discs.

The method can readily be applied to KBS-3H canister locations at Olkiluoto, as described in Appendix B.5. Results have been obtained using the same fracture network data as used in an earlier numerical simulation study of rock movements at Olkiluoto and other sites in Finland due to future earthquakes by /La Pointe and Hermanson 2002/. It is assumed that no fractures in the size range 100 m to 500 m are detected and avoided as emplacement locations, and that all these are the fractures that have the potential to undergo damaging shear movements (movements > 0.1 m).

The expectation value of the number of canisters in the repository that could potentially be damaged by rock shear in the event of an earthquake is calculated to be 16 out of a total number of canisters of 3,000 (i.e. a fraction 0.0053). For KBS-3V, a higher expectation value of 20 is calculated, the difference being largely due to greater vertical extent of a KBS-3V repository and hence its greater vulnerability to movement on the relatively dense population of sub-horizontal fractures). Application of a canister position avoidance criterion, such as the Expanded Full Perimeter Criterion (EFPC) applied in SR-Can, would significantly decrease this number. The marginal probability of encountering an earthquake of sufficient magnitude to induce such movements at Olkiluoto in a 100,000 year time frame has been estimated at 0.02 (Table 5-8 in /La Pointe and Hermanson 2002/).

These results are, however, subject to significant uncertainties and are regarded as preliminary. The fracture network data used by /La Pointe and Hermanson 2002/ and in the present study are based largely the work of /Poteri 2001/ and are likely to be revised in the course of future studies. For SR-Can, a complete fracture model was used that included both sealed and open fractures when computing intersection probabilities. /La Pointe et al. 2000/, however, demonstrated by means of a sensitivity study that fractures with even moderate amounts of cohesion and friction will not slip as a result of earthquakes. Thus, La Pointe and Hermanson adjusted the fracture intensity (P32) of the discrete fracture network model based on the assumption that only open fractures have the potential to slip. Cohesion and friction between the surfaces of fractures

classified as filled or tight was assumed to prevent these fractures from slipping. Cohesive fractures (sealed or partly open) have also been excluded in the data used for the present study. If the assumption were not to hold, it would lead to the expectation value of the number of canisters in the repository that could be damaged by rock shear being an underestimate.

On the other hand, in applying the model of /Hedin 2005/, fractures within a given set are assumed to be distributed randomly throughout the rock. In reality, fractures tend to be concentrated mainly in local zones of abundant fracturing (Section 2.2.3), and such zones are likely to be avoided as canister emplacement locations, particularly if they give rise to groundwater inflow that exceeds 0.1 litres per minute. Individual fractures giving rise to relatively high initial inflows will also be avoided as canister emplacement locations (see the discussion of repository layout in Section 2.2.7). Although the correlation between fracture size and initial inflow is uncertain, fractures giving higher inflows are more likely than others to be sufficiently large to undergo significant rock shear in the event of a large earthquake. This means that, in this respect, the model will tend to overestimate the number of canisters that could be damaged by rock shear.

Another issue for future study is the impact of multiple small (< 0.1 m) rock movements on the safety functions of the buffer and canister. It should be noted, however, that the potential for shear displacements to damage the canisters is a function not only of the total shear displacement, but also of the shear velocity, with a higher shear velocity being more likely to result in canister damage /Börgesson and Hernelind 2006c/. The average shear velocity in the event of multiple small displacements will be significantly less than in the event of a single displacement of the same total magnitude, and the high total stresses induced by a small, sudden displacement will decrease due to pore pressure dissipation and creep before the next event.

In principle, a single, large, sub-horizontal fracture could affect multiple KBS-3H canisters along a drift (Figure 7-5). It is, however, considered likely that any such fracture would be readily detected and the portion of the drift affected by it would be excluded during super-container emplacement. Furthermore, the model of /Hedin 2005/ can be extended to show that, even if such fractures went undetected, the number of canisters that could be damaged in this way in the event of an earthquake is small (about 1 in 2,800 for canister pairs and about 1 in 8,300 for canister triplets) – see Appendix B.5.

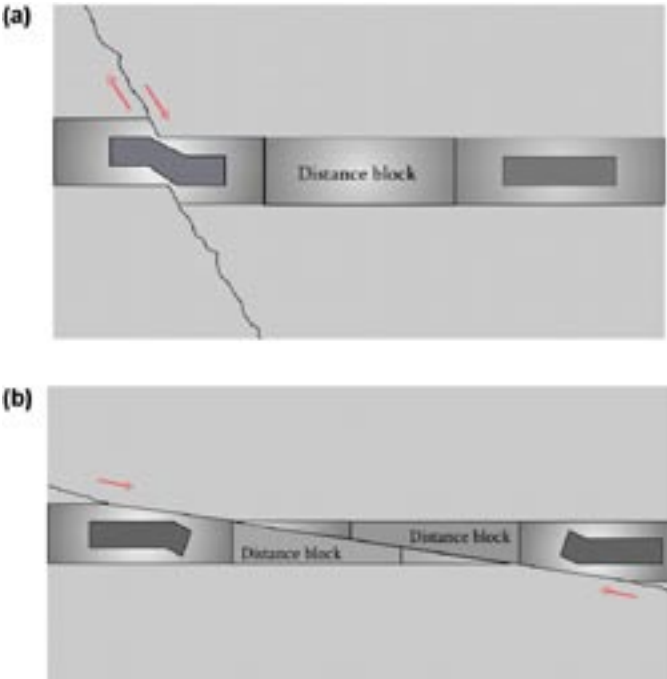


**Figure 7-5.** Shear movements on (a), a subvertical and (b), a subhorizontal fracture intersecting a KBS-3H drift.

Thus, the expectation value of the number of canisters in the repository that could potentially be damaged by rock shear in the event of a large earthquake is taken to be 16 in the current safety studies, with a probability of 0.02 of such an earthquake occurring in a 100,000 year time frame, although there are some significant uncertainties associated with these values that could lead to them giving either an underestimate or an overestimate of the actual likelihood of damage.

### ***Possibility of reduced capacity of the buffer to protect the canisters***

Rock shear movements of less than 0.1 m could conceivably damage the canister if the protection afforded by the buffer is reduced as a result of:

1. Processes occurring during the early phase of evolution, if these were to lead to a local increase in the buffer density around the canisters to a value greater than  $2,050 \text{ kg m}^{-3}$  (see the criteria for buffer safety function indicators – Table 2-3).

The discussion in Section 5.5 indicates that densities greater than  $2,050 \text{ kg m}^{-3}$  will not occur as a result of the loss or redistribution of buffer mass during the early phase of evolution, at least in the case of intact canisters. Higher densities could conceivably arise in the case of a canister with an initial penetrating defect, due to the corrosion and volume expansion of the canister insert (Section 8.5), but in this case that canister will already have failed.

2. The sinking of the canisters through the buffer under their own weight, especially if they come into contact with the drift walls.

Canister sinking is expected to be negligible over a timescale of hundreds of thousands of years (see Section 6.4.3).

3. Chemical alteration processes resulting in a significant increase in buffer stiffness.

As discussed in Section 6.5.3, over a sufficiently long period (up to hundreds of thousands of years) it is possible that mineral transformation of the buffer due to reaction with steel components, particularly the supercontainer shell, could lead to an increase in buffer stiffness. /Börgesson and Hernelind 2006c/ showed that an increase in stiffness of a part of the buffer can result in the impact of rock shear of a given magnitude being more significant in terms of potential canister damage. However, since the 0.1 m limit described above is conservative (in reality, somewhat larger shear movements are also unlikely to result in canister damage; /Börgesson et al. 2004/), and since in the case of iron/bentonite interaction only a small part of the buffer near to the steel components is likely to be affected over a timescale of hundreds of thousands of years, the capacity of the buffer to protect the canisters from rock shear movements smaller than the 0.1 m limit described above, is expected to be maintained.

### **7.4.6 Other potential impacts of rock shear**

Shear movements on fractures intersecting the repository drifts as a result of large earthquakes may cause some mechanical erosion of the buffer. If sufficient erosion were to take place, then advective conditions could become established within the buffer. /Börgesson and Hernelind 2006b/ have calculated the buffer swelling pressure for cases where, in KBS-3V, one, two and three entire bentonite rings surrounding the canister have been omitted, to illustrate the effects of a local loss of large amounts of bentonite. The conclusion was that a mass loss of 1,200 kg to a fracture intersecting the deposition hole would lead to conditions where advective conditions in the buffer must be considered. Due to the similarity between the deposition hole diameter in KBS-3V (1.75 m) and the deposition drift diameter of in KBS-3H (1.85 m), this conclusion can be taken to apply to both alternatives. Although no specific studies have been conducted, shear movements on intersecting fractures are considered unlikely to give rise to mass losses from the buffer of this magnitude.

A further potential impact of rock shear is to increase the transmissivity of fractures intersecting the drifts. The magnitude of such an increase is unknown, and is treated conservatively in the evaluation of radionuclide release and transport in the event of canister rupture due to rock shear in the Radionuclide Transport Report /Smith et al. 2007a/.

#### **7.4.7 Changes in buffer swelling pressure and the possibility of buffer erosion**

As noted earlier in this chapter, penetration of some dilute water to repository depth in association with future glaciations cannot be ruled out, which may lead to some reduction in groundwater salinity. A significant reduction in groundwater salinity at repository depth will increase buffer swelling pressure, and could potentially lead to the erosion by flowing groundwater of buffer (and filling block) material intruded into fractures intersecting the repository drifts if the ionic strength of the water is less than the Critical Coagulation Concentration (CCC); see Section 6.5.2. This process is termed “chemical erosion”

Tentative calculations of chemical erosion in a KBS-3V repository presented in SR-Can suggest that the possibility of advective conditions becoming established at some locations in the buffer cannot be excluded, and that this may occur as early as the next period of glaciation in the least favourably located deposition holes (Section 12.7 of /SKB 2006a/). The same reasoning applied to a KBS-3H repository at Olkiluoto would suggest that this degree of erosion would only occur in association with fractures with transmissivities of around  $3 \times 10^{-8} \text{ m}^2 \text{ s}^{-1}$  or higher. The avoidance of drift sections with initial inflows of more than 0.1 litres per minute as canister and buffer emplacement locations may exclude many such fractures, although there is uncertainty in the relationship between transmissivity and initial inflow (Section 2.2.7), and the bentonite filling blocks used in drift sections with initial inflows up to 1 litre per minute may still be significantly affected by chemical erosion. Furthermore, the model of chemical erosion used in SR-Can is subject to significant uncertainties. It is acknowledged in SR-Can that better understanding of the erosion process could lead to models that yield either lower or higher erosion rates and higher or lower rates of canister failure. An experimental programme and new model development to address this process are currently under development by SKB/KTH (using a preliminary model, /Liu and Neretnieks 2006/) have modelled chemical erosion of the buffer under different flow conditions and for different contents of gypsum in the buffer). It should be noted that, for KBS-3H, the loss of buffer around one canister due to exposure to glacial meltwater may affect the corrosion rate of neighbouring canisters, since the buffer density along the drift will tend to homogenise over time. This also means, however, that the impact on buffer density and on the corrosion rate of the first canister will diminish with time. This is in contrast to the case of KBS-3V, where buffer loss around one canister will not affect the state of the buffer around the other canisters.

It is cautiously assumed in the present safety studies that the conclusion from SR-Can that advective conditions in the buffer could arise during the next period of glaciation also applies to a KBS-3H repository at Olkiluoto. The impact of early canister failure due to corrosion following erosion of the buffer on radionuclide release and transport is considered in the Radionuclide Transport Report /Smith et al. 2007a/.

#### **7.4.8 Buffer liquefaction**

Liquefaction of the buffer could occur during glacial periods if the pressure increase in rock fractures reduces the effective stress (swelling pressure) of the buffer to zero. It has been argued that buffer liquefaction will not occur in a KBS-3V repository at the Swedish sites considered in SR-Can /SKB 2006a/ and these arguments are also expected to apply to a KBS-3H repository at Olkiluoto.

## **8 Evolution of a canister with an initial penetrating defect**

### **8.1 Possibility of occurrence**

The evolution of a canister with an initial penetrating defect is described in the following sections. Given the central role of the canisters in the KBS-3H and KBS-3V safety concepts, the possibility of initial defects that penetrate the copper shell is of crucial importance. As noted in Section 4.2.2, Posiva is not yet taking any position on the likelihood of occurrence of such defects. The evolution of a canister with an initial penetrating defect is described in this report since it provides a convenient basis for exploring various uncertainties affecting radionuclide release and transport in the Radionuclide Transport Report /Smith et al. 2007a/.

### **8.2 Key phases in and aspects of evolution**

The following phases in, or aspects of, the evolution of an initially defective canister can be identified:

- water ingress following penetration of the copper shell;
- interaction of water with the cast iron insert;
- impact of iron and of iron corrosion on the buffer;
- contact of water with the cladding and the fuel pellets and the effects of ionising radiation;
- corrosion of the cladding and other metal components and impact on radionuclide release;
- release of segregated radionuclides;
- fuel dissolution and impact on radionuclide release;
- fate of released radionuclides; and
- the possibility of nuclear criticality inside the canister.

These are described in turn in the following sections.

### **8.3 Water ingress following penetration of the copper shell**

At the time of deposition, void spaces inside the canister will be present:

- in the annulus between the copper shell and the cast iron insert; and
- within the insert around the spent fuel assemblies.

If the copper shell has a penetrating defect, water vapour will start to enter these internal void spaces immediately upon fabrication. Liquid water will also enter these internal void spaces following emplacement as the buffer saturates, driven by the pressure difference between the buffer porewater and the initially relatively low gas pressure inside the canister. The low hydraulic conductivity of the buffer and the localised nature of the defect will, however, provide hydraulic resistances that will limit the rate of inflow.

There is significant uncertainty regarding the extent and accessibility of the different internal void spaces within the canister. It is likely that the annulus between the copper shell and the cast iron insert will close over time, at least partly, as a result of creep deformation of copper caused by the swelling pressure exerted on the canister by the buffer /Knuutila 2001/. Furthermore, unless it has been damaged prior to water ingress, the insert itself will initially prevent access of water to the void spaces around the fuel assemblies.



## 8.4 Interaction of water with the cast iron insert

Water entering a failed canister will react with and corrode the cast iron insert, resulting in:

- the formation of iron corrosion products;
- the weakening of the insert;
- the generation of hydrogen gas; and
- the interaction of iron corrosion products with bentonite located in the vicinity of the defect.

The rate at which these effects occur depends on the corrosion rate of iron and the surface area over which corrosion occurs (see also the discussion of the corrosion of steel components external to the canister in Section 5.6.4).

The behaviour of the water/vapour/gas system in a defective copper-iron canister is complex and has been discussed in various reports /Vieno et al. 1992, Wikramaratna et al. 1993, Bond et al. 1997, Takase et al. 1999, Vieno and Nordman 1999, SKB 2006e, Rasilainen 2004/. The intruding water is expected to be oxygen free, and therefore the corrosion of the insert will be anaerobic. As discussed in Section 5.6.4 in the context of steel components external to the canister, the expected initial corrosion product of steel in the presence of bentonite is magnetite, although, depending on solution conditions, some iron sulphide and siderite may also form. Subsequent film dissolution can produce iron silicates. Electrochemical reactions on the copper surface may have some influence on insert corrosion, although measured corrosion rates of cast iron galvanically coupled to copper are in the same range as those measured without coupling /Smart et al. 2005/, and so the effect is considered to be small.

Initially, the corrosion rate of iron will be high, but will decrease rapidly as a surface film of magnetite develops (magnetite is expected to form as a thin adherent layer with a thickness that is constant in time and an outer, looser layer with poor adhesion). The corrosion rate will then depend on the availability of water and the transport resistance of the inner layer (it has been shown to be independent of both hydrogen gas pressure and the concentration of dissolved Fe(II) in the system; /Smart et al. 2002ab/). For a sufficiently small water inflow rate, all water entering the canister will be consumed by corrosion of iron and the corrosion rate will be limited by the rate of supply of water. For larger inflow rates, water will accumulate in the canister annulus. In this case, the corrosion rate will be limited by the transport resistance of the inner magnetite layer and is expected to remain constant over time. The surface area over which corrosion occurs depends on the accessibility of internal void spaces within the canister, which, as noted above, is subject to uncertainty. Accessibility refers to both liquid water and water vapour; note that both liquid water and water vapour give rise to corrosion and that the anaerobic corrosion rate of iron in the presence of water vapour is the same as in liquid water /Smart et al. 2002ab/. Thus, although liquid water may be present only at the bottom of the void space, corrosion by reaction of water vapour can occur throughout all the connected parts of the internal void space.

The inflowing water will contain some dissolved natural gases from the host rock – mainly methane and hydrogen (Section 2.2.4). Due to the initially lower pressure inside the canister annulus compared with the pore pressure in the buffer, degassing of hydrogen and methane may occur. The gas released in this way will mix with gas initially present in the annulus and gas generated by iron corrosion. Furthermore, as a result of the lowered dissolved gas concentration in water inside the canister, some dissolved hydrogen gas may diffuse from the buffer into the canister annulus, although the impact of this process on overall gas migration will be small.

Assuming that the annulus remains open as water enters, the corrosion products formed by the reaction of water entering this volume with the surface of the insert will gradually fill the open space, since the molar volumes of all relevant corrosion products are larger than the molar volume of the original uncorroded iron. At the same time, the generation of hydrogen gas will increase the gas pressure inside the annulus, since the buffer surrounding the canister has a low permeability to gas flow. As the gas pressure increases, some gas will dissolve in the water inside the canisters and diffuse through the defect into the buffer. The rate of gas dissolution and diffusion is, however, expected to be much lower than the gas production rate, and gas pressure will continue to rise.

The increasing gas pressure will reduce and possibly eventually reverse the driving force for liquid water ingress. Even if all liquid water has either been expelled or consumed by corrosion, corrosion will continue due to vapour, which will diffuse into the canister through the defect. However, as the void space fills with corrosion products, the corrosion rate will drop due to the increasing transport resistance between the defect and the uncorroded surfaces. According to model calculations reported in SR-Can /SKB 2006e/, the annulus will become completely filled with corrosion products about 20,000 years after initial ingress of water into the copper shell.

The subsequent evolution of the system is uncertain. Provided the initial defect where penetration occurs remains small, possibly becoming plugged with bentonite or corrosion products, corrosion of the external surface of the insert is likely to drop to a very low rate, being controlled by the slow migration of water through the defect and corrosion product pore space to the corroding surface or the slow dissolution of the corrosion products and diffusion of the dissolved iron to the defect and into the buffer (Figure 8-1a). On the other hand, the mechanical pressure exerted on the copper shell by the corrosion products could potentially expand the original defect, allowing corrosion of the insert to continue at an increased rate (unlimited water supply), at least over the part of its surface nearest to the defect (Figure 8-1b). In both cases, the canister insert will be weakened by progressive corrosion.

Eventually, weakening of the insert by corrosion will lead to the canister collapsing under the external load. The conditions and timing of the collapse are subject to large uncertainty. For example, it is uncertain whether the collapse of the insert will be accompanied by a further rupturing of the copper shell. The greatest mechanical forces on the canister are likely to arise during or subsequent to a glacial episode. As described in Sections 7.4.4 and 7.4.5, respectively, for an intact canister, the likelihood of collapse due to increased isostatic loading associated with glaciation is negligible, and that of rupture due to rock shear associated with post-glacial earthquakes is small. This is because of the mechanical strength of the insert and, in the case of rock shear, the protection afforded by the plasticity of the buffer. In the case of a defective canister, however, the likelihood of collapse or rupture, especially during and subsequent to a glacial episode, is significant if the canister insert has already been weakened prior to or during glaciation by corrosion. Thus, it is likely that the collapse of a weakened insert will take place during or after a major glaciation, although earlier collapse cannot be excluded.

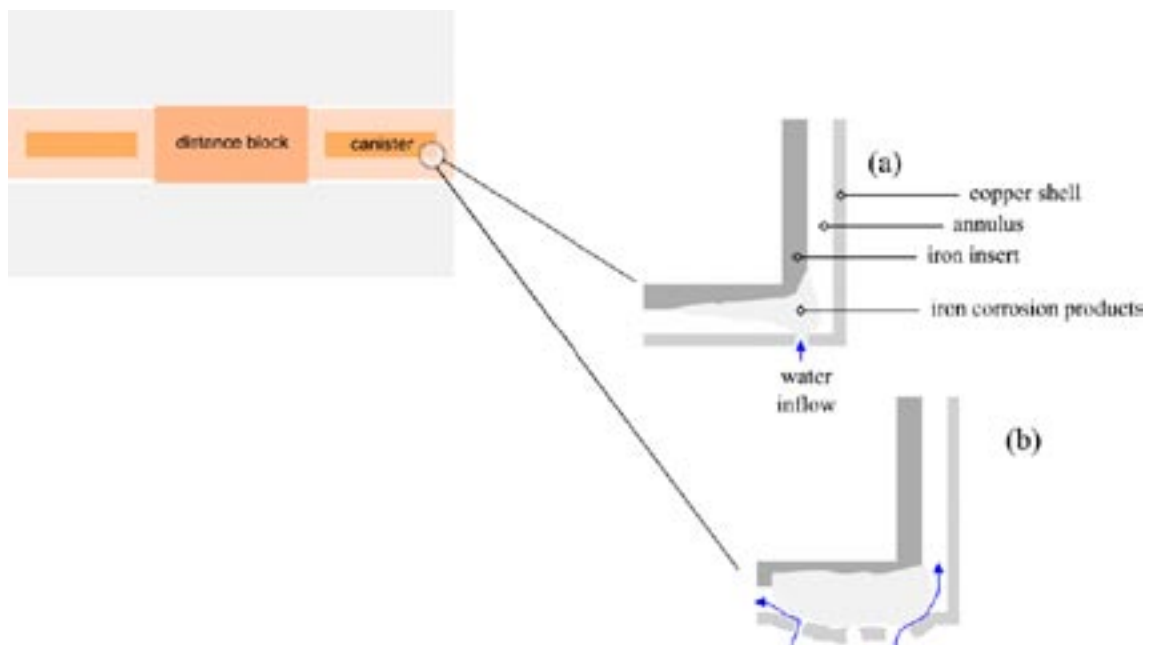


**Figure 8-1.** Possible impacts of iron corrosion on water inflow – (a), corrosion products and bentonite plug the defect in the shell, providing a barrier to further inflow, (b), corrosion products expand the original defect, increasing water inflow

## 8.5 Impact of insert corrosion on the buffer

The corrosion products from the corroding insert may react with swelling clay minerals in the buffer in the vicinity of the canister defect and may change its mineralogical and physical properties. 1-D transport modelling of the interaction between the corrosion products of the steel supercontainer shell and the buffer, as discussed in Section 6.5.3, indicates that transformation of the buffer will be slow, with the affected zone being limited to a few centimetres over a timescale of hundreds of thousands of years or more. The same argumentation can be applied to the impact of insert corrosion on the buffer, but with the additional limiting factor of the residual transport resistance of the defect.

Apart from this chemical interaction, the formation of iron corrosion products with a higher volume than the original metallic iron may also expand the copper shell and lead to a compaction of the buffer, increasing the pressure exerted by the buffer on the canister and rock, and potentially reducing the protection afforded to the (already failed) canister by the buffer against rock shear (Section 7.4.5). In the case of a KBS-3V repository, compaction of the buffer as a result of the expansion of the canister diameter will be offset by the buffer “relaxing” by expansion into, and compaction of, the space above the deposition hole (the crushed rock/bentonite tunnel backfill). This will limit the increase in buffer density and swelling pressure in the gap between the canister and the wall rock. Preliminary modelling by /Bond et al. 1997/ indicates that the overall effect is not significant for KBS-3V. In the case of KBS-3H, creep along the drift may also mitigate, to some extent, the compaction of the buffer around the canister, although, in both repository alternatives, frictional forces within the buffer mean that some increase in buffer density around a failed canister is likely to remain. Assuming pessimistically that only the buffer originally inside the supercontainer and the void space inside the canister take up the increased volume, and that the insert is completely converted to magnetite, a scoping calculation in Appendix B.4 indicates an increase in buffer density around the canister to  $2,160 \text{ kg m}^{-3}$ . This does not satisfy the criteria for the safety function indicators for the buffer, which give a maximum buffer density of  $2,050 \text{ kg m}^{-3}$  (Table 2-3) The calculation is, however, conservative. In reality, there is likely to be some relaxation of the increased density by buffer creep along the drift, although internal friction will mean that some locally increased density around the failed canister is likely to remain.

Buffer with a density above  $2,050 \text{ kg m}^{-3}$  may give reduced protection against rock shear, although the initially defective canister has already failed. Furthermore, the increased buffer swelling pressure could cause some damage to the adjacent rock, although the extent of such damage is likely to be limited to a small region adjacent to the drift wall. Modelling by /Lönqvist and Hökmark 2007/ has found that pressures of the order of 10 MPa are required in the deposition drift to cause opening of intersecting rock fractures. To open these sufficiently to bring them into tension at distances between 0 m and 0.2 m from the drift periphery requires about 20 to 25 MPa. Furthermore, the effects were found to be modest in terms of increase in fracture aperture and distance from the drift wall to which such effects extend.

## 8.6 Contact of water with the cladding and fuel pellets and the effects of ionising radiation

Once water penetrates the cast iron insert and enters the channels in the insert containing the fuel assemblies, it will corrode the channel surfaces, giving rise to further corrosion products and gas. It will contact the surfaces of the cladding and, if the cladding tubes are already ruptured by creep failure, delayed hydrogen cracking (DHC) or failure due to damage during handling (Sections 4.1.3 and 5.7.6), it will also contact the surfaces of the fuel pellets and interact with them.

Ionising radiation from the fuel will cause excitation or ionisation of water molecules near to fuel surfaces and the breaking of their chemical bonds (radiolysis). Even in the case of intact cladding tubes, water inside the fuel channels but outside the tubes will undergo radiolysis. This will be mainly gamma radiolysis because of the relatively low Linear Energy Transfer (LET) and hence long range of gamma radiation. Radiolysis will give rise to a range of products, including stable molecular species such as H<sub>2</sub> and H<sub>2</sub>O<sub>2</sub>, and highly reactive radicals. The contribution of radiolytic hydrogen to overall hydrogen production inside the canisters is expected to be small compared with that from corrosion of the insert, especially since the gamma radiation field from the spent fuel is expected to have decreased markedly by the time significant amounts of water enter the canisters (gamma radiolysis is only relevant for a few hundred years after deposition of the canisters).

## **8.7 Corrosion of the cladding and other metal components and impact on radionuclide release**

The cladding will slowly corrode on contact with water, resulting in the congruent release to solution of activation products embedded within it. Based on experimental studies of the corrosion of titanium /Mattsson and Olefjord 1984, 1990, Mattsson et al. 1990/, which is expected to behave in a similar manner to Zircaloy, it is expected that general corrosion of the cladding will be controlled by the dissolution of the film of zirconium dioxide that will form on, and be tightly bound to, the cladding surfaces. Due to the presence of the zirconium dioxide film, any radiolytically produced nitric acid is expected to preferentially corrode the cast iron insert, and thus not significantly affect the corrosion rate of the cladding tubes. The solubility of zirconium dioxide is low /Bruno et al. 1997/ and corrosion of the cladding will thus proceed slowly at a constant rate estimated at about 2 nm per year /Rothman 1984/. Thus, complete corrosion of the 0.6–0.7 mm thick tubes<sup>30</sup> will require about 400,000 years, although there are uncertainties associated with the extrapolation of the corrosion rate from the results of short-term experiments.

Other metal components in the fuel, which are composed of stainless steels or other nickel based alloys, will also corrode on contact with water and release activation products congruently.

Rupturing of the cladding tubes is likely to take the form of holes or cracks in otherwise relatively intact tubes. The ruptured cladding tubes will, therefore, still provide a partial barrier to the migration of water to the fuel surfaces and the release of radionuclides from the fuel to the canister exterior. There are, however, uncertainties in the probability and extent of rupturing.

In SR-Can, for transport modelling purposes, all cladding tubes are pessimistically assumed to be damaged and to provide no barrier to water ingress and radionuclide release subsequent to canister failure. The same assumption is made in the present study of a KBS-3H repository at Olkiluoto, as described in the Radionuclide Transport Report /Smith et al. 2007a/. In SR-Can, the activation products present in the cladding and in other metal components are conservatively assumed to be released instantaneously upon ingress of water to the canister interior. However, in the Radionuclide Transport Report /Smith et al. 2007a/, release congruent with the corrosion of these materials is explicitly modelled.

## **8.8 Release of segregated radionuclides**

Once water contacts the fuel pellet surfaces through ruptures in the cladding tubes, radionuclides that have been segregated to grain boundaries in the fuel, to pellet cracks and to the fuel/sheath gap will either rapidly enter solution (these radionuclides generally have high solubility and mobility), or, in the case, for example, of C-14, may form volatile products such as methane

---

<sup>30</sup> Zirconium tube thicknesses are given in /Ikonen 2006/.

or carbon dioxide that will mix with hydrogen gas produced principally by corrosion of the insert. These volatile products will be in solubility equilibrium with the water. The release of segregated radionuclides will take place on a timescale in the order of days. The assumption of instant release of all segregated radionuclides is made in the SR-Can safety assessment and is also made in the safety assessment of a KBS-3H repository at Olkiluoto. Instant release fractions are given in the Radionuclide Transport Report /Smith et al. 2007a/, based on values from the SR-Can Data Report /SKB 2006b/.

## 8.9 Fuel dissolution and impact on radionuclide release

Water will also start to interact (but far more slowly) with the surfaces of the fuel matrix, and radionuclides embedded in the fuel matrix, along with radioactive gases present in fission gas bubbles, will be released as the matrix is dissolved or otherwise altered. The rate at which this occurs is determined primarily by redox conditions in the immediate vicinity of the fuel surfaces. Redox conditions will be affected by the composition of water entering the cast iron insert and, potentially, by the radiolysis of water near the fuel surfaces. By the time that liquid water contacts the fuel, the corrosion of the cast iron insert is expected to have produced substantial amounts of hydrogen, part of which will dissolve in the intruding water and be present together with Fe(II) ions. The intruding water will be oxygen free, any oxygen remaining in the repository at the time of closure having been consumed by bacteria, by the reducing minerals in the rock and bentonite and by the surfaces of the copper canisters (Section 5.6.3). When water contacts the fuel (which is likely to be more than several thousand years after disposal), alpha radiolysis is expected to dominate over beta and gamma radiolysis near to the fuel surfaces, the predominant products being  $H_2$  and  $H_2O_2$ . The degree of radiolysis occurring after several thousand years or more is not, however, expected to cause significant oxidative dissolution of the fuel matrix in the presence of hydrogen gas and corroding iron /Werme et al. 2004/.

/Werme et al. 2004/ have proposed fractional fuel dissolution rates to be used in the SR-Can safety assessment on the basis of several recent experimental studies performed on alpha-doped  $UO_2$  and spent fuel under anaerobic, reducing conditions in the presence of a hydrogen atmosphere and in the presence of corroding iron. In SR-Can, rates are sampled from a triangular distribution with a peak at  $10^{-7}$  per year, and upper and lower bounds of  $10^{-6}$  and  $10^{-8}$  per year, to take account of uncertainties in the mechanism of the dissolution process. The distribution is conservative, in that it is expected to over-estimate dissolution rates. In reality, the rate of dissolution or alteration of the fuel matrix may be inhibited over time by the build-up of secondary phase deposits on the fuel surfaces, limiting the amount of water contacting the unaltered fuel. This process has not, however, been quantitatively evaluated. The rate of dissolution will also slowly vary as the wetted surface area of the fuel (including grain boundaries) varies over time. Again, this process has not been quantitatively evaluated, but variations are expected to be insignificant given the slow rate of matrix dissolution or alteration.

The rates assumed in the Radionuclide Transport Report /Smith et al. 2007a/ are also based on the recommendations of /Werme et al. 2004/. The recommended values are based on the expected situation of reducing conditions in the repository and the presence of hydrogen gas and/or corroding iron and iron corrosion products. Fuel dissolution rates are based on measurements taken in solutions of low ionic strength, for which most data is available. /Loida et al. 2004/, however, show that dissolution rates are not significantly affected by salinities up to 5 M NaCl, which is even more severe than the conditions at Olkiluoto. The recommended values have been used without further evaluation, although there remains considerable uncertainty regarding the validity of various proposed models for fuel dissolution, and this remains an important area for further studies (Chapter 12).



## 8.10 Fate of released radionuclides

### 8.10.1 Solubilities and speciation

Radionuclides released from the fuel (including activation products in the metal components) will either enter solution, form volatile species that can mix with repository-generated gas (particularly relevant for C-14<sup>31</sup>), or, if their solubilities in water are low, precipitate either as immobile solids or as colloids.

Solubility limited concentrations used in the Radionuclide Transport Report are based on the study by /Grivé et al. 2007/. Solubilities are dependent on the chemical environment and on temperature. The chemical environment will also affect the speciation of radionuclides in solution. Reducing conditions are expected inside the canisters due to corrosion of the cast iron insert and because the surface of the spent fuel in the presence of dissolved hydrogen is expected to be a strong oxidant scavenger. Other chemical parameters affecting solubilities and speciation, such as pH, the concentrations of strong complexing ligands such as the carbonate ion and salinity are site-specific and have been assessed for a repository at Olkiluoto in /Grivé et al. 2007/. The solubility-limited concentrations of important radionuclides used in SR-Can are reported in /SKB 2006b/, based on /Duro et al. 2006/.

### 8.10.2 Transport mechanisms

Dissolved radionuclides and radionuclides in gaseous form will be transported by gas and water movements (advection) and by diffusion in the interior of the canister, and will exit the canister through the damaged copper shell. The structures inside the canister, including the cladding tubes, other metal parts of the fuel, the cast iron insert and accumulations of iron corrosion products will hinder water movement and provide transport resistances and long transport times for migrating radionuclides (although, as described above, the way in which these features will evolve is uncertain). Sorption of Fe(II) from iron corrosion on the pore surfaces of the buffer may compete with the sorption of some species, such as Ni(II) and Sr(II), and thus weaken the barrier function of the near field for the corresponding radionuclides. The relevance of competitive sorption of Fe(II) is not yet well understood because of lack of experimental data. On the other hand, the surfaces of the structures inside the canister and the newly formed surfaces of their corrosion products display good sorption properties for some radionuclides, offsetting to some extent any detrimental effects of competitive sorption, although it is not currently possible to make any quantitative assessment (these are issues identified for further study – Chapter 12).

Radionuclides in colloidal form will also migrate in water in the canister interior by advection and diffusion. The microporous structure of the buffer is, however, expected to ensure that no radionuclides are transported out of the canister in colloidal form. This structure may be perturbed by processes affecting the evolution of the buffer, including drying/wetting, impact of iron saturation, silica precipitation and strain caused by deformation of the supercontainers, and these potential perturbations require more thorough investigation (Chapter 12). Nevertheless, according to current understanding, none of these processes are likely to reduce the average buffer density between the canister and the rock below that required to filter colloids (1,650 kg m<sup>-3</sup> – see Table 2-3), lead to extensive embrittlement and fracturing of the buffer across its entire thickness, or to canister sinking to the extent that the colloid filter provided by the buffer became ineffective.

The fate of water/vapour/gas and radionuclides in a defective canister depends to some extent on the location of a possible defect in the canister, as well as on the orientation of the canister, the defect size and its evolution, contact surfaces, corrosion rate, etc. This affects the level of the water/gas interface inside the canister, water/gas transport into and out of the canister (possibly including gas-induced porewater displacement) and radionuclide transport. The water ingress – gas generation – water expulsion scenario is more likely to occur in KBS-3H compared with

---

<sup>31</sup> C-14 may be present as carbonate complexes and organic acids, as well as in the form of methane.

KBS-3V. This is because, as described in Section 4.2.2, the initial defect is most likely to occur in the weld region, which is located at the top of the canister in KBS-3V. Defects at locations on the lower part (or at the underside) of the canister cannot be ruled out, but are considered to be significantly less probable than those in the weld at the top of the canister. In contrast, defects in KBS-3H will occur with similar probabilities on the underside and on the upper side of the canister.

### 8.10.3 Conditions for gas-induced displacement of porewater

Model calculations of the fate of water/vapour/gas and radionuclides in a horizontally emplaced canister with a single, small penetrating defect are described in the Process Report /Gribi et al. 2007/.

The model calculations elucidate the conditions under which gas-induced displacement of radionuclide contaminated water from the canister interior through the defect may occur. The relevant processes governing the pressure evolution and water/gas migration into and out of a defect at the underside of a canister are summarised in the following paragraphs.

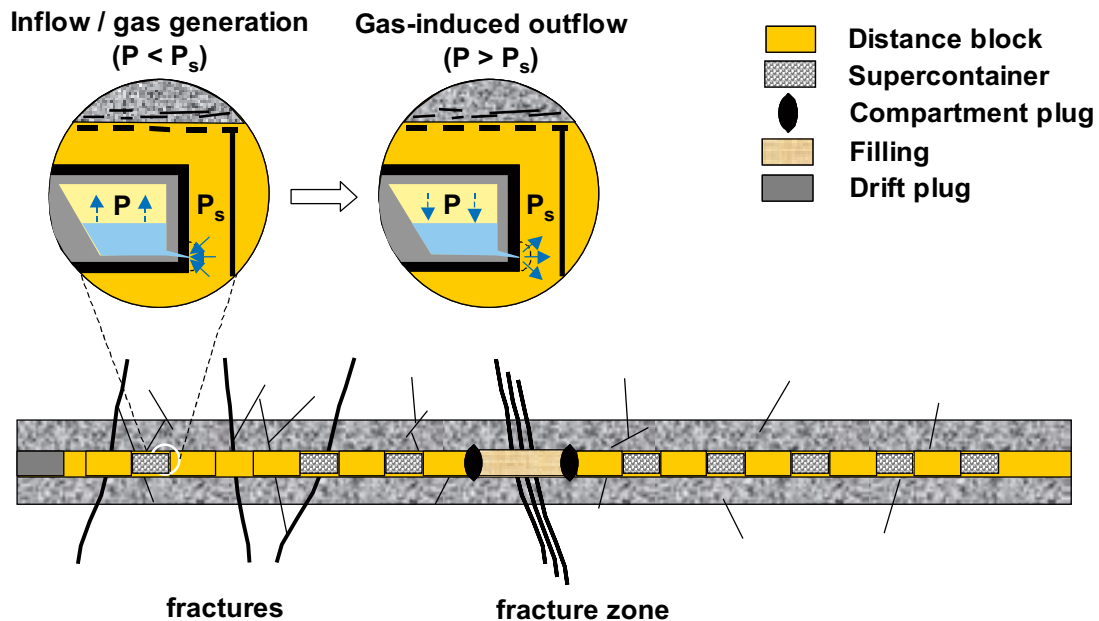
Slow inflow of water from the buffer through the defect into the canister interior will take place as long as the gas pressure within the canister is below the hydrostatic pressure at repository depth. As described in earlier sections, anaerobic corrosion of the cast iron insert will occur, thereby consuming water and generating hydrogen gas. The rate of gas generation is determined by the steel corrosion rate and may be limited by the availability of water inside the canister. When the gas pressure exceeds the hydrostatic pressure, inflow of liquid water will stop, but gas generation may be sustained by transport of water vapour through the hole.

With respect to saturation of the cavity within the canister insert, two limiting situations are of interest:

1. The inflow rate of liquid water exceeds the maximal consumption rate of water by anaerobic steel corrosion. This situation is illustrated in Figure 8-2. In this case, liquid water will slowly accumulate within the cavity until the gas pressure is in equilibrium with the pressure outside the canister ( $P_s$  in Figure 8-2). Due to ongoing gas generation, the pressure inside the canister may further rise. As a consequence, any water previously accumulated within the canister will be slowly squeezed outwards through the hole.
2. The inflow rate of liquid water is smaller than the maximal consumption rate of water by anaerobic steel corrosion. In this case, the cavity remains fully gas saturated.

Model calculations have been performed for various corrosion rates of iron ( $0.1-10 \mu\text{m a}^{-1}$ ) and hydraulic conductivities of the buffer ( $10^{-12}-10^{-13} \text{ m s}^{-1}$ ). The void space accessible to inflowing water assumed in the calculations ( $1 \text{ m}^3$ ) is a typical value for the entire internal void space of the canister (Table 4-2) – i.e. it is assumed that the insert as well as the copper shell has failed. Time-dependence of the accessible void space, e.g. due to the volume expansion of corrosion products, is not taken into account. In modelling cases corresponding to situation (2), it is further assumed that cast iron corrosion and gas generation are the result of the inflow of liquid water only (i.e. any corrosion due to water vapour is not included).

Modelling results indicate that, for the expulsion of dissolved radionuclides by gas to occur (situation (1), above), a relatively high hydraulic conductivity of  $10^{-12} \text{ m s}^{-1}$  must be assumed for saturated bentonite, combined with a low steel corrosion rate of  $0.1 \mu\text{m a}^{-1}$ . For this case, a maximal water saturation of about 3% ( $0.05 \text{ m}^3$  water in  $1 \text{ m}^3$  void space) and a maximal water pressure of about 6 MPa within the canister interior are calculated. In the time period from 2,800 to 4,100 years after initial water ingress, water is expelled through the hole at a maximal rate of 0.02 litres per year. This water flux may convey dissolved radionuclides, mainly from the instant release fraction of spent fuel (assuming that the fuel cladding has ruptured, and water has access to fuel surfaces).



Note: the amount of free gas (light yellow) within the canister is changed by a number of different processes (gas generation, advection and diffusion of dissolved gases, dissolution/degassing).

**Figure 8-2.** Conceptual model for transport of water and gas into and out of a canister with an initial penetrating defect /after Gribi et al. 2007/.

On the basis of the modelling results, the more likely situation is that inflowing water will be completely consumed by steel corrosion (situation (2), above), and there will be no gas-induced displacement of contaminated water through the hole into the saturated bentonite.

#### 8.10.4 Formation of gas pathways in the buffer

Whichever situation occurs in reality, gas pressure inside the canister will continue to rise until it exceeds the gas breakthrough pressure of the bentonite. In some experiments, this pressure has been found to be above 20 MPa for bentonite with a swelling pressure of  $\sim 6$  MPa (Section 2.3.3 of /SKB 2006c/). After breakthrough, gas pressure will fall to a lower value ('shut-in pressure' of about 10 MPa), sufficient to support the pathways and prevent their closure due to swelling pressure. The formation of gas pathways is not expected to displace a significant amount of porewater or dissolved radionuclides /Harrington and Horseman 2003/. Gas pathways may, however, transport radionuclides that are present as volatile species (mainly C-14). The gas pathways will remain open until gas production ceases or is greatly reduced such that it can be dissipated solely by diffusion, at which time the pathways are expected to close and re-seal.

### 8.11 Possibility of nuclear criticality

The risk of criticality, i.e. the risk of a spontaneous and sustained nuclear chain reaction as a result of re-distribution of fissile material at various locations outside a spent fuel canister has been analysed by /Behrenz and Hannerz 1978/ and /Oversby 1996/, the latter study being based on observations from the natural reactor at Oklo. In both cases, the conclusions were that criticality outside the canister has a vanishingly small probability, requiring several highly improbable events to occur.

The possibility of nuclear criticality inside a failed canister has been discussed in a number of studies (see e.g. /SKB 2006a/ and /Nagra 2002/). Calculations by /Agrenius 2002/ and /Nagra 2002/ show that, based on state-of-the-art methods and a reasonable assessment of the uncertainties, burnup credit<sup>32</sup> is a possible way to demonstrate control of the reactivity in the canisters. For the three types of Finnish canisters, /Anttila 2005b/ has shown that the fuel remains subcritical even if the void inside the canister is entirely filled with water.

In the horizontally emplaced canisters in KBS-3H, degraded fuel may accumulate all along the bottoms of the horizontally oriented fuel channels (Section 5.7.7). In such a situation, the re-distributed amount of fissile material per unit channel length would not change compared with the initial fuel configuration. It seems, therefore, highly unlikely that the effective neutron multiplication factor used to evaluate the possibility of criticality would be any different for dis-integrated fuel assemblies as compared with intact fuel assemblies in the horizontal orientation.

Thus, based on the investigations carried out to date, and assuming credit for burnup to be taken, sustained induced fission (criticality) is not expected to occur in any of the types of canisters and for any of fuels that will be disposed of in a Finnish repository.

---

<sup>32</sup> Burn-up credit is a term that applies to the reduction in reactivity of burned nuclear fuel due to the change in composition during irradiation.

## 9 The farthest future

Over a sufficiently long time frame, one or more of the processes described in the previous chapters will lead to the failure of all canisters. Although the possibility of initial penetrating defects is not currently excluded (Section 4.2.2) and there is also some possibility of canister failure due to rock shear associated with post-glacial earthquakes (Section 7.4.5), for the majority of canisters the most likely eventual failure mechanism is the slow corrosion of the copper shell. Calculations reported in SR-Can indicate that, in the absence of buffer erosion or significant perturbations to the buffer/rock interface, around 6 mm of copper will be corroded in a one million year period, compared with an initial copper thickness of 50 mm. A calculation by /Vieno et al. 1992/ based on a sulphide concentration of 1 mg per litre indicated an 18 million year canister lifetime in the absence of defects. The current maximum concentration of sulphide in the groundwater at Olkiluoto at repository depth is, however, higher than that assumed in this calculation, at about 12 mg per litre. Furthermore, additional sulphide could be introduced by microbial activity or by the dissolution of sulphidic minerals. The estimated maximum amount of sulphide produced due to microbial activity in the backfill of a KBS-3V repository at Olkiluoto is 42.3 mg per litre /Pastina and Hellä 2006/. Even for these sulphide concentrations, the maximum calculated amount of corroded copper is in the order of a few millimetres in 100,000 years. It should also be noted that the actual rate of corrosion will depend not only on sulphide concentration, but also on local flow conditions around the drift, which determine the rate at which sulphide in the groundwater is conveyed to the near-field/geosphere interface, and also by the long-term evolution of the diffusion barrier provided by the buffer. Perturbations to the interface by thermally-induced rock spalling, by the presence of potentially porous or fractured corrosion products in contact with the drift wall tighter drift sections and by chemical interaction of the buffer with these corrosion products are described in Chapters 5 and 6. The potential for buffer erosion due to penetration of glacial meltwater to repository depth is described in Section 7.4.7.

Beyond the end of the next glacial cycle, the Quaternary pattern of glacial-interglacial cycling is expected to continue or to be resumed. Based on past glaciation events, cycles are expected to repeat approximately every 120,000 years according to the Quaternary pattern. Over a one million year period, according to the Weichselian-R scenario, approximately 8 glacial cycles are expected, each one featuring at least two ice sheet layers and two glacial melting periods. It is highly uncertain, thus far, how the engineered barrier system and the host rock will react to repeated glacial cycles. So far, in SR-Can it has been assumed that consequences of irreversible processes such as chemical erosion of the buffer are additive, that is, the amount of buffer eroded during the first glacial meltwater period is multiplied by 8 times. However, there is currently little support for the assumption that these processes will be additive. Further knowledge is necessary to elucidate the behaviour of the engineered barrier system in the farthest future.

If the Quaternary pattern is interrupted, for example due to the growth of mountain ranges, changing oceanic circulation patterns (e.g. a breach in the isthmus of Panama) and changes in the distribution of oceanic and continental crust, the periodicity of glaciation cycles will change. The timing of any interruption is uncertain, but current estimates are that this will happen over the next 10 to 100 million years /Crawford and Wilmot 1998/.

Eventually, degradation and transport processes may result in the fuel, radionuclides and repository construction materials becoming widely dispersed in the geological environment. Rates of erosion in the Precambrian Shield areas are extremely low, even during periods of glacial-interglacial cycling. In the hundreds to thousands of millions of years required to exhume the repository horizon, therefore, the geochemical properties of the repository host rock may become similar to a uranium ore body. On the other hand, it is also possible that the copper will be partly replaced by copper sulphide, which is insoluble and not likely to become dispersed, and that the fuel matrix will experience only limited dissolution over time due to its relative geochemical stability.



## 10 Summary of system evolution of a KBS-3H repository at Olkiluoto

### 10.1 Overall evolution

The timescales for the overall evolution of the repository and the site under the Weichselian-R climatic scenario are illustrated in Figure 10-1. The figure assumes a repetition of the last glacial cycle, although the future evolution of the climate and the occurrence of future glaciations are subject to considerable uncertainty, particularly in regard to the long-term impact of anthropogenic emissions, especially greenhouse gases. The figure is adapted from a version developed for a KBS-3V repository evolution in /Pastina and Hellä 2006/. The timescales shown are the same in the KBS-3H case.

### 10.2 Early evolution

Early evolution covers the transient phase starting with the emplacement of the first canister in the repository. Its duration is not well defined, but may be taken as being roughly the period required to saturate the repository external to the canisters, which may take up to several thousands of years.

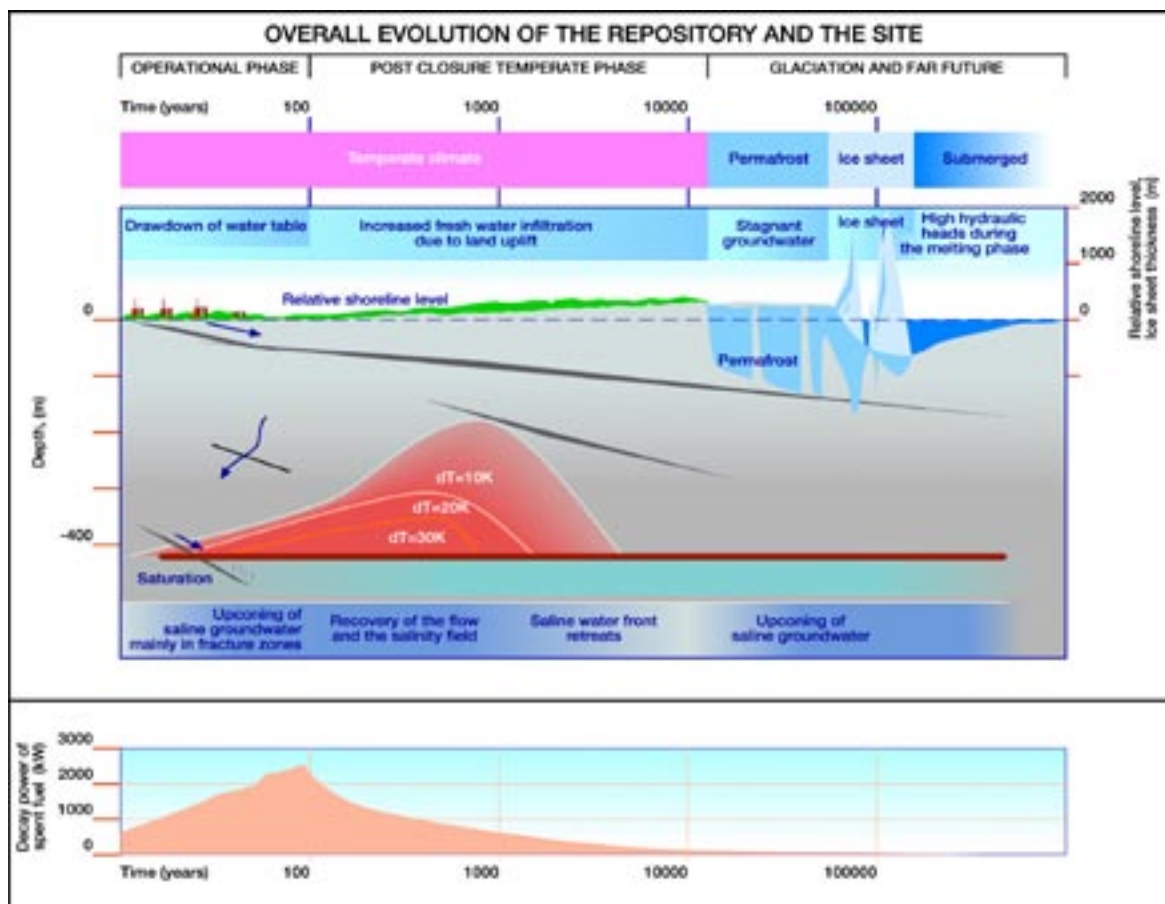


**Figure 10-1.** The timescales for the overall evolution of the repository and the site under the Weichselian-R climatic scenario. The blue arrows show groundwater flow, black lines and dark grey areas mark fractures and deformation zones.

The approximate timescales of key near-field processes and changes in key characteristics of the near field that take place within the transient phase are illustrated in Figure 10-2 (note that changes occurring within this period affect the characteristics and performance of the repository at later times, which is why the time-axis in Figure 10-1 extends to  $10^6$  years).

Operation of a drift, from emplacement of the first canister, through the emplacement of successive distance blocks, supercontainers, compartment plugs and filling materials, to the installation of the drift end plug, is expected to take about 6 weeks, but will depend on the number of compartments into which the drift is divided.

Excavation of ONKALO and of the repository at Olkiluoto may cause a transient drawdown of the water table and an associated reduction of the hydrostatic pressure at repository depth. This could lead to the drawdown of fresh and brackish, sulphate-rich water from closer to the surface and upconing of more saline, deep groundwaters in the period up to saturation of the repository. However, measures to avoid these hydrological disturbances are being taken during the construction of ONKALO and will also be implemented during repository construction. So far, the observed hydrological disturbances have been minimal and this is expected to remain the case in the future /e.g. Ahokas et al. 2006/. The hydrostatic pressure will recover within a couple of years of backfilling and sealing the facility, although perturbed conditions may persist in the immediate vicinity of the repository due to the residual thermal output from the spent fuel, which gives rise to upward convective flow of deep, saline groundwater and increased salinity at repository depth compared with unperturbed conditions lasting for a period of up to several hundreds of years.

Heat generated by the radioactive decay of the spent fuel inside the canisters will be transferred continuously to the surrounding media by conduction, radiation from surfaces, and convection of gas or water in gaps and voids. Model calculations accounting for the first two of these transfer mechanisms show that, for a canister pitch of 11 m and a drift separation of 25 m, temperature at the canister/bentonite interface at the centre of the highest-temperature canister peaks at  $90^{\circ}\text{C}$  after 50 years of repository operation – or about 20 years after deposition of the canister (Finnish BWR spent fuel). For a drift spacing of 40 metres and the same canister pitch, the temperature maximum is slightly lower ( $84^{\circ}\text{C}$ ) and reached somewhat earlier (after 40 years of years of repository operation – or about 10 years after deposition of the canister). During the period of elevated temperature, some limited chemical changes may occur in the buffer (Section 6.2.5). Furthermore, some thermally-induced rock spalling is expected in tighter drift sections, where significant swelling pressure on the drift wall takes more than a few years to develop.

The decay heat of spent nuclear fuel will continue to raise the temperature of the repository and the surrounding bedrock by several tens of degrees for many centuries and by a few degrees for several thousand years.

The distance blocks and the buffer inside the supercontainers will take up water flowing into the drift through intersecting transmissive fractures and water vapour in the air. Water vapour in the air in the deposition drifts will originate from the rock and, during the operational period, from the water cushion system that is proposed for the deposition vehicle (see Section 4.1.2, Air humidity). The infiltrating water will interact chemically with the bentonite. Water uptake will result in swelling of the buffer, and the establishment of a tight contact between the distance blocks and the drift wall. In drift sections with relatively high water inflow through transmissive fractures (hydraulic conductivities of the wallrock greater than about  $10^{-12} \text{ m}^2 \text{ s}^{-1}$ ), a hydraulic separation between the supercontainers is likely to develop during the operational period. In tighter drift sections, humidity-induced swelling will require about three months to provide hydraulic separation between the supercontainers. In the case of the DAWE design variant (Appendix A), drainage will prevent significant water uptake and swelling during the operational period. Following artificial watering at the end of operations, however, hydraulic separation between the supercontainers will be rapidly achieved.

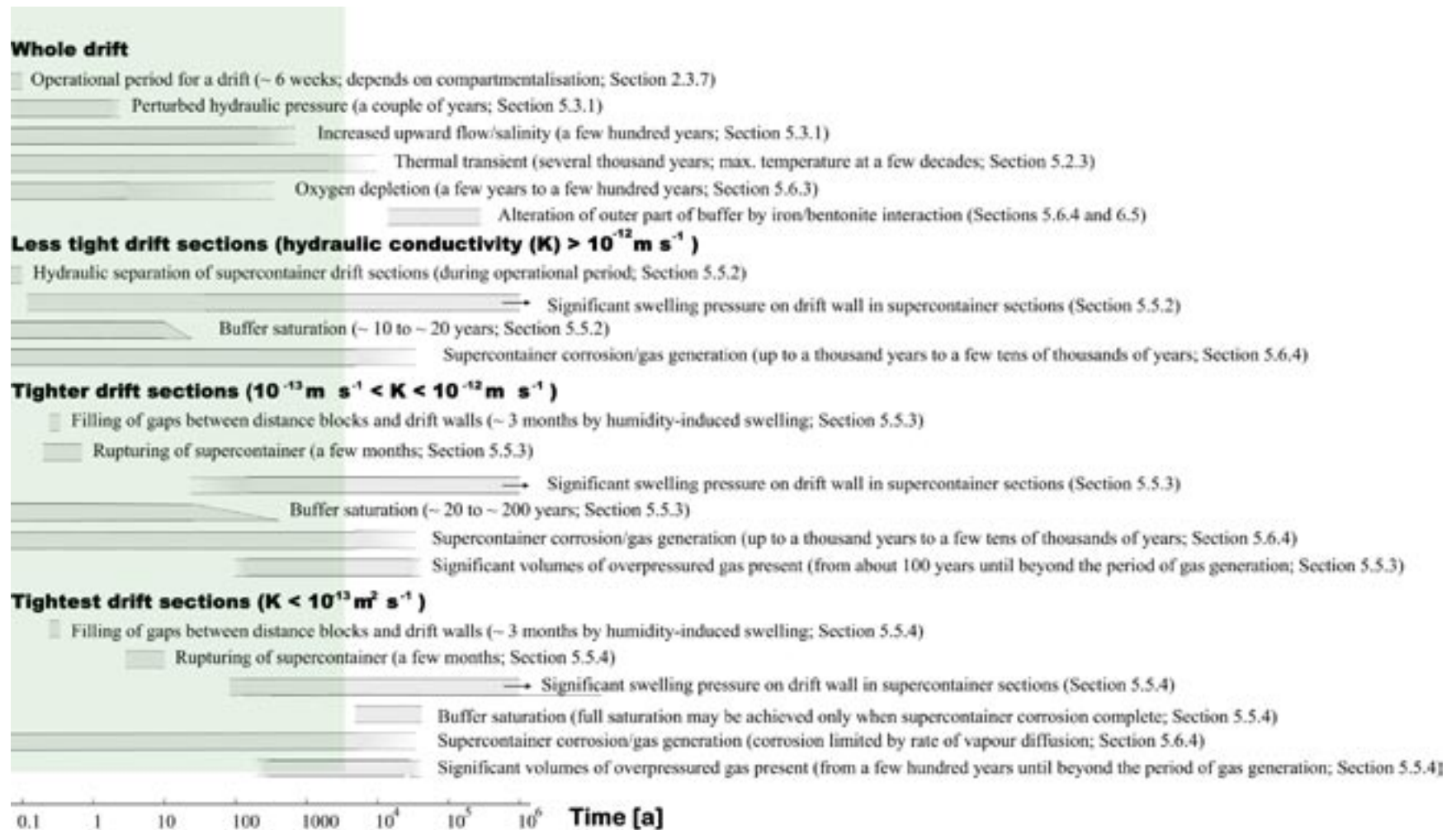


**Figure 10-2.** Approximate timescales of various aspects of system evolution for a KBS-3H repository at Olkiluoto. Uncertainties are indicated by dotted lines. Tapering of the bars is used to indicate spatial variability of process timescales along the length of a deposition drift (e.g. as a result of geological heterogeneity). Background shading indicates the approximate duration of the transient phase (although some of the slowest transient processes may extend beyond this period). Right arrows indicate expected continuation beyond the million year period covered by figure.

Uptake of liquid water by the buffer inside the supercontainers will lead to some extrusion of low-density bentonite through the perforations in the supercontainer shell. Furthermore, the swelling pressure developed on the inner surfaces of the supercontainer due to the uptake of liquid water and, in especially in tighter drift sections, water vapour is expected to lead to deformation and possible rupturing the supercontainers within a few months of emplacement. At the same time, much of the oxygen trapped in the drift will migrate by diffusion to the buffer/rock interface, where it will be consumed over a period of a few years to a few decades principally by fast microbially induced reactions.

Heterogeneity of the near-field rock results in widely differing saturation times for different drift sections. Saturation of the buffer in less tight drift sections (wall rock hydraulic conductivities,  $K$ , of more than  $10^{-12} \text{ m s}^{-1}$ ) will take about a decade, controlled by the ability of the bentonite to take up water. In tighter drift sections ( $10^{-13} \text{ m s}^{-1} < K < 10^{-12} \text{ m s}^{-1}$ ), the rate of saturation is limited by the tightness of the rock. In the tightest drift sections ( $K < 10^{-13} \text{ m s}^{-1}$ ), saturation may be further delayed by the build-up of gas overpressures. Overpressures may persist until the supercontainers and other steel components are fully corroded. This could take up to several thousands of years based on an expected steel corrosion rate of  $1 \mu\text{m a}^{-1}$ . Even in the tightest drift sections, the buffer is expected to retain its initial water content, and will eventually fully saturate, at which time it is expected to perform its full range of safety functions.

As a result of chemical interactions between iron and bentonite, the physical properties of the buffer may change in the vicinity of the supercontainer and other steel components (porosity, hydraulic conductivity, swelling pressure, etc). To date, such changes are difficult to quantify and the impact of iron/bentonite interactions is rather uncertain, but the spatial extent of the affected buffer zone is expected to be very limited for long after the early evolution period.

Gas from the corrosion of steel components external to the canisters may create transport pathways through the buffer, but buffer swelling pressure is expected to reseal these pathways once the gas generation ceases and gas pressure falls. As corrosion products form on the surfaces of the steel components, the volume available to the bentonite will be reduced, and buffer density and swelling pressure will increase. This is due to the higher volume occupied by the corrosion products compared with the original metal. The effect is not, however, expected to be sufficient to compromise the protective function of the buffer.

During early evolution, shear movement on fractures intersecting the deposition drifts may take place as a result of rock excavation and heat load, leading to mechanical forces on the canisters. The plasticity of the buffer is, however, expected to protect the canisters from such movements. The probability of a tectonic earthquake large enough to cause damage to the canisters is expected to be small during this period.

Interactions involving the limited amount of low-pH cement or Silica Sol and stray materials left in the repository are not expected to have a detrimental impact on the buffer, canister or rock, although this is an area requiring further study.

The copper coverage of the canisters is expected to remain intact during early evolution, and with a large safety margin, assuming appropriate quality control procedures during canister encapsulation and emplacement, such that there are no initial penetrating defects. As a consequence, spent fuel and radionuclides are expected to be totally isolated within the canisters throughout this period.

### **10.3 Subsequent evolution prior to major climate change**

Following the transient phase, and before any major climate change, the repository and its geological environment will evolve to a quasi-steady state, in which key safety-relevant physical and chemical characteristics are subject to much slower processes.



By definition, the heat output of fuel will have declined to a level that has no significant effect on the evolution of the repository and its environment. Minor variations in climate are also not expected to have any significant impact on temperatures at repository depth. The reduction in thermal output from the fuel will result in rock stress levels returning to those of the pre-emplacement stage and in a reduction in the thermo-mechanical loads on the canister.

As a result of post-glacial land uplift, the saline water currently at repository depth will start to be replaced by brackish, sulphate-rich and fresher groundwater currently present at shallower depths, and the driving forces for groundwater flow will also change. The changes in the salinity of the groundwater will affect the swelling pressure of the buffer, with lower salinities giving higher swelling pressures.

There is likely to be some intrusion of buffer material into open fractures intersecting the deposition drifts. Significant erosion of this material is not, however, expected.

The buffer will continue to evolve chemically, important processes being ion exchange and the dissolution/precipitation of calcite. Mineral transformation of the buffer due to the presence of Fe(II) from corroding steel components is also likely to extend further into the buffer. 1-D reactive transport modelling results indicate, however, that the Fe(II) front migrating inwards from the supercontainer will penetrate only a few centimetres into the buffer, even after hundreds of thousands of years.

Copper canisters will continue to slowly corrode until they are finally breached. Given the expected anoxic conditions at the canister surface, the only corrosion agent will be sulphide that diffuses through the buffer from the rock. Because of the small diffusive flux of sulphide that is expected to reach the canister surface, the rate of copper corrosion will be very low. Although there is some uncertainty related to perturbations to the buffer/rock interface (e.g. due to thermally-induced rock spalling, the presence of iron corrosion products from the supercontainer shell and iron/bentonite interactions), scoping calculations indicate that a combination of pessimistic assumptions must be made before the canister lifetime drops to one million years or less. No canister failure by corrosion of the copper shell is expected prior to the next glaciation (50,000 years from now according to the Weichselian-R scenario).

## 10.4 Effects of major climate change

The evolution of conditions at repository depth may be significantly affected by major climate change, and in particular by the formation of ice sheets at the ground surface in response to any future change to much colder climatic conditions. The impact of anthropogenic emissions, especially greenhouse gasses, on the magnitude and timing of future major climate changes is uncertain.

The development of permafrost and frozen ground and the advance and retreat of ice sheets are expected to have only limited effects on the ambient temperature at repository depth. Permafrost will also have only a minor influence on hydro-mechanical pressure conditions at repository depth, possibly leading to a more stagnant flow pattern.

The creation of ice sheets, on the other hand, will result in large water pressures and hydraulic gradients in the subsurface. This could conceivably force large volumes of low-salinity and possibly oxidising meltwater into deeper parts of the bedrock. There is a potential for local upconing of saline/brackish groundwater during periods of permafrost and in the presence of an advancing or retreating warm-based ice sheet, as discussed in the KBS-3V Evolution Report (Section 8.3.3 of /Pastina and Hellä 2006/) and in SR-Can (Section 9.4.7 of /SKB 2006a/). Although it is expected that hydrogeological and geochemical characteristics of the geosphere will remain stable below depths of 300 to 400 m, glacial flow conditions are difficult to assess, and penetration of dilute water to repository depth cannot be ruled out. The migration of oxygen to repository depth is, however, unlikely due to oxygen being consumed by microbially-induced reactions and its interaction with minerals in the geosphere.



Glacial loading will affect pore pressures in the rock and in the saturated buffer and the isostatic load exerted on the canisters. No failure of canisters due to this increased load is, however, expected without prior weakening of the insert by corrosion (which could occur, for example, in the case of a canister with an initial penetrating defect).

During the next glacial cycle and in the far future, slow corrosion of the copper surfaces of the canisters will continue to take place by reaction with sulphide from the groundwater, which will diffuse to the canister surface through the buffer. The possibility of dilute water penetrating to repository depth may lead to some erosion of the buffer. If the density of the buffer were to be reduced by erosion to such an extent that advective transport could take place within the buffer region, this could increase the rate at which sulphide migrates to the copper surface, and hence increase the copper corrosion rate, reduce canister lifetime and increase radionuclide migration rates subsequent to canister failure. Currently, the possibility of advective conditions developing in parts of the buffer as early as the next period of glaciation cannot be excluded.

When an ice sheet is present, seismic activity, which is in any case low in the Olkiluoto region, will be further repressed. Post-glacial earthquakes may, however, occur following the retreat of the ice sheet, giving rise to stress changes in the rock that trigger shear movements on smaller-scale fractures that intersect the deposition drifts. The expectation value of the number of canisters in the repository that could potentially be damaged by rock shear in the event of a large earthquake has been estimated at 16 out of the 3,000 canisters in the repository, with a probability of 0.02 of such an earthquake occurring in a 100,000 year time frame, although there are some significant uncertainties associated with these values that could lead to them giving either an underestimate or an overestimate of the actual likelihood of damage.

A further potential impact of rock shear is to increase the transmissivity of fractures intersecting the drifts. The magnitude of such an increase has not, however, been estimated as yet. The retreat of an ice sheet could also cause an infiltration of brackish or saline waters of marine origin, which could also increase the salinity at repository depth (/SKB 2006a/, Section 9.4.7).

## **10.5 Evolution of a canister with an initial penetrating defect**

The possibility that an initial defect will penetrate a copper canister shell (or be sufficiently deep to have significant implications for the timing of failure due to copper corrosion) is not currently excluded.

The behaviour of the water/vapour/gas system in a defective copper-iron canister is complex. Water entering a canister through an initial penetrating defect will react with and corrode the cast iron insert, resulting in the formation of iron corrosion products, the weakening of the insert, the generation of hydrogen gas, and the interaction of iron corrosion products with bentonite located in the vicinity of the defect.

As internal gas pressure within the canister increases, the driving force for liquid water ingress will be reduced and possibly eventually reversed. Furthermore, as the void space fills with corrosion products, the corrosion rate will drop due to the increasing transport resistance between the defect and the uncorroded surfaces.

The canister insert will continue to be weakened by progressive corrosion, although the rate at which this will occur is uncertain, depending, for example, on the extent to which the original defect is expended by the developing corrosion products. Eventually, the canister will collapse. It is likely that the collapse of a weakened insert will take place during or after a major glaciation, although earlier collapse cannot be excluded.

The corrosion products from the insert may react with swelling clay minerals in the buffer in the vicinity of the canister defect, although their effect will extend only very slowly into the buffer. Corrosion of the insert may also expand the copper shell and lead to a compaction of the buffer, increasing the pressure exerted by the buffer on the canister and rock. Due to the low corrosion rate of the insert, this process will also be slow.

Once water penetrates the cast iron insert and enters the channels in the insert containing the fuel assemblies, it will corrode the channel surfaces, giving rise to further corrosion products and gas. It will contact the surfaces of the cladding and, if the cladding tubes are ruptured, it will also contact the surfaces of the fuel pellets and interact with them.

The cladding and other metal components will slowly corrode on contact with water, resulting in the congruent release to solution of activation products embedded within them. Once water contacts the fuel pellet surfaces, radionuclides that have been segregated to grain boundaries in the fuel, to pellet cracks and to the fuel/sheath gap will either rapidly enter solution, or, in the case, for example, of C-14, may form volatile products such as methane or carbon dioxide that will mix with hydrogen gas inside the canister. Water will also start to interact (but far more slowly) with the surfaces of the fuel matrix, and radionuclides embedded in the fuel matrix, along with radioactive gases present in fission gas bubbles, will be released as the matrix is slowly dissolved or otherwise altered.

Radionuclides released from the fuel (including activation products in the metal components) will either enter solution, form volatile species that can mix with repository-generated gas (particularly relevant for C-14), or, if their solubilities in water are low, precipitate either as immobile solids or as colloids. Dissolved radionuclides and radionuclides in gaseous form will be transported by gas and water movements (advection) and by diffusion in the interior of the canister, and may exit through the damaged copper shell. Radionuclides in colloidal form will also migrate in water in the canister interior by advection and diffusion, but will be prevented from migrating into the buffer by its microporous structure.

If the inflow rate of water into the canister exceeds the maximal consumption rate by steel corrosion, water will slowly accumulate within the cavity until the gas pressure is in equilibrium with the pressure outside the canister. Due to ongoing gas generation, the pressure inside the canister may further rise. As a consequence, any water previously accumulated within the canister will be slowly squeezed outwards through the hole, along with any radionuclides that have been released to solution in the intervening period. On the basis of the modelling results, however, the more likely situation is that inflowing water will be completely consumed by steel corrosion, and there will be no gas-induced displacement of contaminated water.

Gas pressure inside the canister will continue to rise until it exceeds the gas breakthrough pressure of the bentonite. Gas pathways will form that may transport radionuclides present as volatile species (mainly C-14). The gas pathways will remain open until gas production ceases or is greatly reduced.

Induced fission (criticality) inside or outside a canister with an initial penetrating defect is not expected to occur in any of the types of canisters and for any of fuels that will be disposed of in a Finnish repository.

## **10.6 The farthest future**

Over a sufficiently long time frame, one or more of the processes described in the previous chapters will lead to the failure of all canisters. For the majority of canisters, the most likely eventual failure mechanism is the slow corrosion of the copper shell, leading to failure after several hundred thousand years or more. The fuel, radionuclides and repository construction materials may eventually become widely dispersed in the geological environment. In the hundreds to thousands of millions of years required to expose the repository horizon to the surface by uplift and erosion, the geochemical properties of the repository host rock may become similar to a uranium ore body. On the other hand, it is also possible that the copper will be partly replaced by copper sulphide, which is insoluble and not likely to become dispersed, and that the fuel matrix will experience only limited dissolution over time due to its relative geochemical stability.

# 11 Implications for radionuclide release and transport

## 11.1 Scenarios and assessment cases

The discussions in the Process Report /Gribi et al. 2007/ and in the present Evolution Report indicate that, while a prolonged period of isolation of the spent fuel and containment of radionuclides in the copper canisters is the expected course of evolution for a KBS-3H repository, there are evolutionary paths or scenarios<sup>33</sup> that cannot currently be excluded in which one or more canisters fail, giving rise to some radionuclide releases. According to the safety concept (Figure 1-3), safety in these scenarios rests principally on complete containment of radionuclides by the remaining canisters and, for the failed canisters, slow release from the spent fuel, slow diffusive transport in the buffer, and slow transport in the geosphere to the biosphere. Each of these is, however, subject to uncertainties. A key purpose of the radionuclide release and transport calculations described in detail in the Radionuclide Transport Report /Smith et al. 2007a/ is to assess the robustness of the safety concept in view of these uncertainties.

Some uncertainties are treated using models, computer codes and parameter values that are conservative, meaning that they tend to over-estimate radiological consequences. Identifying what is a conservative model approach, assumption or parameter value is not, however, always straightforward – what is conservative with respect to one process may not be conservative with respect to another competing process. Furthermore, a purely conservative approach does not give a basis for deciding which uncertainties are the most important in terms of system performance. Thus, many uncertainties are treated by defining a range of assessment cases – i.e. specific model realisations of different possibilities or illustrations of how a system might evolve and perform in the event of canister failure – and analysing these cases in terms of hazard to humans and to other biota, quantified in terms of annual effective dose<sup>34</sup> or nuclide-specific fluxes across the geosphere/biosphere interface (in order to compare with Finnish regulatory guidelines).

The definition of an assessment case includes (i), the canister failure mode that is presumed to lead to the formation of transport pathways between the canister interior and its surroundings, and (ii), the models and data that describe subsequent radionuclide release and transport. The identification of scenarios leading to different canister failure modes is described in the following sections. Given that a key question addressed by the KBS-3H safety studies is whether or not there are safety issues identified in the KBS-3V/KBS-3H difference analysis with the potential to lead to unacceptable radiological consequences, specific assessment cases are defined addressing uncertainties related to features and processes that have a different significance to, or potential impact on, KBS-3H compared with KBS-3V. Additional cases are also analysed to illustrate the impact of other uncertainties in key features of the safety concept. Nevertheless, the range of cases analysed is more limited than that considered, for example, in either TILA-99 /Vieno and Nordman 1999/ or SR-Can /SKB 2006a/, and not all conceivable uncertainties and combinations of uncertainties are covered. The selection of assessment cases for each of canister failure modes is described in the Radionuclide Transport Report /Smith et al. 2007a/. The Radionuclide Transport Report also describes the computer codes, models and data used to analyse the selected cases, and presents the results of these analyses.

---

<sup>33</sup> According to the IAEA definition, a scenario is a postulated or assumed sequence of states defined by the safety functions that are provided by the system components /IAEA 2003/.

<sup>34</sup> Exposure of other biota is not explicitly addressed in the present safety assessment, but is considered in the Biosphere Analysis Report /Broed et al. 2007/.

Consistent with Finnish regulations, assessment cases address radionuclide release and transport over one million year time frame. The consequences of the ultimate failure of the repository multi-barrier system in the farthest future (beyond one million years), including the possible exhumation of the repository, are discussed in the Complementary Evaluations Report /Neall et al. 2007/.

The importance to long-term safety of human intrusion scenarios (e.g. boring a deep water well at the disposal site and core drilling hitting a spent fuel canister) has not been evaluated, although current Finnish regulations indicate that this will be a requirement of any future safety case. Human intrusion has, however, been addressed in the main report of the Swedish SR-Can safety assessment by considering a borehole hitting a canister and then subsequently being used for drinking water abstraction /SKB 2006a/. Drilling occurs 300 years after the sealing of the repository and the calculated doses are in the range of  $10^{-4}$  to  $10^{-3}$  Sv per year, assuming a fuel degradation rate of  $10^{-7}$  per year and water flow through the affected canister of 1,000 litres per year.

## 11.2 Finnish regulatory requirements regarding scenarios

It is a Finnish regulatory requirement given in /STUK 2001/ that:

*“A scenario analysis shall cover both the expected evolutions of the disposal system and unlikely disruptive events affecting long-term safety. The scenarios shall be composed systematically from features, events and processes, which are potentially significant to long-term safety and may arise from:*

- *mechanical, thermal, hydrological and chemical processes and interactions occurring inside the disposal system*
- *external events and processes, such as climate changes, geological processes and human actions”*

Regarding the scenarios to be analysed, regulations go on to state:

*“The base scenario shall assume the performance targets defined for each barrier, taking account of the incidental deviations from the target values. The influence of the declined overall performance of a single barrier or, in case of coupling between barriers, the combined effect of the declined performance of more than one barriers, shall be analysed by means of variant scenarios. Disturbance scenarios shall be defined for the analysis of unlikely disruptive events affecting long-term safety.”*

As noted in Section 1.3, the importance to long-term safety of unlikely disruptive events shall, according to regulations, be assessed. The likelihood and consequence of boring a deep water well at the disposal site, or of core drilling hitting a spent fuel canister and not considered in the present safety studies for KBS-3H, since they do not differ significantly between KBS-3V and KBS-3H repositories.

The methodology applied in the present assessment for identifying the base and variant scenarios is described in the following section.

## 11.3 Methodology for the identification of scenarios leading to canister failure and radionuclide release

The methodology used to identify scenarios leading to canister failure and radionuclide release from a KBS-3H repository is based on that developed for SR-Can. It can be described in terms of the following steps:

1. Consider the safety functions of each of the main components of the disposal system.
2. For each safety function, identify one or more safety function indicators.
3. For each safety function indicator, derive safety function indicator criteria.
4. Develop understanding of the system and its evolution – with a focus on the safety functions.
5. Identify the failure modes (loss of safety functions) that could occur in the course of system evolution.
6. Consider if and when the occurrence of such failure modes is plausible.
7. Consider the implications of loss of one safety function on the others.
8. Identify plausible descriptions of the evolution of safety functions over time.

The products of this methodology – plausible descriptions of the evolution of safety functions over time – are described in the following as “scenarios”, although, in SR-Can, because of the way in which Swedish regulatory guidance is formulated, all those that are considered “probable” are classified as variants within the “base scenario”. Scenarios outside the scope of the base scenario are those that are judged less likely to occur (see Section 11.3 of the main report of SR-Can, /SKB 2006a/).

In the present safety assessment, the Base Scenario for the evolution of a KBS-3H repository at Olkiluoto assumes that the main system components (the canister, the buffer and the host rock) perform the safety functions described in Section 2.4 for a period extending to one million years or more. These safety functions include complete containment of radionuclides by the canister. Thus, in the Base Scenario, there are no canister failures within one million year time frame. On the other hand, for each of the three failure modes, a Base Case and one or more variants are defined.

Process tables that summarise the handling of internal processes in the safety assessment are used as check lists to ensure that no important processes and associated uncertainties have been overlooked in the identification of scenarios (and assessment cases). Process tables for a KBS-3H repository at Olkiluoto are given in /Gribi et al. 2007/.

## 11.4 Application to a KBS-3H repository at the Olkiluoto site

### 11.4.1 Carrying out the steps

The Process Report /Gribi et al. 2007/ provides the most important processes that affect the safety functions of the repository. The present Evolution Report describes these processes in a chronological order and highlights the coupling among different processes. Steps 1–3 and 5 of the methodology are covered in Chapter 2. The main components of the disposal system that are considered to provide safety functions are the canister, the buffer and the host rock. Their safety functions are described in Section 2.4.1. Safety function indicators, safety function indicator criteria and the models by which, in principle, these main components could fail to provide their safety function fully are described in Sections 2.5.2–2.5.4. Current understanding of the initial state of the system and how the system might evolve in different time frames, with a focus on safety functions (Step 4), is described in Chapters 4–8. These chapters also describe the plausibility of different failure modes and implications of loss of one safety function on the others (Steps 6 and 7).



The descriptions of initial state and evolution presented in Chapters 4–8 of this report draw extensively on system understanding developed in the course of SR-Can, /SKB 2006a/ as well as that described in the Evolution Report for a KBS-3V repository at Olkiluoto /Pastina and Hellä 2006/. They also, however, involve consideration of features and processes of specific relevance to KBS-3H which have the potential to lead to significant perturbations to the safety functions. Most of the identified features and processes that have a different significance to, or potential impact on, KBS-3H compared with KBS-3V have the potential to affect, in the first place, the mass transport properties of the buffer and the buffer/rock interface, but can also affect canister lifetime by increasing the rate at which sulphide from the groundwater migrates to, and corrodes, the canister surface. They may also perturb radionuclide transport in the event of canister failure. These features and processes, associated uncertainties and the evaluation of impact of these on the mode and timing of canister failure and on subsequent radionuclide release and transport, are shown in Table 11-1. The table also gives references to specific assessment cases defined in the Radionuclide Transport Report which are used to evaluate the impact of particular KBS-3H-specific features and processes.

A key point to note is that features and processes with a different significance to, or potential impact on, KBS-3H compared with KBS-3V, while they may affect to some extent the timing or rate of canister failure, do not introduce any new modes of canister failure not already considered in SR-Can in the case of a KBS-3V repository at Swedish sites. Canister failure modes that are judged to be plausible for a KBS-3H repository at Olkiluoto are:

- an initial penetrating defect;
- failure due to copper corrosion; and
- rupture due to rock shear.

A fourth mode – collapse due to isostatic loading – is excluded on the basis that the stability of the canister under isostatic loading is ensured with a large safety margin (Sections 5.4.3 and 7.4.4). This failure mode is, therefore, not addressed in analyses of radionuclide release and transport (except as a secondary failure mode in the case of canisters with initial penetrating defects that have been weakened by corrosion of the insert).

#### **11.4.2 Overview of scenarios**

The various scenarios shown in Figure 11-1 have been identified by applying the methodology outlined above. The scenarios are shown as combinations of barrier states (a “no fail” state indicates that all safety functions are assumed to be fulfilled), and are grouped according to the initial canister failure mode that they involve.

As indicated by arrows in Figure 11-1, scenarios involving canister failure and radionuclide release are initiated by:

- the presence of an initial, penetrating defect in one or more of the canisters;
- perturbations to the buffer and buffer/rock interface, giving rise to an increased rate of transport of sulphide from the geosphere to the canister surface and an increased canister corrosion rate;
- penetration of dilute glacial meltwater to repository depth, giving rise to chemical erosion of the buffer an increased rate of transport of sulphide from the geosphere to the canister surface and an increased canister corrosion rate; and
- rock shear movements of sufficient magnitude to give rise to shear failure of the canisters.

**Table 11-1. Features and processes with different significance to, or potential impact on, KBS-3H compared with KBS-3V and summary descriptions of their relevance to radionuclide release and transport major uncertainties and evaluation of their implications for canister failure modes and timing and for radionuclide transport. PR: Process Report /Gribi et al. 2007/, ER: the present Evolution Report, RNT: Radionuclide Transport Report /Smith et al. 2007a/.**

Feature/process	Relevance to RN release and transport	Major uncertainties	Evaluation of impact	
			Impact on canister failure mode/timing	Impact on radionuclide transport (see Table 11-2 and RNT for full lists of cases)
Piping and erosion during the operational phase and during saturation (cf. PR Section 4.5.2; ER Section 5.5.6)	May locally perturb buffer density and increase rate of diffusion of corrosive agents to canister surface and rate of radionuclide diffusion from failed canister	Likelihood of occurrence; amount of bentonite conveyed by piped water; degree of homogenisation after piping/erosion cease	Scoping calculations in ER Appendix B.7	Illustration of impact of increased radionuclide diffusion rates in buffer in assessment case <b>PD-HIDIFF</b>
Processes due to the presence of steel components (external to canister) and their corrosion products (cf. PR Section 4.7.1; ER Sections 5.4.2; 5.6.4; 6.5.3)	May result in chemical alteration of buffer and consequent changes to physical properties; may perturb mass transfer at buffer-rock interface	Degree and spatial extent of perturbation	Scoping calculations in ER Appendix B.7 (impact on capacity of buffer to protect canister in the event of rock shear movements < 10 cm assumed to be negligible)	Illustration of impact of increased radionuclide mass transfer at buffer-rock interface and mixing in outer part of buffer in assessment cases <b>PD-FEBENT1; PD-FEBENT2; PD-FEBENT3</b>
	May provide sorbing surfaces for radionuclides; (which could be released following a change in groundwater chemistry) Fe(II) may compete for sorption sites on buffer; it may also act as a sink for dissolved sulphide, reducing the flux of sulphide to the canister surface.	Quantitative understanding of impact; possibility of release of sorbed radionuclides in the event of change in groundwater chemistry	Favourable effect of iron acting as sink for sulphides not evaluated quantitatively	Impact on sorption not assessed (remaining issue for further study); impact on buffer as a whole of change in groundwater chemistry at 70,000 years due to influx of glacial meltwater illustrated in <b>PD-GWMC</b>
H <sub>2</sub> from corrosion of steel components (external to canister) (cf. ER Sections 5.3.1; 5.6.4; 5.7.4)	May participate in microbial reduction of sulphate to sulphide, which may subsequently corrode canister surface	Quantitative understanding of impact	Scoping calculations in ER Appendix B.7 (minor impact)	None expected
	May perturb groundwater flow and radionuclide transport in the geosphere for the first few thousand years	Quantitative understanding of impact	Minor impact on mass transfer of corrosive agents between geosphere and buffer (not quantitatively evaluated)	Impact on radionuclide transport for an initially defective canister not assessed (remaining issue for further study)

Feature/process	Relevance to RN release and transport	Major uncertainties	Evaluation of impact	
			Impact on canister failure mode/timing	Impact on radionuclide transport (see Table 11-2 and RNT for full lists of cases)
High-pH leachates from cementitious components (cf. ER Section 5.6.5)	May result in chemical alteration of buffer and consequent changes to physical properties; may perturb mass transfer at buffer-rock interface	Degree and spatial extent of perturbation	Scoping calculations in ER Appendix B.7	Illustration of impact of increased radionuclide mass transfer at buffer-rock interface and mixing in outer part of buffer in assessment cases <b>PD-FEBENT1; PD-FEBENT2; PD-FEBENT3</b>
KBS-3H drift and surrounding EDZ/rock spalling (cf. ER Sections 4.1.2; 5.4.5)	May perturb mass transfer at buffer-rock interface	EDZ hydraulic properties; impact of buffer swelling on rock spalling; transport characteristics of spalled zone	Scoping calculations in ER Appendix B.7	Illustration of impact of rock spalling in assessment case <b>PD-SPALL</b>

	System components and failure modes			Time frame (canister failure)	Comments
	Geosphere	Buffer	Canister		
<b>BASE SCENARIO</b>	No fail	No fail	No fail Corrosion failure	Up to a million years or more Farthest future	Expected evolution for most canisters - corrosion failure in the very long term
Scenarios involving an initial penetrating defect in a canister	No fail	No fail	Initial defect ↓ Isostatic collapse or shear failure	Up to future glaciation During or after future glaciation	Expected evolution for canister with initial penetrating defect - eventual major failure following weakening by corrosion of insert
	No fail	Low density / alteration (outer buffer)	Initial defect ↓ Isostatic collapse or shear failure	Up to future glaciation During or after future glaciation	Perturbing phenomena increase radionuclide release across the buffer/rock interface
	Rock damage	Buffer compaction	Initial defect ↓ Isostatic collapse or shear failure	Up to future glaciation During or after future glaciation	Expansion of corroding insert of initially defective canisters gives high buffer swelling pressures that damage rock
Scenarios involving canister failure by corrosion prior to a million years	No fail	Low density / alteration (outer buffer)	No fail Corrosion failure	Up to 100 000 years or more Later times	Perturbing phenomena increase sulphide transport across buffer/rock interface and hence increase canister corrosion rate
	Penetration of dilute water	Advective conditions	No fail Corrosion failure	Up to 100 000 years or more Later times	Relatively rapid canister corrosion due to advective conditions being established in an eroded buffer
Scenarios involving canister failure by shear displacement	Rock shear > 10 cm	No fail (some reduction in buffer transport path length possible)	No fail Shear failure	Up to future major post-glacial earthquake Later times	Damage to canister due to future major post-glacial earthquake

**Figure 11-1.** Potential system states in different time frames analysed in the present safety assessment – the base scenario is shown in red.

Following the requirements given in /STUK 2001/, a Base Scenario is defined which assumes that the performance targets defined for each barrier are met. This is interpreted as meaning that each barrier fulfils the safety functions assigned to it in the safety concept for a period extending to one million years or more. There will thus be no release of radionuclides from a KBS-3H repository within this time frame. This does not imply that the system does not evolve over time in the Base Scenario. Corrosion of the copper canister initially due to oxygen entrapped at the time of deposition, and, in the longer-term, due principally to sulphide present in the buffer and in the groundwater will inevitably occur and eventually lead to failure. However, provided the other components of the system fulfil their safety functions, rates will be low – in the order of a few tens of nanometres per year /Pastina and Hellä 2006/ – and canister integrity should be preserved for at least one million years.

The following sections describe other scenarios, which involve canister failure and radionuclide release within one million year time frame.

### 11.4.3 Scenarios involving an initial penetrating canister defect

#### **General description**

The evolution of a canister with a postulated initial penetrating defect is described in Chapter 8. The defective canister will initially provide some transport resistance, limiting the rate of water ingress and radionuclide release. Corrosion and volume expansion of the insert is, however, expected lead to a reduction of this transport resistance over time. It will also lead to a gradual weakening of the canister and eventual isostatic collapse or shear failure, possibly in association with a future glaciation.

Figure 11-1 depicts three scenarios involving the presence of one or more initial, penetrating defects. In all three, the canister is assumed to undergo eventual isostatic collapse or shear failure during or after a future glaciation.

In the first scenario, the buffer and geosphere are assumed to fulfil all their safety functions for at least one million years.

In the second scenario, the buffer/rock interface is perturbed, leading to enhanced release of radionuclides from the failed canisters across the interface. Features and processes that may lead to perturbations of the buffer/rock interface with different significance to, or potential impact on, KBS-3H compared with KBS-3V are shown in Table 11-1. It should be noted that, while perturbations to the buffer-rock interface may also affect the rate of corrosion of the copper canister (Appendix B.7), the corrosion rate of the copper canister will remain low (isostatic collapse or shear failure will eventually occur, as in the other scenarios involving an initial penetrating defect).

In the third scenario, volume expansion due to corrosion of the cast iron insert is assumed to lead to compaction of the buffer around the canister, and an increase in swelling pressure that damages the rock. A conservative scoping calculation in Appendix B indicates that corrosion of the insert could lead to an increase in buffer density around the canister to about  $2,160 \text{ kg m}^{-3}$ , which could give a swelling pressure of around 10 MPa or greater, depending on the salinity of the groundwater (see Figure 4-7 in /SKB 2006a/). A modelling study by /Lönnqvist and Hökmark 2007/ found that, for a KBS-3H repository at Olkiluoto, a pressure on the drift wall of 10 MPa or more might open pre-existing horizontal fractures intersecting the drift at mid-height, although the effects are expected to be small, even at pressures of 20 to 25 MPa.

The first two scenarios are assessed explicitly in assessment cases defined in the Radionuclide Transport Report /Smith et al. 2007a/. The third scenario is addressed implicitly by defining assessment cases in which the transport resistance of the geosphere is reduced (see Table 11-2 for an overview of assessment cases).

#### **Likelihood of occurrence of initial penetrating defects**

SKB and Posiva are considering different techniques for the closure welding and inspection of copper canisters. As noted in SR-Can /SKB 2006a/, SKB has adopted friction stir welding and has concluded that no penetrating defects are expected.

The differences in Posiva's and SKB's canister designs, including the chosen reference welding technique, are not expected to have any significant impact on the probability of an initial canister defect, which thus is also expected to be low in case of Finnish canisters. In both methods, the seal location is on or within a few cm from the end-face of the canister so that no differences can be identified between electron beam welding and friction stir welding from the long-term safety point of view. Posiva has not yet resolved implementation of quality assurance for canister fabrication, thus it does not as yet take any position on the likelihood of occurrence of defective canisters, except that it will be designed to be low.



#### **11.4.4 Scenarios involving canister failure by corrosion**

##### ***General description***

If the engineered barrier system performs as designed, as assumed in the Base Scenario, there are no canister failures within one million year time frame. There are, however, two scenarios depicted in Figure 11-1 in which canister failure by corrosion occurs before one million years. These are scenarios in which:

1. the buffer/rock interface is perturbed, leading to enhanced mass transfer at the interface; and
2. dilute glacial meltwater penetrates to repository depth, leading to chemical erosion of the buffer and to advective conditions becoming established in the buffer.

These scenarios lead to canister failure times earlier than in the Base Scenario, due to their effects on the transport of sulphide from the groundwater to the buffer and across the buffer, and hence on sulphide concentrations at the canister surface. Features and processes that may lead to perturbations of the buffer/rock interface different significance to, or potential impact on, KBS-3H compared with KBS-3V are summarised in Table 11-1. The impact of these or of other processes potentially altering the buffer transport properties and canister lifetime is assessed in the scoping calculations in Appendix B.7. As discussed in Section 7.4.7, penetration of dilute water to repository depth in association with glacial retreat during future glacial cycles cannot yet be ruled out, although ongoing site characterisation work is exploring whether such event could have happened in the past. Flowing groundwater with a reduced salinity at repository depth could potentially lead to the erosion of buffer material intruded into fractures intersecting the repository drifts if the ionic concentration in the water (proportional to the ionic strength) is less than the Critical Coagulation Concentration (CCC). If, during repeated glacial cycles, the density of the buffer were to be reduced by erosion to such a degree that advective transport takes place within the buffer region, this could increase the rate at which sulphide migrates to the copper surface, and hence increase the copper corrosion rate and reduce canister lifetime.

Following canister failure, radionuclide transport across the buffer will be perturbed by the same features and processes that lead to enhanced sulphide transport to the canister surface. In all assessment cases addressing canister failure by corrosion, it is assumed that transport across the buffer is instantaneous irrespective of the scenario by which corrosion failure occurs (the buffer is treated as a “mixing tank”). This represents a highly conservative representation of a scenario in which only the buffer/rock interface is perturbed. It should be noted, however, that radionuclide transport in assessment cases in which only the outer part of the buffer is treated as perturbed are considered in the context of an initial penetrating defect (Cases PD-SPALL, PD-FEBENT1, PD-FEBENT2 and PD-FEBENT3, as defined in the Radionuclide Transport Report, /Smith et al. 2007a/ – see Section 11.5 for a description of case nomenclature).

##### ***Timing and likelihood of occurrence of canister failure by corrosion***

The scoping calculations presented in Appendix B.7 indicate that corrosion is unlikely to result in a canister lifetime of less than several hundred thousand years, even in cases where mass transport in the buffer is severely perturbed (and for a moderately pessimistic assumption regarding the groundwater flow rate at the buffer/rock interface, see Appendix B.7). It is acknowledged that there are several simplifying assumptions in scoping calculations that could result in somewhat higher or lower canister lifetimes than those calculated. Nevertheless, a canister lifetime in excess of 100,000 years is expected, even in the event of a significantly perturbed buffer/rock interface.

In the case of chemical erosion by glacial meltwater, assuming a repetition of the last glacial cycle, the next glacial retreat and hence the next possibility for penetration of glacial meltwater to repository depth is in 70,000 years time. There is also significant uncertainty associated with anthropogenic emissions, especially greenhouse gasses, which could significantly delay the formation of permafrost and ice sheets (see Section 6.1). Even following partial erosion of the

buffer, the rate of corrosion is expected to remain low due to the limited supply of sulphide from the groundwater. The scoping calculations given in Appendix B.7 indicate that about million years would be required for failure by corrosion even if the entire buffer is treated as a mixing tank, based on the currently observed maximum sulphide concentration in the groundwater at Olkiluoto, and the current hydraulic gradient<sup>35</sup>.

Radionuclide release and transport calculations addressing canister failure due to corrosion assume that failure of a single canister occurs 100,000 years in the future. This failure time is regarded as pessimistic, given the slow rate of canister corrosion even following significant erosion of the buffer.

In neither scenario leading to failure by corrosion can an estimate currently be made of the likelihood or rate of canister failure by corrosion in one million year time frame, given the limited quantitative understanding of relevant processes, such as chemical erosion of the buffer and the impact of methane and hydrogen on the microbial reduction of groundwater sulphate to sulphide (the impact of repository generated hydrogen has been shown to be small). However, for both scenarios leading to this mode of canister failure, the canister positions most vulnerable to failure will be those associated with the highest groundwater flows at the buffer/rock interface. Where the rock adjacent to the drift is relatively tight, it may take many glacial cycles before sufficient buffer erosion occurs for advective conditions to become established in the buffer.

#### **11.4.5 Scenarios involving canister rupture due to rock shear**

##### ***General description***

According to Finnish regulations, the importance to safety of a substantial rock movement occurring in the environs of the repository should be considered. Significant shear movements on fractures intersecting the repository drifts are most likely to occur in association with large earthquakes. As discussed in Section 7.4.5, the buffer is expected to protect the canister against rock shear movements of the order of 0.1 m and smaller with a significant safety margin. The maximum amount of movement is related to fracture size. There is, however, uncertainty in the degree to which large fractures with the potential to slip by more than 0.1 m can be identified and avoided when emplacing canisters along the drift, and so the potential consequences of shear movements greater than 0.1 m at canister emplacement locations need to be assessed.

A single scenario is depicted in Figure 11-1 involving, as the first mode of canister failure, rupture due to rock shear, where the shear movement is in excess of 0.1 m. In this scenario, following failure, the canister is assumed to cease to provide a barrier to water ingress and radionuclide release. There will be deformation and possibly some limited erosion of the buffer, and some increase the transmissivity of fractures intersecting the drifts, although the safety functions of the buffer and the geosphere (including protection of the remaining non-failed canisters) are assumed to be maintained.

##### ***Timing and likelihood of canister rupture due to rock shear***

Any future large earthquakes occurring at the Olkiluoto site are not expected to be uniformly distributed in time. Palaeoseismicity studies support the suggestion that major seismic activity was, in the past, limited to a short period after the last deglaciation, and it may be inferred that this will also be the case in the future (Section 2.2.2). Given that, based on a repetition of the last glacial cycle, the next glacial retreat will be in 70,000 years time, assessment cases addressing canister failure due to rock shear assume that failure occurs 70,000 years in the future.

---

<sup>35</sup> Higher flows are expected in association with glacial retreat, but these would only persist for a few thousand years.

Based on scoping calculations in Appendix B.5, the expectation value of the number of canisters in the repository that could potentially be damaged by rock shear in the event of a large earthquake is 16 out of the total number of 3,000 canisters, although there are some significant uncertainties associated with these values that could lead to them giving either an underestimate or an overestimate of the actual likelihood of damage (see Section 7.4.5). Application of a canister position avoidance criterion would potentially decrease this number, but an efficient criterion has not been developed and tested for KBS-3H. The probability an earthquake occurring that is sufficiently large to cause canister damage in a 100,000 year time frame has been estimated at 0.02 (Table 5-8 in /La Pointe and Hermanson 2002/).

## 11.5 Overview of assessment cases

Table 11-2 gives an overview of assessment cases considered in the Radionuclide Transport Report /Smith et al. 2007a/. Each case is assigned a unique name, comprising two parts separated by a hyphen. The first part of the name indicates the canister failure mode that the case addressed:

PD: canister with an initial penetrating defect;  
CC: canister failure due to copper corrosion; and  
RS: canister failure due to rock shear.

The second part of the name identifies the case either as a Base Case (BC) for a given canister failure mode, or a variant case illustrating the impact of one or more uncertainties.

Cases MD-1, MD-2 and MD-3 illustrate the impact of rock matrix diffusion depth for a hypothetical pulse release from the geosphere, and therefore are not associated with a specific canister failure mode.

Following the methodology applied in SR-Can, the majority of assessment cases illustrating uncertainties not specifically related to a canister failure mode are assigned to the group dealing with an initial penetrating defect. This failure mode provides a convenient basis for exploring these various uncertainties, since, unlike the other failure modes, the transport and retention properties of the buffer and host rock are unaffected by (or need not be perturbed in order to give rise to) canister failure. Using the initial penetrating defect as a reference failure mode for exploring uncertainties also limits the number of cases that need to be analysed, and provides a common basis for comparison with TILA-99.

The variant cases are designed to illustrate specific uncertainties or combinations of uncertainties, including (but not restricted to) those that are of particular relevance to KBS-3H. However, not all conceivable uncertainties and combinations of uncertainties are covered. For example, uncertainties in the transport barrier provided by the geosphere, biosphere uncertainties and uncertainties related to future human actions are either not addressed or are analysed in less detail than others.

In some cases, whether one alternative parameter value is more optimistic or conservative than another is well known from experience in past assessments or is clear from the nature of the release and transport processes involved. For example, a high geosphere transport resistance is clearly a more optimistic assumption than a low transport resistance. On the other hand, in other cases, a sensitivity analysis would, in principle be necessary to explore the impact of variations in one or more parameters on radionuclide releases, before it could be stated what is an optimistic parameter value, and what is conservative. Such sensitivity analyses have not, in general, been performed in the present assessment.

The scope of these cases and the rationale for case selection is discussed further in the Radionuclide Transport Report /Smith et al. 2007a/.

**Table 11-2. Overview of assessment cases.**

<b>Cases assuming a single canister with an initial penetrating defect (PD-)</b>	
<b>Case</b>	<b>Description</b>
PD-BC	Base Case for initial penetrating defect in BWR-type canister
PD-VVER	Initial penetrating defect in VVER-440 PWR type canister
PD-EPR	Initial penetrating defect in EPR type canister
PD-HIFDR	Increased fuel dissolution rate
PD-LOFDR	Reduced fuel dissolution rate
PD-IRF	Evaluates transport only of radionuclides present in instant release fraction <sup>a</sup> (see footnote at the end of the table)
PD-BIGHOLE	Increased defect size
PD-HIDELAY	Increased delay until loss of defect transport resistance
PD-LODELAY	Decreased delay until loss of defect transport resistance
PD-BHLD	Increased defect size plus decreased delay until loss of defect transport resistance
PD-HIDIFF	Increased diffusion rate in buffer
PD-FEBENT1	Perturbed buffer-rock interface – high conductivity, narrow perturbed zone
PD-FEBENT2	Perturbed buffer-rock interface – more extensive perturbed zone (2 different thicknesses)
PD-FEBENT3	
PD-SPALL	Perturbed buffer-rock interface – high conductivity, narrow perturbed zone, lower flow through intersecting fractures than that assumed in cases PD-FEBENT1, 2 and 3
PD-EXPELL	Dissolved radionuclides expelled by gas from canister interior and across buffer to geosphere
PD-VOL-1	C-14 transported in volatile form by gas generated by corrosion (2 rates of gas generation)
PD-VOL-2	
PD-BCN	Initial penetrating defect in BWR-type canister; Nb present in near field and geosphere in anionic form
PD-BCC	Initial penetrating defect in BWR-type canister; C-14 present in geosphere in anionic form (carbonate)
PD-VVERC	Initial penetrating defect in VVER-440 PWR type canister; C-14 present in geosphere in anionic form (carbonate)
PD-EPRC	Initial penetrating defect in EPR type canister; C-14 present in geosphere in anionic form (carbonate)
PD-NFSLV	Near-field solubilities varied according to uncertainties in redox conditions
PD-SAL	Brackish/saline water present at repository depth (all time)
PD-HISAL	Saline water present at repository depth (all time)
PD-GMW	Change from reference (dilute/brackish) water to glacial meltwater at 70,000 years (release also starts at 70,000 years – two alternative meltwater compositions)
PD-GMWV	
PD-GMWC	Change from reference (dilute/brackish) water to glacial meltwater at 70,000 years (release starts at 1,000 years, as in the reference case)
PD-HIFLOW	Increased flow at buffer-rock interface
PD-LOGEOR	Reduced geosphere transport resistance
PD-HIGEOR	Increased geosphere transport resistance
PD-HIFLOWR	Increased flow at buffer-rock interface and reduced geosphere transport resistance

**Table 11-2. (Continued) Overview of assessment cases.**

<b>Cases assuming a single canister failing due to copper corrosion (CC-)</b>	
<b>Case</b>	<b>Description</b>
CC-BC	Base Case for failure due to copper corrosion; buffer treated as mixing tank
CC-HIFDR	Increased fuel dissolution rate
CC-LOFDR	Reduced fuel dissolution rate
CC-GMW	Glacial meltwater present at repository depth (impact on near-field solubilities and geosphere retention parameters)
CC-LOGEOR	Reduced geosphere transport resistance
CC-LOGEORG	Reduced geosphere transport resistance, glacial meltwater <sup>b</sup>
CC-LOGEORS	Reduced geosphere transport resistance, saline groundwater <sup>b</sup>
<b>Cases assuming a single canister failing due to rock shear (RS-)</b>	
<b>Case</b>	<b>Description</b>
RS-BC	Base case for failure due to rock shear
RS-GMW	Glacial meltwater present at repository depth (impact on near-field solubilities and geosphere retention parameters)
<b>Additional cases (hypothetical pulse release to geosphere)</b>	
<b>Case</b>	<b>Description</b>
MD-1	Variations in matrix diffusion depth (3 cases)
MD-2	
MD-3	

<sup>a</sup> Certain radionuclides are enriched at grain boundaries in the fuel, at pellet cracks and in the fuel/sheath gap as a result of thermally driven segregation during irradiation of the fuel in the reactor. These are assumed to enter solution rapidly once water contacts the fuel pellet surfaces, and are termed the instant release fraction (IRF).

<sup>b</sup> Glacial meltwater is a very dilute ice-melting water. Saline groundwater represents water with a TDS (Total Dissolved Solids) content of about 20 g/l. For detailed composition of the waters used in the assessment, see Appendix D of Radionuclide Transport report.



## 12 Issues requiring further work

The description of the evolution of a KBS-3H repository at Olkiluoto given in the previous chapters of this report, and the more detailed process description given in /Gribi et al. 2007/, have identified a range of issues of scientific understanding that may need to be addressed in future research and design development (RD&D). These issues are summarised below. With the exception of erosion due to buffer material falling through supercontainer perforations (Piping and erosion during early evolution, below), none are exclusive to KBS-3H, although their significance to KBS-3V and KBS-3H may differ, for example due to the different nature and amounts of materials likely to be used in the two alternatives. Some, such as iron/bentonite interaction (Iron corrosion, gas generation and the interaction of the buffer with iron corrosion products and hydrogen, below), are of more relevance to KBS-3H than to KBS-3V assuming the current reference KBS-3H design, which employs steel supercontainer shells.

The issues are not prioritised and are to be considered in the context of the development of the KBS-3H design, taking into account programmatic objectives and constraints, such as schedules and resources both in Posiva and SKB.

### 12.1 Issues related to the evolution of the repository and site

#### *Groundwater flow and composition*

The Olkiluoto Site Description 2006 identifies a range of issues and uncertainties concerning the current site model, and discusses the activities being undertaken or proposed to address them (Chapter 10 in /Andersson et al. 2007/). There is a particular focus on groundwater flow and composition, understanding of which is likely to improve significantly as characterisation and modelling of the Olkiluoto site continues. A specific issue for Olkiluoto site is the need for a better estimate on the rate of methane gas production and coupling of the methane gas production to the boundary conditions for other site models.

Specific areas of uncertainty also noted in the present report particularly relevant to the discussions in the present safety assessment include (Section 5.3.1):

- the long-term impact of backfilled and sealed exploration boreholes on groundwater flow (this issue is likely to be clarified as more specific information about the technical methods available to backfill and seal the boreholes becomes available);
- the possible effects on groundwater flow and composition of dissolved gases released from the deeper parts of the rock (methane and hydrogen); and
- the impact of external conditions related to glaciations (e.g. taliks in permafrost, glacial melt water intrusion) on the long-term performance of the geosphere and the engineered barrier.

With regard to the impact of glaciations, additional information is needed to

- better understand rock-water interactions during the transient, high flow conditions associated with glaciation and the role of microbial reactions under glacial and post-glacial conditions;
- determine whether glacial meltwater (and possibly oxygen) penetrated to repository depth during past glaciations;
- provide insight as to the hydrogeology at Olkiluoto during permafrost/glacial conditions; and
- better understand the hydromechanical effects of successive glaciations.

Some potentially significant hydromechanical effects include hydraulic jacking as well as the existence of a highly anisotropic stress field in relation to deglaciation that could possibly open fractures. Modelling work on these issues is underway in Sweden.

A further issue that is particularly relevant if the onset of any future change to glacial conditions is delayed by anthropogenic emissions is the likely reduction in ionic strength of the ground-water during a prolonged period of isostatic uplift (Section 6.5.2). Significant buffer erosion could occur if the ionic strength were to fall below the Critical Coagulation Concentration (CCC). On the basis of current shallow groundwater composition, it is judged unlikely that this would occur (other than in association with glaciation, which is discussed in Section 7.4.3) because of the interaction of this water with the rock and fracture filling materials, but further information is needed.

### ***Piping and erosion during early evolution***

Piping/erosion is a critical issue for repository design as well as safety. The distance blocks in the current reference design have been the subject of extensive experimental and modelling studies to evaluate whether or not significant piping and erosion might occur during saturation (Section 5.5.6). The “tight” blocks have been shown experimentally not to undergo piping in both a reference scenario and a more pessimistic scenario. The more pessimistic scenario involves a 1 litre per minute inflow to the gaps around a supercontainer adjoining a block (higher than the current design limit of 0.1 litres per minute), a 1 MPa per hour rate of hydraulic pressure increase following filling of the gaps with water and a maximum hydraulic pressure difference across the block of 5 MPa. There remains, however, some uncertainty in whether even 5 MPa per hour represents the maximum rate of pressure increase following filling of the gaps around a supercontainer with water. Furthermore, modelling studies suggest that hydraulic pressure differences across a distance blocks separating less tight and tighter drift sections could give rise to deformation, widening the gap between the distance block and the supercontainer and resulting in full hydraulic pressure being exerted on the entire vertical face of a distance block, rather than just a narrow annular region around its periphery (Figure 2-10). This could give rise to displacement of the distance block and to significant piping and erosion. Distance block design alternatives that less sensitive to these phenomena are being developed (see, e.g. Appendix K of Autio et al. 2007/). These designs and the situations in which they might be implemented are likely to be further studied as part of the repository design work.

In the case of the DAWE design option (Appendix A), a further issue of concern is the possible loss of buffer material by erosion during the operation of a compartment and subsequent reduction of final buffer density. In this design option, humidity-induced fracturing of the buffer inside the supercontainers could lead to pieces of the buffer falling through the perforations in the supercontainer shell and onto the drift floor, where they could become dispersed in the water draining along the floor prior to the sealing of the compartment (the gaps around the distance blocks are relatively large in the DAWE design option in order to allow such drainage). If the possibility of significant erosion cannot be excluded in the current design, it is likely that it could be prevented by design refinements, such as reducing the size of the perforations, while maintaining the same percentage of coverage (62%).

### ***Chemical evolution of the buffer***

Strongly reducing conditions will be maintained in the buffer following the depletion of trapped oxygen. Under such conditions, structural iron in smectites, which occurs in the buffer mainly as Fe(III), may be reduced to Fe(II) by electron transfer between the species in solution and in the structure, although the mechanism of this redox process is still controversial and available experimental data are not representative of repository conditions. The key issue for the physical performance of the buffer is the structural change that this might cause. As noted in Section 5.6.2, reduction of Fe(III) to Fe(II) could, in principle, have consequences for the stability and to some extent the swelling pressure and hydraulic properties of the buffer. In the study

by /Carlson et al. 2006/, for example, a substantial increase in hydraulic conductivity was found in some of the samples which had been in contact with iron for a period of up to 3 years. The swelling pressure was, however, rather unaffected in these systems, indicating inhomogeneity, with localised high density/low hydraulic conductivity volumes and low density/high hydraulic conductivity volumes.

More generally, the evolution of the buffer, including drying/wetting, impact of iron saturation, cementation due to silica precipitation and strain caused by deformation of the supercontainers are issues requiring more thorough investigation.

### ***Iron corrosion, gas generation and the interaction of the buffer with iron corrosion products and hydrogen***

The corrosion of the supercontainer shells and the other steel components of a KBS-3H repository will give rise to significant gas pressures in tight drift sections, where the gas cannot readily escape into intersecting transmissive fractures in the rock. The EDZ is a potential migration route for gas away from tight drift sections, but the properties of the EDZ, and thus the magnitude of the gas pressures that will arise in these sections, are subject to uncertainties.

The various strain mechanisms that are involved in the early and long-term evolution of the supercontainer shell have an uncertain and possibly detrimental effect on the outer part of the buffer, depending on how the supercontainer shells deform. Iron/bentonite interaction and the possible alteration of montmorillonite and formation of new minerals are also potentially detrimental and subject to significant uncertainties. The impact of alteration on mass transfer across the buffer/rock interface and the resulting effects on canister corrosion and on radionuclide transport are handled conservatively in the scoping calculations in Appendix B.7 and in the Radionuclide Transport Report /Smith et al. 2007a/ by treating the affected region as a highly permeable mixing tank, and by performing sensitivity analyses on the spatial extent of the affected region. Results of 1-D reactive transport modelling reported in /Wersin et al. 2007/ indicate that the extent of the zone potentially undergoing mineral transformation is likely to remain spatially limited (a few centimetres) for very long times (Section 6.5.3). The transformed buffer may also, in reality, be impermeable and thus continue to limit mass transfer across the buffer/rock interface significantly. Recommendations for continuing studies of iron/bentonite interaction are given in /Wersin et al. 2007/. These include, from the experimental side, long-term iron/bentonite interaction studies that include measurements of physical properties (swelling pressure, hydraulic conductivity) and well-controlled diffusion experiments with Fe(II). From the modelling side, more detailed geochemical modelling is recommended.

Another source of uncertainty is the impact of Fe(II) from the corrosion of the insert of a failed canister on the capacity of the buffer to sorb some radionuclides. Fe(II) could, in particular, compete with the sorption of species such as Ni(II) and Sr(II), and weaken the barrier function of the buffer with respect to Ni and Sr radionuclides. Iron corrosion products will themselves sorb some radionuclides. The ultimate fate of these sorbed radionuclide is not, however, clear. It is possible that changes in geochemical conditions and/or ageing and transformation of the surfaces of the corrosion products could release sorbed radionuclides at a later time. This is also particularly relevant in the case of Ni(II).

There is generally assumed to be no significant interaction between hydrogen from the corrosion of steel and minerals in the buffer. This assumption, however, still awaits experimental verification.

Materials such as titanium are being studied as possible alternatives for the supercontainer shell and some other engineered structures in the drift. Long-term safety implications, such as potential impact of these materials on the safety functions of the buffer, are being addressed in further investigations.

### ***Effect of hydrogen gas on porewater chemistry***

The presence of high hydrogen partial pressures due to the corrosion of the supercontainer shells and the other steel components of a KBS-3H repository, may have an effect on the bentonite porewater chemistry. The impact of hydrogen gas on the bentonite porewater chemistry has not yet been fully evaluated. Various factors need to be considered, including acid-base equilibria and the pH buffering capacity of bentonite, as well as the limited timeframe of hydrogen production of several thousand years. The overall impacts, in particular any effects on the buffer, should be taken into account in future studies.

### ***Microbial activity***

Microbial activity is expected to be suppressed in the highly compacted bentonite buffer and decrease with time due to the increasing buffer swelling pressure. The criterion currently set for negligible microbial activity to be assumed is that the swelling pressure should exceed 2MPa, and this criterion is expected to be met throughout the bulk of the buffer. The highest value of buffer density at which significant microbial activity can occur in compacted bentonite is an issue currently under investigation by SKB.

Lower density bentonite and porous steel corrosion products may, however, be present near the buffer/rock interface, and here there is a greater likelihood of active microbes. Microbial activity together with hydrogen from the corrosion of steel repository components could lead to the reduction of sulphate in the groundwater to sulphide, although the impact on canister lifetime is also expected to be small (see scoping calculations in Appendix B.7). Furthermore, at Olkiluoto there is a potential for microbial activity at the boundary between sulphate rich water and the deeper, methane zone (Section 2.2.4). Although the impact on canister lifetime is also expected to be limited because of the slow migration of microbially-produced sulphide through the bulk of the buffer, this issue needs to be further evaluated, especially with respect to the transport rate of methane and the kinetics of sulphate reduction in the rock.

### ***Impact of cement and stray materials***

Interactions involving cement and stray materials are subject to significant uncertainties including lack of knowledge of the general mechanism of cement/bentonite interaction. Simple mass balance calculations on the impact of alkaline leachates on bentonite have been performed, but these excluded a number of phenomena, such as the precipitation/dissolution of secondary minerals in bentonite. It is argued in Section 5.6.5 that the expected limited amounts of alkaline leachates in the drift will not have significant adverse effects on the safety functions of the canister, buffer or host rock, but this is likely to be the subject of further studies. Stray materials present in the drifts could contain organic substances. As noted in Section 4.2.5, organic substances or their degradation products could form complexes with radionuclides, which would lower radionuclide sorption and thus increase radionuclide transport rates in the event of canister failure and release of radionuclides. Currently, some adverse effects on the mass transport properties of the buffer/rock interface cannot be excluded. The effects of highly alkaline conditions on the solubilities of key elements also need to be assessed, although progress is being made in other programmes dealing with cementitious systems for TRU disposal which are collecting thermodynamic data for these elements at high pH conditions. This is an issue currently being studied. Finally, studies are ongoing to assess the impact of cement additives, e.g. superplasticisers, on radionuclide transport in the event of canister failure.

### ***Evolution of a canister with an initial penetrating defect***

There are many uncertainties in the internal evolution of a canister with an initial penetrating defect, most of which can be treated in safety assessment calculations, e.g. using conservative assumptions. It is possible that a better understanding of, for example, processes leading to water ingress, fuel matrix dissolution and the establishment of a transport pathway from the canister interior to the buffer could allow some of these uncertainties to be reduced.

### ***Buffer erosion by dilute glacial meltwater***

There is currently no adequate quantitative understanding of buffer erosion following the penetration of dilute glacial meltwater to repository depth (Section 7.4.7). The process is modelled in SR-Can, but it is acknowledged that better understanding of the erosion process could lead to models that yield either lower or higher buffer loss rates. This and the effect of subsequent glaciations on the buffer are issues currently being investigated at SKB and Posiva. Potentially significant coupled hydro-mechanical effects due to glaciations that could possibly open fractures, including hydraulic jacking as well as a highly anisotropic stress field resulting from deglaciation, as discussed in Section 9.4.5 of SR-Can Main report /SKB 2006a/, are also issues for further work for both KBS-3H and KBS-3V.

### ***Impact of earthquakes***

The possibility of detecting fractures with the potential to undergo shear movements of 0.1 m or greater in the event of a large earthquake, and of avoiding such fractures during repository construction, has not yet been evaluated in detail. Furthermore, the cumulative effect of the impact of many earthquakes over a prolonged period on the buffer and canisters is an issue for further investigation (Section 7.4.5).

### ***Thermally induced rock spalling***

As noted in Section 5.4.5, pressures much smaller than the full buffer swelling pressure are likely to be sufficient to suppress spalling. The pressure required is thought to be in the order of 150 to 200 kPa, but is uncertain, and is likely to require further investigation. The use of pellets to prevent spalling is being studied in the context of KBS-3V, and such measures may also be considered in future KBS-3H design studies. Ongoing work by Posiva and SKB aims to improve understanding of rock spalling processes, and to find means to reduce or prevent spalling if necessary. For example, the possibility of excavation-induced rock spalling is being further studied via the Prediction-Outcome studies currently underway in Posiva's ONKALO access ramp /Andersson et al. 2007/. Prior to the emplacement of spent fuel, alignment of the deposition drifts with the direction of the principal stress in the rock should ensure that little or no spalling will occur. However, the results of these studies should also provide a firmer basis for predictions of which drift sections may undergo thermally-induced rock spalling subsequent to spent fuel emplacement. This issue is of particular concern in the tightest drift sections, where buffer swelling pressure on the drift wall takes longest to develop. Measures to reduce or prevent thermally-induced rock spalling are also mentioned in the context of design issues in Section 12.2.

## **12.2 Design issues**

The present safety assessment was conducted while design development and associated laboratory testing was still underway. It was necessary to select a reference design for the assessment (the Basic Design), even though there were uncertainties regarding the feasibility of implementing this preliminary design in practice. The feasibility of implementing a given design is assumed in safety assessment, and this assumption must be justified as part of any future safety case. Ongoing design development that should improve the robustness of any future safety case are also summarised below.

### ***Avoidance of distance block displacement and deformation during early evolution***

In the current reference design, the initial gaps between the distance blocks and adjoining supercontainers are made small. If these gaps remain small, then, when the void space around a supercontainer becomes water filled and the water pressure increases towards the hydrostatic pressure at repository depth, this pressure is exerted only on narrow annuli around the outer



perimeters of the vertical faces of the adjoining distance blocks, rather than on the full surface areas of the faces. This is important since, if void space around a neighbouring supercontainer is more slowly filled, then the resulting pressure difference across the separating distance block could result in displacement of this distance block relative to the supercontainer. This could increase the likelihood of piping along the distance block/host rock interface, and would affect the final saturated density of the buffer in a manner that is not possible to predict.

Maintaining a small gap between the distance blocks and adjoining supercontainers is therefore critical in the current reference design. In this design, steel fixing rings will be installed, where necessary, to avoid displacement of the distance blocks prior to the installation of compartment and drift end plugs. It has, however, recently been shown in modelling studies reported the Design Description 2006 /Autio et al. 2007/ that deformation of the blocks may still occur due to hydraulic pressure differences along the drift, which could lead to the adverse consequences described above. Design alternatives that are less sensitive to these phenomena are being developed, including the design variant termed DAWE (Drainage, Artificial Watering and air Evacuation). These designs and the situations in which they might be implemented are likely to be further studied as part of the repository design work.

### ***Avoidance or limitation of thermally induced rock spalling***

In the current reference design, significant thermally induced spalling could occur on a timescale of a few years in relatively tight drift sections (wall rock hydraulic conductivity less than about  $10^{-12} \text{ m s}^{-1}$ ). However, there are indications that pressures much smaller than the full buffer swelling pressure are likely to be sufficient to suppress spalling. The pressure required is thought to be in the order of 150 to 200 kPa, but is uncertain, and is likely to require further investigation. The use of pellets to prevent spalling is being studied in the context of KBS-3V, and such measures may also be considered in future KBS-3H design studies.

### ***Possible alternative supercontainer materials***

A concern with the use of steel in the supercontainer shell and some other engineered structures in the drift is its possible detrimental impact on the physical properties of buffer (Section 12.1.4). Very few relevant experimental studies are currently available and further studies to address the processes involved and their impact on, for example, the swelling and hydraulic properties of bentonite are being initiated. The findings of these studies will be balanced against the favourable qualities of steel, such as the scavenging effects of its corrosion products on sulphide and oxygen, in deciding whether or not steel remains a suitable candidate material for the supercontainer shell.

As a complement to these studies, materials such as titanium are being studied as possible alternatives to steel, since they avoid the complex evolution and uncertainties associated with iron/bentonite interaction at the buffer/rock interface. A preliminary evaluation of the safety implications of using alternative materials has been made /SKB/Posiva 2008/ and the conclusion is that titanium is expected to have a very low reactivity with bentonite and its corrosion rates is lower than that for steel. Nevertheless, the long-term safety implications of these materials, such as their potential impact on the safety functions of the buffer, still need to be more thoroughly addressed.

### ***Layout to avoid potentially problematic fractures***

Shear movements on rock fractures sufficient to damage the canisters in the event of a large earthquake are only possible on fractures above a certain size. In SR-Can, the calculated probability of canister failure is significantly reduced by assuming that the Expanded Full Perimeter Criterion (EFPC) is applied, whereby large fractures intersecting both the full perimeter of a KBS-3V deposition tunnel and the deposition hole are assumed to be readily observable and avoided /Munier 2006/. It is uncertain, however, whether or not a similar line of reasoning can be applied to a KBS-3H repository, without rendering a large proportion of the drift unusable. Thus, no criterion similar to the EFPC is applied in the calculation of the likelihood of canister damage, although this remains an issue for further study.

## References

- Agrenius L, 2002.** Criticality safety calculations of storage canisters. SKB TR-02-17, Svensk Kärnbränslehantering AB.
- Ahokas H, Hellä P, Ahokas T, Hansen J, Koskinen K, Lehtinen A, Koskinen L, Löfman J, Mézaros F, Partamies S, Pitkänen P, Sievänen U, Marcos N, Snellman M, Vieno T, 2006.** Control of water inflow and use of cement in ONKALO after penetration of fracture zone R19. Posiva Working Report 2006-45. Posiva Oy, Olkiluoto, Finland.
- Ahonen L, Vieno T, 1994.** Effects of glacial meltwater on corrosion of copper canisters. Nuclear waste Commission of Finnish Power Companies (YJT), Helsinki, Finland. Report YJT-95-19.
- Andersson C, Eng A, 2005.** Äspö Pillar Stability Experiment. Final experimental design, monitoring results and observations. SKB R-05-02, Svensk Kärnbränslehantering AB.
- Andersson J, Ahokas H, Hudson J A, Koskinen L, Luukkonen A, Löfman J, Keto V, Pitkänen P, Mattila J, Ikonen A T K, Ylä-Mella M, 2007.** Olkiluoto Site Description 2006, POSIVA 2007-03. Posiva Oy, Olkiluoto, Finland.
- Andra, 2005.** Dossier 2005 argile- Tome- Evolution phénoménologique du stockage géologique- rapport Andra n° CRP ADS 04 0025, décembre 2005 (also available in English).
- Anttila P, Ahokas H, Front K, Heikkinen E, Hinkkanen H, Johansson E, Paulamäki S, Riekkola R, Saari J, Saksa P, Snellman M, Wikström L, Öhberg A, 1999.** Final disposal of spent nuclear fuel in Finnish bedrock – Olkiluoto site report, POSIVA 99-10. Posiva Oy, Helsinki, Finland.
- Anttila M, 2005a.** Radioactive characteristics of the spent fuel of the Finnish nuclear power plants. Posiva Working Report 2005-71. Posiva Oy, Olkiluoto, Finland.
- Anttila M, 2005b.** Criticality safety calculations for three types of final disposal canisters. Posiva Working Report 2005-13. Posiva Oy, Olkiluoto, Finland.
- Autio J, Hjerpe T, Siitari-Kauppi M, 2003.** Porosity, Diffusivity and Permeability of EDZ in Crystalline Rock and Effect on the Migration in a KBS-3 Type repository. Proceedings of a European Commission Cluster conference and workshop on Impact of the excavation disturbed or damaged zone (EDZ) on the performance of radioactive waste geological repositories, Luxemburg, 3 to 5 November 2003, EUR 21028 EN, p. 149-155.
- Autio J, Gribi P, Johnson L, Marschall P, 2005.** Effect of Excavation Damaged Zone on Gas Migration in a KBS-3H Type Repository at Olkiluoto. Proc. of the 10th Int. Conf. on Chemistry and Migration Behaviour of Actinides and Fission Products in the Geosphere, Migration'05. Avignon, France, Sept. 18–23, 2005. Special issue of Radiochimica Acta, International Journal for Chemical Aspects of Nuclear Science and Technology. Oldenburg Verlag, Munchen, 2006.
- Autio J, 2007.** KBS-3H Design Description 2005. Posiva Working Report 2007-11 and SKB R-08-29. Posiva Oy, Olkiluoto, Finland and Svensk Kärnbränslehantering AB, Sweden.
- Autio J, Börgesson L, Sandén T, Rönnqvist P-E, Johansson E, Hagros A, Eriksson M, Berghäll J, Kotola R, Parkkinen I, 2007.** KBS-3H Design Description 2006. Posiva Working report 2007-105 and SKB R-08-32. Posiva Oy, Olkiluoto, Finland and Svensk Kärnbränslehantering AB, Sweden.

- Autio J, Anttila P, Börgesson L, Sandén T, Rönnqvist P-E, Johansson E, Hagros A, Eriksson M, Halvarson B, Berghäll J, Kotola R, Parkkinen I, 2008.** KBS-3H Design Description 2007, POSIVA 2008-01 and SKB R-08-44, Posiva Oy, Olkiluoto, Finland and Svensk Kärnbränslehantering AB, Sweden.
- Behrenz P, Hannerz K, 1978.** Criticality in a spent fuel repository in wet crystalline rock. KBS Teknisk Rapport 108, Svensk Kärnbränslehantering AB.
- Bennett D G, Hicks T W, 2005.** The Swedish concept for disposal of spent nuclear fuel: differences between vertical and horizontal waste canister emplacement. SKI Report 2005:58, SKI, Stockholm, Sweden.
- Birgersson M, Johannesson L-E, 2006.** Prototype Repository, statistical evaluation of buffer density. Äspö Hard Rock Laboratory International Progress Report IPR-06-15, Svensk Kärnbränslehantering AB.
- Bond A E, Hoch A R, Jones G D, Tomczyk A J, Wiggin R W, Worraker W J, 1997.** Assessment of a spent fuel disposal canister. Assessment studies for a copper canister with cast steel inner component. SKB TR 97-19, Svensk Kärnbränslehantering AB.
- Broed R, Avila R, Hjerpe T, Ikonen A T K, 2007.** Biosphere analysis for selected cases in TILA-99 and in the KBS-3H safety evaluation, 2007. Posiva Working report 2007-109. Posiva Oy, Olkiluoto, Finland.
- Bruno J, Cera E, de Pablo J, Duro L, Jordana S, Savage D, 1997.** Determination of radionuclide solubility limits to be used in SR 97. Uncertainties associated to calculated solubilities. SKB TR 97-33, Svensk Kärnbränslehantering AB.
- Börgesson L, Hernelind J, 1999.** Coupled thermo-hydro-mechanical calculations of the water saturation phase of a KBS-3 deposition hole – influence of hydraulic rock properties on the water saturation phase. SKB TR-99-41, Svensk Kärnbränslehantering AB.
- Börgesson L, Johannesson L-E, Hernelind J, 2004.** Earthquake induced rock shear through a deposition hole. Effect on the Canister and the Buffer. SKB TR-04-02, Svensk Kärnbränslehantering AB.
- Börgesson L, Sandén T, Fälth B, Åkesson M, Lindgren E, 2005.** Studies of buffers behaviour in KBS-3H concept; Work during 2002–2004. SKB R-05-50, Svensk Kärnbränslehantering AB.
- Börgesson L, Hernelind J, 2006a.** Canister displacement in KBS-3V repository – a theoretical study. SKB TR-06-04, Svensk Kärnbränslehantering AB.
- Börgesson L, Hernelind J, 2006b.** Consequences of loss or missing bentonite in a deposition hole. SKB TR-06-13, Svensk Kärnbränslehantering AB.
- Börgesson L, Hernelind J, 2006c.** Earthquake induced rock shear through a deposition hole – Influence of shear plane inclination and location as well as buffer properties on the damage caused to the canister. SKB TR-06-43, Svensk Kärnbränslehantering AB.
- Carlson L, Karnland O, Olsson S, Rance A, Smart N, 2006.** Experimental studies on the interactions between anaerobically corroding iron and bentonite. Posiva Working Report 2006-60 and SKB R-08-28. Posiva Oy, Olkiluoto, Finland and Svensk Kärnbränslehantering AB, Sweden.
- Cathelineau M, Guillaume D, Mosser-Ruck M, Rousset D, Dubessy J, Charpentier D, Villiéras F, Michau N, 2006.** Dissolution-crystallization processes affecting di-octahedral smectite in presence of iron metal: implication on mineral distribution in clay barriers. Fe-Bentonite Workshop, Basel (CH), 10–11 May 2006.
- Cedercreutz J, 2004.** Future climatic scenarios for Olkiluoto with emphasis on permafrost. POSIVA 2004-06. Posiva Oy, Olkiluoto, Finland.

- Chou N, Martin C D, Christiansson R, 2002.** Suppressing fracture growth around underground openings. In Proc. 5th North American Rock Mechanics Symposium and 17th Tunnel Association of Canada Conference NARMS/TAC 2002, Toronto (Ed. Hammah R, Baden W, Curran J, Telesnicki M), vol. 2, pp 1151–1158, University of Toronto Press, Canada.
- Crawford M B, Wilmot R D, 1998.** Normal evolution of a spent fuel repository at the candidate sites in Finland. POSIVA 98-15. Posiva Oy, Helsinki, Finland.
- David D, 2001.** Analogues archéologiques et corrosion. Andra Report, Chatenay-Malabry, France.
- Dillström P, 2005.** Probabilistic analysis of canister inserts for spent nuclear fuel, SKB TR-05-19, Svensk Kärnbränslehantering AB.
- Duro L, Grivé M, Cera E, Gaona X, Domènech C, Bruno J, 2006.** Determination and assessment of the concentration limits to be used in SR-Can, SKB TR-06-32, Svensk Kärnbränslehantering AB.
- Enescu N, Cosma C, Balu L, 2003.** Seismic VSP and crosshole investigations in Olkiluoto, 2002. Posiva Working Report 2003-13. Posiva Oy, Olkiluoto, Finland.
- Eronen M, Glückert G, van de Plassche O, van de Plicht J, Rantala P, 1995.** Land uplift in the Olkiluoto-Pyhäjärvi area, southwestern Finland, during last 8000 years. Report YJT-95-17. Nuclear Waste Commission of Finnish Power Companies (YJT), Helsinki, Finland.
- Foster M D, 1953.** Geochemical studies of clay minerals: II. Relation between ionic substitution and swelling in montmorillonites. *Amer. Mineral.* 38, 994–1006.
- Fälth B, Hökmark H, 2006.** Seismically induced shear displacement on repository host rock fractures, Results of new dynamic discrete fracture modeling. SKB R-06-48, Svensk Kärnbränslehantering AB.
- Gribi P, Johnson L, Suter D, Smith P, Pastina B, Snellman M, 2007.** Safety assessment for a KBS-3H spent nuclear fuel repository at Olkiluoto – Process Report, POSIVA 2007-09 and SKB R-08-36. Posiva Oy, Olkiluoto, Finland and Svensk Kärnbränslehantering AB, Sweden.
- Grivé M, Montoya V, Duro L, 2007.** Assessment of the concentration limits for radionuclides for Posiva. Posiva Working Report 2007-103. Posiva Oy, Olkiluoto, Finland.
- Hagros A, 2007a.** Estimated quantities of residual materials in a KBS-3H repository at Olkiluoto. Posiva Working Report 2007-104 and SKB R-08-33. Posiva Oy, Olkiluoto, Finland and Svensk Kärnbränslehantering AB, Sweden.
- Hagros A, 2007b.** Foreign materials in the repository – Update of estimated quantities. Olkiluoto, Finland: Posiva Working Report 2007-17. Posiva Oy, Olkiluoto, Finland.
- Hagros A, Öhberg A, 2007.** Hydrological monitoring in the VLJ repository at Olkiluoto during 2006. TVO VLJ Working report VLJ-5/07. (In Finnish with an English abstract).
- Harrington J F, Horseman S T, 2003.** Gas migration in KBS-3 buffer bentonite: sensitivity of test parameters to experimental boundary conditions. SKB TR-03-02, Svensk Kärnbränslehantering AB.
- Hartikainen J, 2006.** Numerical simulation of permafrost depth at Olkiluoto. Posiva Working Report 2006-52. Posiva Oy, Olkiluoto, Finland.
- Hedin A, 2005.** An analytic method for estimating the probability of canister/fracture intersections in a KBS-3 Repository. SKB R-05-29, Svensk Kärnbränslehantering AB.
- Hellä P, Ahokas H, Palmén J, Tammisto E, 2006.** Analysis of Geohydrological Data for Design of KBS-3H Repository Layout. Posiva Working Report 2006-16 and SKB R-08-27. Posiva Oy, Olkiluoto, Finland and Svensk Kärnbränslehantering AB, Sweden.

- Horseman S, Harrington J F, Sellin P, 1999.** Gas migration in clay barriers. *Eng. Geol.* 54, 139–149.
- Hutri K-L, 2007.** An approach to paleoseismicity in the Olkiluoto (sea) area during the early Holocene. STUK-A222, STUK, Helsinki, Finland. ISBN 978-952-478-223-4 (print), ISBN 978-952-478-224-1 (pdf)
- Hökmark H, Fälth B, Wallroth T, 2006.** T-H-M couplings in rock: overview of numerical simulation results of importance to the SR-Can safety assessment. SKB R-06-88, Svensk Kärnbränslehantering AB.
- IAEA, 2003.** Radioactive Waste Management Glossary, 2003 Edition, International Atomic Energy Agency, Vienna, Austria.
- Ikonen K, 2003.** Thermal analysis of KBS-3H type repository. POSIVA 2003-11. Posiva Oy, Olkiluoto, Finland.
- Ikonen K, 2005.** Thermal conditions of open KBS-3H tunnel. POSIVA 2005-04 and SKB R-08-24. Posiva Oy, Olkiluoto, Finland and Svensk Kärnbränslehantering AB, Sweden.
- Ikonen K, 2006.** Fuel temperature in disposal canisters. Posiva Working Report 2006-19. Posiva Oy, Olkiluoto, Finland.
- Ikonen A T K, Hjerpe T, Aro L, Leppänen V, 2007.** Terrain and ecosystems development model of Olkiluoto site, version 2006. Posiva Working Report 2007-110. Posiva Oy, Olkiluoto, Finland.
- IPCC, 2001.** Climate change 2001, The scientific basis. Contribution of working group I to the third assessment report of the intergovernmental panel on climate change (Houghton J T, Ding Y, Griggs D J, Noguer M, Van der Linden P J, Dai X, Maskell K, Johnson C A (eds.)). Cambridge University Press, Cambridge and New York, 881 pp. Available on <http://www.ipcc.ch>
- Jaquet O, Siegel P, 2003.** Groundwater flow and transport modelling during a glacial period. SKB R-03-04, Svensk Kärnbränslehantering AB.
- JNC, 2000.** H12: Project to establish the scientific and technical basis for HLW disposal in Japan. Supporting Report 2. Repository design and engineering technology. JNC TN1410 2000-003, Japan Nuclear Cycle Development Institute, Tokai, Japan.
- Johansson E, Äikäs K, Autio J, Hagros A, Malmlund H, Rautakorpi J, Sievänen U, Wanne T, Anttila P, Raiko H, 2002a.** Preliminary KBS-3H layout adaptation for the Olkiluoto site – Analysis of rock factors affecting the orientation of a KBS-3H deposition hole. Posiva Working Report 2002-57. Posiva Oy, Olkiluoto, Finland.
- Johansson J M, Davis J L, Scherneck H-G, Milne G A, Vermeer M, Mitrovica J X, Bennett R A, Jonsson B, Elgered G, Elósegui P, Koivula H, Poutanen M, Rönnäng B O, Shapiro I I, 2002b.** *Journal of Geophysical Research*, 107.
- Johansson E, Hagros A, Autio J, Kirkkomäki T, 2007.** KBS-3H layout adaptation 2007 for the Olkiluoto site. Posiva Working Report 2007-77 and SKB R-08-31. Posiva Oy, Olkiluoto, Finland and Svensk Kärnbränslehantering AB, Sweden.
- Johnson L H, Tait J C, 1997.** Release of segregated radionuclides from spent fuel. SKB TR 97-18, Svensk Kärnbränslehantering AB.
- Johnson L, Marschall P, Wersin P, Gripi P, 2005.** HMCSBG processes related to the steel components in the KBS-3H disposal concept. Posiva Working Report 2005-09 and SKB R-08-25. Posiva Oy, Olkiluoto, Finland and Svensk Kärnbränslehantering AB, Sweden.
- Kahma K, Johansson M, Boman H, 2001.** Meriveden pinnankorkeuden jakauma Loviisan ja Olkiluodon rannikoilla seuraavien 30 vuoden aikana. Merentutkimuslaitos PGN, Helsinki. 25pp.



- Kalbantner P, Sjöblom R, 2000.** Techniques for freeing deposited canisters. SKB TR-00-15, Svensk Kärnbränslehantering AB.
- Karnland O, Birgersson M, 2006.** Montmorillonite stability with special respect to KBS-3 conditions. SKB TR-06-11, Svensk Kärnbränslehantering AB.
- King F, 2002.** Corrosion of copper in alkaline chloride environments, SKB TR-02-25, Svensk Kärnbränslehantering AB.
- King F, 2004.** The effect of discontinuities on the corrosion behaviour of copper canister. SKB R-04-05, Svensk Kärnbränslehantering AB.
- Knuutila A, 2001.** Canister overpack integrity assessment in handling accidents. Posiva Working Report 2001-28. Posiva Oy, Helsinki, Finland.
- Korhonen K, Kuivamäki A, Paananen M, Paulamäki S, 2005.** Lineament interpretation of the Olkiluoto area. Posiva Working Report 2005-34. Posiva Oy, Olkiluoto, Finland.
- La Pointe P R, Cladouhos T, Outters N, Follin S, 2000.** Evaluation of the conservativeness of the methodology for estimating earthquake-induced movements of fractures intersecting canisters. SKB TR-00-08, Svensk Kärnbränslehantering AB.
- La Pointe P, Hermanson J, 2002.** Estimation of rock movements due to future earthquakes at four Finnish candidate repository sites. POSIVA 2002-02. Posiva Oy, Helsinki, Finland.
- Lahdenperä A-M, Palmén J, Hellä P, 2005.** Summary of overburden studies at Olkiluoto with an emphasis on geosphere-biosphere interface. Posiva Working Report 2005-11. Posiva Oy, Olkiluoto, Finland.
- Lambeck K, Smither C, Johnston P, 1998.** Sea-level change, glacial rebound and mantle viscosity for northern Europe. *Geophys. J. Int.*, 134, 102–144.
- Lanson B, 2006.** Transformation processes of smectite in contact with metal iron: Mechanisms of smectite destabilization and characterization of the newly-formed phases. Fe-Bentonite Workshop, Basel (CH), 10–11 May 2006.
- Lanyon G W, Marschall P, 2006.** Discrete fracture network modelling of a KBS-3H repository at Olkiluoto. POSIVA 2006-06 and SKB R-08-26. Posiva Oy, Olkiluoto, Finland and Svensk Kärnbränslehantering AB, Sweden.
- Lautkaski R, Ikonen K, Hostikka S, 2003.** Consequences of fire of the canister transfer vehicle in repository and access tunnel. Posiva Working Report 2003-35. Posiva Oy, Olkiluoto, Finland.
- Lindberg A, 2007.** Search for glacio-isostatic faults in the vicinity of Olkiluoto. Posiva Working Report 2007-05 (in preparation).
- Liu J, Neretnieks I, 2006.** Physical and chemical stability of the bentonite buffer. SKB R-06-103, Svensk Kärnbränslehantering AB.
- Loida A, Kienzler B, Geckeis H, 2004.** Corrosion Behavior of Pre-oxidized High Burnup Spent Fuel in Salt Brine, Materials Research Society Symposium Proceedings, Volume 807, Scientific Basis for Nuclear Waste Management XXVII (Ed. Oversby, V.M. and Werme, L.O), p. 53–58.
- Löfman J, 1999.** Site scale groundwater flow in Olkiluoto. POSIVA 99-03. Posiva Oy, Helsinki, Finland.
- Löfman J, 2005.** Simulation of hydraulic disturbances caused by decay heat of the repository in Olkiluoto. POSIVA 2005-07. Posiva Oy, Olkiluoto, Finland.

- Lönnqvist M, Hökmark H, 2007.** Thermo-mechanical analyses of a KBS-3H deposition drift at the Olkiluoto site, Posiva Working Report 2007-66 and SKB R-08-30. Posiva Oy, Olkiluoto, Finland and Svensk Kärnbränslehantering AB, Sweden.
- Marcos N, 2003.** Bentonite-iron interactions in natural occurrences and in laboratory – the effects of the interaction on the properties of bentonite: a literature survey. Posiva Working Report 2003-55. Posiva Oy, Olkiluoto, Finland.
- Masurat P, 2006.** Potential for corrosion in disposal systems for high-level radioactive waste by *Meiothermus* and *Desulfovibrio*. Doctoral thesis. Göteborg University, Sweden.
- Mattsson H, Olefjord I, 1984.** General corrosion of Ti in hot water and water saturated bentonite clay. SKB/KBS TR 84-19, Svensk Kärnbränslehantering AB.
- Mattsson H, Olefjord I, 1990.** Analysis of oxide formed on titanium during exposure in bentonite clay. I. The oxide growth. *Werkstoffe und Korrosion* 41, 383–390.
- Mattsson H, Li C, Olefjord I, 1990.** Analysis of oxide formed on titanium during exposure in bentonite clay. II. The structure of the oxide. *Werkstoffe und Korrosion* 41, 578–584.
- Motamedi M, Karnland O, Pedersen K, 1996.** Survival of sulfate reducing bacteria at different water activities in compacted bentonite. *FEMS Microbiology Letters* 141 (1996) 83–87.
- Munier R, Hökmark H, 2004.** Respect distances. Rationale and means of computation. SKB R-04-17, Svensk Kärnbränslehantering AB.
- Munier R, 2006.** Using observations in deposition tunnels to avoid intersections with critical features in deposition holes. SKB R-06-54, Svensk Kärnbränslehantering AB.
- Muurinen A, 2006.** Chemical Conditions in the A2 Parcel of the long-term test of buffer material in Äspö (LOT). Posiva Working Report 2006-83. Posiva Oy, Olkiluoto, Finland.
- Müller Ch, Elagin M, Scharmach M, Bellon C, Jaenisch G-R, Bär S, Redmer B, Goebels J, Ewert U, Zscherpel U, Boehm R, Brekow G, Erhard A, Heckel T, Tessaro U, Tscharncke, D, Ronneteg U, 2006.** Reliability of nondestructive testing (NDT) of the copper canister seal weld. SKB R-06-08, Svensk Kärnbränslehantering AB.
- Mäkiäho J-P, 2005.** Development of Shoreline and Topography in the Olkiluoto Area, Western Finland, 2000 BP–8000 AP. Posiva Working Report 2005-70. Posiva Oy, Olkiluoto, Finland.
- Nagra, 2002.** Project Opalinus Clay: Safety report. Demonstration of disposal feasibility for spent fuel, vitrified high-level waste and long-lived intermediate-level waste (Entsorgungsnachweis). Nagra Technical Report NTB 02-05. Nagra, Wettingen, Switzerland.
- Neall F, Pastina B, Smith P, Gribi P, Snellman M, Johnson L, 2007.** Safety assessment for a KBS-3H spent nuclear fuel repository at Olkiluoto – Complementary Evaluations of Safety, POSIVA 2007-10 and SKB R-08-35. Posiva Oy, Olkiluoto, Finland and Svensk Kärnbränslehantering AB, Sweden.
- Neretnieks I, 2006.** Flow and transport through a damaged buffer – exploration of the impact of a cemented and an eroded buffer. SKB TR-06-33, Svensk Kärnbränslehantering AB.
- Oversby V M, 1996.** Criticality in a high level waste repository. A review of some important factors and an assessment of the lessons learned from the Oklo reactors. SKB TR 96-07, Svensk Kärnbränslehantering AB.
- Pastina B, Hellä P, 2006.** Expected evolution of a spent fuel repository at Olkiluoto. POSIVA 2006-05. Posiva Oy, Olkiluoto, Finland.
- Pedersen K, 2000.** Microbial processes in radioactive waste disposal. SKB TR-00-04, Svensk Kärnbränslehantering AB.

- Pitkänen P, Partamies S, Luukkonen A, 2004.** Hydrogeochemical interpretation of baseline groundwater conditions at the Olkiluoto site. POSIVA 2003-07. Posiva Oy, Olkiluoto, Finland.
- Pitkänen P, Partamies S, 2007.** Origin and Implications of Dissolved Gases in Groundwater at Olkiluoto. POSIVA 2007-04. Posiva Oy, Olkiluoto, Finland.
- Posiva, 2003.** Baseline conditions at Olkiluoto. POSIVA 2003-02. Posiva Oy, Olkiluoto, Finland.
- Posiva, 2005.** Olkiluoto Site Description 2004. POSIVA 2005-03. Posiva Oy, Olkiluoto, Finland.
- Posiva, 2006.** Nuclear Waste Management of the Olkiluoto and Loviisa Power Plants: Programme for Research, Development and Technical Design for 2007-2009. TKS-2006. Posiva, Olkiluoto, Finland.
- Poteri A, 2001.** Estimation of the orientation distributions for fractures at Hästholmen, Kivetty, Olkiluoto and Romuvaara. Posiva Working Report 2001-10. Posiva Oy, Helsinki, Finland.
- Pusch R, Ranhagen L, Nilsson K, 1985.** Gas migration through MX-80 bentonite. Nagra Technical Report NTB 85-36. Nagra, Wettingen, Switzerland.
- Pusch R, Karnland O, 1990.** Preliminary report on longevity of montmorillonite clay under repository-related conditions, SKB TR 90-44, Svensk Kärnbränslehantering AB.
- Pusch R, 1999.** Mobility and survival of sulphate-reducing bacteria in compacted and fully water saturated bentonite – microstructural aspects. SKB TR-99-30, Svensk Kärnbränslehantering AB.
- Påsse T, 1996.** A mathematical model of the shore level displacement in Fennoscandia. SKB TR 96-24, Svensk Kärnbränslehantering AB.
- Påsse T, 1997.** A mathematical model of past, present and future shore level displacement in Fennoscandia. SKB TR 97-28. Svensk Kärnbränslehantering AB.
- Påsse T, 1998.** Lake-tilting, a method for estimation of glacio-isostatic uplift. *Boreas* 27:1, 69–80.
- Raiko H, 2005.** Disposal canister for spent nuclear fuel – Design report. POSIVA 2005-02. Posiva Oy, Olkiluoto, Finland.
- Rasilainen K ed, 2004.** Localisation of the SR-97 process report for Posiva's spent fuel repository at Olkiluoto. POSIVA 2004-05. Posiva Oy, Olkiluoto, Finland.
- Rodwell W R, 2005.** Summary of a GAMBIT Club workshop on Gas Migration in Bentonite, SKB TR-05-13, Svensk Kärnbränslehantering AB.
- Ronneteg U, Cederqvist L, Rydén H, Öberg T, Müller C, 2006.** Reliability in sealing of canister for spent nuclear fuel. SKB R-06-26. Svensk Kärnbränslehantering AB.
- Rothman A J, 1984.** Potential corrosion and degradation mechanisms of Zircaloy cladding on spent fuel in a tuff repository. Lawrence Livermore National Laboratory Report UCID-20172.
- Ruosteenoja K, 2003.** Climate scenarios for Olkiluoto over the next few centuries, Posiva Working Report 2003-21. Posiva Oy, Olkiluoto, Finland.
- Saarelainen S, Kivikoski H, 2002.** Influence of freeze-thaw on the permeability of bentonite and bentonite mixtures – A literature study. Posiva Working Report 2002-31. (In Finnish, English abstract incl.), Posiva Oy, Olkiluoto, Finland.
- Saari J, 1997.** Seismicity in the Olkiluoto area (in Finnish with an English abstract). Posiva Working Report 97-61. Posiva Oy, Helsinki, Finland.

- Saari J, 2006.** Local seismic network at the Olkiluoto Site – Annual Report for 2005. Posiva Working Report 2006-57. Posiva Oy, Olkiluoto, Finland.
- Sandén T, Börgesson L, Dueck A, Goudarzi R, Lönnqvist M, Nilsson U, Åkesson M, 2007.** KBS-3H Buffer tests 2005–2007. SKB R-08-40 and Posiva working report 2008-10. Svensk Kärnbränslehantering AB, Sweden and Posiva, Olkiluoto, Finland.
- SKB, 1999.** SR 97 – Processes in the repository evolution. SKB TR-99-07, Svensk Kärnbränslehantering AB.
- SKB, 2004.** RD&D-Programme 2004 – Programme for research, development and demonstration of methods for the management and disposal nuclear waste, including social science research. Svensk Kärnbränslehantering AB.
- SKB, 2006a.** Long-term safety for KBS-3 repositories at Forsmark and Laxemar – a first evaluation – Main report of the SR-Can project, SKB TR-06-09, Svensk Kärnbränslehantering AB.
- SKB, 2006b.** Data report for the safety assessment SR-Can. SKB TR-06-25, Svensk Kärnbränslehantering AB.
- SKB, 2006c.** Buffer and backfill process report for the safety assessment SR-Can. SKB TR-06-18, Svensk Kärnbränslehantering AB.
- SKB, 2006d.** Geosphere process report for the safety assessment SR-Can. SKB TR-06-19, Svensk Kärnbränslehantering AB.
- SKB, 2006e.** Fuel and canister process report for the safety assessment SR-Can. SKB TR-06-22, Svensk Kärnbränslehantering AB.
- SKB/Posiva, 2008.** Horizontal deposition of canisters for spent nuclear fuel – Summary of the KBS-3H Project 2004–2007. SKB TR-08-03. Posiva report 2008-03. Svensk Kärnbränslehantering AB, Sweden and Posiva Oy, Olkiluoto, Finland.
- Smart N R, Blackwood D J, Werme L, 2001.** The anaerobic corrosion of carbon steel and cast iron in artificial groundwaters. SKB TR-01-22, Svensk Kärnbränslehantering AB.
- Smart N R, Blackwood D J, Werme L, 2002a.** Anaerobic Corrosion of Carbon Steel and Cast Iron in Artificial Groundwaters: Part 1 – Electrochemical Aspects, Corrosion Vol. 58, p547.
- Smart N R, Blackwood D J, Werme L, 2002b.** Anaerobic Corrosion of Carbon Steel and Cast Iron in Artificial Groundwaters: Part 2 – Gas Generation, Corrosion Vol. 58, p547.
- Smart N R, Rance A P, Werme L O, 2004.** Anaerobic corrosion of steel in bentonite. Mat. Res. Soc. Symp. Proc. 807, 441–446.
- Smart N R, Rance A P, Fennell P A H, 2005.** Galvanic corrosion of copper-cast iron couples. SKB TR-05-06, Svensk Kärnbränslehantering AB.
- Smith P, Nordman H, Pastina B, Snellman M, Hjerpe T, Johnson L, 2007a.** Safety assessment for a KBS-3H spent nuclear fuel repository at Olkiluoto – Radionuclide transport report. POSIVA 2007-07 and SKB R-08-38. Posiva Oy, Olkiluoto, Finland and Svensk Kärnbränslehantering AB, Sweden.
- Smith P, Neall F, Snellman M, Pastina B, Nordman H, Johnson L, Hjerpe T, 2007b.** Safety assessment for a KBS-3H spent nuclear fuel repository at Olkiluoto – Summary report. POSIVA 2007-06 and SKB R-08-39. Posiva Oy, Olkiluoto, Finland and Svensk Kärnbränslehantering AB, Sweden.
- Stroes-Gascoyne S, Hamon C J, Kohle C, Dixon D A, 2006.** The effects of dry density and porewater salinity on the physical and microbiological characteristics of highly compacted bentonite. Ontario Power Generation Report No: 06819-REP-01200-10016-R00.

- Stucki J W, Low P F, Roth C B, Golden D C, 1984.** Effects of oxidation state of octahedral iron on clay swelling. *Clays and Clay Minerals* 32, 357–362.
- STUK, 1999.** Government decision on the safety of disposal of spent nuclear fuel (478/1999). Report STUK-B-YTO 195. Radiation and Nuclear Safety Authority (STUK), Helsinki, Finland.
- STUK, 2001.** Long-term safety of disposal of spent nuclear fuel. Guide YVL 8.4. Radiation and Nuclear Safety Authority (STUK), Helsinki, Finland.
- Takase H, Benbow S, Grindrod P, 1999.** Mechanical failure of SKB spent fuel disposal canister – Mathematical modelling and scoping calculations. SKB TR-99-34, Svensk Kärnbränslehantering AB.
- Tanai K, Kanno T, Galle C, 1997.** Experimental study of gas permeabilities and breakthrough pressures in clays. *Mater. Res. Soc. Symp. Proc.* 465, 995–1002. Materials Research Society, Pittsburgh, PA.
- Vieno T, Hautojärvi A, Koskinen L, Nordman H, 1992.** TVO-92 safety analysis of spent fuel disposal. Report YJT-92-33E. Nuclear Waste Commission of Finnish Power Companies, Helsinki, Finland.
- Vieno T, Nordman H, 1996.** Interim report on safety assessment of spent fuel disposal, TILA-96. POSIVA 96-17. Posiva Oy, Helsinki, Finland.
- Vieno T, Nordman H, 1999.** Safety assessment of spent fuel disposal in Hästholmen, Kivetty, Olkiluoto and Romuvaara TILA-99. POSIVA 99-07. Posiva Oy, Helsinki, Finland.
- Vieno T, 2000.** Groundwater salinity at Olkiluoto and its effects on a spent fuel repository. POSIVA 2000-11. Posiva Oy, Helsinki, Finland.
- Vieno T, Lehikoinen J, Löfman J, Nordman H, Mészáros F, 2003.** Assessment of disturbances caused by construction and operation of ONKALO. POSIVA 2003-06. Posiva Oy, Olkiluoto, Finland.
- Vieno T, Ikonen A T K, 2005.** Plan for Safety Case of spent fuel repository at Olkiluoto. POSIVA 2005-01. Posiva Oy, Olkiluoto, Finland.
- Werme L O, Johnson L H, Oversby V M, King F, Spahiu K, Grambow B, Shoesmith D W, 2004.** Spent fuel performance under repository conditions: A model for use in SR-Can. SKB TR-04-19, Svensk Kärnbränslehantering AB.
- Wersin P, Mettler S, 2006.** Workshop on Fe-clay interactions in repository environments, a joint initiative by Andra, SKB and Nagra. Basel 9–10 May 2006. Nagra NAB, Nagra, Wettingen, Switzerland NAB-06-15.
- Wersin P, Birgersson M, Olsson S, Karnland O, Snellman M, 2007.** Impact of corrosion-derived iron on the bentonite buffer within the KBS-3H disposal concept – the Olkiluoto site as case study. POSIVA 2007-11 and SKB R-08-34. Posiva Oy, Olkiluoto, Finland and Svensk Kärnbränslehantering AB, Sweden.
- Wikramaratna R S, Goodfield M, Rodwell W R, Nash P J, Agg P J, 1993.** A preliminary assessment of gas migration from the copper/steel canister. SKB TR 93-31, Svensk Kärnbränslehantering AB.
- Wilson J, Savage D, Cuadros J, Shibata M, Ragnarsdottir K V, 2006.** The effect of iron on montmorillonite stability. (I) Background and thermodynamic considerations. *Geochim. Cosmochim. Acta* 70, 306–322.



### The DAWE design variant

#### A.1 Design description

The DAWE design variant is intended to limit the possibility of buffer erosion by water flow and of mechanical displacement of the supercontainers and distance blocks during the operational period, while allowing the emplacement canisters and buffer in drift sections that would be excluded in the current reference design (referred to as Basic Design, as described in the KBS-3H Design Description 2006, /Autio et al. 2007/). The DAWE design variant is described in Chapter 6 of the Design Description 2006 and is summarised below.

The general approach is to drain the drift of water during operations and then to use artificial watering to accelerate and make more uniform the swelling of the distance blocks and saturation of the void spaces around the supercontainers. Hydraulic pressure differences between neighbouring drift sections that could potentially lead to buffer erosion by water flow and to mechanical displacement of the supercontainers and distance blocks are thus prevented during the operational period of a drift compartment. Furthermore, although hydraulic pressure differences may still develop between drift sections, the fact that they are water filled means that tighter drift sections do not provide sink volumes for potential water flow from less tight drift sections, at least for an initial period following artificial wetting and air evacuation.

As in the current reference design, fractures that could give rise to significant water inflows will be avoided as canister and buffer emplacement locations. Nevertheless, the criteria for transmissive fractures that must be avoided are expected to be less stringent for DAWE compared with the current reference design. Criteria will need to take account of the possibility to drain potentially large water inflows along the drift without perturbing the buffer and the possibility of internal erosion of the buffer after drift closure.

The drainage of inflowing water along the floor of the drift during operations is achieved by inclining the drift towards its entrance. There is a design gap of 37.5–42.5 mm between the distance blocks and the drift walls, which is larger than in the current reference design and should prevent any contact with the water flowing along the bottom of the drift. Drainage of inflowing water along the drift floor is expected to continue until the drift or drift compartment is plugged. Following sealing of a compartment, artificial watering takes place simultaneously with evacuation of air to avoid gas pressurisation. Steel pipes along the surface of the drift are used for watering and air evacuation. The sides of the drift are the preferred position for watering pipes to avoid possible damage during operations.

Nozzles in the watering pipes are distributed along the drift in each supercontainer section to ensure uniform inflow and minimise any axial water flow in the drift that could give rise to bentonite erosion. Water is not directly injected in the sections where the distance blocks are positioned, again to avoid possible erosion.

The watering time is expected to be about 10 hours at most. The flows of water and air during the watering period are illustrated in Figure A-1. It should be noted that only about one third of the total void space (including bentonite pores) will be filled with water in this way, the remaining voids being more slowly saturated. The system remains, therefore, in a partially saturated state even after artificial watering. All supercontainer sections will be filled simultaneously to avoid axial water flows that could give rise to bentonite erosion and redistribution along the drift.

For the DAWE design option to be acceptable, it must be convincingly shown that the pipes used for artificial wetting and drainage can be successfully removed following the injection of water and evacuation of air. It is likely to be difficult or impossible to exclude the formation of

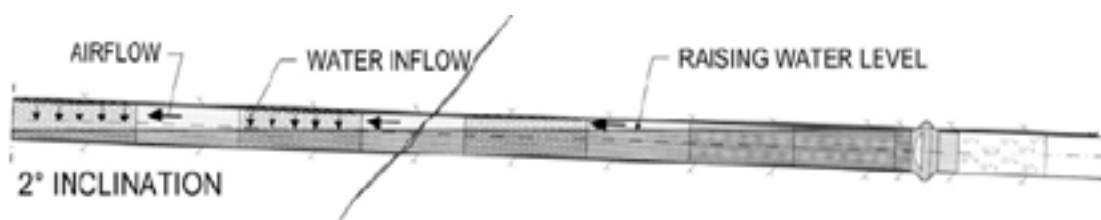


*Figure A-1. The flows of water and air during the watering period.*

preferential transport pathways if this is not the case. Bentonite mud will be pumped in the drift if necessary to fill the open volume left by the pipes during removal. Pipe removal demonstration work at the Äspö Hard Rock Laboratory in Sweden is ongoing.

The drift design, supercontainer design and the length of the distance blocks are the same as in the current reference design. The isolation of unsuitable drift sections by compartment plugs, the sealing of the drift using a drift end plug, and the use of filling blocks similar to the current reference design, although the criteria for defining unsuitable drift sections for canister and buffer emplacement may be somewhat relaxed. Furthermore, the compartment plugs used in the DAWE design variant will be equipped with lead-throughs, valves and collar seals for the wetting and air evacuation pipes, and also for possible drainage.

The operational procedure for implementing the DAWE design variant is given in Box A-1. The overall operational period for a drift is likely to be about a month.

## **A.2 Evolution in the operational period**

During the operational period, water flowing into the drift will migrate around the drift walls to the drift floor, along which it will drain due to the drift inclination. Swelling of the distance blocks during the operational period is likely to be limited and controlled by vapour transport rate in air. The initial water content of the distance blocks (21% by weight) is sufficiently high that no cracking of the blocks is expected during this period (see Appendix K in /Autio et al. 2007/). In the case of the lower initial water content bentonite blocks inside the supercontainers, experimental studies have shown humidity-induced cracking after about 3 months – see Appendix L of /Autio et al. 2007/. Thus, the operational period could, if needed, be extended, but to no more than about a couple of months if the danger that cracking and breaking away of pieces of the distance blocks will interfere with drift drainage is to be avoided.

## **A.3 Artificial wetting and air evacuation and subsequent evolution**

As in the current reference design, saturation of the buffer due to the inflow of groundwater to the drift will continue over a prolonged period following plugging of the drift or drift compartment, and will be strongly affected by the heterogeneity of the surrounding rock.

Following plugging of a compartment (or the installation of the drift end plug in the case of the final compartment in a drift) artificial filling with water (wetting) of the gaps around the distance blocks and supercontainers will force air towards the higher, closed end of the compartment, from where it will be evacuated. The piping used for artificial wetting and air evacuation will then be removed and the compartment plugged.

The water pressure in the gaps around the supercontainers and distance blocks will increase towards the hydrostatic pressure, being hydraulically connected to transmissive fractures intersecting the drift. This hydraulic connection is likely to last for a few days, until it is interrupted by the sealing of the gaps around the distance blocks as the distance blocks absorb water and swell.

**Box A-1**     *The operational procedure for implementing the DAWE design variant in a single compartment*

- Planning of drift specific implementation and definition of positions for design components (e.g. supercontainers, distance blocks, plugs). The positions of compartment borders and of each component are determined before operation starts.
- Preparatory rock works (e.g. installation of drip shields, excavation of grooves and notches). Preparation of positions for steel plugs.
- Installation of attachments to systems and steel structures (mainly steel plugs).
- Installation of drainage, air evacuation and artificial watering systems for the deposition compartment.
- Emplacement of distance blocks, supercontainers and other design components to one compartment. The estimated longest time for this step is 5 days.
- When all supercontainers and other components have been installed in the drift the necessary auxiliary systems (drainage mat etc) are removed. The estimated longest time for this step is one shift (7 hours).
- The collar of compartment steel plug with necessary cuffs and lead-throughs is inserted. The estimated longest time for this step is one shift.
- Necessary pipes are extended through the cuffs and lead-throughs. The estimated longest time for this step is one shift.
- The compartment plug is installed. The estimated longest time for this and the following step is one shift.
- The free space behind the plug is filled (see Figure 2-11).
- The air evacuation pipe and watering pipes are connected to relevant systems and the function is checked.
- The watering and air evacuations start. The estimated longest time for this and the previous step is two shifts.
- When the drift is filled (water comes from air evacuation pipe) the pipes are removed through cuffs and necessary supporting measures are taken (e.g. shutting of valves etc).
- When the drift is plugged and sealed and all system parts are removed, the deposition compartment operation is completed.

As long as no hydraulic gradient exists along the drift, there will be no possibility of piping and erosion. In drift sections intersected by sufficiently transmissive fractures, the injected water taken up by the buffer inside the supercontainers will be replaced by inflow from the rock, and a hydraulic pressure close to the hydrostatic pressure will be maintained within the gaps around the supercontainers. Saturation and buffer swelling will then proceed as in the case of the current reference design in less tight drift sections. In tighter drift sections, however, the artificially injected water taken up by the buffer may not be replaced at an equal rate by inflow from the rock, and, in such cases, the hydraulic pressure in the gaps will fall. Because of the size of the gap between the distance blocks and the rock surface in the DAWE design variant, it is uncertain whether a swelling pressure will be exerted on the drift wall before all the injected water is taken up by the buffer. Furthermore, even if a swelling pressure is developed, this may decrease as water infiltrates into the buffer at a rate faster than water is supplied from the host rock. This behaviour is suggested by preliminary unpublished results from a small-scale laboratory test carried out in support of the Large Scale Gas Injection Test (LASGIT) project at the Äspö Hard Rock Laboratory. The test showed that bentonite swelled initially, but after some time the swelling pressure decreased and, when the test cell was opened, the bentonite had desiccated and

shrinkage cracking was observed. Although the test was performed on small-scale samples with no heating, and although the observed cracking may have been affected by the stress release caused by opening the test chamber, the observation of cracking suggests that the process may also be of concern at a larger, repository scale, and requires investigation.

As the buffer takes up water, some air in the buffer pore spaces may be displaced, opening up gaps at the distance block/rock interface and accumulating at the top of the gaps around the supercontainers. The potential for transient water flows between wet and tight drift sections sufficient to cause significant buffer erosion, or for hydraulic and swelling pressure differences to cause significant mechanical displacement of supercontainers and distance blocks, will, however, remain low for the reasons discussed in the context of the current reference design in Sections 5.5.3 and 5.5.4. Saturation and buffer swelling will thus proceed as in the current reference design in the tighter and tightest drift sections.

#### **A.4 Rock spalling**

The LASGIT results also indicate that, in spite of the observed desiccation and shrinkage cracking, the buffer will continue to exert a swelling pressure on the drift wall. It is currently uncertain whether or not this is sufficiently large to prevent thermally-induced rock spalling (as noted in Section 5.4.5, pressures as low as around 150 to 200 kPa may be sufficient to suppress spalling). If spalling were to occur in a repository based on the DAWE design, it could conceivably affect several successive supercontainer and distance block sections, creating flow and transport pathways along the drift. In the current reference design, it is likely to affect only the supercontainer sections, because of the small gap between the distance blocks and the drift wall in the “tight” distance block components, which would readily be filled by humidity-induced buffer swelling, so that continuous pathways along the drift are not expected.

#### **A.5 The final saturated state**

The final saturated state of the buffer should, in most respects, be identical for the current reference design and for DAWE. Since, however, DAWE is designed to reduce the possible adverse effects of emplacing supercontainers and distance blocks in drift sections intersected by transmissive fractures that, in the current reference design, must be avoided by compartmentalising the drift, the final saturated state may differ in that there may be more compartments separated by plugged drift sections in the case of the current reference design compared with DAWE. Furthermore, as noted in Section A.4, the extent of drift sections affected by thermally-induced rock spalling may also differ between the two designs.

### **References for Appendix A**

**Autio J, Börgesson L, Sandén T, Rönnqvist P-E, Johansson E, Hagros A, Eriksson M, Berghäll J, Kotola R, Parkkinen I, 2007.** KBS-3H Design Description 2006. Posiva Working Report 2007-105 and SKB R-08-32. Posiva Oy, Olkiluoto, Finland and Svensk Kärnbränslehantering AB, Sweden.

### Scoping calculations

#### B.1 Types of scoping calculations and input data

This appendix describes various scoping calculations that have been carried out (i), to provide feedback from long-term safety considerations to design, and (ii), to develop a tentative quantitative understanding of certain key aspects of the evolution of a KBS-3H repository at Olkiluoto. In the first category are calculations addressing the implications for long-term safety of the:

- hydraulic properties of fractures intersecting the drift at canister and buffer emplacement locations (Section B.2);

since these calculations indicate which fractures would ideally be avoided at canister and buffer emplacement locations, because of long-term safety considerations.

In the second category are calculations addressing:

- saturation of tight drift sections adjacent to more permeable sections (Section B.3);
- processes leading to loss or redistribution of buffer mass (Section B.4);
- numbers of canisters potentially affected by a post-glacial earthquake (Section B.5);
- impact of limited availability of water on steel corrosion rates (Section B.6);
- impact of uncertainties in the generation and transport of sulphide on canister lifetime (Sections B.7 and B.8).

Many of the calculations are also presented in the Process Report /Gribi et al. 2007/.

Input parameter values, their use in the scoping calculations and their derivation or origin in this and other reports are presented in Tables B.1-1 to B.1-5. These are data extracted from Appendix A of the Process Report, along with specifically added data for these calculations given in Table B.1-4 and B.1-5. Data used in this report are based on the preliminary information available at the time of report writing (2006–2007). Input data were selected on the basis of the KBS-3H Design Description 2006 /Autio et al. 2007/, laboratory data, field data, modelling calculations, and, in some cases, expert judgment. A generic report on data, models, codes, and databases that will apply both to KBS-3V and KBS-3H will be produced at a later time. It should be noted that there are uncertainties and variabilities in some of the parameter values (e.g. the buffer block radius inside a supercontainer). These are too small to have a significant impact on the calculations, and only reference values are shown in the tables. Engineering tolerances for the drift and for the supercontainer components are also given in Appendix A of the Process Report.



**Table B.1-1. Parameters describing near-field geometry and quantities of materials.**

Parameter	Symbol	Value	Source	Usage
Number of canisters in repository	$N_c$	Approximately 3,000	/Saanio et al. 2004/	App. B.5
Drift diameter	$2r_t$	1.850 m	/Börgesson et al. 2005/	App. B.2, B.3, B.4, B.7
Distance block length	$\rho$	5.475 m	/Autio et al. 2007/ (see note 1)	App. B.3, B.4, B.5
Length of supercontainer	$l_s$	5.525 m	/Johansson et al. 2007/	App. B.3, B.4, B.5, B.6
Combined length of buffer ring blocks within a supercontainer	$l_{rb}$	4.810 m	–	App. B.3, B.6
Combined length of buffer end blocks within a supercontainer	$l_{eb}$	0.7 m	/Börgesson et al. 2005/	App. B.3, B.6
Buffer block diameter within a supercontainer	$2r_B$	1.739 m	/Autio et al. 2007/	App. B.3, B.6
External diameter of supercontainer	$2r_{s,o}$	1.765 m	/Börgesson et al. 2005/	App. B.4, B.6
Internal diameter of supercontainer	$2r_{s,i}$	1.749 m	/Börgesson et al. 2005/	App. B.4, B.6
Thickness of end plates	$t_s$	$8 \times 10^{-3}$ m	/Autio et al. 2007/	App. B.4
Degree of perforation of supercontainer walls (end plates not perforated)	$Z$	62%	/Börgesson et al. 2005, Autio et al. 2007/	App. B.4
Void volume within and around supercontainers	$V_{void}$	1.5 m <sup>3</sup>	/Autio 2007/ (see note 2)	App. B.3
Supercontainer surface area	$F_0$	~ 40 m <sup>2</sup>	/Autio et al. 2007/ (see note 3)	App. B.6
Supercontainer shell mass (incl. feet)	$M_{sc}$	1,071 kg	/Autio et al. 2007/	App. B.4
External diameter of canister	$2r_c$	1.05 m	/Raiko 2005/	App. B.2, B.4, B.5
Length of canister	$l_c$	4.8 m	/Raiko 2005/ (see note 4)	App. B.4, B.5, B.7
Thickness of copper canister shell	$d$	0.05 m	/Raiko 2005/	App. B.2, B.7
Mass of iron and steel in canister	$M_{insert}$	$13.4 \times 10^3$ kg	Table 4-2 (see note 4)	App. B.4
Canister internal void space	$V_{canvoid}$	0.95 m <sup>3</sup>	Table 4-2 (see note 4)	App. B.4
Drift separation	$s$	25 m	/Johansson et al. 2007/	App. B.4

Notes

1. The distance block is composed of a “tight” component 1 m in length and a 4.475 m long “loose component” /Autio et al. 2007/.
2. Void space inside and outside supercontainer excluding unsaturated buffer pores and spaces within and around adjacent distance blocks.
3. 35.73 m<sup>2</sup> internal + external surface area + feet; 41.52 m<sup>2</sup> internal + external surface area + hole edges.
4. Data are for BWR-type fuel and canisters (Olkiluoto 1–2).

**Table B.1-2. Parameters describing physical properties of the buffer.**

Parameter	Symbol	Value	Source	Usage
Initial water content of buffer ring blocks within a supercontainer	$w_{rb}$	10% by weight	/Börgesson et al. 2005/	App. B.3, B.6
Initial dry density of buffer ring blocks within a supercontainer	$\rho_{rb}$	1,885 kg m <sup>-3</sup>	/Autio et al. 2007/	App. B.3, B.6
Initial water content of end blocks within a supercontainer	$w_{eb}$	10% by weight	/Autio et al. 2007/	App. B.3, B.6
Initial dry density of buffer end blocks within a supercontainer	$\rho_{eb}$	1,753 kg m <sup>-3</sup>	/Autio et al. 2007/	App. B.3, B.6
Saturated buffer porosity	$\varepsilon$	0.44	/Autio et al. 2007/	App. B.3
Effective diffusion coefficient of anions in the saturated buffer	$D_e$	10 <sup>-11</sup> m <sup>2</sup> s <sup>-1</sup>	SR-Can (Table A-11 of /SKB 2006b/)	App. B.2, B.7
Coefficient used to model buffer saturation	$D$	10 <sup>-9</sup> to 3 × 10 <sup>-10</sup> m <sup>2</sup> s <sup>-1</sup>	See discussion in App. B.3	App. B.3
Hydraulic conductivity of saturated buffer	$K_B$	10 <sup>-13</sup> to 10 <sup>-14</sup> m s <sup>-1</sup>	SR-Can (Figure 4-8 of /SKB 2006a/; see note 1)	App. B.3
Density of saturated buffer	$\rho_o$	2,000 kg m <sup>-3</sup>	/Autio et al. 2007/	App. B.4
Bentonite mineral density	$\rho_s$	2,750 kg m <sup>-3</sup>	Section 4.2.8 in /SKB 2006a/	App. B.3, B.6

**Notes**

1. Figure gives hydraulic conductivity as a function of dry density. A saturated density of 2,000 kg m<sup>-3</sup> corresponds to a dry density of about 1,570 kg m<sup>-3</sup> (Section 4.2.8 in /SKB 2006a/).

**Table B.1-3. Parameters describing physical properties of the host rock.**

Parameter	Symbol	Value	Source	Usage
Max. hydraulic conductivity of EDZ	$K_{EDZ}$	$3 \times 10^{-12} \text{ m s}^{-1}$	See note 1, below	App. B.3
Max. pressure differences along drift, or between the drift and the undisturbed rock, during saturation	$\Delta P$	$4 \times 10^6 \text{ Pa}$	/Lanyon and Marschall 2006/	App. B.2, B.3
EDZ thickness	$t_{EDZ}$	$2.3 \times 10^{-2} \text{ m}$	App. D of /Johnson et al. 2005/; see note 2, below	App. B.3
Hydraulic length (from drift to nearest major fracture zone)	$l_h$	50	/Lanyon and Marschall 2006/, see note 3	App. B.2
Undisturbed hydraulic gradient	$i_o$	0.01	/Löfman 1999/	App. B.2
Max. radius of fractures that are assumed to escape detection	$r_{max}$	500 m	/Hedin 2005/	App. B.5
Critical shear displacement at canister position	$d_{crit}$	0.1 m	Section 7.4.5	App. B.5
Constant in fracture radius/displacement relationship (Eq. B.5-3)	$b$	0.001	/Hedin 2005/	App. B.5

## Notes

1. /Johnson et al. 2005/, Appendix C, gives the average intrinsic permeability of the EDZ as  $3 \times 10^{-19} \text{ m}^2$ . The permeability was measured in a full-scale experiment at the Olkiluoto Research Tunnel under fully gas-saturated conditions. Taking this value as an upper bound for the transport of water in the EDZ, the maximal hydraulic conductivity of the EDZ is  $3 \times 10^{-12} \text{ m s}^{-1}$ . EDZ properties at repository depth are, however, highly uncertain at present.
2. Combined thickness of crushed zone (0–4 mm from wall), microfractured zone (4–9 mm) and zone of minor damage (9–23 mm).
3. Assumed distance to constant head hydrostatic boundary in discrete fracture network modelling.

**Table B.1-4. Fracture network data used in Appendix B.5 (orientation and size distribution parameters from /Poteri 2001/; fracture intensity adjusted to account only for open fractures, following /La Pointe and Hermanson 2002/).**

Set	Orientation parameters		Size distribution parameters		Intensity
	Mean pole plunge $\theta_p$ (in degrees)	Dispersion $\kappa$	Exponent $k$	Min. radius $r_o$	$P_{32}$
Horizontal	70	6.9	2.50	0.53 m	0.0480 $\text{m}^{-1}$
N-NW	2	16	2.72	0.59 m	0.0109 $\text{m}^{-1}$
E-NE	17	2	2.66	0.58 m	0.0262 $\text{m}^{-1}$

**Table B.1-5. Further miscellaneous parameters used in scoping calculations.**

Parameter	Symbol	Value	Source	Usage
Gravitational acceleration	$g$	9.81 m s <sup>-2</sup>	–	App. B.2, B.3
Density of water	$\rho_w$	1,000 kg m <sup>-3</sup>	–	App. B.2, B.3, B.6
Viscosity of water	$\mu$	10 <sup>-3</sup> Pa s	–	App. B.2
Diffusion coefficients of ions in free water	$D_w$	2 × 10 <sup>-9</sup> m <sup>2</sup> s <sup>-1</sup>	–	App. B.2, B.7
Diffusion coefficient for eroded bentonite particles in water	$D_b$	2 × 10 <sup>-9</sup> m <sup>2</sup> s <sup>-1</sup>	Conservatively set equal to $D_w$	App. B.2
Effective vapour diffusion constant in partly desaturated rock matrix	$D_v$	2.6 × 10 <sup>-10</sup> m <sup>2</sup> s <sup>-1</sup>	For partly saturated rock, see note 1, below	App. B.6
		10 <sup>-9</sup> m <sup>2</sup> s <sup>-1</sup>	For unsaturated buffer	
Density of copper	$\rho_c$	8,900 kg m <sup>-3</sup>	–	App. B.2, B.7
Density of iron/steel	$\rho_{Fe}$	7,800 kg m <sup>-3</sup>	–	App. B.4, B.6
Molar weight of copper	$N_c$	64 g mol <sup>-1</sup>	–	App. B.2, B.7
Molar weight of sulphide (bisulphide anions)	$N_s$	33 g mol <sup>-1</sup>	–	App. B.2, B.7
Molar weight of water	$N_w$	18 g mol <sup>-1</sup>	–	App. B.6
Molar weight of iron	$N_{Fe}$	56 g mol <sup>-1</sup>	–	App. B.6, B.7
Constant in the aperture/transmissivity relationship (Eq. B.2-2)	$c$	2 s <sup>-1/2</sup>	/Lanyon and Marschall 2006/	App. B.2
Maximum bentonite mass assumed to be carried as particles by flowing water	$C_{max}$	50 kg m <sup>-3</sup>	/SKB 2006a/; see also note 2, below	App. B.2, B.4
Factor for uneven corrosion of copper (Eq. B.2-6)	$C_{local}$	50	See note 3, below	App. B.2, B.7
Steel corrosion rate	$R$	10 <sup>-6</sup> m a <sup>-1</sup>	/Smart et al. 2004/	App. B.6
Universal gas constant	$R_0$	8.3145 J K <sup>-1</sup> mol <sup>-1</sup>	–	App. B.6

**Notes**

1. For fully gas saturated conditions, see /Johnson et al. 2005/, p. 149.
2. This corresponds to a total suspended solids ratio (weight ratio bentonite/suspension) of 5%. Weight ratios have been measured experimentally for MX-80 bentonite and found to be in the range 0.1–1% (see Section 4.5.2, /Börgesson et al. 2005/). 5% is thus a pessimistic value, outside the measured range.
3. A lower value of 5 was used in earlier studies in Finland (p. 94 of /Vieno et al. 1992/). A higher and more conservative value is, however, consistent with current understanding, as described, for example, in SR-Can, where a factor of about 35 is used.

## B.2 Hydraulic properties of fractures intersecting a drift at canister and buffer emplacement locations

### Introduction

In determining where along a deposition drift canisters and buffer can be emplaced, a key consideration is the avoidance of significant buffer loss or redistribution by piping and erosion phenomena during saturation. The potential for transient water flows to cause piping and erosion is described in Section 5.5.6. There, it is noted that laboratory and modelling studies indicate that, for the current reference design, piping will not occur provided the inflow rate to a supercontainer drift section comprising a supercontainer plus a distance block during saturation is 0.1 litres per minute or less, and provided there is no significant deformation and displacement of the distance blocks relative to the supercontainers (this is an issue addressed on ongoing design developments).

There are, however, considerations related to the evolution of the repository subsequent to saturation that also have a bearing on the suitability of particular drift sections as emplacement locations. In particular, it is at least desirable that any flow through the intersecting fractures be such that:

- there is no significant long-term erosion of the buffer by flowing water that could affect its barrier function;
- the rate at which species with the potential to corrode the copper shell of the canister can migrate from the rock via the buffer to the canister surface does not lead to an unacceptable rate of loss of copper coverage, and hence early canister failure by corrosion; and
- the rock provides an effective barrier to the transport of released radionuclides in the event of canister failure.

It is also clearly desirable that canister positions are not intersected by fractures capable of undergoing potentially damaging slip as a result of large earthquakes. The buffer is expected to protect the canisters from shear displacements smaller than 0.1 m. The issue of potential larger shear movements caused by large, post-glacial earthquakes is discussed in Section 7.4.5.

The rate of groundwater inflow to the drift during saturation is related to the transmissivity and frequency of fractures intersecting the drift. Hence, it is also related to the long-term flow subsequent to saturation (the relationship is, however, complicated by a number of factors mentioned in Section 2.2.7 and also below). The purpose of the scoping calculations presented below is to discuss how design requirements related to the saturation period and, in particular, the requirement that inflow is 0.1 litres per minute or less, compare to desirable properties related to the post-closure evolution and performance of the repository.

The calculations assume that the system is implemented as planned. Perturbing features and processes, such as the presence of initial defects in the canisters, poor emplacement of the buffer and the possibility of processes that could disturb the buffer/rock interface (rock spalling and iron/bentonite interaction, cement-bentonite interaction) are assumed to be of negligible importance or avoided by design. Such features and processes are, however, taken into account in the overall description of system evolution in the main part of this report. The specific issue of the impact of disturbances to the buffer/rock interface on canister lifetime is also addressed in the scoping calculations presented in Appendices B.8 and B.9.

## Hydrodynamic relationships and assumptions

### Inflow and transmissivity

Assuming that saturation in a drift section occurs principally due to radial inflow from the rock (rather than water migration parallel to the drift), a relationship between fracture transmissivity and the rate at which a drift section saturates with water in the early phase of evolution may be obtained from Darcy's law in a radial configuration (Thiem's equation). Assuming that  $n$  fractures intersect the section:

$$Q = 2\pi \frac{\Delta P}{\rho_w g \ln(l_h / r_i)} \sum_{i=1}^n T_i \quad (\text{Eq. B.2-1})$$

with:

$Q$  inflow from the  $n$  intersecting fractures [ $\text{m}^3 \text{s}^{-1}$ ]

$T_i$  fracture transmissivity [ $\text{m}^2 \text{s}^{-1}$ ]

$\Delta P$  magnitude of the maximum hydraulic pressure difference between the drift and the undisturbed rock during saturation [Pa] (Table B.1-3)

$l_h$  hydraulic length (from drift to nearest major fracture zone) [m] (assumed to be 50 m, Table B.1-3)

$r_i$  drift radius [m] (Table B.1-1).



According to this equation, a single fracture with a transmissivity  $3 \times 10^{-9} \text{ m}^2 \text{ s}^{-1}$  will deliver an initial inflow of about 0.1 litres per minute, which is currently taken to be the maximum allowable value if the possibility of piping and erosion is to be avoided.

As noted in Section 2.2.7, there are other factors that may affect the initial inflow from transmissive fractures such that fractures with transmissivities above  $3 \times 10^{-9} \text{ m}^2 \text{ s}^{-1}$  could potentially give initial inflows of less than 0.1 litres per minute. Firstly, it may be possible to reduce the initial inflow through some larger aperture fractures by injecting grout, such that significant piping and erosion do not occur during the operational period and subsequent buffer saturation, but this grout is likely to become degraded and ineffective in reducing flow in the longer term (in view of current uncertainties in the performance of any grout, an inflow of less than 0.1 litres per minute prior to grouting is used as a criterion for a drift section to be suitable for the emplacement of canisters and buffer in deriving a preliminary repository layout). Furthermore, initial inflows may also be reduced by drawdown of the water table, which will give a reduction in the hydrostatic pressure at repository depth, by the impact of other open repository tunnels and drifts, and potentially by mineral precipitation and degassing in the fracture. These are generally transient effects which do not affect flow in the longer term, once the drifts are saturated. Finally, inflow is determined not only by the hydraulic properties of fractures intersecting the drift, but also by those of other connected fractures in the wider fracture network.

The impact of fracture network effects on the initial rate of inflow to a drift at canister and buffer emplacement locations is illustrated by the results of the discrete fracture network (DFN) modelling of /Lanyon and Marschall 2006/. Lanyon and Marschall constructed a series of model variants in which one or more KBS-3H drifts were positioned within a network of deterministically positioned major fracture zones and stochastically generated local fracture zones and discrete water-conducting fractures in the background rock, each with a distribution of transmissivities based on field measurements at Olkiluoto. Based on the above consideration of Thiem's equation, fractures intersecting the drift with transmissivities above about  $3 \times 10^{-9} \text{ m}^2 \text{ s}^{-1}$  were considered unsuitable as supercontainer and distance block emplacement locations, but were rather assumed to be sealed using filling blocks or compartment seals. Flow simulations were carried out in order to evaluate, among other issues, the time to fill the supercontainer gap volumes (assumed to be  $1.38 \text{ m}^3$ ). From these times, the inflow rates<sup>36</sup> to drift sections containing supercontainers, which are intersected by one or more fractures with transmissivities of  $3 \times 10^{-9} \text{ m}^2 \text{ s}^{-1}$  or less can be evaluated (Table B.2-1).

In none of the simulations did the inflow rate to the gap around a supercontainer exceed about 0.05 litres per minute, implying a 0.1 litre per minute maximum inflow rate to a drift section containing a supercontainer plus distance block. In most cases, inflow was significantly less than this. This indicates that the initial inflow criterion of 0.1 litres per minute might be satisfied if it were possible to exclude fractures with transmissivities above  $3 \times 10^{-9} \text{ m}^2 \text{ s}^{-1}$  at supercontainer and distance block locations. It does not, however, necessarily show that avoiding locations with inflows greater than 0.1 litres per minute will ensure that there are no intersecting fractures with transmissivities greater than  $3 \times 10^{-9} \text{ m}^2 \text{ s}^{-1}$ . In practice, characterisation of fractures intersecting the drift is likely to be based largely on observations made at the drift wall, including inflow. It must further be kept in mind that the impact of repository excavation on the hydrostatic pressure around the drift, and hence on inflow, was not been considered in the model used to generate Table B.2-1. Nor have the possibilities of mineral precipitation and degassing reducing initial inflow been considered. All these issues require further investigation. Thus, the possibility that, in reality, some higher transmissivity fractures are present must be acknowledged.

---

<sup>36</sup> The inflow rate will, in reality, decrease with time as the gap is filled and the pressures of the fluids (water and air) inside the gap increase. The storage model used in the calculations was, however, set up in such a way that this decrease was small (high compressibility while the gap volumes are being filled).

**Table B.2-1. Inflow rates to the gap around a supercontainer calculated for four single drift models (derived from Table 5-6 in /Lanyon and Marschall 2006/).**

Drift	Number of supercontainers	Number intersected by features in model	Inflow rate [litres per minute]		
			Max.	Av.	Min.
W01T01	23	6	0.048	0.015	0.009
W01T12	25	9	0.019	0.006	0.003
W01T22	19	5	0.025	0.011	0.005
W01T23	17	4	0.022	0.017	0.007

In the following sections and in the majority of radionuclide transport calculations in the safety assessment /Smith et al. 2007/, the flow around a deposition drift is calculated based on the assumption that the drift section containing the canister under consideration is intersected by a fracture with a transmissivity of  $3 \times 10^{-9} \text{ m}^2 \text{ s}^{-1}$ . This is viewed as a moderately pessimistic assumption, but is not necessarily the “worst case”. Intersection of the drift by a higher transmissivity fracture at the location of a failed canister is, however, considered in some variant cases in radionuclide transport calculations.

### Transmissivity and aperture

Fracture transmissivity and aperture are clearly related, although the form of the relationship depends on the geometry of the fracture (the presence of constrictions, etc). For the purposes of this appendix and in the radionuclide transport calculations in the safety assessment /Smith et al. 2007/, following /Lanyon and Marschall 2006/, it is assumed that the fracture half-aperture  $b_v$  [m] is related to transmissivity via the equation:

$$b_v = \frac{\sqrt{T}}{2c} \quad (\text{Eq. B.2-2})$$

where  $c[\text{s}^{-1/2}]$  is a constant (Table B.1-5).

### Flow around a deposition drift

In the following sections, it is assumed that a fracture (transmissivity  $3 \times 10^{-9} \text{ m}^2 \text{ s}^{-1}$ ) intersects the drift at a canister location with the fracture plane perpendicular to the drift and aligned with the regional hydraulic gradient of 0.01 (Table B.1-3). In reality, more than one fracture may intersect a drift section, which will tend to increase overall flow, whereas flow will tend to be reduced by the dip of the fractures with respect to the regional gradient. Furthermore, fractures that will intersect the drift at a range of angles and other connected fractures will have a perturbing effect on the flow. These effects are again illustrated in the DFN modelling of /Lanyon and Marschall 2006/, where DFN models variants with different cut-off transmissivities are used to evaluate the flow into and out of a cylindrical volume of rock around a drift element containing a supercontainer, with its outer surface 0.5 m from the drift wall (1.425 m from the drift centre line). Values obtained by Lanyon and Marshall vary significantly between drift sections, but are never more than  $4 \times 10^{-11} \text{ m}^3 \text{ s}^{-1}$  (Table B.2-2). A single  $3 \times 10^{-9} \text{ m}^2 \text{ s}^{-1}$  fracture aligned with the regional gradient and with the fracture plane perpendicular to the drift axis would give rise to a similar flow of  $\sim 4 \times 10^{-11} \text{ m}^3 \text{ s}^{-1}$  into and out of this cylindrical volume ( $3 \times 10^{-9} \text{ m}^2 \text{ s}^{-1} \times 0.01 \times 2 \times 0.66 \text{ m}$ )<sup>37</sup>. It is therefore concluded that basing the flow around a deposition drift on a

<sup>37</sup> The solution of Darcy’s Law for flow around an impermeable circular drift shows that the fluid velocity in a fracture along a line passing through the drift centre and normal to the flow direction is  $v = V(1+r_t^2/r^2)$  for  $r > r_t$ , where  $r$  is distance from the drift centre,  $r_t$  is drift radius and  $V$  is the undisturbed water velocity at large distances from the drift. By integrating  $v$  with respect to  $r$  between  $r = r_t$  and  $r = r_t + 0.5 \text{ m}$ , it can be shown that, because of distortion of the flow by the drift, the flow passing through the cylindrical volume is equivalent to the flow passing through a fracture of width  $2 \times 0.66 \text{ m}$  in the undisturbed rock.

**Table B.2-2. Flows across supercontainers calculated from steady state DFN flow models for two model drifts (after Table B-1 in /Lanyon and Marschall 2006/).**

Drift	Model transmissivity cut-off [m <sup>2</sup> s <sup>-1</sup> ]	Supercontainers not intersected	Flow [× 10 <sup>-11</sup> m <sup>3</sup> s <sup>-1</sup> ]	
			Max.	Av.
W01T01	10 <sup>-10</sup>	15	4	1.5
W01T01	10 <sup>-11</sup>	1	4	0.6
W01T02	10 <sup>-10</sup>	14	5	0.2

single fracture with the properties described above represents a reasonable assumption in safety assessment.

### Buffer erosion

The swelling pressure of the buffer of a KBS-3H repository following saturation may be sufficient to cause bentonite to be extruded into open fractures intersecting the drift. The advancing clay front will be composed of a soft clay gel, which may potentially be eroded by flowing groundwater. There are two broad ways in which this might happen:

- mechanical erosion, in which the viscous force exerted by the flowing water on the particles of the clay gel exceeds the average particle bond strength; and
- chemical erosion, in which the concentration of cations in solution at the gel/water interface falls below the value required to maintain the stability of the gel (e.g. as a result of the penetration of dilute waters to repository depth in association with glaciation).

Either of these mechanisms may in principle cause the gel to break up and disperse in the form of colloids. They are discussed in turn below.

### Mechanical erosion

The shear stress (traction) exerted by a laminar flow through a fracture on the buffer,  $\tau$  [Pa], is given by Newton's law of viscosity:

$$\tau = \mu \frac{dv}{dy} \quad (\text{Eq. B.2-3})$$

where  $v$  [m s<sup>-1</sup>] is the groundwater velocity in the fracture, averaged across its aperture,  $y$  [m] is normal distance from the buffer/rock interface and  $\mu$  [Pa.s] is the viscosity of water (about 10<sup>-3</sup> Pa.s). The influence of the interface on the water velocity in the fracture extends to a distance of a few fracture apertures from the interface /Liu and Neretnieks 2006/. The velocity gradient perpendicular to the buffer/rock interface is therefore of the order:

$$\frac{dv}{dy} \cong \frac{v}{b_v} \quad (\text{Eq. B.2-4})$$

Considering a single fracture intersecting the deposition drift, and neglecting the distortion in the streamlines caused by the cylindrical shapes of the buffer, the groundwater velocity in the fracture away from the influence of the interface is given by:

$$v = \frac{T \cdot i_0}{2b_v} \quad (\text{Eq. B.2-5})$$

where  $i_0$  is hydraulic gradient (0.01 – Table B.1-3).

From Eq. B.2-3 to B.2-5:

$$\tau \cong \frac{\mu T i_0}{2b_v^2} \quad (\text{Eq. B.2-6})$$

If a fracture intersecting the drift at supercontainer and distance block emplacement locations is assumed to have a transmissivity of  $3 \times 10^{-9} \text{ m}^2 \text{ s}^{-1}$ , then, according to Eq. B.2-2, the fracture half-aperture is in the order of  $10^{-5} \text{ m}$ . For a hydraulic gradient of 0.01, Eq. B.2-6 gives a shear stress in the order of  $10^{-4} \text{ Pa}$ . In practice, the fracture aperture is likely to vary locally around the buffer/rock interface, giving some corresponding variability in the shear stress, which may be higher or lower than the  $10^{-4} \text{ Pa}$  indicated above. However, while a locally smaller aperture will, according to Eq. B.2-6, give rise to a higher shear stress, this does not take account of the mitigating effect of channelling – i.e. flow will tend to be channelled around any local constrictions, offsetting to some extent the effect of the smaller aperture on shear stress.

The typical Bingham yield stress of the gel front is strongly dependent on the composition of the clay and ionic strength of the water, but a review of experimentally determined values by /Liu and Neretnieks 2006/ indicates that 1.0 Pa may be taken as a conservative estimate of the minimum shear stress required for mechanical erosion. The expected shear maximum stress is around four orders of magnitude smaller than this once the influence of transient pressure gradients associated with repository saturation has passed, which implies that no mechanical erosion will occur once the repository is saturated, in spite of the uncertainties noted above associated with the variability of aperture, the effects of channelling and the possibility that fractures with transmissivities greater than  $3 \times 10^{-9} \text{ m}^2 \text{ s}^{-1}$  will intersect the drift at canister and buffer emplacement locations. Some limited erosion associated with piping during the saturation phase cannot, however, currently be excluded.

### **Chemical erosion**

The next glacial retreat, and hence the next possibility for penetration of glacial meltwater to repository depth, is assumed to be in 70,000 years time, according to the Weichselian-R climate scenario. Penetration of glacial meltwater to repository depth could lead to some chemical erosion of the buffer (Section 7.4.7).

Significant erosion is here defined as that required for advective conditions to occur within the buffer. /Börgesson and Hernelind 2006a/ have calculated the buffer swelling pressure for cases where, in KBS-3V, one, two and three entire bentonite rings surrounding the canister have been omitted, to illustrate the effects of a local loss of large amounts of bentonite. The conclusion was that a mass loss of 1,200 kg to a fracture intersecting the deposition hole would lead to conditions where advective conditions in the buffer must be considered. Due to the similarity between the deposition hole diameter in KBS-3V (1.75 m) and the deposition drift diameter of in KBS-3H (1.85 m), this conclusion can be taken to apply to both alternatives. It should be noted that, for KBS-3H, the loss of buffer around one canister due to exposure to glacial meltwater may affect the corrosion rate of neighbouring canisters, since the buffer density along the drift will tend to homogenise over time. This also means, however, that the impact on buffer density and on the corrosion rate of the first canister will diminish with time. This is in contrast to the case of KBS-3V, where buffer loss around one canister will not affect the state of the buffer around the other canisters.

A model of chemical erosion has been developed by SKB for SR-Can. If the model is applied to a KBS-3H repository at Olkiluoto, the results indicate that significant erosion could occur in a single glacial cycle if fractures intersecting the buffer have transmissivities in excess of about  $3 \times 10^{-8} \text{ m}^2 \text{ s}^{-1}$ . The SKB model is, however, tentative (a new model is currently under development by SKB/KTH) and model uncertainties are probably too great to draw any firm conclusions regarding those fractures that should be avoided in emplacing supercontainers and distance blocks.

### Canister corrosion

A model for the time required for canister failure by corrosion to occur for a given set of flow conditions around the drift and a given groundwater sulphide concentration is given in Appendices B.8 and B.9. Assuming that no processes occur that lead to detrimental perturbations to the buffer or buffer/rock interface, canister lifetime ( $t_a$  [s]) is given by:

$$t_a = \frac{d}{c_{local} j_a} \quad (\text{Eq. B.2-7})$$

with:

$d$  thickness of the copper canister shell [m] (Table B.1-1)

$c_{local}$  factor for uneven corrosion of copper [-] (Table B.1-5)

$j_a$  copper corrosion rate [m s<sup>-1</sup>].

Noting that 2 moles of copper are corroded per mole of sulphide arriving at the canister surface, the maximum rate of uniform copper corrosion is given by:

$$j_a = \frac{2f_{max}}{\rho_c} \frac{N_c}{N_s} \quad (\text{Eq. B.2-8})$$

with:

$\rho_c$  density of copper [kg m<sup>-3</sup>] (Table B.1-5)

$N_c$  molar weight of copper [g mol<sup>-1</sup>] (Table B.1-5)

$N_s$  molar weight of sulphide [g mol<sup>-1</sup>] (Table B.1-5)

$f_{max}$  rate of arrival of sulphide at the canister surface at the location where this is the highest (directly opposite the fracture/drift line of intersection) [mol s<sup>-1</sup>].

$f_{max}$  is given by:

$$f_{max} = \frac{\pi D_e C_s}{2(r_t - r_c)} \frac{1}{\log_e \left( \frac{2(r_t - r_c)}{b_v} \right)} \frac{Q_b}{Q_b + Q_f} \quad (\text{Eq. B.2-9})$$

with:

$D_e$  effective diffusion coefficient of anions in the saturated buffer [m<sup>2</sup> s<sup>-1</sup>] (Table B.1-2)

$r_t$  drift radius [m] (Table B.1-1)

$r_c$  canister radius [m] (Table B.1-1)

$b_v$  fracture half aperture (from Eq. B.2-2)

$C_s$  concentration of sulphide in groundwater approaching the drift [kg m<sup>-3</sup>] (see below).

$Q_b$  [m<sup>3</sup> s<sup>-1</sup>] and  $Q_f$  [m<sup>3</sup> s<sup>-1</sup>] are transfer coefficients given by:

$$Q_b = \frac{A_{frac}}{\pi} \sqrt{\frac{2D_w T \cdot i_0}{r_t b_v}} \quad (\text{Eq. B.2-10})$$

and

$$Q_f \approx \frac{\pi D_e A_{frac}}{2b_v \log_e \left( \frac{2(r_t - r_c)}{b_v} \right)} \quad (\text{Eq. B.2-11})$$



$D_w$  [ $\text{m}^2 \text{s}^{-1}$ ] is the diffusion coefficient of ions in free water (Table B.1-5) and  $A_{frac}$  [ $\text{m}^2$ ], the area of intersection of the fracture with the drift, is given by:

$$A_{frac} = 4\pi b_v r_t \quad (\text{Eq. B.2-12})$$

In deriving Eq. B.2-9, it is assumed that the buffer has uniform transport properties from the canister surface to the drift wall. In reality, there are a number of features and processes that could perturb mass transfer in the buffer and at the buffer/rock interface (see Table 11-1). The impacts of such features and processes are considered in Appendix B.7.

Figure B.2-1 shows the calculated canister lifetime as a function of the transmissivity of a fracture assumed to intersect the drift adjacent to a canister position, for different values of groundwater sulphide concentration:

- 12 mg  $\text{l}^{-1}$  (the highest currently observed value);
- 42.5 mg  $\text{l}^{-1}$  (the maximum value calculated for future times – see /Pastina and Hellä 2006/).

The results show that the canister lifetime exceeds the minimum design lifetime of  $10^5$  years by one to two orders of magnitude in the case of a transmissivity of  $3 \times 10^{-9} \text{m}^2 \text{s}^{-1}$ . It continues to exceed the minimum, though by a reduced margin, as fracture transmissivity is increased. This is because, even at high transmissivities, the barrier to sulphide transport provided by the buffer severely limits the rate at which sulphide can reach the canister surface. Consideration must, however, be given to the possibility of chemical erosion of the buffer at high transmissivities, as discussed in Section Buffer erosion (this and the impact of other possible perturbations to the buffer and the buffer/rock interface are discussed in Appendix B.7).

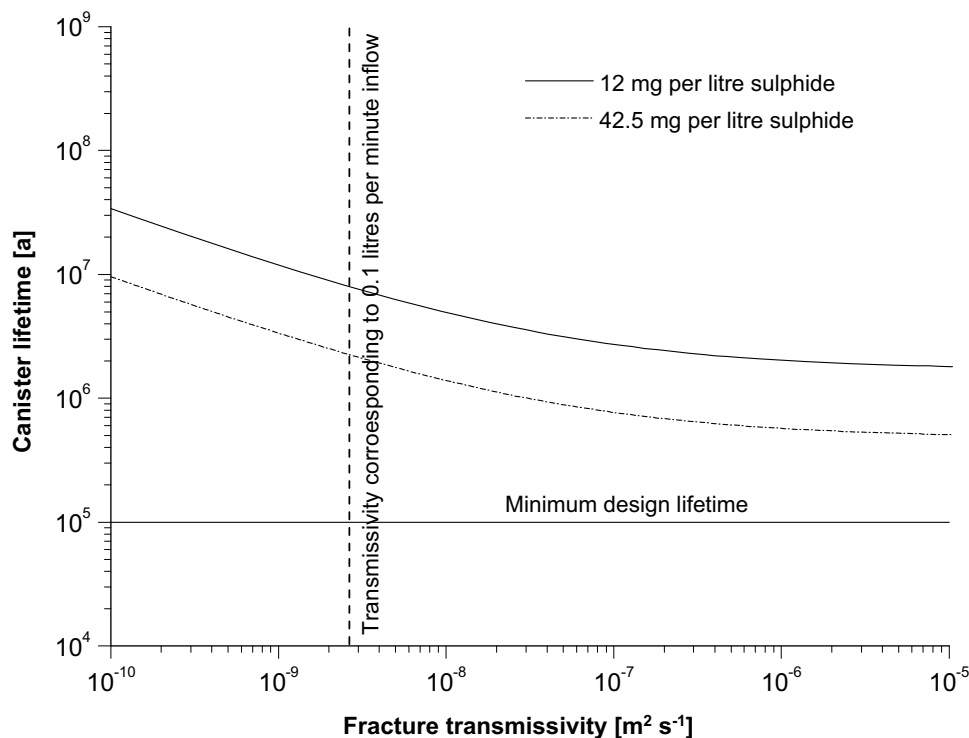


**Figure B.2-1.** Canister lifetime as a function of fracture transmissivity for two different groundwater sulphide concentrations

## Geosphere transport barrier

In terms of the hydrogeological properties of the rock, the effectiveness of the geosphere and a transport barrier to radionuclides released in the event of canister failure is a function of the “transport resistance”, defined as  $WL/Q$ , where  $W$  [m] is the width of a representative transport path within the fracture network,  $L$  [m] is the transport distance along this path and  $Q$  [ $\text{m}^3 \text{a}^{-1}$ ] is the flow through the path. Experience from past Posiva safety assessments is that a value of  $WL/Q$  of a few thousands or more years per metre provides an effective barrier to the transport of many safety relevant radionuclides (the median value for all sites given in TILA-99 is  $5 \times 10^4$  years  $\text{m}^{-1}$  – see Section 11.6 in /Vieno and Nordman 1999/).

The transport resistance of a single fracture may also be expressed in terms of transmissivity:

$$\frac{WL}{Q} = \frac{L}{Ti_0} \quad (\text{Eq. B.2-13})$$

In a heterogeneous geosphere, the transport resistance is additive along different sections of the overall transport path. It is, however, likely that, where the migrating radionuclides encounter higher-transmissivity features, low transmissivity fractures between the near-field/geosphere interface and some point within the geosphere, perhaps a few tens of metres away, dominate the transport resistance.

Figure B.2-2 shows transport resistance plotted against transmissivity for transport path lengths of 10 m, 50 m and 100 m, where transmissivity is to be understood as the transmissivity of fractures intersecting the drift near a canister emplacement position, and transport path length is the assumed distance from the drift to the most highly transmissive features along the transport path.

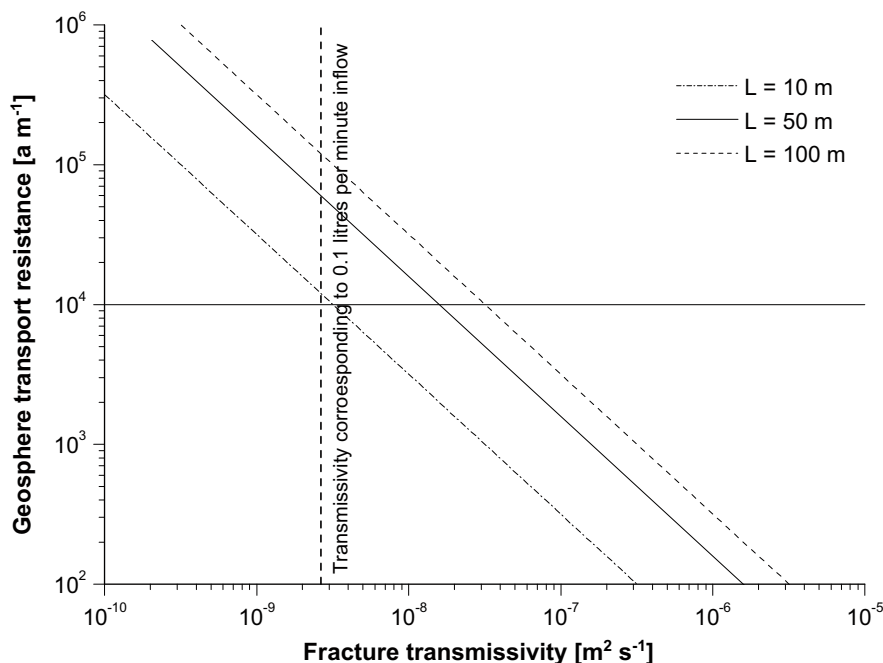


**Figure B.2-2.** Transport resistance plotted against transmissivity for different transport path lengths. The figure indicates the fracture transmissivity which is assumed to give rise to a maximum 0.1 litre per minute inflow during saturation (see, however, the caveats given in Section Hydrodynamic relationships and assumptions).

The figure shows that, for a pessimistic transport path length of 10 m to the nearest higher-transmissivity fracture, a transmissivity of about  $3 \times 10^{-9} \text{ m}^2 \text{ s}^{-1}$  provides a transport resistance of the order of 10,000 years per metre, and thus an effective geosphere transport barrier for many safety-relevant radionuclides (this is roughly equivalent to the transmissivity giving rise to a maximum 0.1 litre per minute inflow during saturation).

/Lanyon and Marschall 2006/ carried out steady state flow modelling using their discrete fracture representation of the Olkiluoto site, and evaluated transport resistances from various supercontainer deposition locations to the outer boundary of their model, 50 m from the modelled deposition drift. Histograms of the results for model drift W01T01, which were obtained using particle tracking, are shown in Figure B.2-3. Particles are released at the intersection of fracture sub-planes with the 1D supercontainer drift elements and are then tracked within the detailed pressure field from the steady-state solution. The advective travel time and the F-quotient<sup>38</sup> are calculated for each particle. The results show that none of the particle tracks gave transport resistances less than about  $5 \times 10^4 \text{ years m}^{-1}$ , the highest value being obtained for supercontainer location W01T01:CO16. The results for other modelled drifts gave still higher minimum transport resistances (see Figure B-3 parts b–d in /Lanyon and Marschall 2006/). Figure B.2-4 shows particle tracks from which the lowest transport resistance was calculated (supercontainer location W01T01:CO16, which is circled in red). In this realisation of the DFN model, supercontainer location W01T01:CO16 is separated by a distance block from a 10 m section of filling blocks intersected by a fracture with a relatively high transmissivity of about  $10^{-7} \text{ m}^2 \text{ s}^{-1}$ . Even in this location, although the smallest transport resistance is about  $5 \times 10^4 \text{ years m}^{-1}$ , the mean is about an order of magnitude higher.

This discussion suggests that an assumption of a transport resistance of  $5 \times 10^4 \text{ years m}^{-1}$  is conservative for the purposes of geosphere transport modelling, and is assumed in analysing many of the assessment cases in the Radionuclide Transport Report /Smith et al. 2007/.

## Conclusions

The scoping calculations presented above illustrate the impact of the hydraulic properties of fractures intersecting a drift, and particularly the impact of transmissivity, on various processes relevant to long-term safety.

Considering the possibility of failure by corrosion, the canister lifetime will remain well in excess of the minimum design lifetime of 100,000 years, irrespective of fracture transmissivity (the impact of perturbations to the buffer on canister lifetime is considered in Appendix B.7). Mechanical erosion of the buffer is shown to be irrelevant even at high transmissivities. In the case of chemical erosion due to the penetration of dilute glacial meltwater to repository depth, model uncertainties are probably too great to draw any firm conclusions regarding those fractures that should be avoided in emplacing supercontainers and distance blocks. It should, however, be noted that the next possibility for penetration of glacial meltwater to repository depth is in 70,000 years time and, even if advective conditions then become established in parts of the buffer, it will take time for canister failure to occur – thus the minimum design lifetime may still be achieved.

In terms of the transport barrier provided by the geosphere, a 10 m long transport path having a transmissivity of about  $3 \times 10^{-9} \text{ m}^2 \text{ s}^{-1}$  provides a transport resistance in the order of 10,000 years per metre, which corresponds to an effective geosphere transport barrier for many safety-relevant radionuclides. This is also roughly the transmissivity giving rise to a maximum

<sup>38</sup> In numerical codes where transport calculations are based on particle tracking, like e.g. ConnectFlow, F is calculated as the sum of advective travel time,  $t$ , divided by half-aperture,  $b$ , in individual transport segments along the path (in the most general sense an integral). This definition and concept used by SKB is described in /Andersson et al. 1998/ and used in /Hartley et al. 2006ab/. Regarding flow rates the F-quotient (or F-factor) for a single planar fracture can be defined as  $F=2WL/Q$  ( $= t/b$ ), where  $W(m)$  is the channel width over which  $Q$  has been determined.

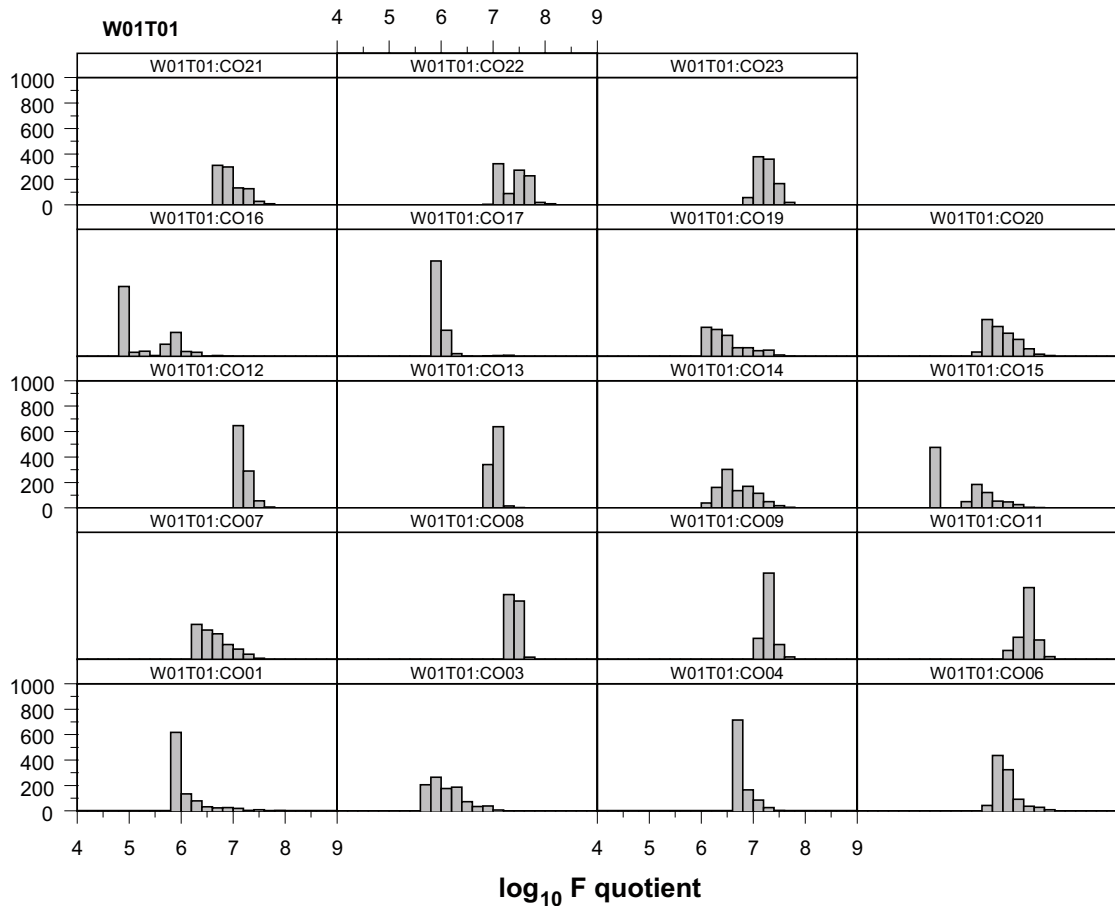


**Figure B.2-3.** Histograms of transport resistances (termed here  $F$  quotient in  $\log (am^{-1})$ ), from particles released at different supercontainer locations in a DFN model of the Olkiluoto site (after Figure B-3 of /Lanyon and Marschall 2006/).

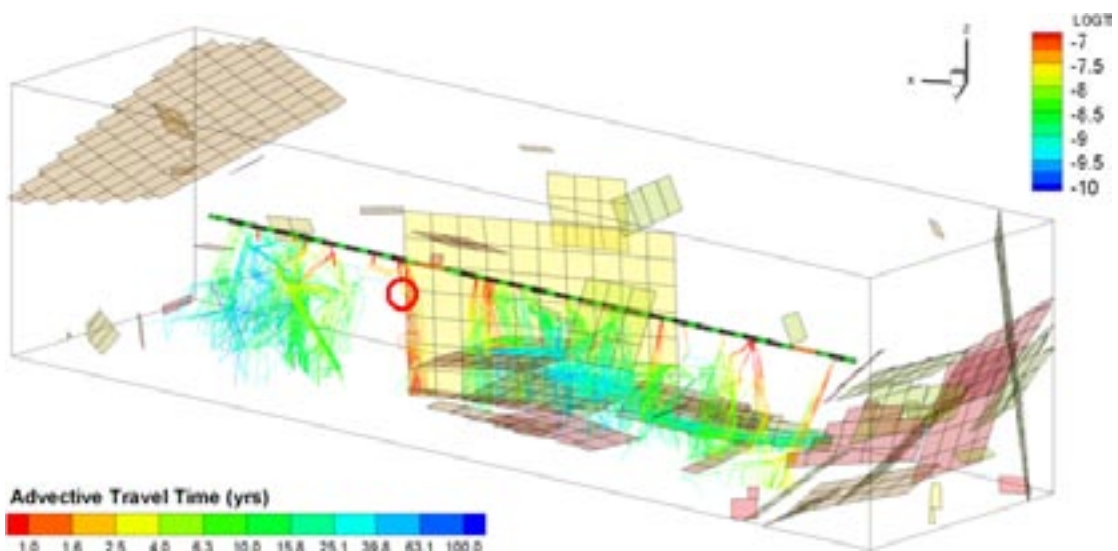


**Figure B.2-4.** Particle tracks from supercontainer drift elements. Supercontainer location  $W01T01:CO16$ , which gives the lowest calculated transport resistances, circled in red. Tracks coloured by travel time. Features coloured by log transmissivity, only features with transmissivity greater than  $10^{-8} m^2/s$  are shown (after Figure B-1 of /Lanyon and Marschall 2006/).

0.1 litre per minute inflow during saturation – i.e. the maximum inflow if the possibility of piping and erosion is to be avoided – see, however, the caveats given in Section Hydrodynamic relationships and assumptions.

Overall, it is concluded that a transmissivity limit of about  $3 \times 10^{-9} \text{ m}^2 \text{ s}^{-1}$  for fractures intersecting the drift at canister and buffer emplacement locations desirable from the point of view of long-term safety. This criterion is derived in the first place from considerations of the geosphere transport barrier, being the most restrictive of those described in this appendix. In practice, however, it is unlikely that a transmissivity criterion can be applied directly in selecting locations for canister and buffer emplacement. Characterisation of fractures intersecting the drift is likely to be based largely on observations made at the drift wall, and other quantities including inflow, that can be measured directly, rather than on transmissivities inferred from a model that are therefore subject to greater uncertainty.

### B.3 Saturation of tight drift sections adjacent to less tight sections

#### Overview

Scoping calculations have been performed to estimate the saturation time of a relatively tight drift section (a supercontainer and distance block unit section) adjacent to a less tight drift section. The relevant processes are sketched in Figure B.3-1.

The saturation time of the buffer initially inside a supercontainer is determined by the void volume to be filled with water,  $V$  [ $\text{m}^3$ ], and the inflow rate of water,  $Q$  [ $\text{m}^3 \text{ a}^{-1}$ ]:

$$T_{sat} = \frac{V}{Q} \quad (\text{Eq. B.3-1})$$

where

$$V = V_{void} + \varepsilon_B V_B (1 - S_{B,0}) \quad (\text{Eq. B.3-2})$$

with:

$V_{void}$  the void volume within and around a supercontainer (not including unsaturated buffer pores) [ $\text{m}^3$ ] (Table B.1-1)

$V_B$  the initial bulk volume of buffer inside a supercontainer [ $\text{m}^3$ ]

$\varepsilon_B$  initial buffer porosity

$S_{B,0}$  initial buffer saturation.

The evaluation of Eq. B.3-2 is complicated by the fact that the initial dry density and water content of the buffer ring blocks ( $\rho_{rb}$  [ $\text{kg m}^{-3}$ ] and  $w_{rb}$  [% by weight]) around the canister are different to those of the end blocks ( $\rho_{eb}$  [ $\text{kg m}^{-3}$ ] and  $w_{eb}$  [% by weight]) at each side of the supercontainer.

The initial buffer porosity of the ring blocks,  $\varepsilon_{rb}$ , is given by:

$$\varepsilon_{rb} = 1 - \frac{\rho_{rb}}{\rho_s} \quad (\text{Eq. B.3-3})$$

with:

$\rho_s$  mineral density of bentonite [ $\text{kg m}^{-3}$ ] (Table B.1-2).



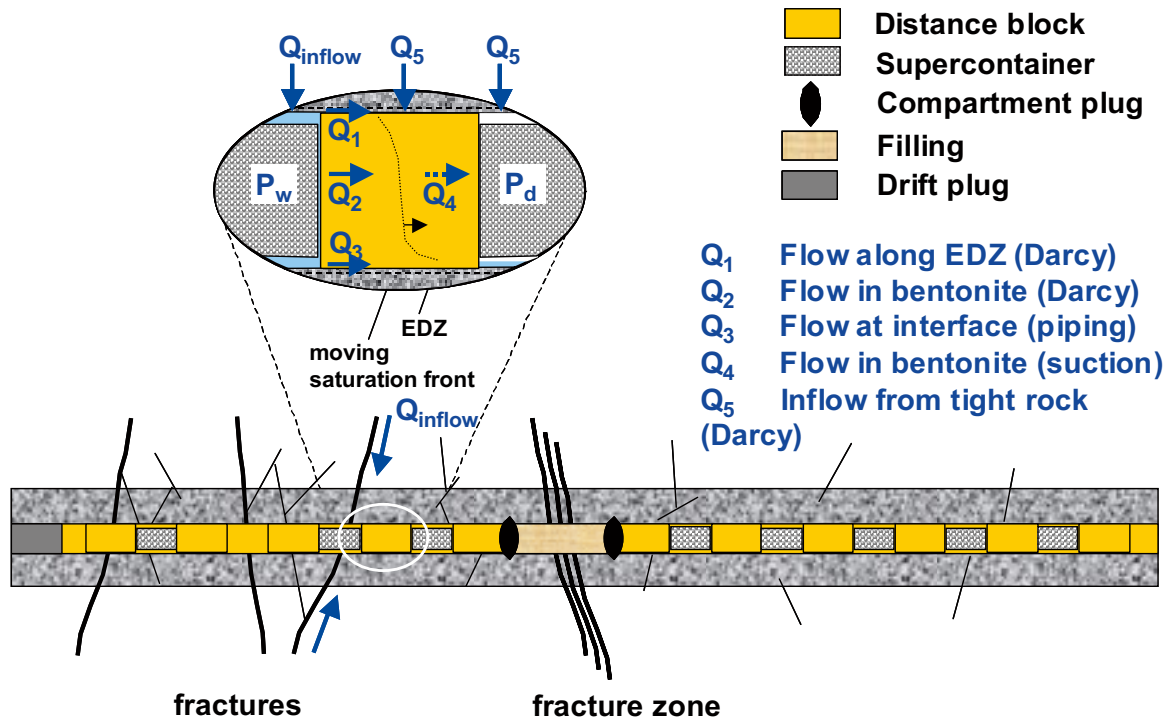


**Figure B.3-1.** Processes relevant to the transport of water from a less tight drift section towards a supercontainer located in a relatively tight section of the deposition drift.

The initial water content of the ring blocks is related to their saturation,  $S_{rb}$ , by:

$$\frac{w_{rb}}{100} = \frac{\epsilon_{rb} S_{rb} \rho_w}{(1 - \epsilon_{rb}) \rho_s + \epsilon_{rb} S_{rb} \rho_w} \quad (\text{Eq. B.3-4})$$

with:

$\rho_w$  density of water [ $\text{kg m}^{-3}$ ] (Table B.1-5).

Similar equations apply to the end blocks.

Using these equations, Eq. B.3-2 can be written:

$$V = V_{\text{void}} + \pi \left[ l_{rb} (r_B^2 - r_c^2) \left[ \left( 1 - \frac{\rho_{rb}}{\rho_s} \right) - \frac{\rho_{rb}}{\rho_w} \left( \frac{w_{rb}}{100} \right) \right] + l_{eb} r_B^2 \left[ \left( 1 - \frac{\rho_{eb}}{\rho_s} \right) - \frac{\rho_{eb}}{\rho_w} \left( \frac{w_{eb}}{100} \right) \right] \right] \quad (\text{Eq. B.3-5})$$

with:

$r_c$  canister radius (Table B.1-1)

$r_B$  buffer block radius within a supercontainer [m] (Table B.1-1)

$l_{rb}$  combined length of buffer ring blocks within a supercontainer (Table B.1-1)

$l_{eb}$  combined length of buffer end blocks within a supercontainer (Table B.1-1).

Based on the parameter values given in Appendix B.1,  $V$  takes a value of about  $2.7 \text{ m}^3$  (about  $1.5 \text{ m}^3$  of open space and an unsaturated bentonite pore volume of about  $1.2 \text{ m}^3$ ).

In the following, the saturation time of the buffer in a tight drift section is estimated on the basis of the alternative assumptions that it is controlled by (i), the rate of water flow from a permeable drift section via the EDZ adjacent to the distance block ( $Q_1$  in Figure B.3-1), (ii), the rate of water flow through the distance block ( $Q_4$  in Figure B.3-1 prior to distance block saturation and  $Q_2$  after saturation), and (iii), the rate of water flow through (poorly transmissive) fractures in the host rock. The possible impact of piping on saturation times is also assessed.

A summary of the results of the scoping calculations of saturation times, described one-by-one in the following sections, is given in Figure B.3-2.

### Water flow along EDZ

The transport of liquid water in the EDZ surrounding a distance block separating less tight and tight drift sections,  $Q_1$  [ $\text{m}^3\text{a}^{-1}$ ], can be estimated using Darcy's law:

$$Q_1 = \pi(2r_i + t_{EDZ})t_{EDZ}K_{EDZ} \frac{\Delta P}{\rho_w g p} \quad (\text{Eq. B.3-6})$$

with:

$r_i$  drift radius [m] (Table B.1-1)

$t_{EDZ}$  EDZ thickness [m] (Table B.1-3)

$K_{EDZ}$  maximum hydraulic conductivity of EDZ [ $\text{m s}^{-1}$ ] (Table B.1-3)

$\Delta P$  magnitude of the pressure difference in the EDZ between the fully saturated ("less tight") drift section and the dry ("tight") drift section [Pa] (Table B.1-3)

$g$  gravitational acceleration [ $\text{m s}^{-2}$ ] (Table B.1-5)

$p$  distance block length [m] (Table B.1-1).

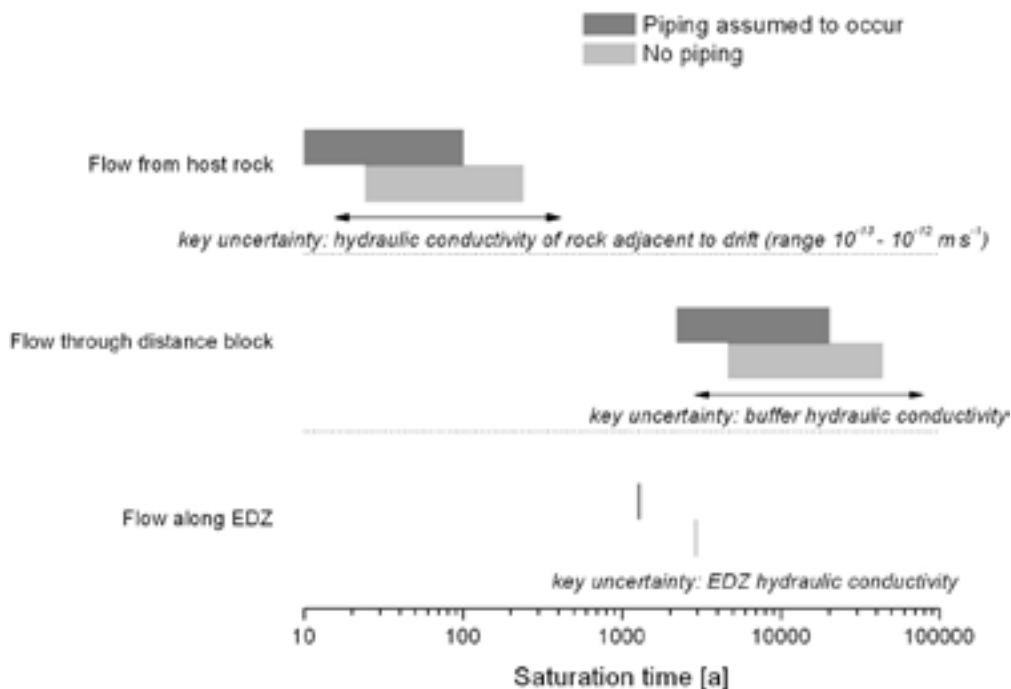


**Figure B.3-2.** Summary of results of scoping calculations of water saturation of a tight drift section (supercontainer and distance block unit section) adjacent to a more permeable drift section (dark grey bars: piping assumed to occur; light grey bars: no piping).

The less tight section is expected to be fully water saturated within about 10 years after spent fuel emplacement and sealing of the deposition drift, due to the presence of one or more transmissive fractures (see Figure 5-7). The tight section (including its EDZ) will remain in an unsaturated state for some time before it is slowly filled with water. Here, it is assumed that the interface between the saturated and unsaturated parts of the EDZ coincides approximately with the interface between the distance block and the supercontainer in the tight section (i.e. the EDZ adjacent to the distance block is assumed to be fully saturated). Assuming that the interface is static, the water pressure in the EDZ at the interface is equal to the gas pressure minus the capillary pressure in the EDZ. This can be estimated using Young's equation. Based on the mean aperture of fractures in the EDZ of 2  $\mu\text{m}$  (/Johnson et al. 2005/, Appendix C), a capillary pressure of 0.15 MPa is calculated. This means that the downstream water pressure in the EDZ is lower than the gas pressure by 0.15 MPa. The gas pressure itself is initially atmospheric and gradually increases due to the slow inflow of water and generation of hydrogen gas by anaerobic corrosion of steel.

Based on a maximal pressure difference of 4 MPa, the maximal water flow rate through the EDZ is estimated to be 1 litre  $\text{a}^{-1}$  and the corresponding minimal saturation time of the buffer is 2,800 years.

In reality, the distance block will remain partially saturated for a prolonged period of time (see below) especially in the vicinity of the tight drift section. During transport along the EDZ, some water may thus be sucked from the EDZ radially into the bentonite, leading to a sustained unsaturated state in the EDZ. By this process, the saturation of the distance block is speeded up and the saturation of the tight drift section is slowed down. This coupling of processes, which has not been taken into account in the above scoping calculations, would result in an even longer saturation time for the tight drift section.

### Water flow through the distance block

Upon contact with water entering through the permeable fractures in the less tight drift section, the face of the distance block exposed to water starts to take up water by suction and swells, while the remaining part of the distance block is still in its initial (partially saturated) state. In the course of time, a saturation front moves axially through the distance block. It is well established that the dominant water movement in unsaturated bentonite takes place by transport of vapour when the water content is low and by transport of liquid water when the water content is high. Transport of water in unsaturated bentonite may be represented as a diffusion-like process (see, e.g. /Börgesson 1985, Pusch 2000, JNC 2000/), described by:

$$\frac{\partial S}{\partial t} = \frac{D}{\varepsilon} \frac{\partial^2 S}{\partial z^2} \quad S(0,t) = 1 \text{ for } t > 0; S(z,0) = S_0 \text{ for } z > 0 \quad (\text{Eq. B.3-7})$$

with:

- $D$  an empirical coefficient [ $\text{m}^2 \text{s}^{-1}$ ] (Table B.1-2)
- $\varepsilon$  buffer porosity (Table B.1-2)
- $S$  saturation of bentonite [-]
- $z$  axial distance into the distance block from its interface with the supercontainer in the permeable drift section [m].

The distance block porosity will vary slightly with time as the bentonite swells into the gaps surrounding the blocks, but this small effect is neglected here.

Applying this 1-D equation and boundary conditions to the distance block assumes that a free water phase exists across the entire wetted vertical face of the distance block. In reality, contact between the supercontainer and the distance block will restrict the flow of water to the distance block, particularly once the distance block starts to swell, and Eq. B.3-7 will thus tend to overestimate the rate at which water migrates into the block. It also disregards the impact on the saturation process of the boundary with the supercontainer in the permeable drift section; the impact of this simplification has not been evaluated.

The analytical solution to Eq. B.3-7 is:

$$S(z, t) = S_0 + (1 - S_0) \operatorname{erfc} \left[ \frac{z}{2\sqrt{Dt/\varepsilon}} \right] \quad (\text{Eq. B.3-8})$$

where  $S_0$  is the initial saturation of the distance block.

$J$  [ $\text{m}^3$ ], the amount of water that enters the distance block in time  $t$  is given by:

$$J = -\pi r_i^2 D \int_0^t \left. \frac{\partial S}{\partial z} \right|_{z=0} dt \quad (\text{Eq. B.3-9})$$

From Eq. B.3-8 and Eq. B.3-9:

$$J = 2\pi r_i^2 (1 - S_0) \sqrt{\frac{\varepsilon D t}{\pi}} \quad (\text{Eq. B.3-10})$$

An identical equation is obtained if the saturation process is modelled as a moving saturation front, with flow upstream of the front described by Darcys Law, driven by a “suction pressure”  $p_s$  [Pa] given by:

$$\frac{p_s}{\rho g} = \frac{2D}{\pi K_B} \quad (\text{Eq. B.3-11})$$

where  $K_B$  [ $\text{m a}^{-1}$ ] is the hydraulic conductivity of saturated bentonite.

It can be assumed that the distance block is saturated when the amount of water that enters the distance block is equal to the initial unsaturated pore space within the distance block (or equivalently when the saturation front reaches the downstream boundary of the distance block):

$$J = 2\pi r_i^2 (1 - S_0) \sqrt{\frac{\varepsilon D t}{\pi}} = \varepsilon \pi r_i^2 (1 - S_0) p \quad (\text{Eq. B.3-12})$$

$$t = \frac{\pi \varepsilon p^2}{4D} \quad (\text{Eq. B.3-13})$$

with  $p$  [m] being the distance block length (Table B.1-1).

The critical parameter for this process is the effective water diffusion constant which depends on a number of variables (water content, temperature, etc). /Börgesson 1985/ and /Pusch 2000/ provide a value of  $3 \times 10^{-10} \text{ m}^2 \text{ s}^{-1}$ . /JNC 2000/ gives effective diffusion constants of  $10^{-9} - 10^{-10} \text{ m}^2 \text{ s}^{-1}$ , for a range of volumetric water contents of 0.05–0.3 and for a temperature range of 25–60°C. Using an effective diffusion constant of  $10^{-9} \text{ m}^2 \text{ s}^{-1}$ , Eq. B.3-14 gives a saturation time of about 300 years. Alternatively, the time to saturation is about 1,000 years for an effective water diffusion constant of  $3 \times 10^{-10} \text{ m}^2 \text{ s}^{-1}$ .

Once the distance block is largely saturated, water will flow through the distance block from the permeable drift section at a rate  $Q_2$  [ $\text{m}^3 \text{a}^{-1}$ ] that can be estimated using Darcy's law:

$$Q_2 = \pi r_i^2 K_B \frac{\Delta P}{\rho_w g p} \quad (\text{Eq. B.3-14})$$

with:

- $r_i$  drift radius [m] (Table B.1-1)
- $p$  distance block length [m] (Table B.1-1)
- $K_B$  hydraulic conductivity of saturated buffer [ $\text{m s}^{-1}$ ] (Table B.1-2)
- $\Delta P$  maximum pressure difference along the drift [Pa] (Table B.1-3)
- $\rho_w$  density of water [ $\text{kg m}^{-3}$ ] (Table B.1-5)
- $g$  gravitational acceleration [ $\text{m s}^{-2}$ ] (Table B.1-5).

This yields an estimated water flow rate through a fully water saturated distance block of 0.06 to 0.6 litres per year for the range of buffer hydraulic conductivities given in Table B.1-2 and a saturation time of the 2.7  $\text{m}^3$  total void volume in a supercontainer section of 4,300 to 43,000 years, calculated from the time of distance block saturation. Adding the time of distance block saturation, gives a total saturation time in the range of above 4,600 to 44,000 years.

### Inflow from tight rock

The inflow of liquid water from the tight rock directly into the tight section can also be estimated using Darcy's law in a radial configuration (Thiem's equation), as given by Eq. B.2-1, expressed in terms of the hydraulic conductivity of the rock adjacent to the drift section containing a supercontainer ( $K$  [ $\text{m s}^{-1}$ ]):

$$Q_5 = 2\pi l_s K \frac{\Delta P}{\rho_w g \ln(l_h / r_i)} \quad (\text{Eq. B.3-15})$$

with:

- $l_s$  the length of a supercontainer [m] (Table B.1-1)
- $l_h$  hydraulic length (from drift to nearest major fracture zone) [m] (Table B.1-3).

Tighter drift sections, as defined in Section 5.5.1, have hydraulic conductivities in the range  $10^{-13}$  to  $10^{-12} \text{ m s}^{-1}$ . This gives water flow rates in the range 11–110 litres per year and saturation times of the buffer in the range 24 to 240 years. Where hydraulic conductivities exceed the higher end of this range, saturation times will be controlled not by fracture transmissivity, but rather by the ability of the bentonite to take up water. Thus, in accordance with the results shown in Figure 5-7, saturation will take a minimum of about 10 years.

For tightest drift sections, saturation will be hindered even more by the build-up of gas pressure due to anaerobic corrosion of steel, as described in Section 5.5.4.

### Possible impact of piping on the time to saturation

The potential for transient water flows to cause piping and erosion is described in Section 5.5.6. If piping were to occur, significant water flow (conveying some suspended bentonite) could take place through the pipes from a less tight drift section down gradient to a tighter section. In Section 5.5.6, it is noted that laboratory and modelling studies indicate, in the case of the current reference design (the Basic Design), transient hydraulic pressure differences along the drifts will not develop sufficiently rapidly to cause piping provided the inflow rate to a supercontainer drift section comprising a supercontainer plus a distance block during saturation is 0.1 litres



per minute or less (and provided there is no displacement of the distance blocks relative to the supercontainers caused by hydraulic pressure differences along the drift). This is a design criterion for supercontainer and distance block emplacement.

Even if piping were to occur, its duration and impact would be limited. Once all open voids in the tight section (excluding unsaturated bentonite pores) became filled with the water/bentonite suspension due to piping and erosion, the pressure gradient along the pipes would decrease, the flow through the pipes would stop and the pipes would be closed by bentonite swelling provided that the outer plug is tight. The time needed to fill all open voids within and around a supercontainer ( $V_{void}$  – about  $1.5 \text{ m}^3$ ) is estimated to be several days to weeks, mainly depending on the pressure gradient and on the rate of water inflow into the less tight drift section. Thereafter, gradual saturation of the remaining pore volume ( $2.5 \text{ m}^3 - 1.5 \text{ m}^3 = 1.0 \text{ m}^3$ ) will occur by the same processes as described above ( $Q_1, Q_2, Q_4, Q_5$ ).

- For saturation via a flow of 1 litre per year along the EDZ ( $Q_1$ ), the minimum time to saturation is reduced from 2,900 years to 1,300 years;
- For saturation via flow of between 0.06 and 0.6 litres per year through a saturated distance block ( $Q_2$ ), the time to saturation of a supercontainer section is reduced from between 4,300 and 43,000 years to between 1,900 and 19,000 years; combined with a distance block saturation time of 300 to 1,000 years (via  $Q_4$ ), this gives a total saturation time in the range of above 2,200 to 20,000 years, compared with a range without piping of 4,600 to 44,000 years; and
- For saturation via inflow from the rock a rate of between 11 and 110 litres per year ( $Q_5$ ), the time to saturation is reduced from between 24 and 240 years to between about 10 and 100 years; for lower hydraulic conductivities, the impact of gas is likely to extend the time to saturation to several thousand years.

## **B.4 Processes leading to loss or redistribution of buffer mass**

### **Overview**

Scoping calculations have been performed to estimate the impact of processes that could lead to a loss of bentonite mass from, or redistribution of bentonite mass in, a drift compartment especially in the early phase of repository evolution including the operational phase.

The processes addressed include:

- axial displacements of distance blocks and supercontainers caused by differential saturation and swelling along the deposition drift;
- water flows between less tight and tight supercontainer sections due to piping along the bentonite/rock interface units and causing erosion and redistribution of bentonite;
- bentonite erosion into fractures, which may be of concern during the operational phase, namely if a sealed compartment is hydraulically connected to some nearby open rock excavation (in contrast, long-term erosion of bentonite into fractures has been investigated in previous studies and found to be of less concern);
- vertical displacement (lifting) of the supercontainer by off-centred swelling; and
- bentonite compaction due to volume changes arising from the formation of iron corrosion products (initially mainly magnetite, but also some iron sulphide and siderite).

In this last case, both the corrosion of the supercontainer, and the corrosion of the canister insert in the case of a failed canister are considered.

These processes, which are considered one-by-one in the following sections, may give rise to changes in mass,  $\Delta m$  [kg], and/or changes in the available volume,  $\Delta V$  [ $\text{m}^3$ ], in a given system component (a supercontainer section and/or distance block).

In the case of processes assumed principally to affect a distance block, the resulting change in saturated buffer density,  $\Delta\rho$  [ $\text{kg m}^{-3}$ ], is given by:

$$\Delta\rho = \frac{\rho_0 V_0 + \Delta m}{V_0 + \Delta V} - \rho_0 \quad (\text{Eq. B.4-1})$$

with:

$\rho_0$  the density of the saturated buffer [ $\text{kg m}^{-3}$ ] (Table B.1-2)

and

$$V_0 = \pi r_t^2 p \quad (\text{Eq. B.4-2})$$

with:

$r_t$  the drift diameter [m] (Table B.1-1)

$p$  the distance block length [m] (Table B.1-1).

In the case of processes assumed to affect principally the buffer originally inside a supercontainer:

$$\Delta\rho = \frac{\rho_0 V_{B,0} + \Delta m}{V_{B,0} + \Delta V} - \rho_0 \quad (\text{Eq. B.4-3})$$

$$V_{B,0} = \pi \left( r_t^2 l_s - r_c^2 l_c - \left( 1 - \frac{Z}{100} \right) (r_{s,o}^2 - r_{s,i}^2) (l_s - 2t_s) - 2r_{s,o}^2 t_s \right) \quad (\text{Eq. B.4-4})$$

with:

$l_s$  the length of a supercontainer [m] (Table B.1-1)

$l_c$  the length of a canister [m] (Table B.1-1)

$r_c$  the canister radius [m] (Table B.1-1)

$Z$  the degree of perforation of the supercontainer walls [%] (Table B.1-1)

$r_{s,o}$  the outer radius of the supercontainer [m] (Table B.1-1)

$r_{s,i}$  the inner radius of the supercontainer [m] (Table B.1-1)

$t_s$  the thickness of the supercontainer end plates [m] (Table B.1-1).

### Displacement of distance blocks and supercontainers

Differential saturation and swelling along the deposition drift due to the heterogeneous rate of water inflow from the host rock could potentially give rise to either (1), gradual or (2), more abrupt displacement of distance blocks and supercontainers.

**Case 1:** Gradual displacement could occur as a result of the development of differential swelling pressures along the drift. Upon contact with water entering through permeable fractures in a less tight drift section, the exposed face of the distance block starts to take up water by suction and swells, while the remaining part of the distance block is still in its initial (partially saturated) state. In the course of time, the saturation front moves axially through the distance block. This may result in an axial volume expansion of the swelling distance block, while the part closest to the less tight drift section is kept in place by the high swelling pressure exerted on the rock surface. As a consequence, the bentonite density of the distance block would be decreased and the buffer density in the adjacent tight section(s) would be increased due to axial compaction of vertical open slots. The slots affected may be both outside and inside the supercontainer, because the steel shell may be deformed or ruptured due to the stresses exerted by the swelling distance block. The density of the buffer in the less tight drift section remains unchanged in this situation.

**Case 2:** More abrupt displacement could occur due to a large hydraulic pressure difference between less tight and tight drift sections. This is particularly of concern if there is a slot between the distance block and the supercontainer in a less tight drift section, increasing the surface of the distance block exposed to the hydraulic pressure and thus resulting in a higher total force on the distance block (and on any supporting rings, if used). As a consequence of the displacement, the buffer density in the less tight unit is decreased and the buffer density in the adjacent tight section(s) is increased due to the compaction of voids, while the density of the distance block remains unchanged.

These two possibilities of mass redistribution by displacement are similar in their effects on the final saturated bentonite density, but differ in their evolutionary pathway from emplacement until full saturation. In both cases, the saturated bentonite density variation of the distance block adjacent to the less tight drift section (Case 1) and of the buffer in the less tight drift section (Case 2) can be estimated based from Eq. B.4-1 with<sup>39</sup>:

$$\Delta V = \pi r_i^2 f n; \quad \Delta m = 0 \quad (\text{Eq. B.4-5})$$

and with:

$\Delta V$  total change of bentonite volume in distance block (Case 1) and in buffer (Case 2) [m<sup>3</sup>]

$f$  total linear compaction by reduction of void space (per dry supercontainer unit) [m]

$n$  number of dry supercontainer units compacted by the displacement process [-].

Similarly, the bentonite density variation in the buffer of each compacted supercontainer unit can be calculated from:

$$\Delta V = \pi r_i^2 f; \quad \Delta m = 0 \quad (\text{Eq. B.4-6})$$

For Case 1, assuming  $f = 2$  (with 10 as a variant) cm per supercontainer unit<sup>40</sup>, the change of volume of the swelling distance block is 0.054 (0.27) m<sup>3</sup> if only one supercontainer unit is compacted ( $n = 1$ ). For each additional supercontainer ( $n > 1$ ) the bentonite volume gained by compaction increases accordingly. The corresponding saturated densities of the distance block next to the less tight drift section are:

- 1,993 (1,964) kg m<sup>-3</sup>, if only 1 supercontainer unit is compacted
- 1,985 (1,930) kg m<sup>-3</sup>, if 2 supercontainer units are compacted
- 1,971 (1,864) kg m<sup>-3</sup>, if 4 supercontainer units are compacted
- 1,957 (1,802) kg m<sup>-3</sup>, if 6 supercontainer units are compacted.

Similarly, for case 2, again assuming  $f = 2$  (10) cm per supercontainer unit, the corresponding saturated buffer densities in the less tight drift section are:

- 1,990 (1,950) kg m<sup>-3</sup>, if only 1 supercontainer unit is compacted
- 1,980 (1,903) kg m<sup>-3</sup>, if 2 supercontainer units are compacted
- 1,960 (1,815) kg m<sup>-3</sup>, if 4 supercontainer units are compacted
- 1,941 (1,735) kg m<sup>-3</sup>, if 6 supercontainer units are compacted.

Thus, the scoping calculations indicate that the displacement of distance blocks and supercontainers in a KBS-3H deposition drift has no significant effect on the density of bentonite

<sup>39</sup> It can be shown by a force balance consideration, that the friction forces are not sufficient to counteract the axial forces exerted by the swelling pressure of the wetted distance block (Section 4.6.1 of /Gribi et al. 2007/). Friction is, therefore, not taken into account in the calculations of bentonite density variation.

<sup>40</sup> The total linear compaction  $f$  is a measure of the extent to which a supercontainer unit may be axially compacted. It sums contributions from inside the supercontainer (gaps between individual bentonite blocks as well as gaps between blocks and steel wall) and from outside the supercontainer (gaps between steel wall and distance block).

(i.e. buffer density remains within the range 1,890 to 2,050 kg m<sup>-3</sup> discussed in Section 5.3.2), only if:

- the total linear compaction per supercontainer unit is not too large; and/or
- the number of supercontainer units affected is also not too large.

Note, however, that, under the assumption that  $f = 2$  cm, the saturated buffer densities of the compacted supercontainer units fulfil the criterion that density  $< 2,050$  kg m<sup>-3</sup>, irrespective of the case considered and of the number of compacted sections. If  $f = 10$  cm, the buffer density of the compacted supercontainer units marginally exceeds the criterion (2,052 kg m<sup>-3</sup>).

The number of units affected by the displacement process depends on various factors, including the resistance of the supercontainer against compaction, the distance to the next less tight drift section (where full counterforces are developed), the distance to the next steel ring/steel plug and friction forces opposing any displacements. It can be shown by the force balance considerations – Section 4.6.1 of /Gribi et al. 2007/ – that the friction force of tight drift sections is not sufficient to counteract the force exerted by the swelling pressure of the wetted distance block). Furthermore, the axial stiffness of the supercontainer in a tight drift section is not expected to be able to withstand the swelling pressure of a nearby distance block. It will thus be deformed or ruptured and any voids within it will be compacted. There is the possibility that the broken parts of the supercontainer are pressed against the drift walls and block any further displacement. It is, however, difficult to demonstrate that this mechanism actually occurs (for this reason, no credit is taken for this process in the scoping calculations). These considerations suggest that the displacement can only be stopped by the counterforce of a nearby wetted/fully swollen supercontainer unit.

If the total linear compaction per supercontainer is assumed to take the more conservative value of 10 cm, then the maximal distance to the next fully water saturated unit or reinforced unit must be shown not to exceed about 2–3 supercontainer units, to keep the bentonite density above a lower bound of 1,890 kg m<sup>-3</sup>.

### Piping and erosion

If piping were to occur along the bentonite/rock interface then, as long as the pipes persisted, significant water flow (conveying some suspended bentonite) could take place through the pipes from a less tight drift section to a tight drift section. The redistribution of bentonite mass in this way would persist until all open voids in the tight section (excluding unsaturated bentonite pores) are filled with the water/bentonite suspension. At that point, the pressure gradient along the pipes will vanish, the flow through the pipes will stop and the pipes will close due to bentonite swelling. As also noted in Appendix B.3, the time needed to fill all open voids within and around a supercontainer (about 1.5 m<sup>3</sup>) is estimated to be several days to weeks.

The average bentonite density decrease in the distance block adjacent to the less tight drift section is calculated based on Eq. B.4-1 with:

$$\Delta V = 0; \quad \Delta m = -V_{\text{void}} C_{\text{max}} n \quad (\text{Eq. B.4-7})$$

and with:

$\Delta m$  total change of bentonite mass in distance block [kg]

$V_{\text{void}}$  void volume around a supercontainer [m<sup>3</sup>] (Table B.1-1)

$C_{\text{max}}$  maximum bentonite mass assumed to be carried as particles by flowing water [kg m<sup>-3</sup>] (Table B.1-5)

$n$  number of supercontainer units filled with water/bentonite suspension [-].

Similarly, the average bentonite density increase due to accumulation of bentonite in each affected supercontainer unit can be calculated from:

$$\Delta V = 0; \quad \Delta m = V_{\text{void}} C_{\text{max}} \quad (\text{Eq. B.4-8})$$

Local density changes in the distance blocks are initially likely to be greater in parts of the distance blocks where erosion has occurred compared with the average. Due to the plasticity of bentonite, it is considered possible that large local density reductions would homogenise over long periods of time, although the timescale is uncertain. Two cases are thus considered:

**Case 1:** the situation after full homogenisation has taken place; and

**Case 2:** the situation of an extremely localised density reduction, in which the loss of bentonite affects only 10% of the designed volume and mass of the distance block.

Using the values given in Appendix B.1,  $\Delta m = 75$  kg. For each additional supercontainer ( $n > 1$ ) the bentonite mass lost by piping/erosion increases accordingly. The average saturated densities of the distance block next to the less tight drift section (i.e. Case 1) are thus:

- 1,995 kg m<sup>-3</sup>, if only 1 supercontainer unit is filled with a water/bentonite suspension
- 1,990 kg m<sup>-3</sup>, if 2 supercontainer units are filled
- 1,985 kg m<sup>-3</sup>, if 3 supercontainer units are filled
- 1,898 kg m<sup>-3</sup>, if 20 supercontainer units are filled.

In the supercontainer units that become filled with the water/bentonite suspension, the average saturated densities of the buffer originally inside the supercontainers are changed to 2,007 kg m<sup>-3</sup>, irrespective of the number of filled units.

In Case 2, the local density changes of the distance block next to the less tight drift section are:

- 1,949 kg m<sup>-3</sup>, if only 1 supercontainer unit is filled with a water/bentonite suspension
- 1,896 kg m<sup>-3</sup>, if 2 supercontainer units are filled
- 1,847 kg m<sup>-3</sup>, if 3 supercontainer units are filled
- 981 kg m<sup>-3</sup>, if 20 supercontainer units are filled.

The above considerations seem to indicate that the redistribution of bentonite by piping/erosion in a KBS-3H deposition drift has no significant effect on the density of bentonite (i.e. buffer density remains within the range 1,890 to 2,050 kg m<sup>-3</sup> discussed in Section 5.3.2), provided that (i), the total suspended solids ratio is not too large (in the order of a few weight% – note that the 5% weight ratio of bentonite/suspension assumed in these calculations is a pessimistic, high value, see Appendix B.1), (ii) the volume available to be filled with suspension is not too high – i.e. only a few supercontainer units are filled, and (iii), local density changes are quickly homogenised by the plasticity of bentonite. Moreover, the increase in bentonite density in each of the filled supercontainer units is marginal, i.e. 2,007 kg m<sup>-3</sup>, irrespective of the number of filled units.

### **Erosion into fractures during the operational phase**

Plugs and compartments will be positioned in such a way that no highly transmissive fracture pathways exist from a sealed drift section into any open rock excavations. There may, however, be some less transmissive fractures that provide a hydraulic connection between a sealed drift compartment and:

- an open central tunnel via a fracture bypassing the plug at the end of the drift;
- an open neighbouring drift via a fracture through the near-field rock; or
- an open compartment in the same drift, by-passing the compartment plug.

These fractures could convey significant amounts of water and suspended bentonite if the sealed compartment is quickly saturated and pressurised so that large hydraulic gradients are established between the sealed compartment and any nearby open rock excavations. Thus the relevant process during the operational phase is mechanical erosion of bentonite (particle entrainment by flowing water). Although it seems likely that such fractures would be self-sealed by accumulation and swelling of the intruded bentonite, there is a risk of ongoing bentonite



erosion if the fracture aperture is too large. In the following calculations no credit is taken for the possible sealing of fractures.

If the breakthrough of any significant flows of water, possibly conveying some suspended bentonite, were observed in the open rock excavations, measures would be taken to stop the flow (grouting, etc). In the following calculations, it is therefore assumed (though in practice it cannot be taken for granted) that the flow of water could be stopped in due time, e.g. within less than a year.

As in the case of erosion by piping, local density changes in the distance blocks are initially likely to be greater in parts of the distance blocks where erosion has occurred compared with the average; two limiting cases are considered:

**Case 1:** the situation after full bentonite homogenisation has taken place; and

**Case 2:** the situation of an extremely localised density reduction, in which the loss of bentonite affects only 10% of the designed volume and mass of the distance block.

The average bentonite density variation in the buffer adjacent to a transmissive fracture conveying water/bentonite suspension is calculated based on Eq. B.4-1 with:

$$\Delta V = 0; \quad \Delta m = -Q \tau C_{\max} \quad (\text{Eq. B.4-9})$$

where:

$\Delta m$  total change of bentonite mass in buffer next to the fracture [kg]

$Q$  flow rate through fracture from sealed drift into open excavation [ $\text{m}^3 \text{a}^{-1}$ ]

$C_{\max}$  maximum bentonite mass assumed to be carried as particles by flowing water [ $\text{kg m}^{-3}$ ]

$\tau$  time needed to stop the flow of water through the fracture [a].

In Eq. B.4-9 it is pessimistically assumed that any bentonite lost into the fracture stems from the buffer originally contained within a single supercontainer. In reality, neighbouring supercontainer buffer sections and distance blocks may also be affected, which would mitigate the effects of erosion on the saturated bentonite density.

If a fracture intersecting an open drift also intersects a sealed compartment in a parallel drift, and this sealed compartment contains water-filled void space with a high hydraulic conductivity, then the proportion of the total inflow to the open drift that passes through this void space may be approximated as:

$$\frac{r_i C}{\pi s} = 0.024 \quad (\text{Eq. B.4-10})$$

with:

$s$  drift separation [m] (Table B.1-1).

$C$  is a flow concentration factor accounting for the convergence of the streamlines towards the sealed compartment, set to 2.

Assuming a high inflow rate via the fracture to the drift of 0.1 litres per minute, the corresponding flowrate conveying suspended buffer material from the sealed compartment is  $2.4 \times 10^{-3}$  litres per minute<sup>41</sup>. The average saturated densities of the buffer next to the permeable fracture connecting the sealed section with any open excavation (i.e. Case 1) are:

- virtually unchanged, if the flow of water is stopped within 1 month
- $1,996 \text{ kg m}^{-3}$ , if the flow of water is stopped within 1 year.

<sup>41</sup> Lower rates are calculated on the basis of the DFN modelling reported in /Lanyon and Marschall 2006/. In particular, using the model of two adjacent drifts W01T22 and W01T23, net steady-state fluxes through a supercontainer section are calculated as having a mean value of  $3 \times 10^{-4}$  litres per minute and a maximum of  $10^{-3}$  litres per minute.

In Case 2, the local density changes are:

- 1,997 kg m<sup>-3</sup>, if the flow of water is stopped within 1 month
- 1,958 kg m<sup>-3</sup>, if the flow of water is stopped within 1 year.

These results indicate that the redistribution of bentonite by erosion into a permeable fracture connecting a sealed KBS-3H deposition drift with any open rock excavation is unlikely to have a detrimental effect on the capacity of the eroded buffer to perform its safety functions (i.e. buffer density remains within the range 1,890 to 2,050 kg m<sup>-3</sup> discussed in Section 5.3.2).

### Vertical displacement (lifting) of supercontainer by off-centred swelling pressure

Water accumulating in the lower part of the drift can lead to bentonite extruding through the holes in the lower part of the supercontainer, whereas bentonite extrusion in the upper part would occur more slowly due to a somewhat later contact with liquid water (Section 5.4.4). Also, the wetted bentonite in the lower part of the buffer has a higher thermal conductivity than the drier bentonite in the upper part, which further accentuates the off-centred saturation of the buffer. As a result, the supercontainer may be subject to off-centred swelling pressure, causing lifting of the supercontainer to the top of the deposition drift and a corresponding lowering of bentonite density in the lower part of the drift (Figure B.4-1).

The average bentonite density decrease in the lower half of the buffer is calculated based on Eq. B.4-1 with:

$$\Delta V = 2r_t (r_r - r_{s,o})l_s; \quad \Delta m = 0 \quad (\text{Eq. B.4-11})$$

and with:

$r_t$  radius of drift [m] (Table B.1-1)

$r_{s,o}$  external radius of supercontainer [m] (Table B.1-1)

$l_s$  length of supercontainer [m] (Table B.1-1).

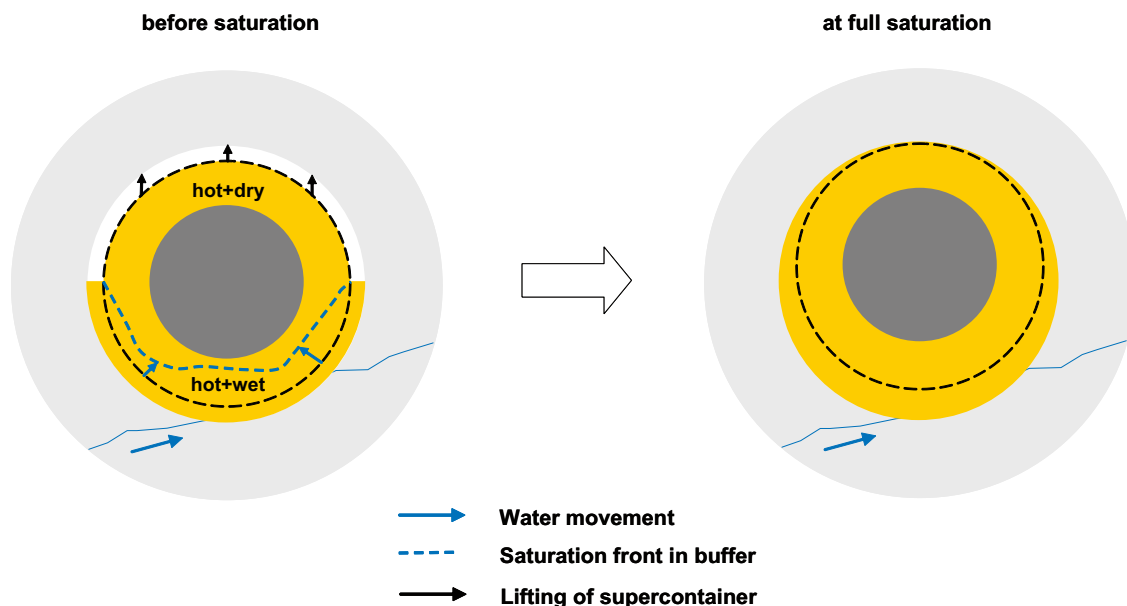


**Figure B.4-1.** Vertical displacement (lifting) of a supercontainer due to off-centred bentonite swelling.

The calculated average saturated buffer density in the lower half of the drift<sup>42</sup> is 1,921 kg m<sup>-3</sup>. The corresponding *increase* in average saturated buffer density in the upper half of the drift is 2,086 kg m<sup>-3</sup>. The higher density is outside the bound specified by the safety function indicator criteria in Table 2-3. However, as the remaining buffer saturates, the initially higher density and swelling pressure in the upper part of the drift will tend to homogenise and return the canister to a more central position in the drift, although some small eccentricity may remain.

### Formation of corrosion products

Corrosion of steel components affects the final density of the buffer due to the greater volume of the corrosion products compared with uncorroded steel. The dominant corrosion product is initially expected to be magnetite, although, depending on solution conditions, some iron sulphide and siderite may also form.

In the case of the corrosion of the supercontainer, the change in average bentonite density in the buffer is calculated based on Eq. B.4-1 with:

$$\Delta V = \frac{M_{sc}}{\rho_{Fe}}(1 - \delta); \quad \Delta m = 0 \quad (\text{Eq. B.4-12})$$

and with:

$\Delta V$  total change of bentonite volume in buffer due to formation of corrosion products [m<sup>3</sup>]

$M_{sc}$  mass of supercontainer iron (including feet) [kg] (Table B.1-1)

$\rho_{Fe}$  density of iron/steel [kg m<sup>-3</sup>] (Table B.1-5)

$\delta$  volume increase factor relative to iron [-] (Table B.4-2).

The resulting saturated bentonite densities for the buffer are given in Table B.4-1, based on the volume increase factors also given in the table.

These results indicate that the volume increase due to corrosion of the supercontainer will not have a detrimental effect on the capacity of the eroded buffer to perform its safety functions (i.e. buffer density remains within the range 1,890 to 2,050 kg m<sup>-3</sup> discussed in Section 5.3.2), except if it assumed that the corrosion product is siderite. The production of siderite is, however limited by the availability of carbonate from bentonite (in the form of calcite) or from the host rock. The buffer contains only very limited amounts of calcite, which may release some carbonate upon dissolution (0.1% for siderite and calcite combined – /SKB 2006a). Moreover, the molar volumes of calcite and siderite are similar. This means that even if some carbonate could be provided by the bentonite enabling siderite formation, no significant volume increase would be involved with this process. At Olkiluoto, the present carbonate content of groundwaters at a depth of 400–500 m is below 1 mmol per litre /Andersson et al. 2007/. During the operational phase, carbonate rich groundwaters from above may flow towards the drift. In the brackish groundwaters at depths down to 300 m, the carbonate content is up to 4–5 mmoles per litre.

**Table B.4-1. Summary of steel corrosion processes and corresponding changes in saturated density of the buffer.**

Corrosion product	Process	Volume increase factor (relative to iron) [-]	Saturated density of buffer [kg m <sup>-3</sup> ]
Magnetite	$3\text{Fe} + 4\text{H}_2\text{O} \rightarrow \text{Fe}_3\text{O}_4 + 4\text{H}_2$	2	2,026
Iron sulphide	$\text{Fe} + \text{HS}^- + \text{H}^+ \rightarrow \text{FeS} + \text{H}_2$	2.5	2,040
Siderite	$\text{Fe} + \text{HCO}_3^- + \text{H}^+ \rightarrow \text{FeCO}_3 + \text{H}_2$	4.7	2,101

<sup>42</sup> Including the buffer in the gap between the supercontainer and the drift wall in the lower and upper halves of the drift.

As noted in Appendix B.3, during saturation, about 2.7 m<sup>3</sup> of groundwater (containing maximally about 10–15 moles of carbonate) are needed to fill all voids and pores within and around supercontainer. After saturation and pressure equilibration, some 0.0035 m<sup>3</sup> a<sup>-1</sup> of groundwater may flow through a supercontainer unit, assuming that there is a permeable fracture intersecting the drift (transmissivity 3 × 10<sup>-9</sup> m<sup>2</sup> s<sup>-1</sup>, hydraulic gradient 0.01 m m<sup>-1</sup>, flow convergence factor of 2), conveying some 0.02 moles of carbonate per year. An additional 0.5 moles of carbonate per year may be provided by diffusion through the intact host rock (effective diffusion constant 10<sup>-10</sup> m<sup>2</sup> s<sup>-1</sup>, carbonate concentration gradient 5 mol m<sup>-4</sup>). At such transport rates, the complete conversion of the supercontainer (1,071 kg – see Table B.1-1 – or 19,000 moles of iron) to siderite would take some tens of thousands of years, compared with an expected corrosion time of a few thousand years. This is a clear indication, that the transformation of iron to siderite is limited by the availability of carbonate. The value given in Table B.4-2 for siderite is therefore likely to overestimate the buffer density increase under the expected repository conditions.

In the case of corrosion of the insert following canister failure the change in average bentonite density in the buffer around a supercontainer is calculated based on Eq. B.4-1 with:

$$\Delta V = \frac{M_{insert}}{\rho_{Fe}}(1 - \delta) + V_{canvoid}; \quad \Delta m = 0 \quad (\text{Eq. B.4-13})$$

and with:

$M_{insert}$  mass of iron and steel inside the canister [kg] (Table B.1-1)

$V_{canvoid}$  void space inside the canister [m<sup>3</sup>] (Table B.1-1).

Here, it is assumed that the corrosion products will preferentially fill the void space inside the canister; only once this is filled is the buffer compacted.

The resulting change in volume ( $\Delta V$ ) to be taken up by the buffer is 0.77 m<sup>3</sup> and the resulting density is 2,160 kg m<sup>-3</sup>, assuming the corrosion product to be magnetite. This does not satisfy the criteria for the safety function indicators for the buffer, which give a maximum buffer density of 2,050 kg m<sup>-3</sup>. The calculation is, however, conservative. In particular, it is assumed that the only part of the buffer to be compacted is that originally inside the supercontainer. In reality, there is likely to be some relaxation of the increased density by buffer creep along the drift, although internal friction will mean that some locally increased density around the failed canister is likely to remain.

## B.5 Numbers of canisters potentially affected by a post-glacial earthquake

### Introduction

Shear movements along fractures intersecting a KBS-3H deposition drift have the potential to damage the canisters if these movements are sufficiently large. Although Finland is located in a region that is currently tectonically quiet, significant movement on fractures could occur in the future in conjunction with the retreat of a major glacier. According to the methodology proposed in the context of a KBS-3V repository in Sweden in /SKB 2006a/ and in more detail in /Munier and Hökmark 2004/, canisters should not therefore be placed in the vicinity of major deformation zones that may undergo post-glacial earthquakes. Additionally, canister deposition positions should, if possible, not be placed at positions where the drift is intersected by fractures above a certain size to avoid the possibility of secondary shear movements larger than typically 0.1 m, which has been demonstrated to provide a reasonable margin for canister failure /Börgesson et al. 2004/. There is, however, uncertainty in the degree to which large fractures with the potential to slip by more than 0.1 m can be identified and avoided when emplacing canisters along the drift, and so the potential consequences of shear movements greater than 0.1 m at canister emplacement locations need to be assessed.

A methodology for calculating the probability of a KBS-3V canister location being intersected by a fracture exceeding a prescribed size, assuming that such fractures are not detected and avoided when the canisters are deposited, is given in /Hedin 2005/. Hedin applied the method using data from the Forsmark site in Sweden. This appendix describes how the method can also be applied to KBS-3H canister locations at Olkiluoto, and can be easily extended to evaluate the special case of two or more adjacent KBS-3H canisters in a drift being affected by the same fracture.

### The model for KBS-3V

The model presented in /Hedin 2005/ is based on the notion that, if the distributions of fracture sizes and orientations in a host rock are known, and if a canister is emplaced randomly in that host rock, then it is possible to calculate the probability that the canister is intersected by a fracture of specified properties, and in particular by a fracture that exceeds a certain size. The fracture population is described as several fracture sets, each with specified distributions of sizes and orientations. The distributions of sizes and orientations within a set are assumed to be uncorrelated. Furthermore, all fractures are assumed to be infinitesimally thin, circular discs.

The model assumes a power-law probability density function of fracture sizes,  $f(r)$ :

$$f(r) = \frac{kr_0^k}{r^{k+1}}, \quad r_0 \leq r < \infty \quad (\text{Eq. B.5-1})$$

with:

$r$  fracture radius [m]

$r_0$  the smallest fracture radius considered in the model [m] (Table B.1-4)

$k$  a dimensionless model parameter (Table B.1-4).

The fracture intensity and fracture size distribution gives rise to an average fracture area per unit volume of host rock, a  $P32$ -value, expressed in units of  $\text{m}^2$  per  $\text{m}^3$ . Part of the  $P32$ -value is associated with fractures that exceed a certain size and this critical part,  $a$  [ $\text{m}^{-1}$ ] is given by Eq. 11 in /Hedin 2005/:

$$a = P_{32} (k - 2) \left\{ \left( \frac{r_0}{r_{Max}} \right)^{k-2} \left[ \frac{1}{2-k} + \left( \frac{r_{Min}}{r_{Max}} \right)^2 \frac{1}{k} \right] - \left( \frac{r_0}{r_{Min}} \right)^{k-2} \left[ \frac{1}{2-k} + \frac{1}{k} \right] \right\} \quad (\text{Eq. B.5-2})$$

with:

$r_{Max}$  the size above which a fracture is assumed to be readily observable, and thus avoided [m] (Table B.1-3)

$r_{Min}$  the minimum fracture size that could give rise to potentially damaging displacement [m].

It is assumed that:

$$r_{Min} = \frac{d_{Crit}}{b} \quad (\text{Eq. B.5-3})$$

with:

$d_{Crit}$  the minimum displacement that may cause damage to a canister [m] (Table B.1-3)

$b$  a dimensionless model parameter (Table B.1-3).

For a given rock volume,  $V$  [ $\text{m}^3$ ], the total critical fracture area – i.e. the area of fractures exceeding the critical size – is equal to  $aV$  [ $\text{m}^2$ ]. In KBS-3V, the cylindrical canisters are to be deposited with their axes oriented vertically. If a fracture of critical size is horizontal, then a canister centre-point positioned within half the canister height on either side of the fracture will result in the fracture intersecting the canister position, giving a total canister intersection zone width around a horizontal fracture equal to the canister length  $l_c$  [m]. The corresponding width for a vertical fracture equals the canister diameter  $2r_c$  [m]. The intersection zone half-width  $L/2$  [m] for a single fracture the pole of which has a plunge angle  $\theta$  is illustrated in Figure B.5-1.



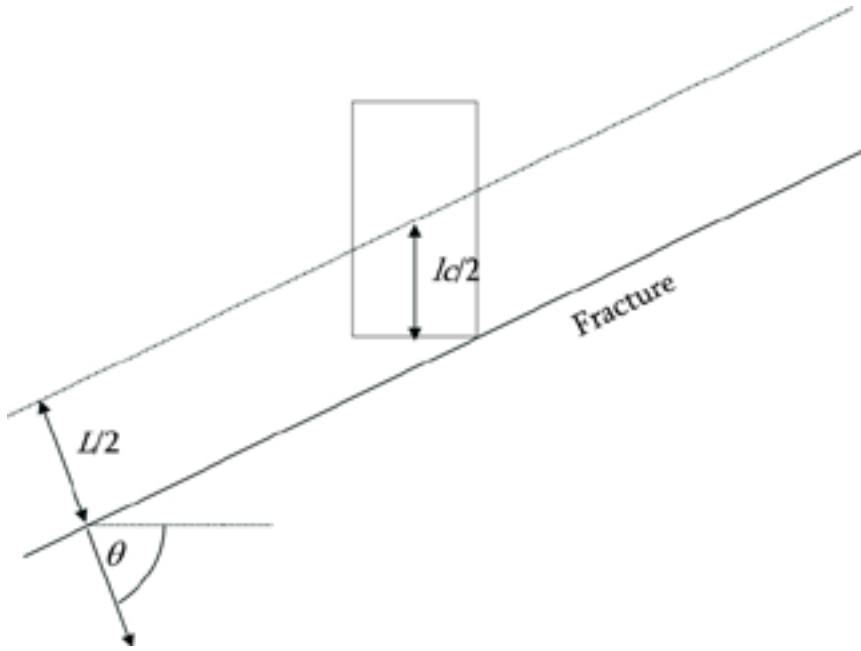


**Figure B.5-1.** The intersection zone half-width  $L$  for a single fracture the pole of which has a plunge angle  $\theta$  (after Figure 2-2 in /Hedin 2005/).

More generally, for distribution of fracture orientations, a mean intersection zone width  $\langle L \rangle$  [m] can be calculated using Eq. 15 in Hedin 2005:

$$\langle L \rangle = \int_{\theta'=0}^{\pi} \int_{\varphi=0}^{2\pi} L(\theta) \frac{\kappa \sin \theta' \exp(\kappa \cos \theta')}{\exp(\kappa) - \exp(-\kappa)} \frac{1}{2\pi} d\varphi d\theta' \quad (\text{Eq. B.5-4})$$

where:

$$L(\theta) = h_{Can} |\sin \theta| + d_{Can} \sqrt{1 - \sin^2 \theta} \quad (\text{Eq. B.5-5})$$

and

$$\sin \theta = -\cos \theta_p \sin \theta' \cos \varphi - \sin \theta_p \cos \theta' \quad (\text{Eq. B.5-6})$$

In deriving Eq. B.5-4, it is assumed that each fracture set is characterised by a principal orientation, around which the orientation of fractures is described by a Fisher distribution for which the probability density function  $g(\theta')$  is given by:

$$g(\theta') = \frac{\kappa \sin \theta' \exp(\kappa \cos \theta')}{\exp(\kappa) - \exp(-\kappa)} \quad (\text{Eq. B.5-7})$$

where  $\kappa$  is a dimensionless measure of the degree of concentration around the principal orientation. The pole of a fracture with the principal orientation has a plunge angle  $\theta_p$ . Eq. B.5-4 is solved by a numerical integration scheme.

Given the mean total critical fracture area,  $a$ , and the mean intersection zone width,  $\langle L \rangle$ , a mean value of the volume of rock within which canisters would intersect fractures of critical size is calculated as  $a \cdot V \cdot \langle L \rangle$ .  $\varepsilon$ , the expectation value of the portion of canister positions that are intersected by fractures that may cause damage is thus given by:

$$\varepsilon = a \langle L \rangle \quad (\text{Eq. B.5-8})$$

$N$ , the expectation value of the number of canisters positions that are intersected by fractures that may cause damage, is given by:

$$N = N_c a \langle L \rangle \quad (\text{Eq. B.5-9})$$

where  $N_c$  is the number of canisters in the repository.

### Adaptation of the model to KBS-3H

For single canister positions, it is trivial to adapt this model to deal with canisters emplaced horizontally by redefining  $\theta$  as  $\pi/2$  – the plunge angle of a fracture pole – i.e. the fracture dip (Figure B.5-2).

For KBS-3H, it is also of interest to evaluate the likelihood that the same potentially damaging fracture (or fractures) will affect two or more adjacent canisters in a deposition drift. The situation of concern is sketched in Figure B.5-3.

To adapt the model described in the previous section to evaluate this situation, the intersection zone width  $L(\theta)$  must be modified, as illustrated in Figure B.5-4.

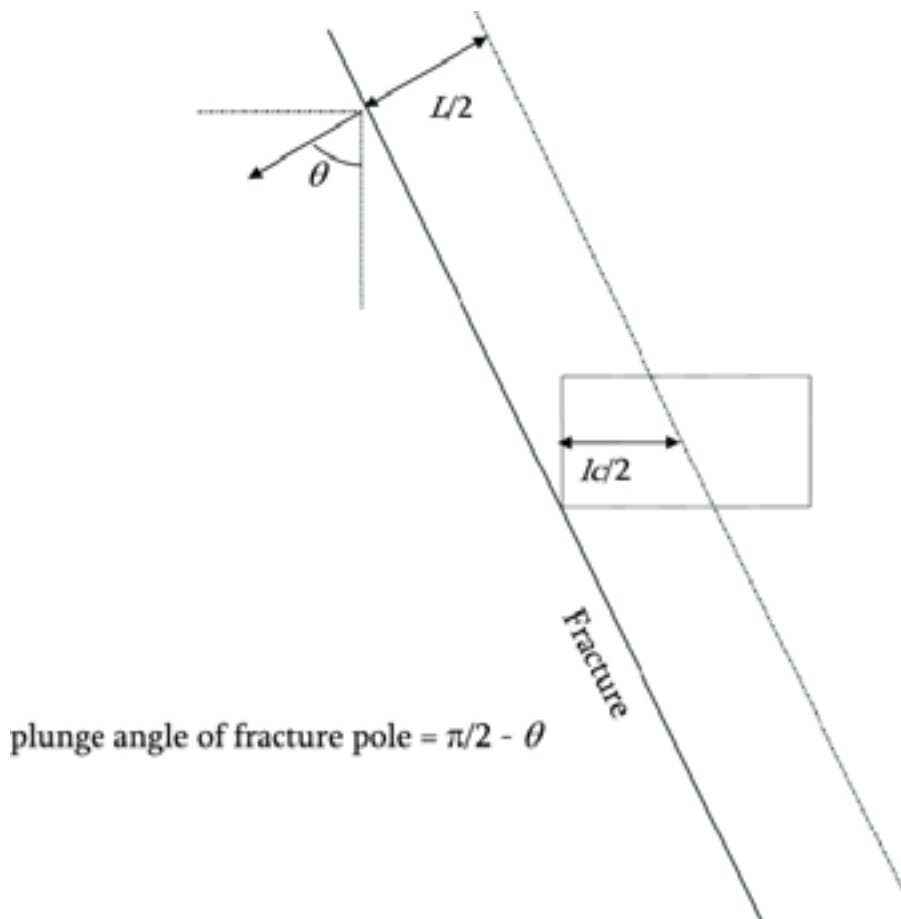


**Figure B.5-2.** Redefinition of  $\theta$  for the horizontal (KBS-3H) canister case.

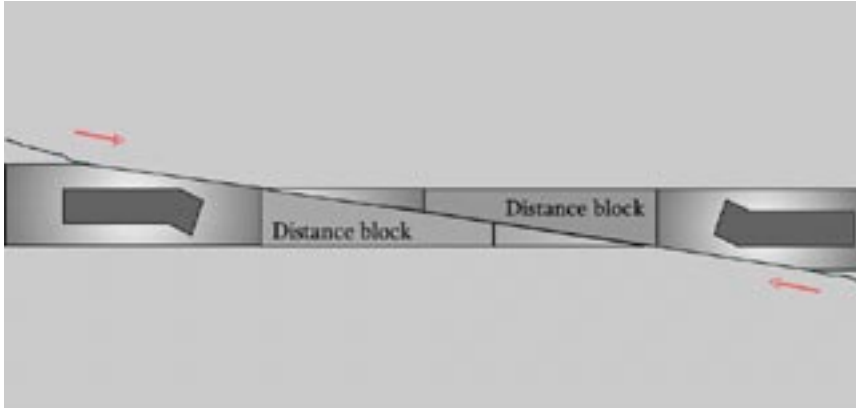


**Figure B.5-3.** A single fracture affecting two adjacent canisters.

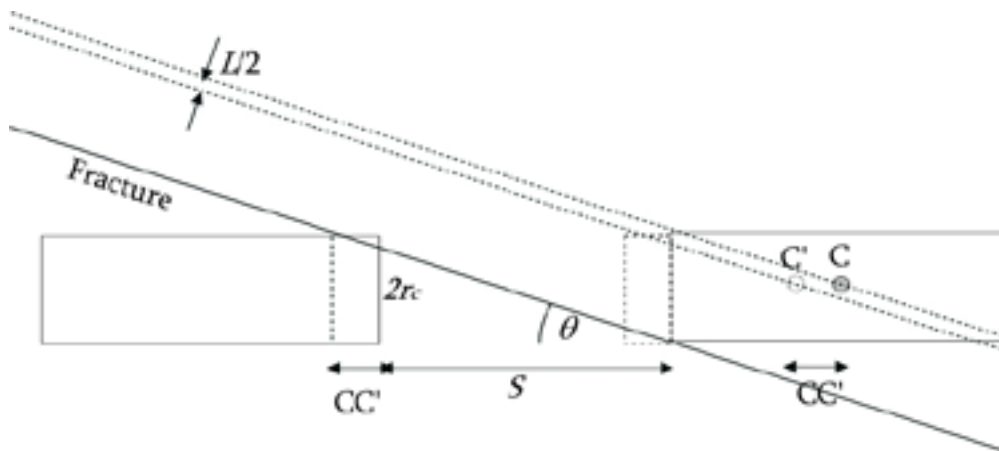


**Figure B.5-4.** The intersection zone half-width  $L/2$  for a single fracture affecting two adjacent canisters (a similar zone exists at an equal distance on the other side of the fracture).

In Figure B.5-4, C denotes the centre of the right-hand canister. If the canister centre were further to the right, the right-hand canister would no longer be intersected by the fracture shown as a diagonal solid line. On the other hand, if the canister centre were further to the left than C', the fracture would no longer intersect the left-hand canister. The distance  $CC'$  is given by:

$$CC' = \frac{r_c}{|\tan \theta|} - S \quad (\text{Eq. B.5-10})$$

with:

$r_c$  canister radius [m] (Table B.1-1)

$S$  the distance between canisters (i.e. the supercontainer length,  $l_s$  + the distance block length,  $P$  – the canister length,  $l_c$ ) [m].

If  $CC'$  is positive, then:

$$L(\theta) = 2CC'|\sin \theta| = 2(2r_c \sqrt{1 - \sin^2 \theta} - S|\sin \theta|) \quad (\text{Eq. B.5-11})$$

If  $CC'$  is negative, then the fracture is too steeply dipping to intersect both canisters simultaneously (i.e. its dip is greater than  $\arctan(d/S)$ ) and  $L(\theta)$  is set to zero.

$L(\theta)$  defined in this way is substituted into Eq. B.5-4 and the resulting  $\langle L \rangle$  into Eq. B.5-8 to evaluate the expectation value of the portion of adjacent canister pairs that are both affected by the same potentially damaging fracture (or fractures). By redefining  $s$  as the distance separating the first and last canister in a set of three adjacent canisters, the expectation value of the portion of sets of three adjacent canisters that are all affected by the same potentially damaging fracture (or fractures) can be evaluated.

It should be noted that the method only takes into account one deposition drift at a time. As the distance between drifts is only 25 m, there is also the possibility that the same fracture will cause canister damage in adjacent drifts. This possibility has not been evaluated quantitatively in the present study.

### Fracture network data

Fracture network data used in the present preliminary application of the model are given in Table B.1-4. The data are the same as those of the discrete fracture network model of /La Pointe and Hermanson 2002/, which was used in an earlier study to make estimates of rock movements at Olkiluoto and other sites in Finland due to future earthquakes by numerical simulation. Orientation and size distribution parameters are originally from a study by /Poteri 2001/. Data are based on a size scaling analysis of observations of lineaments with a trace length scale in the order of 1 km and greater, and, at a smaller scale, of outcrops and boreholes, which are on the scale of meters to tens of meters. Fractures have been classified as open, filled or tight. Filled and tight fractures are assumed not to be subject to slip during earthquakes, since sensitivity analyses carried out by /La Pointe et al. 2000/ suggest that fractures with even moderate amounts of cohesion and friction will not slip as a result of earthquakes unless these earthquakes are extremely large and within a few hundred meters of a fracture. Thus, in /La Pointe and Hermanson 2002/, the intensity of the open fractures was used for calibrating the fracture intensity of the discrete fracture network model (P32).

### Results

The expectation values of the portion of canister positions and of the total number of canister positions that are intersected by potentially damaging fractures are presented in Table B.5-1 for vertical emplacement (KBS-3V) and in Table B.5-2 for horizontal emplacement (KBS-3H). Intermediate results are also shown.

**Table B.5-1. The expectation values of the portion of canister positions and of the total number of canister positions that are intersected by potentially damaging fractures in the case of vertical emplacement (KBS-3V), along with intermediate results.**

	Fracture sets			Total
	Horizontal	N-NW	E-NE	
$a$ [ $m^{-1}$ ]	0.0012	0.00012	0.00036	
$\langle L \rangle$ [m]	4.41	1.96	3.04	
$\varepsilon$	0.0055	0.00023	0.0011	<b>0.0068</b>
N	16.5	0.7	3.3	<b>20</b>

**Table B.5-2. The expectation values of the portion of canister positions and of the total number of canister positions that are intersected by potentially damaging fractures in the case of horizontal emplacement (KBS-3H), along with intermediate results.**

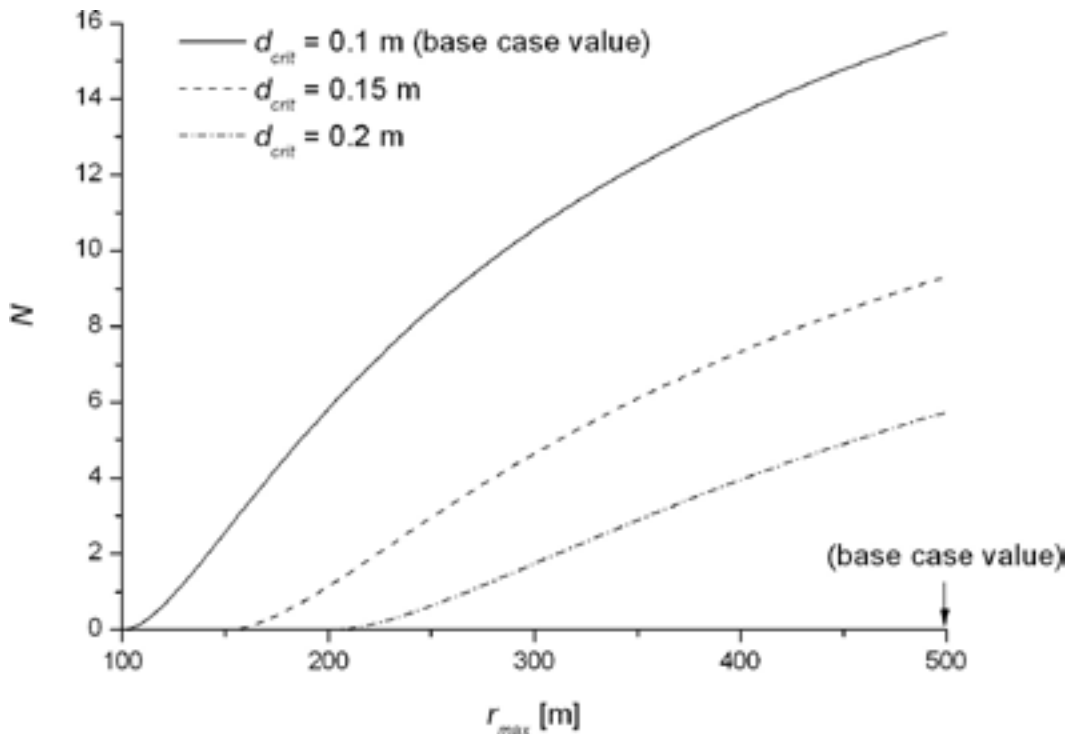
	Fracture sets			Total
	Horizontal	N-NW	E-NE	
$a$ [ $m^{-1}$ ]	0.0012	0.00012	0.00036	
$\langle L \rangle$ [m]	2.72	4.82	3.64	
$\epsilon$	0.0034	0.00055	0.0013	<b>0.0053</b>
N	10.2	1.7	3.9	<b>16</b>

Figure B.5-5 shows the sensitivity of  $N$ , the expectation value of the total number of canister positions that are intersected by potentially damaging fractures, to:

- $r_{max}$  – the maximum radius of fractures that are assumed to escape detection; and
- $d_{crit}$  – the critical shear displacement at a canister position, above which damage is assumed to occur.

The figure shows how the expectation value increases with the threshold size for fracture detection, and decreases with the threshold shear displacement (note that, for  $d_{crit} = 0.1$  m, fractures of radii less than 100 m are assumed not to have the potential to cause damage).

The expectation value of the portion of adjacent canister pairs in KBS-3H that are affected by the same potentially damaging fracture (or fractures) is presented in Table B.5-3, again along with intermediate results. Table B.5-4 presents results for sets of three adjacent canisters.



**Figure B.5-5.** The sensitivity of  $N$ , the expectation value of the total number of canister positions that are intersected by potentially damaging fractures, to  $r_{max}$ , the maximum radius of fractures that are assumed to escape detection, and  $d_{crit}$ , the critical shear displacement at a canister position, above which damage is assumed to occur. Base case values refer to values given in Appendix B.1.



**Table B.5-3. The expectation value of the portion of adjacent canister pairs in KBS-3H that are both affected by the same potentially damaging fracture (or fractures), along with intermediate results.**

	Fracture sets			Total
	Horizontal	N-NW	E-NE	
$a$ [m <sup>-1</sup> ]	0.0012	0.00012	0.00036	
$\langle L \rangle$ [m]	0.26	$1.20 \times 10^{-6}$	0.11	
$\varepsilon$	0.00032	$1.38 \times 10^{-10}$	0.000038	<b>0.00036</b>

**Table B.5-4. The expectation value of the portion of sets of 3 adjacent canisters in KBS-3H that are all affected by the same potentially damaging fracture (or fractures), along with intermediate results.**

	Fracture sets			Total
	Horizontal	N-NW	E-NE	
$a$ [m <sup>-1</sup> ]	0.0012	0.00012	0.00036	
$\langle L \rangle$ [m]	0.080	$2.69 \times 10^{-7}$	0.038	
$\varepsilon$	0.00010	$3.09 \times 10^{-11}$	0.000014	<b>0.00011</b>

## Discussion and conclusions

According to the results of the model calculations, about one in every 150 vertically emplaced canisters will be affected by a potentially damaging fracture (20 canisters out of 3,000), assuming that fractures with radii below 500 m are not detected and avoided as deposition positions. The number is slightly lower for horizontally emplaced canisters – about 1 in every 190 or 16 canisters out of 3,000. This is largely due to the lesser effect of subhorizontal fractures in the case of horizontal emplacement – the mean intersection zone width for subhorizontal fractures is 4.41 m for vertical deposition and only 2.72 m in the horizontal case.

The possibility of two adjacent horizontally deposited canisters being affected by displacement on the same fracture or fractures is indicated to be very low – about 1 in 3,000 canister pairs. Fractures that intersect canister pairs predominantly belong to the sub-horizontal fracture set. Almost no fractures in the relatively steeply dipping N-NW fracture set intersect two adjacent canisters. This number drops to about 1 in 9,000 for sets of 3 adjacent canisters.

As discussed in the conclusions of /Hedin 2005/, there are several uncertainties that are not treated in this approach, or are treated conservatively. For example, all fractures are pessimistically assumed to slip by an amount determined only by the secondary fracture size, irrespective of their distance from, and orientation with respect to, the major deformation zone on which the earthquake occurs.

It should also be noted that the criterion that the canister may fail if slips are greater than 0.1 m is conservative, particularly if slip occurs in a plane approximately parallel to, rather than normal to, the canister axis, as in the case of a single fracture affecting two horizontally emplaced canisters /Börgesson and Hernelind 2006/ investigated the impact of shear direction showed that a shear inclination of 45° is more harmful to the copper shell of the canister than shear either parallel or perpendicular to the canister axis). Sensitivity analysis shows how the number of canister positions intersected by potentially damaging fractures decreases if this criterion is relaxed.

## B.6 Impact of limited availability of water on steel corrosion rates

### Rate of water consumption by steel corrosion

Based on the corrosion process involving magnetite as the dominant corrosion product, the rate of water consumption by corrosion of steel with an unlimited supply of water to the corroding surfaces,  $R_c$  [ $\text{m}^3 \text{a}^{-1}$ ], is given by:

$$\dot{n}_{w,\max} = \frac{4}{3} R F_0 \frac{N_w \rho_{Fe}}{N_{Fe} \rho_w} \quad (\text{Eq. B.6-1})$$

with:

$R$  steel corrosion rate [ $\text{m a}^{-1}$ ] (Table B.1-5)

$F_0$  total steel surface (supercontainer and feet) [ $\text{m}^2$ ] (Table B.1-2)

$\rho_{Fe}, \rho_w$  densities of iron and water [ $\text{kg m}^{-3}$ ] (Table B.1-5)

$N_{Fe}, N_w$  molar weights of iron and water [ $\text{kg mol}^{-1}$ ] (Table B.1-5).

The reference steel corrosion rate (also based on the assumption of an unlimited supply of water) is  $1 \mu\text{m a}^{-1}$ . From Eq. B.6-1, to sustain the reference corrosion rate over the total steel surface of  $F_0 \sim 40 \text{ m}^2$  per supercontainer, about  $0.1 \text{ litres a}^{-1}$  of water are needed. This appendix considers the possibility that the rate of corrosion of steel components external to the canisters is limited by the availability of water in the drift.

### Availability of liquid water

In many drift sections, as long as a significant hydraulic gradient towards the drift persists, inflow rates of liquid water from the rock will be sufficient to maintain the reference steel corrosion rate of  $1 \mu\text{m a}^{-1}$ . For example, even in tighter drift sections, with hydraulic conductivities in the range  $10^{-13}$  to  $10^{-12} \text{ m s}^{-1}$ , initial inflow rates will be 11 to 110 litres  $\text{a}^{-1}$  (Appendix B.3), i.e. 2 to 3 orders of magnitude higher than the  $0.1 \text{ litres a}^{-1}$  of water are needed to maintain the reference steel corrosion rate. Over time, however, gas overpressures may develop in these tighter drift sections, reducing water inflow rates and possibly leading to a partial desaturation of the rock. Water may still, however, migrate to the corroding surfaces in the form of vapour, both from the rock and from the buffer, as described in the following sections.

Even where there is no inflow from the rock, there is a substantial amount of water present in the partly saturated buffer. The buffer initially inside the supercontainer consists of ring blocks fitted around the canister, and end blocks on either side. The volume of liquid water initially within the ring blocks,  $V_{rb}$  [ $\text{m}^3$ ], is given by:

$$V_{rb} = \pi (r_B^2 - r_c^2) l_{rb} \left( \frac{w_{rb}}{100} \right) \left( \frac{\rho_{rb}}{\rho_w} \right) \quad (\text{Eq. B.6-2})$$

with:

$\rho_{rb}$  initial dry density of the ring blocks [ $\text{kg m}^{-3}$ ] (Table B.1-2)

$\rho_w$  density of water [ $\text{kg m}^{-3}$ ] (Table B.1-5)

$w_{rb}$  initial water content of the ring blocks [% by weight] (Table B.1-2)

$r_c$  canister radius (Table B.1-1)

$r_B$  buffer block radius within a supercontainer [ $\text{m}$ ] (Table B.1-1)

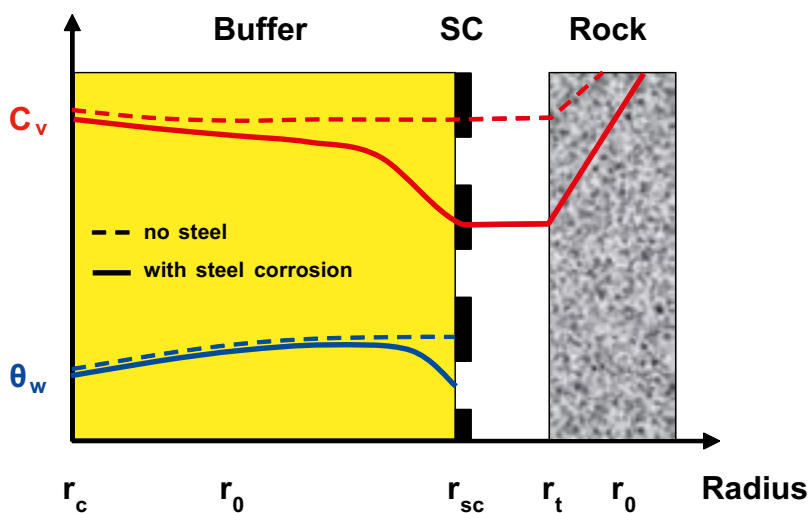
$l_{rb}$  combined length of buffer ring blocks within a supercontainer (Table B.1-1).

This gives a water volume of 1,350 litres initially contained within the ring blocks. A similar expression, also with data given in Tables B.1-1 and B.1-2, gives about 300 litres of water initially contained within the end blocks. The conversion of the total mass of steel (about 1,071 kg per supercontainer including feet) to magnetite would require 382 litres of water. Thus, there is sufficient water initially inside the buffer to corrode the steel. The question arises, however, whether water can be withdrawn from the buffer and from the near-field rock by evaporation/vapour diffusion at a sufficient rate to maintain corrosion.

### Supply of water by vapour diffusion from the near-field rock and from bentonite

The dominant driving force for vapour transport between corroding steel surfaces and liquid water present in both the near-field rock and the buffer is the vapour pressure gradient that is established by a gradient in the relative humidity (which in turn is a function of the total suction potential) and by a temperature gradient. Other gradients, such as the osmotic gradient, density gradient and gravity, are less important. Note that vapour transport by a temperature gradient (thermal diffusion) can be viewed as being part of vapour transport driven by a gradient in the relative humidity. This is because a temperature difference causes a vapour pressure difference, which drives vapour from the warmer part to the cooler part.

Steel corrosion and suction/condensation in the buffer will take up moisture from the gas phase and tend thus to maintain a vapour pressure gradient from the rock towards the drift (Figure B.6-1). This is opposed by the temperature gradient that, by thermal diffusion, tends to evaporate water near the heat source (canister) and to drive water vapour outwards to cooler areas where condensation takes place. The importance of thermal diffusion, however, decreases with time due to the gradual decrease of temperature at the canister surface. After a transient phase, a steady-state vapour flux is likely to be established, where the consumption of water at the steel surface (the sink) is balanced by transport of vapour towards the sink. It is important to note that the conversion of water to corrosion products is an irreversible process and is thus a true sink, whereas the uptake/condensation of moisture in bentonite may be reversed by evaporation/removal (drying of bentonite). As a matter of fact, drying of bentonite is common in the fabrication of bentonite blocks or pellets.



Note that the figure represents a situation where a thermal gradient exists from the canister towards the rock. In this situation, water in bentonite pores is driven outwards by vapour diffusion.

**Figure B.6-1.** Schematic radial profile of water content ( $\theta_w$ ) and vapour concentration ( $C_v$ ) in bentonite and at the interface supercontainer/near-field rock, with and without the effect of steel corrosion (vapour sink).

The steady-state transport rate of vapour from a source of water, located at some radial distance  $r_o$ , to the sink (supercontainer shell), located at the radius  $r_{s,i}$ , may be estimated as follows:

$$Q_v = 2\pi D_v S_g l_s \frac{C_v(r_o) - C_v(r_{s,i})}{\ln(r_o / r_{s,i})} \quad (\text{Eq. B.6-3})$$

with:

- $Q_v$  vapour transport rate [ $\text{kg a}^{-1}$ ]
- $D_v$  effective vapour diffusion constant of porous medium [ $\text{m}^2 \text{a}^{-1}$ ] (Table B.1-5)
- $S_g$  average gas saturation of the porous medium [-]
- $C_v$  vapour concentration in gas phase [ $\text{kg m}^{-3}$ ]
- $l_s$  length of supercontainer [m] (Table B.1-1)
- $r_{sc}$  radius of supercontainer, taken to be  $(r_{s,i} + r_{s,o})/2$  [m] (Table B.1-1)
- $r_o$  radial location of water source [m].

The concentration of vapour in the gas phase is given by:

$$C_v = \frac{N_w P_{v,sat} r_H}{R_0 T} \quad (\text{Eq. B.6-4})$$

with:

- $P_{v,sat}$  saturated vapour pressure [Pa]
- $r_H$  relative humidity [-]
- $N_w$  molar weight of water [ $\text{kg mol}^{-1}$ ] (Table B.1-5)
- $R_0$  universal gas constant [ $\text{J K}^{-1} \text{mol}^{-1}$ ] (Table B.1-5)
- $T$  temperature [K].

In the case of vapour diffusion from the near-field rock into the drift, the vapour pressure gradient is spanned by a relative humidity of 1 within the rock, assumed to be saturated at a radial distance of 0.1 m from the rock surface, and by a relative humidity of 0.6 near to the steel surface of the supercontainer. Note that corrosion is strongly reduced for relative humidities below 0.6. In the presence of hygroscopic salts on the steel surface, the threshold value for the relative humidity above which significant corrosion can occur may be even lower (in the order of 0.4). The saturated vapour pressure at an assumed temperature of 60°C at the steel surface is about  $2 \times 10^4$  Pa. Based on these values and on an average gas saturation in the pores of the rock matrix of 0.1, one obtains:

$$Q_v = \begin{cases} 0.010 \text{ kg a}^{-1} & (r_H = 0.6) \\ 0.015 \text{ kg a}^{-1} & (r_H = 0.4) \end{cases} \quad (\text{Eq. B.6-5})$$

This is about an order of magnitude lower than the minimal rate of water supply (0.1 litres per year, or 0.1 kg per year) that is required to maintain corrosion at a rate of 1  $\mu\text{m}$  per year.

In the case vapour diffusion within the pores of the buffer an additional equation is needed to relate the relative humidity within the buffer pores to the total suction potential,  $\psi$  [Pa]. Neglecting osmotic effects, this relationship reduces to Kelvin's equation:

$$\psi = \frac{\rho_w R_0 T}{N_w} \ln(r_H) \quad (\text{Eq. B.6-6})$$

For an initial water content of 10% by weight, a total suction potential of -70 MPa /SKB 2006b/ to -100 MPa (/JNC 2000/, Figure B5-13) is reported. The total suction potential does not show a strong dependence on temperature (/JNC 2000/, Figure B5-11). From Eq. B.6-6, the relative humidity within bentonite pores can be calculated (Table B.6-1).

**Table B.6-1. Relative humidity within bentonite pores as a function of the water content and of the temperature.**

Water content [% w]	Total suction potential [MPa]	Temperature [°C]	Relative humidity [-]
10	-70	10 <sup>1</sup>	0.58
	-100	10	0.46
20	-20	10	0.86
	-70	60 <sup>2</sup>	0.63
-100		60	0.52
20	-20	60	0.87
10	-70	80 <sup>3</sup>	0.65
	-100	80	0.54
20	-20	80	0.88

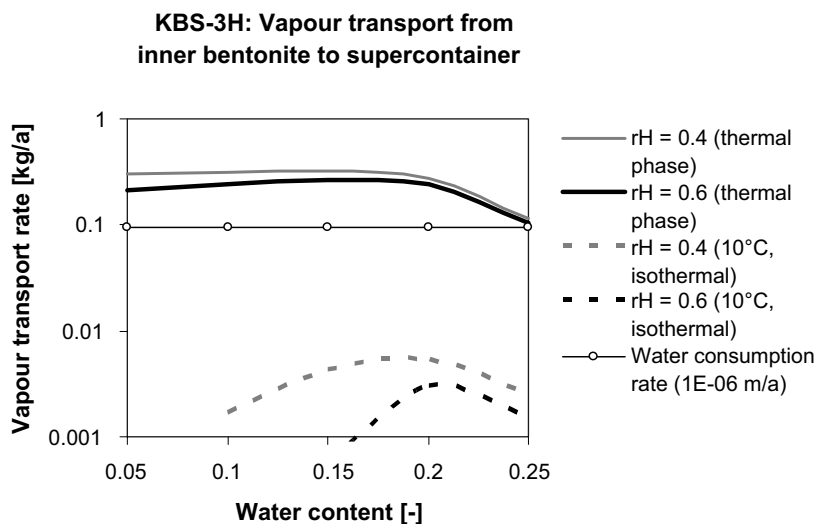
<sup>1</sup> Ambient rock temperature at 400 m depth.

<sup>2</sup> Average temperature of supercontainer during early thermal phase.

<sup>3</sup> Average temperature of inner bentonite during early thermal phase.

From the values in Table B.6-1, and using Eqs. B.6-3, B.6-4 and B.6-6, the rate of vapour transport from the inner part of the buffer to the steel surface of the supercontainer (where a constant relative humidity of 0.6 or 0.4 is assumed) can be calculated. The resulting vapour transport rates are presented in Figure B.6-2 as a function of the average water content and of the relative humidity at the steel surface. Two sets of curves are shown:

- Thermal phase (upper curves): Temperature of 80°C and a saturated vapour pressure of about  $5 \times 10^4$  Pa in the inner part of the bentonite buffer (halfway between the canister and the supercontainer); temperature of 60°C and a saturated vapour pressure of about  $2 \times 10^4$  Pa near the supercontainer shell.
- Isothermal conditions (lower curves): Uniform temperature of 10°C throughout the near field, saturated vapour pressure of about  $1.2 \times 10^3$  Pa.



Note that the initial water content inside the supercontainer is 10–18% by weight.

**Figure B.6-2.** Vapour transport from the inner part of the buffer to the supercontainer shell as a function of the water content in buffer (by weight) for the transient thermal phase (upper curves) and for isothermal conditions after the transient thermal phase.

The vapour transport rate during the transient thermal phase is a factor of 1–3 higher than the minimal rate of water supply ( $0.1 \text{ kg a}^{-1}$ ) that is required to maintain corrosion at a rate of  $1 \text{ } \mu\text{m a}^{-1}$ . After roughly 100 years of cooling, the heat flux from the canister is reduced to about half its initial value. By then, the supply of water vapour has dropped to values below  $0.1 \text{ kg a}^{-1}$ . In the course of further cooling, the temperature gradient gradually decreases until – after a few thousand years – the temperature returns to ambient conditions (about  $10^\circ\text{C}$ ). For these conditions, the vapour transport rate is below  $0.01 \text{ kg a}^{-1}$ . Some additional water vapour is provided by the rock (see above) and from the two adjacent distance blocks towards the supercontainer. The latter contribution has not been quantified, but is considered to be smaller than the water vapour supply from the buffer due to geometrical reasons.

Table B.6-2 summarises the estimated water supply rates from the near-field rock and from the inner part of buffer to the supercontainer shell for various conditions and transport processes.

## B.7 Impact of uncertainties in the generation and transport of sulphide on canister lifetime

### Introduction

The interaction of the copper canister with sulphide from the groundwater is considered to be the most important canister corrosion process in the long term (i.e. after oxygen-free conditions are established). Critically, the barrier to sulphide transport provided by the buffer severely limits the rate at which sulphide can reach the canister surface. Scoping calculations reported in Appendix B.2 that indicate canister lifetimes exceeding the minimum design lifetime of  $10^5$  years by more than an order of magnitude, even in the case that the drift is intersected near the canister location by a fracture with a transmissivity at the higher end of the expected range – i.e. about  $3 \times 10^{-9} \text{ m}^2 \text{ s}^{-1}$  (although, as noted in Appendix B.2, the possibility of some higher transmissivity fractures intersecting the drift near a supercontainer location cannot be excluded on the basis of the current 0.1 litres per minute inflow criterion). In this appendix, the impact on canister lifetime of features and processes that could perturb sulphide concentration at the buffer/rock interface, and transport of sulphide across the interface and through the buffer, are evaluated.

Methane and hydrogen are present naturally in the groundwater and hydrogen will also be generated by the corrosion of the steel repository components, principally the supercontainer shell. These gases could participate in the reduction of groundwater sulphate to sulphide in the presence of sulphate reducing bacteria, increasing the sulphide concentration (Section 5.3.1).

**Table B.6-2. Water supply rates from the near-field rock and from the inner part of buffer to the supercontainer shell.**

Situation	Critical parameter	Water supply	Time period
Drift sections in permeable and moderately tight rock	Hydraulic conductivity above about $10^{-11} \text{ m s}^{-1}$	unlimited <sup>1</sup>	0 to 4,000 years (steel corrosion rate $1 \text{ } \mu\text{m a}^{-1}$ )
Drift sections in tighter rock			
advective inflow	Hydraulic gradient	unlimited <sup>1</sup>	0 to a few 100 years (up to gas/water pressure equilibration)
vapour transport	Vapour pressure gradient	limited <sup>2</sup>	from a few 100 years until the end of steel corrosion (several 1,000 to several 10,000 years, depending on the effective corrosion rate)

<sup>1</sup> Water supply is sufficient to maintain corrosion at a rate of  $1 \text{ } \mu\text{m a}^{-1}$ .

<sup>2</sup> Water supply is, however, likely sufficient to maintain corrosion at a rate of  $0.1 \text{ } \mu\text{m a}^{-1}$ .



Features and processes with the potential to perturb the transport of sulphide across the buffer/rock interface, and through a limited layer of buffer or rock adjacent to the interface, include:

- thermally-induced rock spalling (Section 5.4.5);
- the presence of potentially porous or fractured corrosion products in contact with the drift wall relatively tight drift sections (see Section 5.5.2);
- chemical interaction of the buffer with these corrosion products (Sections 5.6.4 and 6.5.3); and
- chemical interaction of the buffer with high-pH leachates from cementitious components (Section 5.6.5).

In addition, limited piping and erosion during the operational phase of the repository and during saturation of the drift (Section 5.5.6) could lead to a loss of buffer density and an increase in the rate of solute diffusion across the buffer. Finally, chemical erosion of the buffer by glacial melt-water (Section 7.4.3) has the potential to perturb a greater thickness of the buffer, and to give rise to advective transport conditions between the canister and the drift wall. It may, however, still require considerable time for a canister to fail after advective conditions are established, particularly if the erosion rate is limited by the supply of sulphide from the rock.

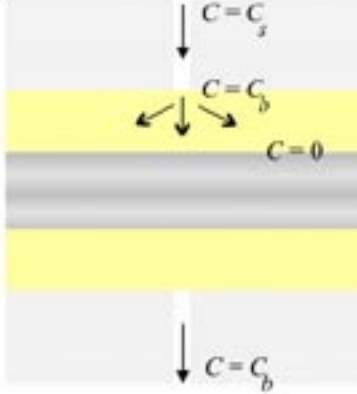
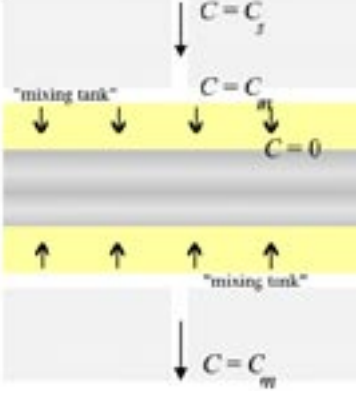
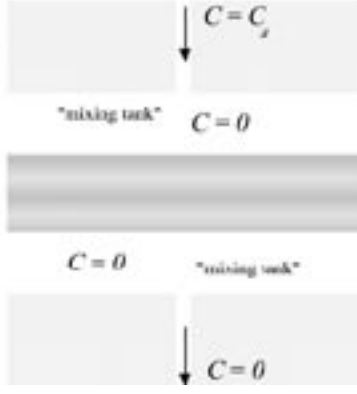
The impact of these features and processes on canister lifetime is assessed in the present appendix. The impact on radionuclide transport subsequent to canister failure is addressed by the radionuclide release and transport calculations described in the Radionuclide Transport Report /Smith et al. 2007/.

### Cases considered

The cases addressed in the scoping calculations described in this appendix are shown schematically in Figure B.7-1. In all cases, it is assumed that a drift section containing a canister is intersected perpendicularly by a single transmissive fracture.

In Case (a), the above-mentioned features and processes are assumed to cause no significant perturbation to the flow in the fracture around the perimeter of the drift.  $C_s$  [ $\text{kg m}^{-3}$ ] is defined as the concentration of sulphide in groundwater approaching the drift. Some of this sulphide diffuses into the buffer and is consumed by reaction with the copper, and some passes into the downstream part of the fracture. Diffusive mass transfer between the fracture and the buffer takes place in a thin “boundary layer” in the fracture along its interface with the buffer. The concentration in the boundary layer is modelled as being constant ( $C_b$  [ $\text{kg m}^{-3}$ ]) around the perimeter of the drift. Groundwater exiting the boundary layer and passing into the downstream part of the fracture also has a sulphide concentration  $C_b$ . All sulphide reaching the canister surface is assumed to be consumed by reaction with copper, so that a zero sulphide concentration boundary condition is applied at the surface. Two variants are considered: (i), in which diffusion in the buffer is unperturbed by processes such as piping and erosion during early evolution, and (ii), in which the rate of diffusion in the buffer is assumed to be increased by such processes.

In Case (b), the above-mentioned features and processes give rise to a highly conductive annular zone at the buffer/rock interface. This zone is treated as a mixing tank, within which sulphide has a constant concentration  $C_m$  [ $\text{kg m}^{-3}$ ], and from which sulphide can diffuse into the buffer or pass into the downstream part of the fracture. The length of this mixing tank along the drift is set equal to the canister length. Groundwater exiting the mixing tank and passing into the downstream part of the fracture also has a sulphide concentration  $C_m$ . Again, reaction with copper is assumed to reduce the sulphide concentration to zero at the canister surface. Two variants are considered: (i), in which the mixing tank has negligible thickness, and (ii), in which it occupies 10% of the buffer thickness.

Case	Description
<p>(a)</p> 	<p>No perturbation to buffer/rock interface</p> <ul style="list-style-type: none"> <li>(i) diffusion in buffer unperturbed</li> <li>(ii) rate of diffusion in buffer increased, e.g. by piping and erosion during early evolution</li> </ul>
<p>(b)</p> 	<p>Perturbed interface zone, treated as mixing tank:</p> <ul style="list-style-type: none"> <li>(i) thickness of zone treated as negligible</li> <li>(ii) zone assumed to occupy 10% of buffer thickness</li> </ul>
<p>(c)</p> 	<p>The entire buffer is treated as mixing tank</p>

**Figure B.7-1.** Cases considered in the current scoping calculations. Symbols are defined in the main text.

In Case (c), the mixing tank is assumed to extend throughout the buffer (e.g. due to loss of buffer mass by chemical erosion). Reaction with copper is pessimistically assumed to consume all sulphide entering the mixing tank. As in Cases (a) and (b), the rate at which sulphide enters the mixing tank is controlled by its supply from the host rock via the fracture, in which sulphide has a concentration  $C_s$ .

In Cases (a), (b) and (c), corrosion is evaluated as a function of sulphide concentration in the groundwater. The possible impact of sulphate-reducing bacteria on the concentration of sulphide in groundwater approaching the drift in the presence of hydrogen from the corrosion of steel components is also considered. The possible impact of dissolved hydrogen and methane naturally present in the groundwater remains an issue for further investigation (Chapter 12).

## Mathematical models

### Case (a)

In Case (a), the mass of sulphide reaching the boundary layer by advection along the fracture must balance the mass lost from the boundary layer by advection in out-flowing water, and the mass lost by diffusion into the buffer and reaction with copper.

The rate at which sulphide enters the boundary layer from the approaching flowing water is  $C_s Q_b$  [kg a<sup>-1</sup>], and the rate at which sulphide in the boundary layer is advected downstream of the drift is  $C_b Q_b$  [kg a<sup>-1</sup>], where  $Q_b$  [m<sup>3</sup> a<sup>-1</sup>] an equivalent flowrate given:

$$Q_b = \frac{A_{frac}}{\pi} \sqrt{\frac{2D_w T \cdot i_0}{r_t b_v}} \quad (\text{Eq. B.7-1})$$

(see e.g. Eq. 3-10 in /Vieno and Nordman 2000/), with:

$T$  the fracture transmissivity [m<sup>2</sup> s<sup>-1</sup>] (set an assumed moderately pessimistic value of  $3 \times 10^{-9}$  m<sup>2</sup> s<sup>-1</sup>, see Appendix B.2)

$b_v$  the fracture half aperture [m] (related to transmissivity using Eq. B.2-2)

$r_t$  the drift radius [m] (Table B.1-1)

$i_0$  the hydraulic gradient [-] (Table B.1-3).

$A_{frac}$  [m<sup>2</sup>] is the area of intersection of the fracture with the drift and is given by:

$$A_{frac} = 4\pi b_v r_t \quad (\text{Eq. B.7-2})$$

If  $Q_f$  [m<sup>3</sup> a<sup>-1</sup>] is the transfer coefficient between the boundary layer and the canister surface through the buffer (i.e. the rate of mass loss by diffusion into the buffer and reaction with copper is  $C_b Q_f$ ), then mass balance requires that:

$$C_s Q_b = C_b Q_b + C_b Q_f \quad (\text{Eq. B.7-3})$$

It is shown in Appendix B.8 that the transfer coefficient  $Q_f$  may be approximated by:

$$Q_f \approx \frac{\pi D_{eff} A_{frac}}{2b_v \log_e \left( \frac{2(r_t - r_c)}{b_v} \right)} \quad (\text{Eq. B.7-4})$$

where  $r_c$  [m] is the canister radius (Table B.1-1) and  $D_{eff}$  [m<sup>2</sup> s<sup>-1</sup>] is the effective diffusion coefficient of sulphide ions in the buffer, which is set, in variant (i), to:

- $D_e$  [m<sup>2</sup> s<sup>-1</sup>], i.e. the effective diffusion coefficient of anions in the unperturbed buffer (Table B.1-2);

and, in variant (ii), which represents an increased rate of buffer diffusion due to loss and redistribution of buffer mass by piping and erosion during early evolution, to:

- $\varepsilon D_w$  [ $\text{m}^2 \text{s}^{-1}$ ], where  $\varepsilon$  is the buffer porosity (Table B.1-2), and  $D_w$  is the diffusion coefficient of ions in free water (Table B.1-5).

Eq. B.7-4 is slightly different to the equation for  $Q_f$  given by Eq. 3-9 in /Vieno and Nordman 2000/, and different again to that given in /Neretnieks 1985/ due to minor differences in the way the problem is formulated. For the parameter ranges used here, the three expressions give similar results (see e.g. Appendix B.8, Figure B.8-2).

It is also shown in Appendix B.8 that the rate of arrival of sulphide at the canister surface at the location where this is the highest (directly opposite the fracture/drift line of intersection) is:

$$f_{\max} = \frac{\pi D_{\text{eff}} C_b}{2(r_t - r_c) \log_e \left( \frac{4(r_t - r_c)}{b_v} \right)} \quad (\text{Eq. B.7-5})$$

From Eqs. B.7-3 and B.7-5:

$$f_{\max} = \frac{\pi D_{\text{eff}} C_s}{2(r_t - r_c) \log_e \left( \frac{4(r_t - r_c)}{b_v} \right)} \frac{1}{Q_b + Q_f} \quad (\text{Eq. B.7-6})$$

Noting that 2 moles of copper are corroded per mole of sulphide arriving at the canister surface, the maximum rate of copper corrosion ( $j_a$  [ $\text{m a}^{-1}$ ]) is:

$$j_a = \frac{2 f_{\max} N_c}{\rho N_s} \quad (\text{Eq. B.7-7})$$

where  $\rho$  [ $\text{kg m}^{-3}$ ] is the density of copper, and  $N_c$  and  $N_s$  are, respectively, the molar weight of copper and sulphide (Table B.1-5).

Finally, the canister lifetime ( $t_a$  [a]) is given by:

$$t_a = \frac{d}{c_{\text{local}} j_a} \quad (\text{Eq. B.7-8})$$

where  $d$  [m] is the canister wall thickness (Table B.1-1) and  $c_{\text{local}}$  is a factor for uneven corrosion (Table B.1-5).

### Case (b)

In Case (b), the mass of sulphide reaching the mixing tank by advection along the fracture must balance the mass lost from the boundary layer by advection in out-flowing water, and the mass lost by diffusion into the buffer and reaction with copper. If the rate of groundwater flow through the mixing tank is  $Q_m$  [ $\text{m}^3 \text{a}^{-1}$ ], and  $Q_{fm}$  [ $\text{m}^3 \text{a}^{-1}$ ] is the transfer coefficient between the canister surface and the mixing tank through the buffer (i.e. the rate of mass loss by diffusion into the buffer and reaction with copper is  $Q_{fm} C_m$ ), then:

$$C_s Q_m = C_m Q_m + Q_{fm} C_m \quad (\text{Eq. B.7-9})$$

$Q_m$  depends on the hydraulic conductivity and thickness of the mixing tank. If the product of these parameters is sufficiently large, however,  $Q_m$  tends towards a limiting value:

$$Q_m = 4T i_0 r_t \quad (\text{Eq. B.7-10})$$

i.e. the mixing tank “captures” the flow from a portion of the fracture that is twice the drift diameter (note: this factor of 2 is due to a convergence of flow lines towards the drift).

If the inner radius of the mixing tank is  $r_m$  [m], the concentration in the buffer inside this boundary,  $C$ , is given by the solution to Laplace’s equation (i.e. the steady-state diffusion equation) in cylindrical geometry:

$$C = C_m \frac{\log_e \left( \frac{r'}{r_c} \right)}{\log_e \left( \frac{r_m}{r_0} \right)} \quad (\text{Eq. B.7-11})$$

where  $r'$  [m] is the radial distance from the drift axis. The rate of transport of sulphide across the buffer is:

$$Q_{fm} C_m = -2\pi r' l_c D_e \frac{dC}{dr'} = 2\pi l_c D_e C_m \frac{1}{\log_e \left( \frac{r_m}{r_c} \right)} \quad (\text{Eq. B.7-12})$$

where  $l_c$  [m] is the canister length (Table B.1-1).

From Eq. B.7-9:

$$C_m = C_s \frac{Q_m}{Q_m + Q_{fm}} \quad (\text{Eq. B.7-13})$$

The rate of arrival of sulphide at the canister surface is given by:

$$Q_{fm} C_m = C_s \frac{Q_{fm}}{1 + Q_{fm} / Q_m} \quad (\text{Eq. B.7-14})$$

The maximum rate of copper corrosion ( $j_b$  [m a<sup>-1</sup>]) is:

$$j_b = \frac{C_s}{\pi r_c l_c \rho} \frac{N_c}{N_s} \frac{Q_{fm}}{1 + Q_{fm} / Q_m} \quad (\text{Eq. B.7-15})$$

$Q_{fm}$  is evaluated using Eq. B.7-12. In variant (i),  $r_m$  is set equal to  $r_t$ . In variant (ii), it is set equal to  $r_t - 0.1(r_t - r_c)$ .

The canister lifetime in this case ( $t_b$  [a]) is:

$$t_b = \frac{d}{c_{local} j_b} \quad (\text{Eq. B.7-16})$$

### Case (c)

In Case (c), all of the sulphide that is collected by the mixing tank is assumed to contact the canister surface and to react with it. Any limitation by the kinetics of the corrosion reaction is thus pessimistically neglected. The rate of arrival of sulphide at the canister surface ( $F_d$  [kg a<sup>-1</sup>]) is given by:

$$F_d = C_s Q_m \quad (\text{Eq. B.7-17})$$

The maximum rate of copper corrosion ( $j_c$  [ $\text{m a}^{-1}$ ]) is:

$$j_c = \frac{F_d}{\pi r_c l_c \rho} \frac{N_c}{N_s} \quad (\text{Eq. B.7-18})$$

and the canister lifetime in this case ( $t_c$  [a]) is:

$$t_c = \frac{d}{c j_c} \quad (\text{Eq. B.7-19})$$

### Calculated canister failure time as a function of sulphide concentration in the water

Figure B.7-2 shows canister failure time as a function of groundwater sulphide concentration for each of the cases described in Figure B.7-1. With no perturbation of the buffer/rock interface, a very long canister lifetime in the order of millions of years is calculated (see also Figure B.2-2), which is only slightly reduced if an increased sulphide diffusion coefficient in the buffer is assumed (e.g. due to early piping and erosion). If iron/bentonite interaction results in a highly conductive “mixing tank” around the buffer/rock interface, the resulting higher flux of sulphide to the canister surface results in a significantly reduced canister lifetime. Canister lifetime is further reduced, though only slightly, if the mixing tank extends to a finite depth into the buffer (10% of the buffer thickness). The impact of treating the entire buffer thickness as a mixing tank is also quite limited, indicating that the transport resistance provided by the buffer does not dominate the transport of sulphide to the canister surface. The canister lifetime falls below one million years only if sulphide concentrations significantly above the currently observed maximum level at Olkiluoto are assumed.

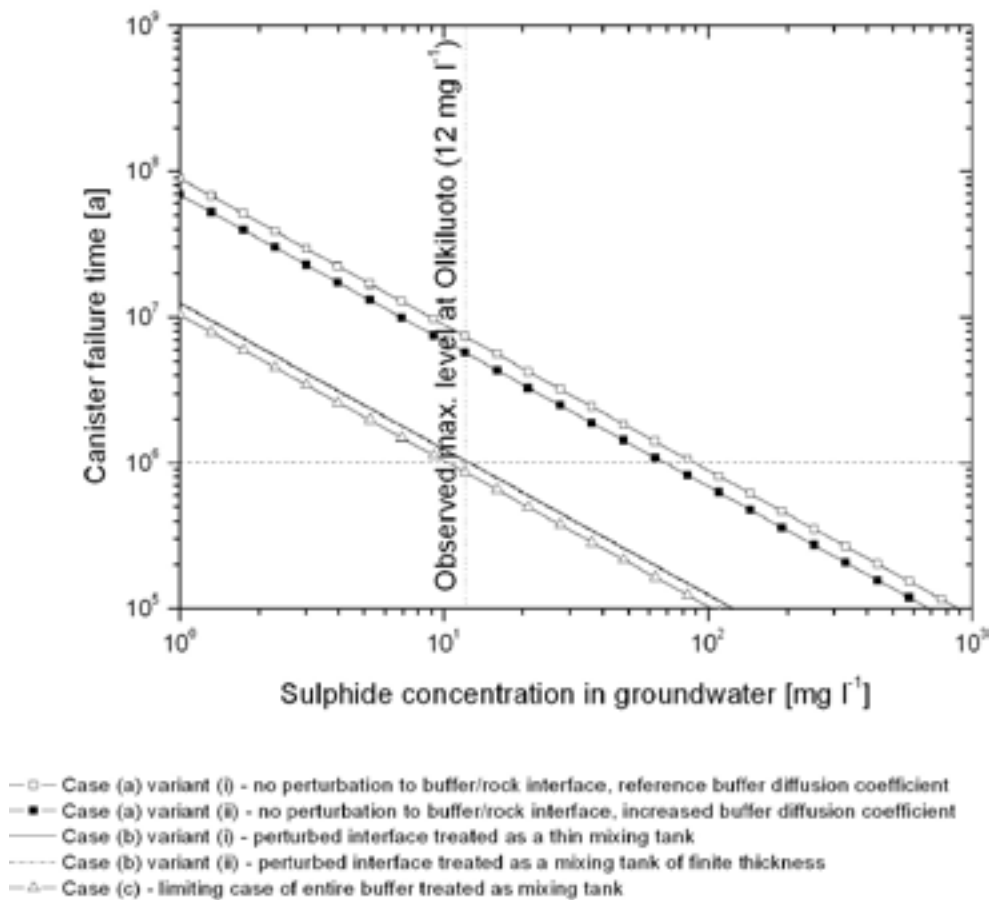


**Figure B.7-2.** Canister failure time as a function of groundwater sulphide concentration for the cases defined in Figure B.7-1. Note that the results for case (b), variants (i) and (ii), approximately coincide.



## Impact of hydrogen from steel corrosion

The possible impact of sulphate-reducing bacteria on the concentration of sulphide in groundwater approaching the drift in the presence of hydrogen from the corrosion of steel components is considered below, assuming a steel corrosion rate of 1  $\mu\text{m}$  per year (Table B.1-5) and a variant rate of 0.1  $\mu\text{m}$  per year (Appendix A of /Gribi et al. 2007/).

The conversion of steel to magnetite (the expected initial corrosion product) proceeds according to the reaction:



and results in the production of hydrogen gas. Corrosion at a rate of  $R$  [ $\text{m a}^{-1}$ ] produces hydrogen at a rate of 9.5 moles per year for a corrosion rate of 1  $\mu\text{m}$  per year, and 0.95 moles per year for a corrosion rate of 0.1  $\mu\text{m}$  per year (see Table 5-9 of /Gribi et al. 2007/). The largest contribution to hydrogen gas generation comes from the supercontainer shell (there are smaller contributions from other steel components external to the canisters, i.e. the fixing rings and spray and drip shields). The thickness of the supercontainer shell is 8 mm. Assuming this to be corroded from both sides, the hydrogen generation period is 4,000 years for a corrosion rate of 1  $\mu\text{m}$  per year, and 40,000 years for a corrosion rate of 0.1  $\mu\text{m}$  per year.

In Case (a), sulphate enters the boundary layer at the buffer/rock interface at a rate  $C_{\text{sulphate}} Q_b$  moles per year, where  $C_{\text{sulphate}}$  [ $\text{mol m}^{-3}$ ] is the sulphate concentration in groundwater. According to /Andersson et al. 2007/, the current sulphate concentration below around 300 m depth at Olkiluoto does not exceed about 100 mg per litre (Figure 11-8 of /Andersson et al. 2007/). Ionic strengths are expected to remain below this value throughout the period considered, as illustrated, for example, in Figure 4-1.  $Q_b$ , evaluated using Eq. B.7-1, is about  $1.6 \times 10^{-4} \text{ m}^3 \text{ a}^{-1}$ , and so the rate at which sulphate enters the boundary layer is not expected to exceed  $100 \text{ g m}^{-3} \times 1.6 \times 10^{-4} \text{ m}^3 \text{ a}^{-1} / (96 \text{ g per mole}) = 1.7 \times 10^{-4}$  moles per year, which will require  $6.7 \times 10^{-4}$  moles per year of hydrogen to reduce it to sulphide according to the reaction:



Thus, in Case (a), as long as hydrogen production persists, there is more than enough hydrogen present to reduce this sulphate to sulphide, even for a low corrosion rate of 0.1  $\mu\text{m}$  per year. Even in Case (c), which represents an extreme case of buffer perturbation where the entire buffer is treated as a mixing tank, sulphate enters the mixing tank at a rate  $C_{\text{sulphate}} Q_m$  moles per year.  $Q_m$ , evaluated using Eq. B.7-10, is about  $3.5 \times 10^{-3} \text{ m}^3 \text{ a}^{-1}$ , and so the maximum rate at which sulphate enters the mixing tank is  $100 \text{ g m}^{-3} \times 3.5 \times 10^{-3} \text{ m}^3 \text{ a}^{-1} / (96 \text{ g per mole}) = 3.6 \times 10^{-3}$  moles per year, which will require 0.014 moles per year of hydrogen to reduce it to sulphide. Thus again, as long as hydrogen production persists, there is more than enough hydrogen present to reduce this sulphate to sulphide. The impact of this sulphide is, however, confined to the duration of hydrogen generation.

In Case (a), if sulphate migrating through a fracture is converted to sulphide and this sulphide then enters the boundary layer at a rate of  $2.1 \times 10^{-4}$  moles per year, the resultant canister lifetime, according to Eq. B.7-8, will be about 900,000 years for variant (i) (reference diffusion coefficient in buffer) and 700,000 years for variant (ii) (increased diffusion coefficient due, e.g., to piping and erosion). If hydrogen generation ceases at 4,000 years (1  $\mu\text{m}$  per year steel corrosion rate), the canister will only be between 0.4% and 0.6% corroded at this time. The corresponding range for a 0.1  $\mu\text{m}$  per year corrosion rate is 4% to 6%. The same equations apply, and the same results are obtained, if sulphate is converted to sulphide at or near the surfaces of the corroding steel surfaces, rather than in a host-rock fracture. Thus, copper thickness is only slightly reduced by corrosion during the period of hydrogen generation.

In Case (c), with the entire buffer is treated as a mixing tank and with sulphate converted to sulphide and entering the mixing tank at a rate of  $4.5 \times 10^{-3}$  moles per year, the resultant canister lifetime, according to Eq. B.7-19, will be about 100,000 years. If hydrogen generation ceases at 4,000 years (1  $\mu\text{m}$  per year steel corrosion rate), the canister will only be about 4% corroded

at this time. The corresponding value for a 0.1 µm per year corrosion rate is 40%. Assuming the sulphide concentration then falls currently observed maximum value of about 12 mg per litre, based on the results shown in Figure B.7-2, the remaining 60% will require about another 600,000 years to corrode before the canister fails. Thus, even in this highly pessimistic case, an overall canister lifetime of several hundred thousand years is expected. Only in the case of a high sulphide concentration of 100 mg per litre being maintained, e.g. by microbial activity, for some tens of thousands of years is canister lifetime reduced below about 100,000 years. This is not expected to occur as a result of hydrogen from the corrosion of steel, since all steel components external to the canister will corrode away within a shorter time frame. Methane and hydrogen naturally present in the groundwater could, in principle, play a role in sustaining microbial activity over a longer period. As noted in Chapter 12, the impact of these dissolved gasses on sulphate reduction by microbes is an issue for both KBS-3H and KBS-3V and requires further investigation.

### **Limitations of the scoping calculations**

In the scoping calculations presented in this appendix, it is assumed that the groundwater is the only source of sulphate or sulphide. In reality, pyrite in the buffer may also provide a source of sulphide (although part of this may be oxidised before and after emplacement in the drift, and act as a source of sulphate which might later be reduced to sulphide). In the case of a KBS-3V deposition hole, sulphide originating from pyrite dissolution has been estimated to lead to, at most, 0.1 mm of corrosion at the sides of the canister, and 0.5 mm at the top /Hedin 2004/. This estimate is based on a simple diffusive transport model in which sulphide concentration in the buffer is solubility limited, with 0.07+/-0.05 weight % pyrite assumed to be present in the buffer. Thus, corrosion caused by the pyrite initially present in the buffer has negligible impact on the copper thickness in KBS-3V, and the same conclusion is expected to apply to KBS-3H.

The scoping calculations also assume that groundwater is the only source of sulphate available for reduction to sulphide in the presence of hydrogen and sulphate-reducing bacteria. In reality, dissolution of gypsum in the buffer could also provide a source of sulphate internally within the buffer. This could migrate by diffusion to the buffer/rock interface, where it could be reduced to sulphide by sulphate reducing bacteria, increasing the overall sulphide concentration. While neglecting this source of sulphide is non-conservative, it is further (and conservatively) assumed that sulphide from whatever source passing the buffer/rock interface and migrating through the buffer remains in solution (is not solubility limited) and does not react with any porewater constituents or repository components other than the copper canister. In reality, the large amount of iron present in KBS-3H at the buffer/rock interface is likely to react with sulphide, forming iron sulphides that have low solubility and reducing the flux of sulphide to the canister surface. Furthermore, reaction with sulphide may increase the corrosion rate of the steel components, and reduce the period of hydrogen generation during which sulphate may be reduced to sulphide in the presence of hydrogen and sulphate-reducing bacteria.

Finally, it is assumed that hydrogen from corrosion of steel components participates directly in the reduction of sulphate to sulphide. In reality, the hydrogen generated may also oxidise any carbon dioxide present in the system and form methane ( $4\text{H}_2 + \text{CO}_2 \rightarrow \text{CH}_4 + 2\text{H}_2\text{O}$ ), which may later play a role in the microbial reduction of sulphate. The overall impact of hydrogen production on canister corrosion is, however, likely to be similar.

Overall, there are several simplifying assumptions in these scoping calculations presented in this appendix that could result in somewhat higher or lower canister lifetimes than those calculated. The provisional finding, however, is that corrosion is unlikely to result in a canister lifetime of less than several hundred thousand years, even in cases where mass transport in the buffer is severely perturbed.

## B.8 Maximum mass transfer rate to the canister surface from an intersecting fracture

The steady-state concentration distribution between a canister surface and an intersecting fracture has been derived by /Neretnieks 1985/ and, for slightly different boundary conditions, by /Liu and Neretnieks 2004/. The general solution involves a sum over infinite terms and equation roots that must be obtained numerically.

In the present context, the entire concentration distribution is not of interest. Rather, it is the maximum sulphide concentration gradient at the canister surface (i.e. the gradient along a line on the canister surface directly opposite the fracture/drift line of intersection) and the transfer coefficient through the buffer between the canister surface and the buffer/rock interface that are required, and much simpler approximate expressions for these quantities may be obtained.

The steady-state concentration within the buffer is governed by Laplace's equation (i.e. the steady-state form of the diffusion equation):

$$\nabla^2 C = 0 \quad (\text{Eq. B.8-1})$$

According to the uniqueness theorem, real solutions of Laplace's equation within a bounded region where either concentration (Dirichlet) or flux (Neumann) boundary conditions apply are unique. It follows from the uniqueness theorem that if a solution to Laplace's equation can be found that satisfies the required boundary conditions by any means whatever, then that solution is the correct one since only one solution exists. This observation is the basis of the method of images, which is the approach used to solve the present problem. In the method of images, a system of sources and sinks in a hypothetical unbounded medium is considered such that the boundary conditions required around the more spatially limited physical problem domain are satisfied.

In order to simplify the solution, the curvature of the canister and drift wall surfaces is neglected (as in /Neretnieks 1985/) and the fracture aperture is assumed to be much smaller than the buffer thickness, such that the fracture can be treated as a line source of small but finite radius  $r_D$  [m], shown as a shaded circle in Figure B.8-1. External to this source, and in the absence of other sources or sinks, the concentration gradient is given by the solution to the 1-D form of Laplace's equation:

$$\frac{dC}{dr} = \frac{A}{r} \quad r > r_D \quad (\text{Eq. B.8-2})$$

where  $A$  [ $\text{kg m}^{-3}$ ] is a constant and  $r$  [m] is the distance from the centre of the source in the direction of the canister surface.

In order to maintain a zero concentration at the canister surface, an equal and opposite line sink (represented by an open circle) is placed a distance  $\Delta$  below the canister surface, i.e. a distance  $2\Delta$  below the line source representing the fracture, where:

$$\Delta = (r_i - r_e) \quad (\text{Eq. B.8-3})$$

This sink, however, leads to a non-zero concentration gradient in the  $r$  direction at the drift wall, which requires a further sink to be considered at a distance  $2\Delta$  above the line source representing the fracture. This, in turn, requires a further source to be considered below the canister surface in order to maintain a zero concentration at this surface. The resulting 1-D array of sources and sinks is illustrated in Figure B.8-1. The system of sources and sinks extends infinitely above and below the buffer, but the sources and sinks have a diminishing effect on the concentration distribution within the buffer as distance from the buffer increases.

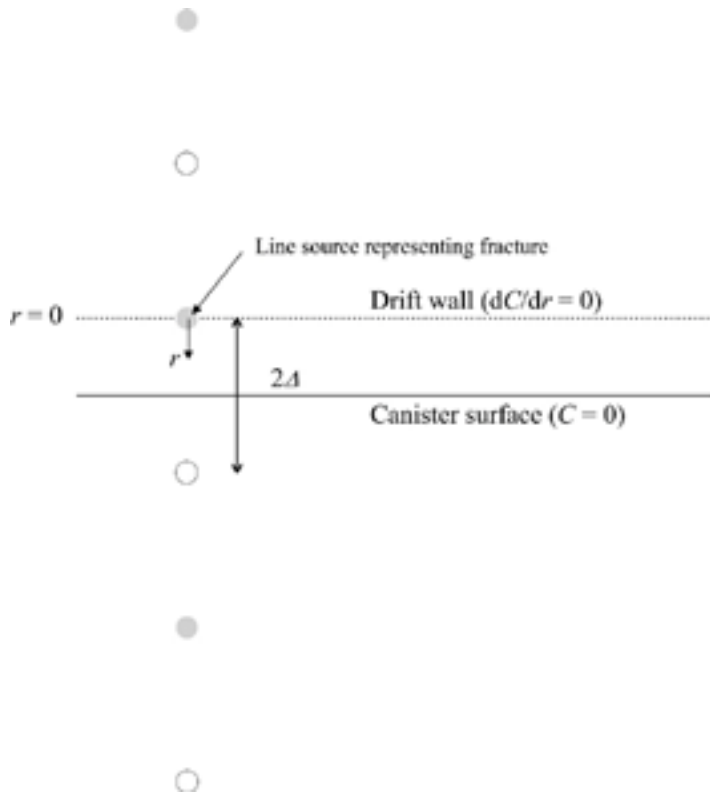


**Figure B.8-1.** Array of image sources (shaded circles) and sinks (open circles) extending infinitely along the  $r$ -axis and representing the concentration field in the buffer.

Considering the entire array of sources and sinks, the concentration gradient at a point inside the buffer at a distance  $r$  from the fracture is thus given by:

$$\frac{dC}{dr} = A \left[ \left( \frac{1}{r} + \frac{1}{2\Delta - r} \right) - \left( \frac{1}{2\Delta + r} + \frac{1}{4\Delta - r} \right) + \dots \right] \quad (\text{Eq. B.8-4})$$

Integrating Eq. B.8-4 from the source, where the concentration is  $C_b$ , along the shortest line to the surface of the canister, where the concentration is zero:

$$C_b = -A \frac{\Delta}{r_D} \left[ (\log_e r - \log_e (2\Delta - r)) - (\log_e (2\Delta + r) - \log_e (4\Delta - r)) + \dots \right] \quad (\text{Eq. B.8-5})$$

$r_D$  [m], the diameter of a source or sink, is set such that the half-surface area is equal to the fracture area intersecting the drift wall:

$$r_D = \frac{2b_v}{\pi} \quad (\text{Eq. B.8-6})$$

Since  $r_D \ll \Delta$ :

$$C_b \approx A \left[ \left( \log_e \left( \frac{r_D}{\Delta} \right) - \log_e 2 \right) - \left( \log_e \left( \frac{2}{3} \right) - \log_e \left( \frac{4}{3} \right) \right) + \dots \right] \quad (\text{Eq. B.8-7})$$

This sum can also be written:

$$\begin{aligned}
C_b &\approx A \left( \log_e \left( \frac{r_D}{\Delta} \right) - \log_e 2 + \sum_{n=1}^{\infty} (-1)^n \left( \log_e \frac{2n}{2n+1} \right) - \log_e \left( \frac{2(n+1)}{2n+1} \right) \right) \\
&= A \left( \log_e \left( \frac{r_D}{\Delta} \right) - \log_e 2 \prod_{n=1}^{\infty} \left( 1 - \frac{1}{4n^2} \right) \right) = A \left( \log_e \left( \frac{r_D}{\Delta} \right) + \log_e \frac{\pi}{4} \right) \\
&= A \log_e \left( \frac{b_v}{2\Delta} \right)
\end{aligned} \tag{Eq. B.8-8}$$

The release rate of sulphide from the source (i.e. the rate of mass loss by diffusion into the buffer) is:

$$Q_f C_b = -D_e A_{frac} \frac{dC}{dr} \Big|_{r=r_D} \approx -D_e A_{frac} \frac{\pi A}{2b_v} \tag{Eq. B.8-9}$$

From Eqs. B.8-8 and B.8-9:

$$Q_f \approx \frac{\pi D_e A_{frac}}{2b_v \log_e \left( \frac{2\Delta}{b_v} \right)} \tag{Eq. B.8-10}$$

The rate of arrival of sulphide at the canister surface at the location where this is the highest (directly opposite the fracture/drift line of intersection) is:

$$f_{max} = -D_e \frac{dC}{dr} \Big|_{r=\Delta} \tag{Eq. B.8-11}$$

From Eq. B.8-4:

$$\frac{dC}{dr} \Big|_{r=\Delta} = -\frac{2A}{\Delta} \sum_{n=1}^{\infty} (-1)^n \frac{1}{2n-1} = \frac{\pi A}{2\Delta} \tag{Eq. B.8-12}$$

From Eqs. B.8-8, B.8-11 and B.8-12:

$$f_{max} = \frac{\pi D_e C_b}{2\Delta \log_e \left( \frac{4\Delta}{b_v} \right)} \tag{Eq. B.8-13}$$

As a test of this solution, the release rate of sulphide from the source calculated using Eq. B.8-10 can be compared with the solutions given in /Neretnieks 1985/ and in /Liu and Neretnieks 2004/. There are some differences in the problem addressed by the two solutions. Most significantly, the solution given by Eq. B.8-10 is for the case where diffusion parallel to the drift is unbounded. The solution given in /Neretnieks 1985/ considers the case of a KBS-3V deposition hole, in which there is mass transfer from the deposition hole to the tunnel backfill, which is located a vertical distance  $a$  [m] above the centre plane of the (horizontal) rock fracture. The solutions should, however, give similar results from the case in which  $a$  is much greater than either  $b$  or  $\Delta$ .

For the case of zero mass transfer from the deposition hole to the tunnel backfill (which is also the case considered in /Liu and Neretnieks 2004/), and for  $b \ll a$ , the solution given in /Neretnieks 1985/ reduces to:

$$Q_f = \frac{D_e A_{frac}}{F} \quad (\text{Eq. B.8-14})$$

where:

$$F \cong 2a \sum_{n=1}^{\infty} \frac{\tanh\left(\frac{n\pi\Delta}{a}\right) \sin\left(\frac{n\pi b}{a}\right)}{(n\pi)^2} \quad (\text{Eq. B.8-15})$$

The ratio of the two solutions is plotted in Figure B.8-2 as a function of  $a$  across a wide range of values.  $b$  is set to  $10^{-4}$  m and  $\Delta$  to 0.4 m. Good agreement (within a few percent) between the solutions is found for all values of  $a$  more than a few metres, such that the condition that  $a$  much greater than either  $b$  or  $\Delta$  is satisfied.

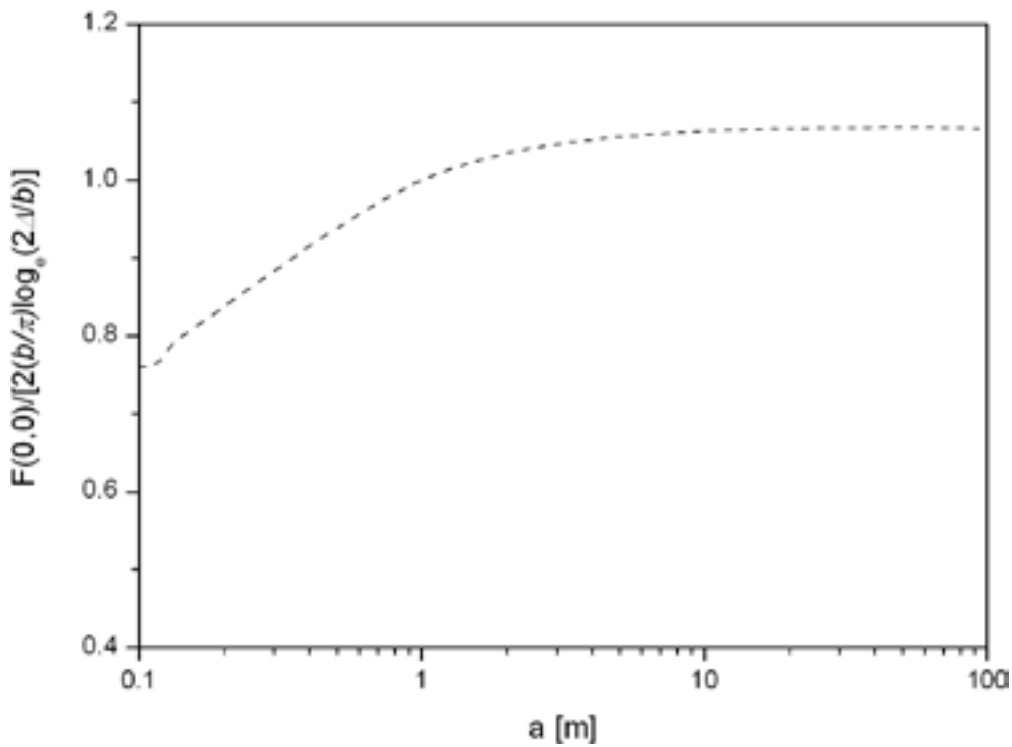


**Figure B.8-2.** Ratio of solutions for the release rate of sulphide from the source, calculated using the solution given in /Neretnieks 1985/ and /Liu and Neretnieks 2004/ and the solution given by Eq. B.8-10.



## References for Appendix B

- Andersson J, Hermansson J, Elert M, Gylling B, Moreno L, Selroos J-O, 1998.** Derivation and treatment of the flow wetted surface and other geosphere parameters in the transport models FARF31 and COMP23 for use in safety assessment. SKB R-98-60, Svensk Kärnbränslehantering AB.
- Andersson J, Ahokas H, Hudson J A, Koskinen L, Luukkonen A, Löfman J, Keto V, Pitkänen P, Mattila J, Ikonen A T K, Ylä-Mella M, 2007.** Olkiluoto Site Description 2006, POSIVA 2007-03. Posiva Oy, Olkiluoto, Finland.
- Autio J, 2007.** KBS-3H Design Description 2005. Posiva Working Report 2007-11 and SKB R-08-29. Posiva Oy, Olkiluoto, Finland and Svensk Kärnbränslehantering AB, Sweden.
- Autio J, Börgesson L, Sandén T, Rönnqvist P-E, Johansson E, Hagros A, Eriksson M, Berghäll J, Kotola R, Parkkinen I, 2007.** KBS-3H Design Description 2006. Posiva Working Report 2007-105 and SKB R-08-32. Posiva Oy, Olkiluoto, Finland and Svensk Kärnbränslehantering AB, Sweden.
- Börgesson L, 1985.** Water flow and swelling pressure in non-saturated bentonite-based clay barriers. Eng. Geology, Vol. 21, pp. 229–237.
- Börgesson L, Johannesson L-E, Hernelind J, 2004.** Earthquake induced rock shear through a deposition hole. Effect on the Canister and the Buffer. SKB TR-04-02, Svensk Kärnbränslehantering AB.
- Börgesson L, Sandén T, Fälth B, Åkesson M, Lindgren E, 2005.** Studies of buffers behaviour in KBS-3H concept; Work during 2002-2004. SKB R-05-50, Svensk Kärnbränslehantering AB.
- Börgesson L, Hernelind J, 2006.** Earthquake induced rock shear through a deposition hole – Influence of shear plane inclination and location as well as buffer properties on the damage caused to the canister. SKB TR-06-43, Svensk Kärnbränslehantering AB.
- Börgesson L, Hernelind J, 2006a.** Consequences of loss or missing bentonite in a deposition hole. SKB TR-06-13, Svensk Kärnbränslehantering AB.
- Gribi P, Johnson L, Suter D, Smith P, Pastina B, Snellman M, 2007.** Safety assessment for a KBS-3H spent nuclear fuel repository at Olkiluoto – Process Report, Posiva Report 2007-09 and SKB R-08-36. Posiva Oy, Olkiluoto, Finland and Svensk Kärnbränslehantering AB, Sweden.
- Hartley L, Hoch A, Jackson P, Joyce S, Mc Carthy R, Rodwell W, Swift B, Marsic N, 2006a.** Groundwater flow and transport modelling during the temperate period for the SR-Can assessment Forsmark area – version 1.2. SKB R-06-98, Svensk Kärnbränslehantering AB.
- Hartley L, Hoch A, Jackson P, Joyce S, Mc Carthy R, Swift B, Gylling B, Marsic N, 2006b.** Groundwater flow and transport modelling during the temperate period for the SR-Can assessment. Laxemar subarea – version 1.2. SKB R-06-99, Svensk Kärnbränslehantering AB.
- Hedin A, 2004.** Integrated near field evolution model for a KBS-3 Repository. SKB R-04-36, Svensk Kärnbränslehantering AB.
- Hedin A, 2005.** An analytic method for estimating the probability of canister/fracture intersections in a KBS-3 Repository. SKB R-05-29, Svensk Kärnbränslehantering AB.
- JNC, 2000.** H12 Project to establish the scientific and technical basis for HLW disposal in Japan – Repository design and engineering technology (Supporting Report 2). Japan Nuclear Cycle Development Institute, Japan.
- Johansson E, Hagros A, Autio J, Kirkkomäki T, 2007.** KBS-3H layout adaptation 2007 for the Olkiluoto site. Posiva Working Report 2007-77 and SKB R-08-31. Posiva Oy, Olkiluoto, Finland and Svensk Kärnbränslehantering AB, Sweden.

- Johnson L, Marschall P, Wersin P, Gribi P, 2005.** HMCEBG processes related to the steel components in the KBS-3H disposal concept. Posiva Working Report 2005-09 and SKB R-08-25. Posiva Oy, Olkiluoto, Finland and Svensk Kärnbränslehantering AB, Sweden.
- La Pointe P R, Cladouhos T, Outters N, Follin S, 2000.** Evaluation of the conservativeness of the methodology for estimating earthquake-induced movements of fractures intersecting canisters. SKB TR-00-08, Svensk Kärnbränslehantering AB.
- La Pointe P, Hermanson J, 2002.** Estimation of Rock Movements due to Future Earthquakes at Four Candidate Sites for a Spent Fuel Repository in Finland. POSIVA 2002-02. Posiva, Olkiluoto, Finland.
- Lanyon G W, Marschall P, 2006.** Discrete fracture network modelling of a KBS-3H repository at Olkiluoto. POSIVA 2006-06 and SKB R-08-26. Posiva, Olkiluoto, Finland and Svensk Kärnbränslehantering AB, Sweden.
- Liu J, Neretnieks I, 2004.** Coupled transport/reaction modelling of copper canister corrosion aided by microbial processes. *Radiochim. Acta* 92, pp. 849–854.
- Liu J, Neretnieks I, 2006.** Physical and chemical stability of the bentonite buffer. SKB R-06-103, Svensk Kärnbränslehantering AB.
- Löfman J, 1999.** Site scale groundwater flow in Olkiluoto. POSIVA 99-03. Posiva Oy, Olkiluoto, Finland.
- Munier R, Hökmark, H, 2004.** Respect Distances. Rationale and Means of Computation. SKB R-04-17, Svensk Kärnbränslehantering AB.
- Neretnieks I, 1985.** Stationary transport of dissolved species in the backfill surrounding a waste canister in fissured rock: some simple analytical solution. *Nuclear Technology*, Vol. 72, pp. 194–200.
- Pastina B, Hellä P, 2006.** Expected evolution of a spent fuel repository at Olkiluoto, POSIVA 2006-05. Posiva Oy, Olkiluoto, Finland.
- Poteri A, 2001.** Estimation of the orientation distributions for fractures at Hästholmen, Kivetty, Olkiluoto and Romuvaara. Posiva Working Report 2001-10. Posiva Oy, Olkiluoto, Finland.
- Pusch R, 2000.** On the effect of hot water vapor on MX-80 clay. SKB TR-00-16. Svensk Kärnbränslehantering AB.
- Raiko H, 2005.** Disposal canister for spent nuclear fuel – Design report. POSIVA 2005-02. Posiva, Olkiluoto, Finland.
- Saario T, Kirkkomäki T, Sacklén N, Autio J, Kukkola T, Raiko H, 2004.** Spent nuclear fuel repository at Olkiluoto – Preliminary design – Stage 1. Posiva Working Report 2003-74. (In Finnish). Posiva Oy, Olkiluoto, Finland.
- SKB, 2006a.** Long-term safety for KBS-3 repositories at Forsmark and Laxemar – a first evaluation – Main report of the SR-Can project. SKB TR-06-09, Svensk Kärnbränslehantering AB.
- SKB, 2006b.** Buffer and backfill process report for the safety assessment SR-Can. SKB TR-06-18, Svensk Kärnbränslehantering AB.
- Smart N R, Rance A P, Werme L O, 2004.** Anaerobic corrosion of steel in bentonite. *Mat. Res. Soc. Symp. Proc.* 807, 441–446.
- Smith P, Nordman H, Pastina B, Snellman M, Hjerpe T, Johnson L, 2007.** Safety assessment for a KBS-3H spent nuclear fuel repository at Olkiluoto – Radionuclide transport report. POSIVA 2007-07 and SKB R-08-38. Posiva Oy, Olkiluoto, Finland and Svensk Kärnbränslehantering AB, Sweden.

**Vieno T, Hautojärvi A, Koskinen L, Nordman H, 1992.** TVO-92 Safety Analysis of Spent Fuel Disposal. Report YJT-92-33E, Nuclear Waste Commission of Finnish Power Companies, Helsinki, Finland.

**Vieno T, Nordman H, 1999.** Safety assessment of spent fuel disposal in Hästholmen, Kivetty, Olkiluoto and Romuvaara TILA-99, POSIVA 99-07. Posiva Oy, Helsinki, Finland.

**Vieno T, Nordman H, 2000.** Updated compartment model for near-field transport in a KBS-3 type repository. Posiva Working report 2000-41. Posiva Oy, Helsinki, Finland.